In vitro reproduction of a gut on a microfluidic chip

Marine Verhulsel

Université Pierre et Marie Curie

Ecole doctorale 'Physique en Ile de France'

Institut Curie, UMR168 / Equipe Macromolécules et Microsystèmes en Biologie et en Médecine

Reproduction *in vitro* d'un intestin sur puce microfluidique

Présentée par Marine Verhulsel

Thèse de doctorat de Biophysique

Dirigée par Stéphanie Descroix, Danijela Matic Vignjevic, Jean-Louis Viovy

Jury :

Mme Ferrand Audrey

M Leclerc Eric (Rapporteur)

M Théry Manuel (Rapporteur)

M Viovy Jean-Louis (Directeur de thèse)

M Voituriez Raphaël

Mme Wilhelm Claire

Mme Descroix Stéphanie (Co-directeur de thèse, membre invité)

Mme Vignjevic Danijela (Co-directeur de thèse, membre invité)

ABBREVIATIONS:

ECM	Extracellular matrix
2D	Two dimensional
3D	Three dimensional
ISC	Intestinal stem cell
TA	Transit amplifying
BM	Basement membrane
GAG	Glycosaminoglycan
CBC	Crypt base columnar
αSMA	α smooth actin
PEGDA	Poly(ethylene glycol) diacrylate
PEG	Poly(ethylene glycol)
PA	Peptides amphiphiles
RGD	Arginyl-glycyl-aspartic acid
PDMS	Polydimethylsiloxane
S	Spread parameter
Wcc	Cell-cell adhesion per unit area
Wsc	Cell-substrate adhesion per unit area
PLL	Poly L lysine
EGF	Epithelial growth factor
PMMA	Poly(methyl methacrylate)
PLGA	poly-lactic-glycolic acid
LOX	Lysyl oxidase
S(f)	Frequency dependent fluctuation spectrum
k	Spatial mode
R	Radius of the laser
G*	Complex viscoelastic modulus

G’	Elastic modulus
G’’	Viscous modulus
E	Young modulus
MEF	Mouse embryonic fibroblasts
IPN	Interpenetrating polymer network
SIPN	Semi interpenetrating polymer network
HA	Hyaluronic acid
GM	Gycidyl methacrylate
AGE	Advanced glycation end product
MMP	Matrix metalloproteinase
SIS	Small intestine submucosa
lp	Persistance length
Lc	Contour length

TABLE OF CONTENTS

CHAPTER 1: INTRODUCTION

Tissue engineering has greatly expanded over the last 20 years as evidenced by the exploding number of publication since 2000 (Fisher and Mauck 2013). This large number of publications is directly correlated to the multiple fields of applications of tissue engineering such as regenerative medicine, pharmaceutics, fundamental and applicative research. The world-leading biotechnology researcher, Robert Langer, first described tissue engineering as 'an interdisciplinary field that applies the principles of engineering and life sciences to the development of biological substitutes that restore, maintain, or improve tissue function' (Langer 2000). In a more restricted approach, tissue engineering mainly consists in manufacturing a scaffold that would resemble the native extracellular environment of cells and would therefore deliver the signaling needed for the cells to differentiate and survive as a functional tissue (Katari, Peloso, and Orlando 2015). Cells could either be seeded within or on this scaffold. Tissue engineering appears as an alternative between the complexity of *in vivo* studies and the lack of realism of conventional cell culture (Figure 1). Indeed cells cultured in artificial cell matrix exhibit features (different phenotype, gene expression and polarity) that are close to the *in vivo* ones and are not expressed in traditional culture (Ramanan et al. 2014). Meanwhile, as for standard culture, it allows working with well-characterized cells and facilitates the use of DNA recombination techniques as cells are in a controlled confined area compared to *in vivo* experiments. The fact that cells, matrix components and properties can be selected independently facilitated the read-out of the experiments compared to *in vivo* experiments. Furthermore, as shown in figure 1, its low cost, compared to laboratory animal models, favors high throughput investigations. The main deficit of engineered tissues is that they are not integrated in a body. Therefore, they do not integrate signals from adjacent tissues, humoral or immune factors that could induce changes in tissue phenotype. From that perspective, they lack the full complexity that characterize *in vivo* studies (Ramanan et al. 2014).

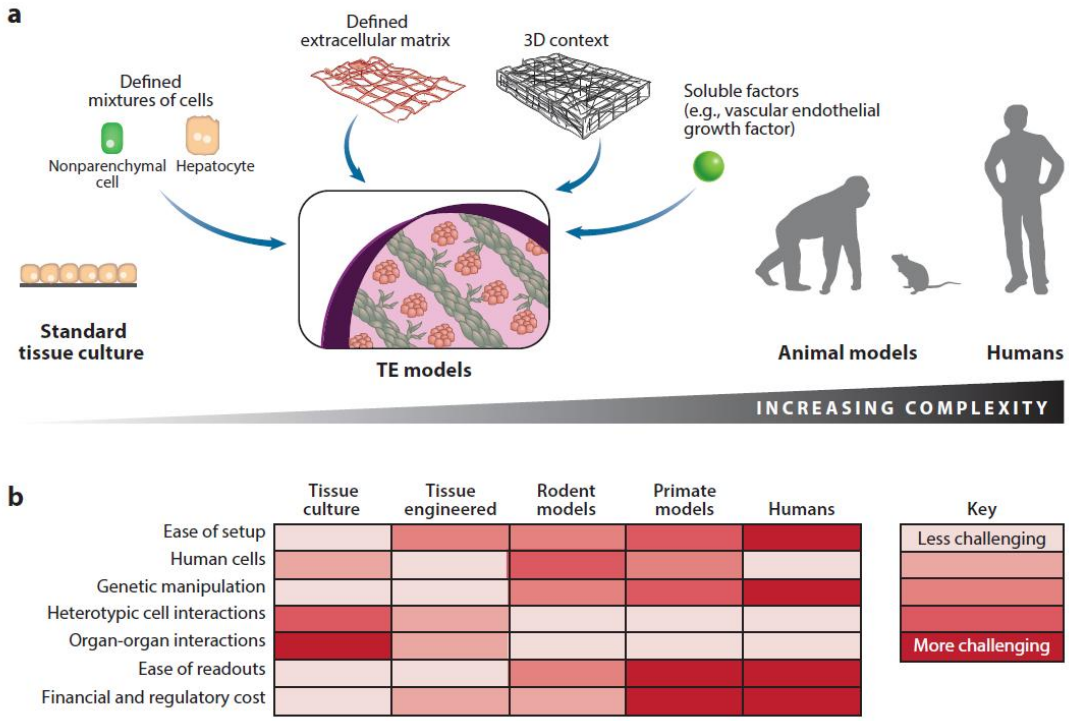

Figure 1: *The intermediate position of tissue engineering in today's research. a) the increasing complexity of the environment from conventional monolayer cell culture to integrated bodies. Tissue engineering belongs half-way between these two extremes by providing a controlled biomimetic environment to the cells. b) Main advantages and drawbacks of tissue engineering compared to conventional culture and in vivo studies. Imported from* (Ramanan et al. 2014)

Tissue engineering offers great opportunities in regenerative medicine since manufactured tissues and organs could be implanted in an injured body. In this perspective, the United-Kingdom has invested £25M to create a Regenerative Medicine Platform. This platform is composed of 5 interdisciplinary centers working on the translation of in vitro tissues from bench to clinical practice (http://www.ukrmp.org.uk). Artificial skin and cartilage are examples of engineered tissues that have already been approved by the FDA.

Pharmacological trials have already been greatly improved thanks to tissue engineering. Indeed, due to species variable sensitivity, 80% of the drugs that efficiently cure cancer in mice are inefficient in human (Holzapfel et al. 2015; Villasante and Vunjak-Novakovic 2015). Working with human engineered tissues alleviates ethical problems related to animal testing, increases standardization, and allows more thorough studies of toxicity, metabolism and life cycle of putative drugs before entering clinical testing (Bricks et al. 2015). This could, in turn, reduce the duration, cost failure rate and risk of clinical trials.

Finally, fundamental research also shows growing interest for artificial matrix as there are now clear evidences that cell environment affects cell phenotype. This is, in particular, illustrated by the increasing number of companies that offer extracellular matrix (ECM)-like hydrogels as support for

cell culture (Lifetechnologies, Sigma, Corning…). In these 2D or 3D hydrogels cells exhibit significantly different morphology, proliferation capacity, differentiation status and gene expression profile than in traditional cell culture. As an example, it has been demonstrated that cancer cells express numerous genes in native environment that are down-regulated in conventional cell culture (Villasante and Vunjak-Novakovic 2015). Furthermore, owing to a greater control of the properties of cell microenvironment, the influence of each parameter on cell proliferation, migration or differentiation can be investigated independently and in accurate manner.

The main challenge of tissue engineering is to reconstitute *in vitro* a cellular environment that induces the differentiation of cells and their organization in an ordered functional tissue. In this perspective, the small intestine is particularly ambitious. As a matter of fact, since intestinal epithelium acts as a barrier between the outer and the inner environment of the body, this organ is submitted to multiple signals with various origins. Although the special interaction with the external environment might participate in the maintenance of intestinal homeostasis, it can also be harmful for this tissue. The presence of bacteria and the irritation related to nutrients digestion may cause various inflammatory intestinal diseases like Crohn disease or intestinal ulcers that are widespread diseases but still not fully understood. Similarly, disruption of intestinal epithelium homeostasis can promote the development of cancers (colonic cancer is the third more widespread cancer in Canada) but initiation steps are not well established.

The ability for *in vitro* systems to analyze the influence of each intestinal signaling independently should complement *in vivo* studies to better understand the normal physiology of the gut and, thereafter, would facilitate figuring out the mechanism of such diseases. In this regard, my PhD aims to recapitulate on chip the biological, chemical and physical characteristic of the *in vivo* intestine to induce the growth of an intestinal tissue *in vitro*.

I Introduction to the intestine

The small intestine is composed of three structural parts: duodenum, jejunum and ileum. The intestinal epithelium secrete the enzymes to lyze the nutrients and to complete the digestion initiated earlier in the stomach. The intestinal epithelium, also ensure most of nutrient absorption. The peristaltic motion makes the nutrient move forward into the intestine. This motion results from the contraction of the muscular layers surrounding the gut (Figure 2). Finally, the intestinal epithelium also acts as a barrier between the external lumen and the body. To ensure the integrity of this barrier the epithelium is renewed every 4-5 days, which makes the intestine the organ that renews the most in adult mammalian (van der Flier and Clevers 2009).

As shown in figure 2, the intestinal wall is comprised of four layers: mucosa, submucosa, muscularis externa and serosa (T Komuro and Hashimoto 1990). These four layers are very distinct and

complementary with regards to their structure and function. The muscularis externa is composed of several muscular layers that contract cyclically. These layers give the intestinal wall the contractility needed to ensure the peristaltic motion. Right above the muscular layer, the submucosa is mostly constituted of a dense network of interwoven type I collagen fibrils: the lattice (Terumasa Komuro 1988). These interwoven collagen fibrils provide the intestinal wall resistance to the shear stress induced by the flow of nutrients. The intestinal mucosa ensures the absorptive function and is composed of the epithelium, the lamina propria and the lamina muscularis mucosae (Figure 2). Lamina muscularis mucosae draw the line between the mucosa and the submucosa and consist of 3-5 layers of smooth muscle cells. These cells are oriented longitudinally but not as densely organized as in the muscularis externa. Some muscle cells involved in contraction of the villus, are found in the core of the villi oriented longitudinally to the axis of the villi (Figure 2) (T Komuro and Hashimoto 1990).

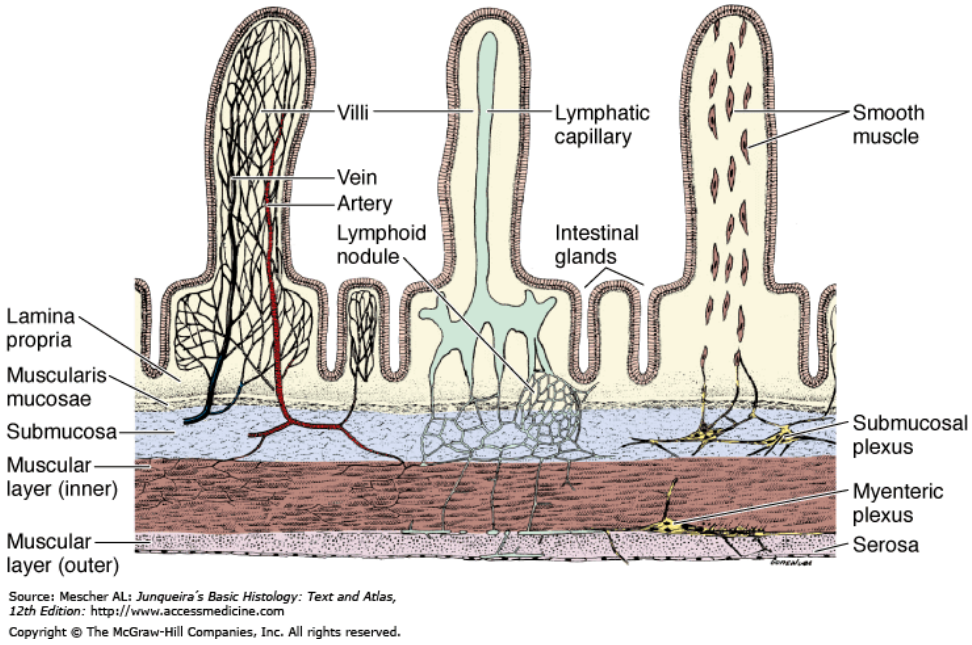

Figure 2: *Schematic representation of the intestinal wall.*

Above the lamina muscularis mucosae, the lamina propria and the epithelium display the morphology characteristic of the intestine made of villi surrounded by 5-10 crypts (Figure 3). Villi are finger-like structures that rise into intestinal lumen and maximize the surface area for digestion and absorption (Barker 2014). Intestinal crypts are tubular invaginations in the lamina propria that shelter intestinal stem cells.

The intestinal epithelium consists of a cellular monolayer that entirely covers the surface of the intestine wall. Villi are coated with 5 of the 6 differentiated intestinal cell types: the enterocytes, the goblet cells, the enteroendocrine cells, the Tuft cells and the M cells (Clevers 2013; van der Flier and Clevers 2009). Enterocytes represent 80% of the intestinal epithelial cells and are considered as the

absorptive lineage (van der Flier and Clevers 2009). They are highly polarized and present an apical brush border consisting of thousands of microvilli that greatly expand their absorptive surface (Louvard, Kedinger, and Hauri 1992). Goblet cells secrete protective mucus and are required for the movement and effective expulsion of gut content (van der Flier and Clevers 2009). Enteroendocrine cells synthesize intestinal hormones and are subdivided into 15 subtypes with specific morphology and secretory content (van der Flier and Clevers 2009). Tuft cells are chemosensory cells and are supposed to be involved in chemotransduction (Gerbe, Legraverend, and Jay 2012). Finally, M cells are involved in the mucosal immunity and function as an interface between the luminal content and the underlying immune cells (Kucharzik et al. 2000).

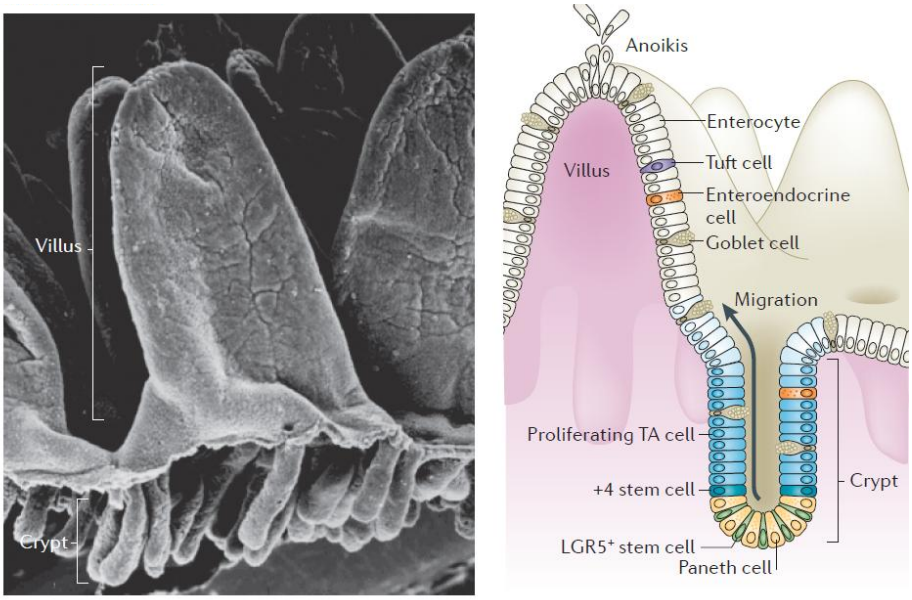

Figure 3: *Epithelial organization in the small intestine. On the left: scanning electron micrograph of the villi surrounded by crypts. On the right: schematic representation of the intestine: its self-renewal and constitutive cell types. Imported from* (Barker 2014)

Intestinal crypts contain the intestinal stem cells (ISCs), the transit amplifying cells and the last differentiated cell type: Paneth cells. As all stem cells, the ISC are multipotent and they have the ability to self-renew (Gracz and Magness 2014). Stemness of the ISC is most likely not an intrinsic property but more a state induced and maintained by the surrounding microenvironment (van der Flier and Clevers 2009; Yen and Wright 2006). The signals involved in the maintenance of ISC stemness mainly originate from Paneth cells, the underlying myofibroblasts and extracellular matrix (ECM) of the crypt (Barker 2014; van der Flier and Clevers 2009). Therefore intestinal crypts have been defined as stem cell niches (Barker 2014; van der Flier and Clevers 2009; Gracz and Magness 2014; Yen and Wright 2006). Transit amplifying cells are ISC progeny. They proliferate faster than the ISC but only achieve four to five division cycles. They exhibit a more restricted pluripotency than the ISC and they differentiate into one of the 6 lineages as they reach the crypt-villus junction (Clevers 2013) (Figure 2). Paneth cells are intercalated between ISC at the bottom of the crypt (Figure 2). In addition to

secrete factors constitutive of the niche, Paneth cells also secrete antimicrobial peptides into the intestinal lumen. Their renewal rate is much lower (3-6 weeks) than the other epithelial cell types (3-5 days) (Barker 2014).

All intestinal epithelial cells are anchored to the basement membrane (BM) at their basal pole. Basement membrane is a thin layer (100-200nm) composed of two interconnected layers of specialized extracellular matrix molecules composed mainly of laminin, nidogen, type IV collagen and heparin sulfate proteoglycans (Glentis, Gurchenkov, and Vignjevic 2014; Louvard, Kedinger, and Hauri 1992). The basement membrane may act as a barrier between the lumen and the body since its structure is very dense except on the upper two third of the villi were it exhibits fenestrations (Figure 4) (T Komuro and Hashimoto 1990). These fenestrations allow free immune cells and basal protrusion of epithelial cells to cross the basement membrane (Figure 4).

Once transit amplifying cells are differentiated, they migrate on this basement membrane upwards to the top of the villi. Paneth cells are very specific because they are the only cell type that is found in the crypt and not in the villi. Although some authors speculate that some transit amplifying cells might migrate downwards and differentiate as Paneth cells, this hypothesis has not been verified *in vivo*. Therefore, it is more likely that Paneth cells directly differentiate from the dividing stem cells in the lowest part of the crypt. At the top of the villi, differentiated cells undergo anoikis: cells detach from the basement membrane and the loss of cell-matrix adhesion induces cell apoptosis (Fouquet et al. 2004; Gracz and Magness 2014). Since stem cells and transit amplifying cells are constantly dividing in the crypt, apoptosis ensures the homeostasis of the tissue both at the base of the crypt to control the number of stem cells and at the villus tip by the shedding of differentiated cells (Fouquet et al. 2004).

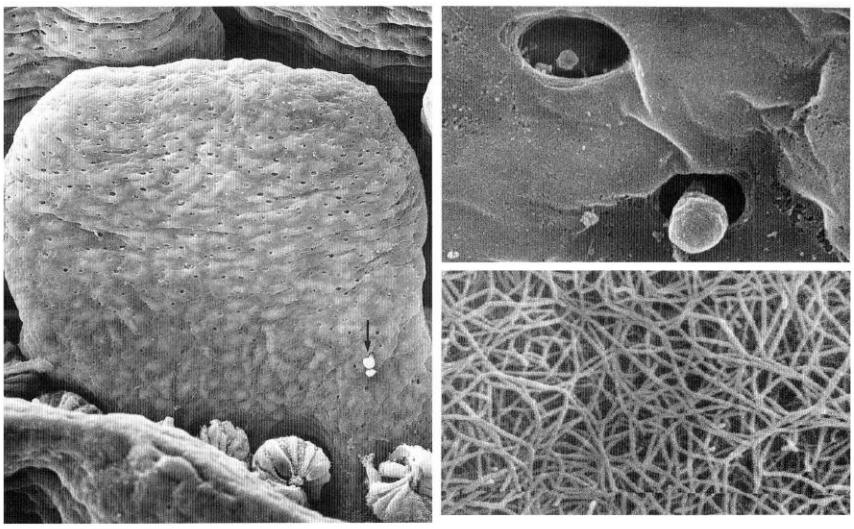

Figure 4: *Structure of the lamina propria. On the left: scanning electron micrograph of the basement membrane of the rat intestinal villi. Black arrow indicates cell processes passing through the fenestration (× 430). On the top right: higher magnification of the fenestration (× 8 600). On the bottom right: collagen fibrils constitutive of the underlying layer of the basal lamina (× 12 000).*

The lamina propria is constituted by basement membrane and the underlying stromal matrix mainly composed of type I and III collagen and glycosaminoglycan (GAG) (Louvard, Kedinger, and Hauri 1992). Beneath the basement membrane, collagen fibers form a supportive network together with subepithelial fibroblasts. This network is is denser around the crypt with greater abundance of fibroblasts and collagen fibrils (Hosoyamada and Sakai 2005). Lymphocytes, neurons and capillaries are also common part of the lamina propria (Gracz and Magness 2014).

Since we are interested in reproducing the entity composed of the intestinal epithelium and its underlying lamina propria, it is important to understand how these layers acquire such specific morphology during the embryonic development and how this functional architecture is maintained at the adult stage.

I.1.Embryonic morphogenesis of the intestine

Morphogenesis shapes cells organization and distribution into the morphology of the tissue they will belong to. Cells then acquire the function associated to their tissue through the differentiation process. Morphogenesis and differentiation are controlled by different cascades of biochemical and physical signals very well-orchestrated in space and time (P. Simon-Assmann et al. 1995).

In the rat, the small intestine first appears as a tube resulting from the folding of the endodermal sheet. At embryonic day 15, villi start to form; cells progressively differentiate in the villi while proliferative cells are restricted to intervillus pocket regions (Figure 5). Crypts start to appear around postnatal day 7 (Barker 2014; Crosnier, Stamataki, and Lewis 2006). The number of crypts then rapidly expands by growth and fission of existing crypts. During crypt fission, a crypt is duplicated starting from the bottom upwards rather than de novo from the top (Clarke 1972). The maximum of crypt fission is reached at 21 days (25% of crypts undergo crypt fission) and then decrease to the adult value of around 7% (St Clair and Osborne 1985).

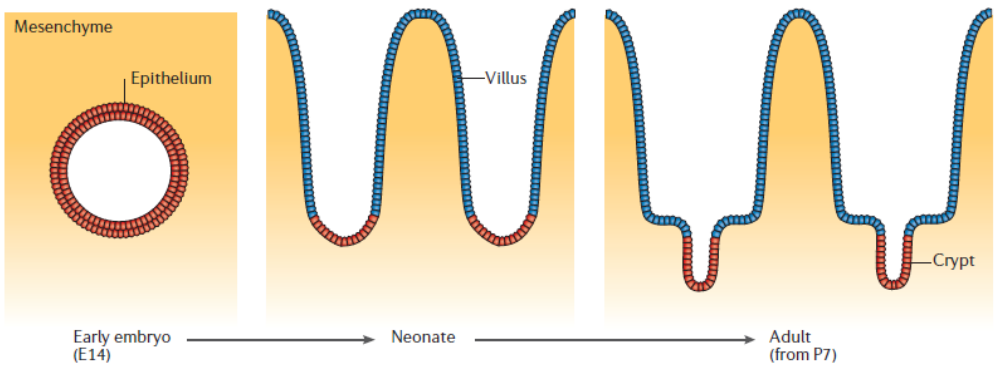

Figure 5: *Schematic representation of the 3 main stages in the intestinal morphogenesis of the mouse. Imported from* (Crosnier, Stamataki, and Lewis 2006)

Multiple signals trigger the morphogenesis of villi and crypts during embryogenesis. The nature of these signals could be chemical or physical as it will be discussed in the following sections.

I.1.1) Heterotypic cell signaling

At early stage of development mesenchymal and epithelial cells interact and strongly induce formation of the villi through the hedgehog signaling pathway. Hedgehog ligands (Sonic hedgehog (Shh) and Indian hedgehog (Ihh)) are secreted by epithelial cells while the expression of Hedgehog receptors (Patched 1 (Ptch1) and patched 2 (Ptch2)) is restricted to the underlying mesenchymal cells (Barker 2014; Crosnier, Stamataki, and Lewis 2006). Madison et al (Madison et al. 2005) generated transgenic mice expressing pan-hedgehog inhibitor. They noted that shutting down hedgehog signaling results in a complete absence of villi and the persistence of highly proliferative epithelium. This observation suggests that hedgehog paracrine signaling from epithelial cells to mesenchyme is necessary to induce villi morphogenesis.

I.1.2) Homotypic cell signaling

Interactions between epithelial cells are also required through the process of villi formation. These interactions are mediated through the juxtacrine Ephrin (ligand)/Eph (receptor) pathway. Epithelial cells either express Ephrin b1 ligand or EphB2/EphB3 receptors at the surface of their membrane (Crosnier, Stamataki, and Lewis 2006). Juxtacrine signaling only occurs when two cells: one carrying the receptor and the other the ligand are physically in contact. Regarding Ephrin/eph signaling, it induces repulsive forces between the interacting cells. In mice embryo, the ephrinb1 expression is restricted to the differentiated cells of the villus while EphB2 and EphB3 are located at the intervillus region. In their study, Batle E et al (Batlle et al. 2002), observed (deficient for these two receptors) an absence of the boundary between proliferative cells and differentiated cells in EphB2/EphB3 mutants (deficient for these two receptors). Proliferative cells were no more restricted to the intervillus pocket domain and appeared in the villus domain. Ephrin-based repulsion is thus critical regarding segregation between differentiated and proliferative cells. This homotypic signaling is of major importance since the restriction of proliferative cells to the intervillus pockets and of differentiated cells to villi is a necessary step to ensure the normal morphogenesis of the intestine.

I.1.3) ECM composition

Intestinal embryonic development is also associated with changes in ECM composition. For instance, maximal synthesis of laminin 1, the BM major component, occurs at the 16-18 days of gestation when the intestinal cells start differentiating (Louvard, Kedinger, and Hauri 1992; P. Simon-Assmann et al. 1995). Variations in the ratio of the isoforme of this molecule are also observed. The proportion of α1 laminin chain is maximal during villus formation compared to β1 and γ1 laminin chains (P. Simon-Assmann et al. 1995). This is of particular interest since laminin α is assumed to promote the

polarization of epithelial cells (Louvard, Kedinger, and Hauri 1992). In ECM, the amount of glycosaminoglycan (GAG) is maximal during fetal stages. GAGs are large hydrophilic molecules which can be solvated by water in the matrix and provoke its swelling. Therefore any variation in GAG proportion induces matrix remodeling. The reduction of GAG amount after birth can also bring at the ECM surface some ligands that were previously inaccessible due to matrix swelling (Louvard, Kedinger, and Hauri 1992). The asynchronous expression of some ECM components causes local changes in the microenvironment of the cells. The transduction of the extracellular spatio-temporal heterogeneities to the intracellular compartments via integrins induces cell maturation, differentiation and migration required for intestinal morphogenesis (Louvard, Kedinger, and Hauri 1992).

I.1.4) Mechanical forces

During embryonic development, the mesenchymal cells underneath the future epithelium also differentiate into muscular layers. The apparition of such muscular layers imposes mechanical constrains to the epithelial tissue proliferation. Shyer et al (Shyer et al. 2013) observations attest of the strong influence of the underlying muscular layers on the formation of villi in the chicken embryo. The flat chicken epithelium passes through two intermediate morphological stages before acquiring its final structure.

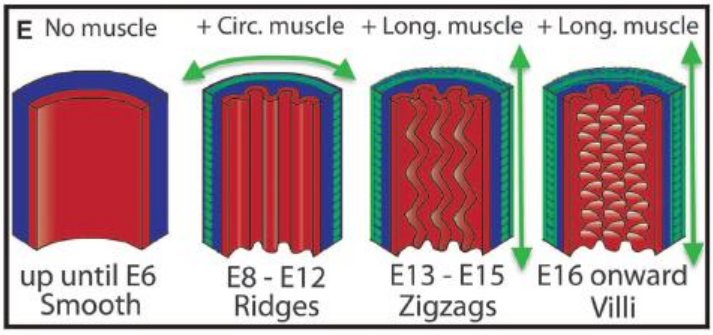

Figure 6: *Schematic representation of the correlation between muscular differentiation and epithelium morphological stage through time in the chicken embryo. Imported from* (Shyer et al. 2013)

First ridges appear at embryonic days E8-E12, then they evolved to a zig-zag structure at E13-E15 and finally at E16 villi are observed (Figure 6). Shyer et al have established a close correlation between the apparition of a new muscular layer and the transition from one morphological stage to the next one. At first, the circumferential layer is formed. The future epithelium is constrained and ridges appear. Then a second muscle layer differentiated into the longitudinal muscle layer. The gut is thus compressed biaxially inducing a switch from ridges to zig-zag morphology. Finally, the differentiation of an additional longitudinal muscular layer gives rise to the villi. In conclusion the smooth muscle constrains the expansion of the above mesenchyme and epithelium by compressing these layers from different axis. It is worth noting that the apparition of the peristaltic motion does not influence the acquisition of the successive stages.

In conclusion, during embryonic morphogenesis, the intestinal development is influenced by short range signaling (adjacent epithelial cell, BM) and from long range signaling (mesenchymal cells, ECM). These signals are complementary and precisely orchestrated over time. They ensure the acquisition of the adult crypt-villi structure and the segregation of proliferative and differentiated cells in their dedicated morphological subunits. One of the key challenges of the adult stage is to maintain both structure and functionality to guarantee the homeostasis of the intestinal epithelium.

I.2 The maintenance of epithelium homeostasis in the adult small intestine

Homeostasis of the intestinal epithelium is ensured by the continuous cells division in the crypt and apoptosis both in the crypt and at the top of the villi. Maintenance of stem cell, cell migration and apoptosis are precisely orchestrated by biochemical and mechanical signaling. As previously discussed in embryonic morphogenesis of the intestine, those signals have various origins: homotypic and heterotypic signaling, cell matrix interaction and long range interactions with regards to the underlying tissues like muscular layers. The following sections details how these actors support intestinal homeostasis. With respect to the aim of tissue engineering which is to recreate a microenvironment that induces the differentiation of cells into a specific tissue, evaluating the influence of each parameters is essential in order to simulate them *in vitro*.

I 2 1) Stem cells and epithelium renewal

The following section introduces the specific location of stem cells in the crypt, how they self-renew and generate their progeny. The factors responsible for their maintenance and the induction of a specific fate to their progeny are also presented. The spatial restriction of these factors to the low part of the crypt confirms the vision of the crypt as a stem cell niche.

Stem cell hierarchy and crypt plasticity

In 1974, crypt base columnar (CBC) cells localized at the bottom of the crypt were first identified as stem cells by Cheng & Leblond (Cheng and Leblond 1974). They injected tritiated thymidin in mice to determine where the dividing cells were located. Unfortunately the β-radiation of the tritium killed the CBC cells undergoing mitosis during the injection in the crypt. Apoptotic CBC cells were phagocytosed by their neighboring CBC cells thus exhibiting a large radiolabeled phagosome. After 12 hours, phagosomes were founded in the mid crypt and after 30 hours they appeared in the enterocytes and Paneth cells. Since phagosomes were first identified in the CBC cells and then in differentiated cell types, they concluded that CBCs behave as the stem cells of the epithelium as they are multipotent and have the ability to self-renew (Cheng and Leblond 1974). More recently, the location of CBC stem cells was precisely determined in the study of Barker et al (Barker et al. 2007), who identified Lgr5 as a marker of those cells. They located cells expressing Lgr5 ($Lgr5^+$ cells) at the

bottom of the crypt intercalated between Paneth cells and counted approximatively 3-4 $Lgr5^+$ cells per crypt.

They then used Cre recombinase to follow their progeny. Cre-recombinase catalyzes recombination across DNA sequences called lox P. Cre recombinase can be associated to estrogen receptor (ERT) to permit temporal activation of the cre-recombinase. When Cre recombinase is bound to estrogen receptor it cannot enter the nucleus and therefore is not active. In presence of tamoxifen, tamoxifen binds to the ERT receptor and induces a change in its conformation that allows the cre-ERT construct to enter the nucleus and induce targeted mutation namely the fusion of two lox P sequences and the excision of the intermediate sequence. (Figure 7)

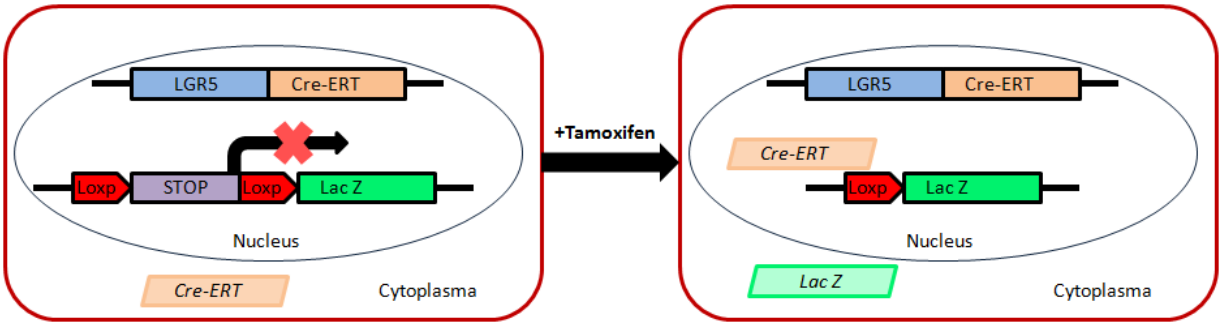

Figure 7: *Cre recombinase technique in cells expressing Lgr5. In absence of tamoxifen Cre recombinase bound to ERT is restricted to the cytoplasma and Lac Z is not expressed. Following the addition of tamoxifen, Cre recombinase translocates to the nucleus, recombines loxp sequences resulting in the expression of LacZ*

In this study, the gene coding for the enzyme Cre-recombinase-ERT was located in the first exon of the gene coding for Lgr5. As a result, Cre recombinase-ERT was only present in the cytoplasm of cells expressing Lgr5. In the nucleus two lox P sequences flanked a silence sequence. When Cre recombinase was absent this silence sequence was transcribed. In the presence of Cre recombinase the two lox P were fused, the silence sequence was excised and the Lac Z gene following the second lox P sequence was transcribed (Figure 7). Therefore following tamoxifen injection, Lac Z was expressed only in the $Lgr5^+$ cells. After 5 days, they observed ribbons of cells expressing Lac Z starting from the bottom of the crypt and reaching the top of the villus. It confirmed that the progeny of $Lgr5^+$ cells can differentiate into the 6 differentiated cell types. After 60 days cells expressing Lac Z were still found testifying of the ability of $Lgr5^+$ to self-renew (Figure 8).

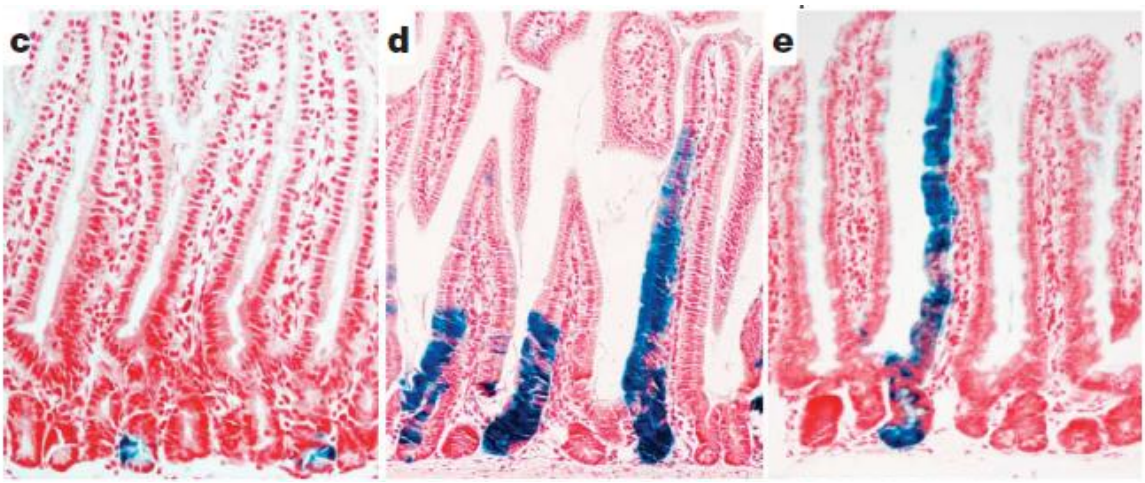

Figure 8: *Lineage tracing in the small intestine. Analysis of Lac Z expression (blue cells) c)1 day after tamoxifen induction, d) 5 days after injection and e) 60 days after injection. Imported from* (Barker et al. 2007)

In 1977, Potten suspected the existence of another stem cell subpopulation located at the +4 location (fourth position starting from the crypt base) in the crypt as those cells were also sensible to irradiation (C S Potten 1977). Since those cells were also able to retain labeled DNA over cell cycles (C S Potten, Kovacs, and Hamilton 1974), it was suggested that these +4 cells could be stem cells. Indeed the fact that these cells retain labeled DNA indicates that they divide asymmetrically: DNA template strand is preserved in the stem cell while newly synthesized strands with potential errors are sent to the daughter cell (C S Potten 1977). In addition, their sensitivity to radiation resembles the behavior of stem cells that undergo apoptosis in case of damage to avoid the apparition of errors in their template DNA strands (Christopher S Potten, Owen, and Booth 2002). The study of Sangiorgy et al (Sangiorgi and Capecchi 2008) confirmed that +4 cells can be considered as intestinal stem cells since after 12 months, their lineage was still present testifying of their ability to self-renew and the five differentiated cell types were found in their progeny. In their experiments, they defined Bmi1 as a marker of those +4 and used the Cre recombinase approach to follow the cells expressing Bmi1 and their progeny. They also noticed that +4 stem cells were slow cycling cells; this observation could explain their ability to retain DNA. Since some crypts did not expressed Bmi1 stem cells but where still active, they confirmed the existence of the additional Lgr5 stem cell subpopulation.

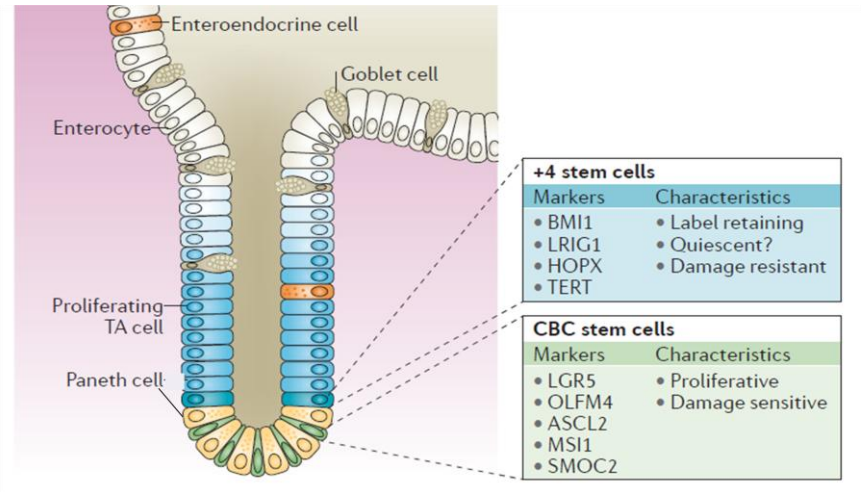

Figure 9: *Summary of the characteristics and the markers of the two subpopulations of stem cells: the crypt base columnar (CBC/ Lgr5+) stem cells and +4 stem cells. Imported from* (Barker 2014) *with modifications*

The existence of two subpopulations of stem cells in the crypt is now globally admitted and provides a more plastic model of the origin of stem cells (Figure 9). The Lgr5+ / CBC cells are considered as the active stem cells responsible for daily epithelial homeostasis while +4 stem cell population represents a more quiescent/ slow cycling population that is activated following tissue injury (Barker 2014; Gracz and Magness 2014; C S Potten 1977; Sangiorgi and Capecchi 2008). In case of major injury TA cells ($Lgr5^-$) are able to dedifferentiate and to adopt the stem cell fate (Lgr5+) (Barker 2014; Gracz and Magness 2014). Such observations suggest some hierarchy among the stem cells present in the crypts (Barker 2014; Christopher S Potten, Owen, and Booth 2002). The plasticity of the cell populations in the crypt might be sustained by the specific signaling and microenvironment occurring in the stem cell niche (Barker 2014).

Asymmetrical stem cell division vs neutral drift in the crypt

Despite the permanent dividing stem cells, intestinal tissue homeostasis imposes the total number of cells to remain constant. Therefore it implies some asymmetry in the fate of daughter cells, half of them remaining stem cells. This asymmetry can be assessed at the scale of individual stem cell (division asymmetry) or of the whole crypt population (population asymmetry) (Lopez-Garcia et al. 2010). In population asymmetry, the loss of one stem cell dividing into two TA daughter cells is compensated by the division of another stem cell into two daughter stem cells.

Potten (C S Potten 1977) first made the assumption that asymmetric division was the rule regarding individual stem cell division. Template DNA strands segregates from newly synthesized strands and remains in the stem cells to avoid the emergence of any error in the stem cell DNA. This hypothesis was experimentally confirmed by Quyn et al (Quyn et al. 2010) study. They labeled the newly synthesized DNA with EdU in the crypt and observed that for the cell located at position 4 and below,

the mitotic spindle of dividing cells was oriented perpendicular to the surface and that in most cases division was asymmetric. (Figure 10)

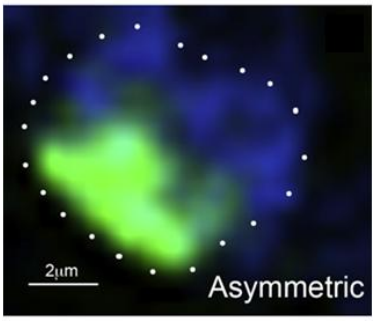

Figure 10: *Asymmetric distribution of DNA in dividing stem cells 1 day after EdU injection. Newly synthesized DNA EdU labeled (in green) and template DNA labeled with Dapi (blue). Imported from* (Quyn et al. 2010)

However controversial studies are in favor of an asymmetry at the population level. A first observation was performed on chimaeric mice which are mice that are constituted of two populations of genetically distinct cells (Schmidt, Winton, and Ponder 1988). Two days after birth, the crypts that were at the borders between two chimaeric patches expressed cells of each population indicating the existence of stem cells of both populations (polyclonality). Two weeks after, mixed crypts tended to express one cell population more than the other with a gradual disappearance of mixed crypts. At the adult stage all crypts were only formed with one population of cells indicating the prevalence of one stem cell type in each crypt (monoclonality). In conclusion, the crypts that were initially polyclonal shift to monoclonality over time (Schmidt, Winton, and Ponder 1988). This phenomenon called neutral drift was also observed in adult mice. Snippert et al (Snippert et al. 2010), generated crypts with stem cells with random colors in a 10 weeks old mutant mice using the Cre recombinase approach previously presented. The genetic recombination generated stem cells that expressed either green nucleus, blue membrane, or yellow or red cytoplasm in presence of tamoxifen. The injection of tamoxifen thus genetically modifies randomly the $Lgr5^+$ cells resulting in stem cell clones with different colors in the crypt (polyclonal crypt). In the following weeks the authors observed the prevalence of one color per crypt (Figure 10). After 8 weeks almost all crypts were single colored indicating that they drift to monoclonality through time. The villi are however polyclonal since their cellular turn-over is fueled by several surrounding crypts (Figure 11). One explanation for this neutral drift is that $Lgr5^+$ stem cells rather divide symmetrically generating two potential $Lgr5^+$ stem cells, then local signaling from the niche and competition for available niche space determines the fate of the daughter cells. Thus the asymmetry that guarantees the homeostasis of the tissue is noticed at the population level and would be the result of neutral competition between equal stem cells in the crypt (Snippert et al. 2010).

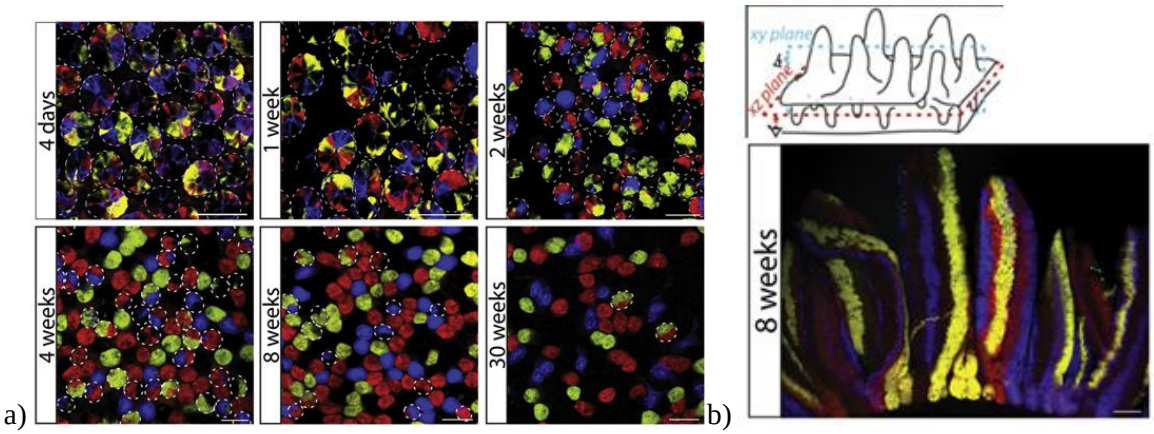

Figure 11: *Neutral drift from polyclonality to monoclonality through time in crypt. a) lineage tracing at the bottom of the crypts in the x-z plane polyclonal crypts are marked with a white dashed circle. b) Transversal cut of polyclonal villi and surrounding monoclonal crypts in the intestine 8 weeks after tamoxifen injection.*

Regarding these controversial studies, it is hard to conclude weather asymmetrical or symmetrical stem cell division is prevalent in the crypt. It remains however certain that some stem cells are maintained in the crypt since several studies could follow the lineage of single stem cells during months (Barker et al. 2007; Cheng and Leblond 1974; Sangiorgi and Capecchi 2008; Snippert et al. 2010). In order to maintain stemness at the bottom of the crypt, two major signaling pathways, Wnt and the Notch, were identified as crucial.

Wnt and Notch pathways

Wnt ligands are known to be secreted by both Paneth cells and myofibroblasts underlying the epithelial layer. A recent study suggests the presence of an additional source of Wnt since the integrity of the crypts were maintained even though signal emanating from both Paneth and myofibroblasts were inhibited (San Roman et al. 2014). Wnt ligand binds to the membrane receptor and induces the inactivation of the β catenin degradation pathway. β catenin then accumulates in the cytoplasm, translocates to the nucleus and binds to the promoters of the transcription complex of Wnt target genes (van der Flier and Clevers 2009). The amount of Wnt in the crypt is tightly regulated through a feedback loop from Wnt target genes. As an example among the genes that are express upon Wnt activation, Lgr5 gene amplifies Wnt signal whereas Rhf43 and Troy down regulate it (Barker 2014). Since Wnt sources are mostly located at the bottom of the crypt, Wnt diffuses as a gradient along the crypt axis (M. H. Wong 2004). Therefore the stemness of stem cells is maintain as they are under the direct influence of Wnt but as cells migrate upwards in the crypt they receive low level of Wnt and therefore are engaged in the differentiation process (M. H. Wong 2004). In this respect, Sansom et al (Sansom et al. 2004) reported that an overexpression of Wnt strongly impedes differentiation by reducing the number of differentiated cells and increasing the number of transit amplifying cells.

Wnt also participates in the segregation between stem cells and differentiating cells as it upregulates the expression of EphB2 and EphB3 receptors and down regulate the expression of ephrin b1 ligand (see § 1.1.b for the mechanism of Eph/ephrin interaction). Therefore, a decreasing gradient of EphB2 receptor is observed from the bottom to the top of the crypt in direct correlation with Wnt gradient, while ephrin b1 gradient follows the opposite tendency (Figure 12). The repulsive forces generated between cells carrying ephrin ligand and those carrying Eph receptors participate in cell segregation and could promote the upward migration of differentiating cells. Similarly, the expression EphB3 receptors at the surface of Paneth cells could be responsible for their downward migration (Batlle et al. 2002).

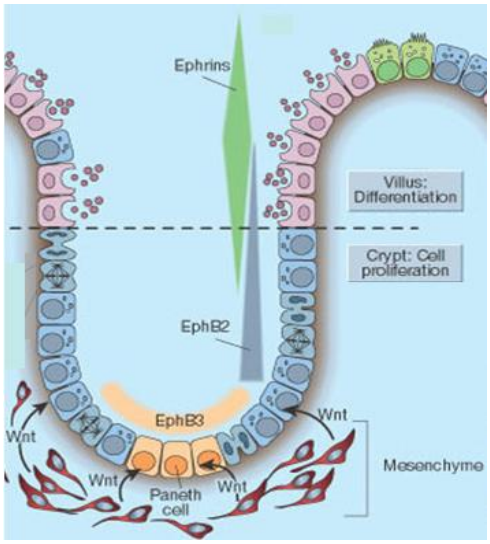

Figure 12: *Wnt induce spatial segregation between proliferative and differentiated cells by upregulating the expression of EphB 2 and down regulating the expression of ephrins. Adapted from* (Peifer 2002).

Wnt is also involved in the differentiation process as it drives the maturation of Paneth cells and promotes the differentiation of secretory lineages. Pinto et al (Pinto et al. 2003) observed that the inhibition of the Wnt pathway in mice mutant secreting Dickkopf 1 (Wnt inhibitor) correlates with the loss of crypts and the lack of secretory lineage although absorptive lineage did not seem affected. Wnt would thus have longer range of action than expected and can confer TA cells the potentiality to differentiate into secretory lineage.

Notch signaling is also involved in stem cells maintenance. Notch is a juxtacrine signaling. Therefore, Notch ligands and receptors are expressed at the membrane surface epithelial cells and physical contact between two adjacent cells is needed for this pathway to be activated. Notch expression is restricted to intestinal crypts (van der Flier and Clevers 2009). Inhibition of Notch signaling leads to a conversion of all cells to the secretory lineage, even in the crypt where proliferation is stopped. The overexpression of Wnt in those crypts is not sufficient to overcome this stemness loss, indicating that both Wnt and Notch signaling are required for stem cell maintenance (Crosnier, Stamataki, and Lewis

2006). When Notch is overexpressed, the number of secretory cells is reduced and most of the cells differentiated into enterocytes. Therefore Notch signaling is considered to balance between the differentiation into secretory versus absorptive lineage (Crosnier, Stamataki, and Lewis 2006; van der Flier and Clevers 2009).

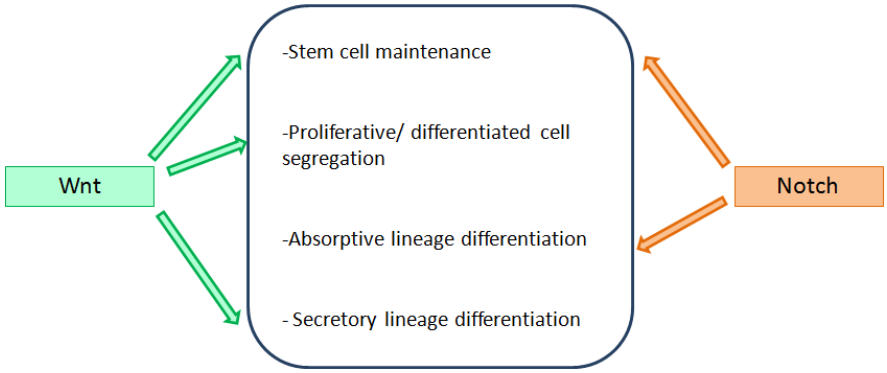

Figure 13: *Summary outline of the different functions induced by Wnt or Notch signaling.*

Wnt and Notch pathways both play key roles in the maintenance of the stem cells in the crypt (Figure 13). In this regards their respective concentration in crypts has to be optimal to ensure the homeostasis of the intestinal tissue. Homeostasis of the intestinal tissue is ensured by a constant division of stem cells in the crypt and apoptosis of differentiated cells at the villus tip but, in the meantime, it implies that epithelial cell directionally migrate from crypt to villus.

Stem cell division as a possible driving force of the directional migration in the epithelium

As evidenced by the studies that follow the evolution of labeled stem cell progeny (Sangiorgi and Capecchi 2008; Snippert et al. 2010), epithelial cells in the intestine migrate upwards from the basal part of the crypt to the tip of the villi in approximately 5 days. Stem cells are hypothesized to drive cell migration as they exert a mitotic pressure by dividing at the bottom of the crypt (Meineke, Potten, and Loeffler 2001). The directionality of this pressure driven passive movement is set by dividing cells at the bottom of the crypt and the gap left by apoptotic cells at the top of the villus. However, Frey et al (Frey, Golovin, and Polk 2004) noted that the ability for cell to migrate depends on their gene expression. In their experiment, they noticed that EGF (Epidermal Growth Factor) simulated migration in epithelial cell expressing active P38 protein (member of MAPK signaling family) whereas it induced the proliferation of cells with inactive P38. This finding suggests that migration can be induced by external factors but only in the cells expressing the right proteome. Other studies suggest that cell migration is more an active than passive driven phenomenon. Kaur et Potten (Kaur and Potten 1986a) actually observed that epithelial cells were still migrating even though cell division erased by either irradiation or drugs administration. Migrating cells normally express motility proteins and exhibit a motile phenotype. Even though the presence of lamellipodia on the basal part of epithelial cells has still not been observed *in vivo*, Kaur et Potten noticed that the inhibition of protein synthesis

in vivo induce an inhibition of cell migration in the crypt but not in the villi. Therefore they deduced that cell migration in the crypt was achieved through motility protein synthesis. On the contrary, cell migration in the villi was disrupted when noradrenaline, a drug that blocks smooth muscle contraction, was administered to the mice. They thus assumed that smooth muscle contraction stimulates cell migration in the villi. The distinct mechanisms driving cell migration in the crypt or in the villi might explain the fact that migration velocities measured in the villi and in the crypt are not correlated in time driving (Kaur and Potten 1986b). Subepithelial fibroblasts underneath the BM might also be involved in epithelial cell migration.

I.2.2) Subepithelial fibroblasts and epithelium homeostasis

Subepithelial fibroblasts are essential to the balance of the intestine under various aspects. Indeed, they secrete constituent of the ECM and of the basement membrane, act as mechanical support of the villi structure, induce both maintenance epithelial stemness and differentiation through paracrine signaling, and are possibly induce epithelial cell migration.

Subepithelial fibroblasts are present just below the basement membrane in the lamina propria (Figure 14 a). At the lower part of the crypt, they exhibit a spindle shape and are organized in two to three overlapping layers surrounding the bottom of the crypt. In this portion of the crypt, the fibroblasts are so densely packed that they are the only mesenchymal cells in contact with the BM (Marsh and Trier 1974a; Parker, Barnes, and Kaye 1974). Their sheet-like processes, beneath the BM, cover an area of approximately height adjacent epithelial cells. In the upper part of the crypt and proximal portions of the villi, the density of fibroblast decreases as they are organized in a single discontinuous layer. This discontinuous network allows other mesenchymal cell types (plasma cells, endothelial cells, leukocytes or macrophages) to be in direct contact with the BM (Marsh and Trier 1974a). From the basal part to the top of the villi, network of fibroblasts gets even sparser. The fibroblasts are more stellate and they interact with the BM through finger-like processes (Marsh and Trier 1974a). In the villi, fibroblasts processes together with collagen fibrils form a reticular sheet with numerous pores ranging from 3 to 7µm called foramina (Furuya and Furuya 2007).

a) 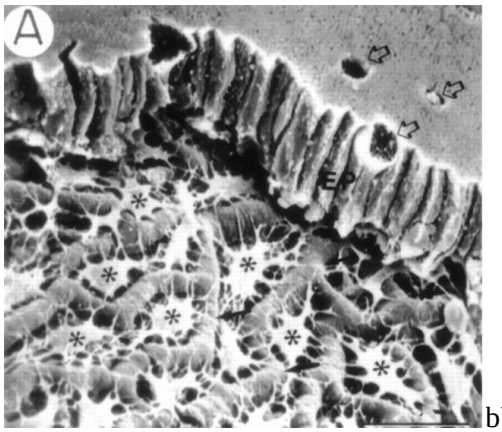

b) 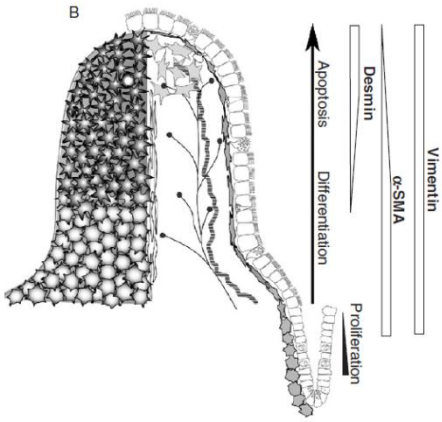

Figure 14: *Cellular network of intestinal subepithelial fibroblasts. (a) Scanning electron micrograph of subepithelial fibroblasts (*) connected as a syncitium underneath columnar epithelial cells (EP) in rat villi. Arrows indicate apical surface goblet. Scale bar 20µm. Imported from* (Desaki, Fujiwara, and Komuro 1984).*(b) Schematic representation of subepithelial fibroblasts along the crypt villus axis. Spindle shaped fibroblasts proliferate in the crypt and then differentiate as they migrate along the crypt-villus axis. While they migrate they switch from spindle shape to stellate shape, their level of expression of αSMA decreases but level of desmin increases. Imported from* (Furuya and Furuya 2007)

The first layer of pericryptal fibroblasts were identified as myofibroblasts due to their contractile apparatus made of α smooth muscle actin (αSMA) and non-muscle myosin (Mifflin et al. 2011). They are attached to the ECM through specialized fibronexus adhesion complex connecting actin bundles to extracellular fibronectin in a plaque-like structure. Fibronexus are particularly efficient to mechano transduce the external ECM tension to the stress fibers but also to transmit cell contraction to the external matrix (Hinz 2006; Mifflin et al. 2011; Tomasek et al. 2002). Spindle shaped myofibroblast contains high level of αSMA and low level of desmin. On the contrary, stellate fibroblasts in the villi exhibit a high level of desmin but low αSMA (Furuya and Furuya 2007) (Figure 14 b). As desmin happens to be a marker of fibroblast differentiation and also because the organelles, Golgi and granular apparatus were absent or immature in pericryptal fibroblasts, fibroblasts in the villi were considered as more mature than pericryptal fibroblasts (Furuya and Furuya 2007; Parker, Barnes, and Kaye 1974).

Marsh et al (Marsh and Trier 1974b) observed that subepithelial fibroblasts were able to divide in the low crypt region and to migrate upwards to the distal villi part. Tritiated thymidine injection in mice revealed that subepithelial fibroblasts were dividing slower than epithelial stem cells. However, fibroblasts seemed to precede epithelial cells during upward migration. Taken together these observations suggest that subepithelial fibroblasts differentiate while they migrate along the crypt villus axis but also that their migration could initiate epithelial cell migration. It is however important to notice that other studies failed to prove the existence of this co-migration (Neal and Potten 1981).

All epithelial fibroblasts (myofibroblasts and fibroblasts) are connected through gap junction (Furuya and Furuya 2007; Mifflin et al. 2011). Gap junctions are made of connexins assembled in a tubular transmembrane structure that ensures direct communication between two adjacent cell cytoplasma. Information is thus rapidly transmitted to the whole network of fibroblasts. It is particularly efficient in case of injury: the damaged epithelium secretes ATP which is transduced in subepithelial fibroblasts and results in fibroblast contraction due to a sudden increase of calcium level. Calcium wave propagates to other fibroblasts via gap junction provoking the contraction of the whole fibroblast network (Furuya and Furuya 2007). Fibroblasts contraction reduces the size of the sieving of the collagen/ fibroblast network and therefore temporary modifies the mechanical properties of the villi and also its absorptive properties. Other substances like substance P neurotransmitter secreted by neurons from lamina propria or endothelin from endothelial cells also trigger the increase of Ca^{2+} intracellular level in subepithelial fibroblasts (Furuya and Furuya 2013). In consequence subepithelial fibroblast network is necessary to integrate external signals and to provide the villi the adequate mechanical properties in response to these stimuli (Furuya and Furuya 2007).

Subepithelial fibroblasts are also involved in the maintenance of differentiated/ proliferative cells segregation through Bmp signaling pathway. They secrete Bmp4 ligand that binds type I and type II serine/ threonine kinase receptors in the epithelium. Bmp4 expression is restricted to villi portions and the inhibition of Bmp4 signaling leads to the formation of crypt along the length of the villi. Therefore BMP4 heterotypic signaling is involved in cell segregation.

In conclusion, subepithelial fibroblasts form together with collagen fibers a network that acts as a structural support of the intestinal morphology. They are contractile cells and their global tension depends on both mechanical and chemical modification of the environment. They are thus able to modify temporarily and locally the mechanical properties of the villi and to adjust nutrients absorption in response to external stimuli. In addition, subepithelial fibroblasts might induce epithelial cell migration as they co-migrate with epithelial cells. They are also involved in the maintenance of proliferative and the spatial segregation between differentiated cells and proliferative cells through paracrine signaling. Finally, they also have an indirect action on intestine homeostasis due to the ECM components they secrete.

I. 2. 3) The role of the epithelial environment on intestinal homeostasis

In the previous sections we have described the importance of dynamic cell-cell interactions, both homotypic and heterotypic, in the maintenance of stem cells, cell differentiation and migration homeostasis. However epithelial cells also interact with ECM and, although it seems inert, its chemical composition and mechanical properties play a major role in intestinal homeostasis.

Basement membrane

In the histological description of the intestine, we have reported that the epithelium relies on the basement membrane at its basal pole. In addition to the two major component (type IV collagen and laminine) introduced previously, entactin/ nidogen, heparin sulfate proteoglycan, fibronectin, tenascin and type III collagen also constitute the basement membrane (Louvard, Kedinger, and Hauri 1992; Trier et al. 1990). Simon-Assman et al (P Simon-Assmann et al. 1988) proved that basement membrane constituents originate from both mesenchymal and epithelial cells by hybridizing a mouse epithelium with a chicken endoderme. The hybrid was left to grow in nude mice and the immunolabelling revealed that the matrix formed at the frontier between the two cell types was of both origins. This global observation can be refined depending on basement membrane constituents as it was established that collagen IV had a mesenchymal origin whereas heparin sulfate was exclusively synthesized by epithelial cells (Patricia Simon-Assmann et al. 1990). The case of laminin is more complex since the chains constitutive of laminin molecule are of various origins: laminin α1 chain is expressed by the epithelium and α2 by the mesenchyme (Teller et al. 2007).

At the adult stage the constitution of the basement membrane is stable in time compared to the massive changes experienced during the embryonic development (§ embryonic morphogenesis/ ECM composition). Although its global composition is stable the constituents of the BM are constantly renewed. Its renewing was first supposed to precede the migrating epithelial cells BM so that it acts as a treadmill that conveys epithelial cells from the bottom of the crypt to the top of the villi. The study of Trier et al (Trier et al. 1990) disproved this hypothesis: they injected an antibody against laminin in mice and observed that laminin turnover happens in period of weeks whereas epithelial cells are renewed in few days. They also noticed that laminin renewing was not homogeneous in the BM but occured more in a mosaic of new laminin patches among old ones.

The renewing of the basement membrane has to be perfectly orchestrated between epithelial and mesenchymal cells since the composition of the basement membrane is not homogeneous along the crypt villus axis. Indeed as shown in Figure 15 the distribution of basement membrane constituent is topographically defined. As an example laminin α2 is located in the crypt while laminin α3 and α5 are expressed in the villi (Teller et al. 2007). This specific distribution can be correlated to the spatial expression of adhesion receptors in epithelial cells (Figure 15). For instance, integrin subunit (β4A) is present in intestinal epithelium under two distinct forms: one functional and one immature that are spatially distributed so that the pattern of functional subunit coincides with the repartition of its ligand, laminin α5, which is restricted to the villi (Basora et al. 1999). This spatial heterogeneity in the composition of basement membrane is transduced in the cell cytoplasm through transmembrane receptor. The basement membrane composition is thus supposed to play a significant role in the maintenance of stem cell, the induction of migration or differentiation, but it seems difficult to be

experimentally proven. Benoit et al (Benoit et al. 2012) succeeded in showing that the loss of RGD interaction (composed of extracellular fibronectin, transmembrane integrin and intracellular vinculin) increased cell migration out of the crypt and affects cell survival signaling in the crypt. RGD signaling would thus be needed to preserve the integrity of the crypt. The differential composition of basement membrane might also drive the apoptosis at the top of the villi. Indeed, fibronectin provides great cell adhesion and is expressed as a decreasing gradient from the bottom of the crypt to the top of the villi while tenascin, to which cells adhere less, exhibits the opposite pattern (Beaulieu 1992; P. Simon-Assmann et al. 1995). These complementary distributions might induce the cell shedding process resulting in the complete loss of cell-matrix adhesion at the villi top. Matrix detachment induces a rapid loss of cell-cell adhesion mediated by E-cadherin and is responsible for anoikis (Beaulieu 1992).

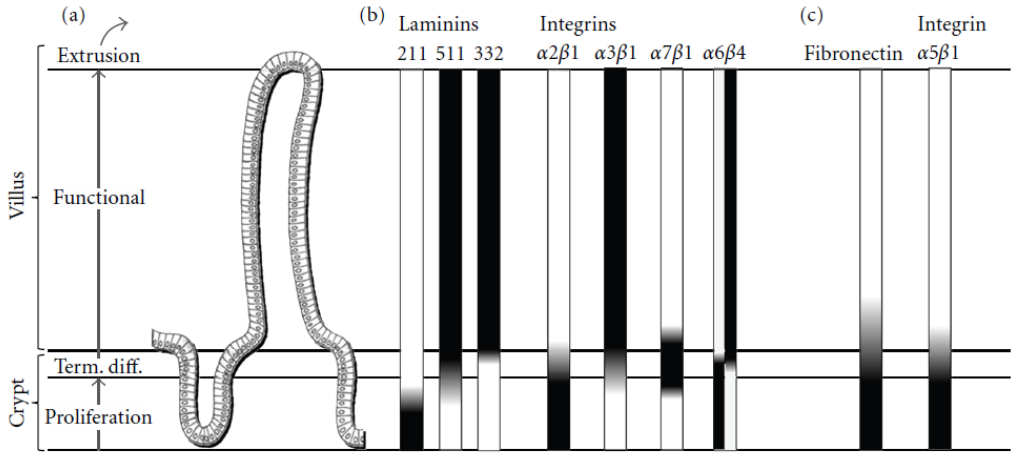

Figure 15: *Schematic representation of the heterogeneities of distribution of adhesion molecules in the BM and cell adhesion receptors along the crypt-villus axis. Imported from*(Benoit et al. 2012)

To conclude, basement membrane is secreted by subepithelial fibroblasts together with epithelial cells and presents a complex spatial composition. This spatial heterogeneity in its chemical composition might play a key role in tissue homeostasis. However, regarding intestine mechanical properties, it has been demonstrated that the contribution of basement membrane to the mechanical properties of the intestine is negligible(V. I. Egorov et al. 2002).

Mechanical properties of intestine wall

The mechanical strength of the intestine is of major importance; since it ensures the maintenance of the topography (villus & crypt) of the epithelium. Egorov et al (V. I. Egorov et al. 2002) estimated the tensile strength of each layers starting from cadaveric gut that had their intestinal wall sectioned. They sutured back the layers (lamina propria, submucosa and muscular layers) independently of each other to evaluate the strength of each layer and compared to the sutured entire wall. They concluded that the submucosa contributes for up to 70 to 75% to the mechanical strength of the intestine structure while

muscular layer contributes only for 15-20%. The input of lamina propria is quite negligible and counts for 5-10% (V. I. Egorov et al. 2002). The mechanical properties of the submucosa are related to the collagen lattice. In the lattice, collagen fibers are arranged into two arrays of collagen fibers interweaved to form a unified sheet (Figure 16). This organization confers more strength than aligned collagen fibers. It also provides some elasticity, as it can undergo peristaltic motion, even though it is composed of non-elastic collagen fibers (Terumasa Komuro 1988).

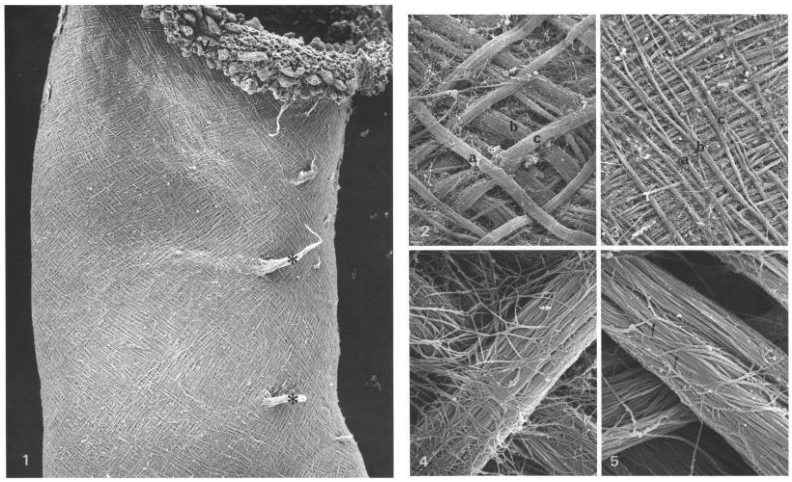

Figure 16: *Arrangement of collagen fibers in the lattice of the submucosa. Scanning electron microscopy micrographs of: a) Global structure of the lattice with the traces of blood vessels (*) (*× 80) *and b) 300 fold magnification of the two interweaved arrays of collagen fibers. Imported from* (Terumasa Komuro 1988)

Collagen organization varies as a function of the intestine localization. In the lamina propria, collagen fibers together with fibroblasts form a loosely arranged network in the villi with a moderate amount of collagen. On the opposite, in the crypt region, pericryptal fibroblasts are arranged into two to three layers, collagen fibers are thicker, more numerous and arranged circumferentially around the crypt (Parker, Barnes, and Kaye 1974). The mechanical tension generated by the contracted myofibroblasts at the crypt base permits the expulsion of cryptal luminal content in the intestinal lumen. In the villi fibroblasts together with the smooth muscle cells oriented longitudinally can contract and retract the villi. Meanwhile the interstitial pressure generated by the blood flow in the capillaries of the villi tends to extend the villi. These two opposite forces generate a dynamic inward tension that avoids the collapsing of the villi. In addition the extension of the villi related to blood pressure might facilitate the upward migration of epithelial cells (Hosoyamada and Sakai 2005).

In the intestinal wall, the mechanical properties of the different layers are combined to ensure the peristaltic motion, to hold and maintain the 3D structure of the epithelium. However the exact influence of the topography of the lamina propria on the epithelium dynamic has never be demonstrated experimentally.

In this first part of the introduction, the dynamic driving the epithelium renewal has been described. We have pointed out the main actors of the intestinal wall that are likely to play a role in stem cell maintenance, cell migration, differentiation and apoptosis. Although other distant entities in the body can provide long range signaling like hormonal signaling (glucocorticoid/ insulin-like growth factor) that can also induce epithelial or mesenchymal cell proliferation and differentiation (Frey, Golovin, and Polk 2004; Louvard, Kedinger, and Hauri 1992). The microbiota may also provide the cell information regarding spatial positioning as the bacteria distribution is heterogeneous along the crypt villus axis (Li et al. 2007).

The main challenge of my PhD is to reproduce *in vitro* the main parameters responsible for intestinal homeostasis in order to induce the growing and differentiation of intestinal tissue starting from isolated intestinal stem cell. Although, with regards with existing technologies, it appears still very challenging to implement *in vitro* all the criteria previously exposed with their level of complexity. Hopefully, in many cases, recapitulating the level of refinement of the *in vivo* environment is not necessary to induce cell growth into a functional tissue. The second part of this chapter describes the tools and approaches developed in the tissue engineering field to promote tissue morphogenesis with a special focus on the recent trends towards the development of multicellular systems with definite architectures, called organ-on-chip. Most of the following paragraphs are extracted from the review we published last year entitled 'Combining microfabrication and hydrogels biochemical engineering towards micro-organs on chip'(Verhulsel et al. 2014).

II Introduction to 3D scaffolds for tissue engineering

At first, the cell substrate is of particular importance, since *in vivo* the extracellular space is occupied by the ECM. The chemical composition of the ECM and the resulting mechanical properties are both important aspects, as the transduction of both chemical and physical signals via cellular adhesion molecules affects cell shape, polarization, migration and differentiation (Burute and Thery 2012; Kaivosoja et al. 2012; Peyton et al. 2007). Furthermore, the ECM topography orients tissue polarity and the morphogenesis of new organs (Burute and Thery 2012; Vogel and Sheetz 2006).

Crude *in vitro* substrates that lack these features are therefore often insufficient for guiding the assembly and coordination of isolated cells to form a coherent tissue with a common global orientation and polarity. New devices that mimic the microscale structures of the ECM are needed and are now being developed thanks to the fast evolving fields of microfabrication and microfluidics. Microfabrication allows researchers to structure space at the right order of scale (from micrometers to centimeters) and to position individual cells according to the architectures they experienced *in vivo*. Microfluidics also provides new tools for controlling the transport and availability of chemical and biochemical signals on such micron scales. The cells can be seeded in an enclosed area with volume restrictions and transport properties favoring autocrine and paracrine communication, allowing users

to build more realistic and/or more specific culture conditions than can be achieved in traditional cell culture. The resulting autonomous and functional tissues shaped with a morphology that attempts to recapitulate conditions seen *in vivo* organs has led to the concept of 'organs on chip'.

The first subpart describes the main chemical and mechanical features needed to create an artificial extracellular matrix that recapitulates in vivo ECM as closely as possible, in order to induce cell differentiation. The second section presents the techniques to structure artificial matrix and already existing devices.

II.1 Artificial extracellular matrix

The *in vivo* ECM consists mainly of collagen fibers, elastin fibers, glycoproteins and polysaccharides. It acts as a mechanical support to the cells it surrounds and plays an important role in cell shape, cell polarity, cell migration, resistance to external forces, and signal transduction. The primary focus of tissue engineering is to achieve an *in vivo*-like cellular environment, by developing *in vitro* artificial ECM. In regenerative medicine applications, such scaffolds could either be directly introduced into an injured organ in order to induce in vivo genesis, or first seeded with cells in vitro and then transplanted once those cells have differentiated. For *in vitro* research and testing applications, they are generally directly used as a substrate. In all cases, the artificial structures need to recapitulate the in vivo environment signals responsible for cell differentiation into the desired tissue. In the following sections, we discuss the different ways of generating and controlling artificial ECM properties. We also underline how the possibility of uncoupling biochemical and physical parameters has opened the route for a deeper understanding of the influence of cell microenvironment on cell fate.

II.1.1) Chemical composition

Biomaterial scaffolds are essentially made of hydrogels. Based on their ability to retain water by swelling, they mimic the high water content of the extracellular matrix (Jason a. Burdick and Murphy 2012). Hydrogels can be classified into two distinct categories: the natural and the synthetic hydrogels (Jason a. Burdick and Murphy 2012; Cushing and Anseth 2007; Schindler, Nur-E-Kamal, and Ahmed 2006). Natural hydrogels include collagen (Cross et al. 2010; Helary et al. 2005; K. E. Sung et al. 2009), fibrin (Thomson et al. 2013), hyaluronic acid (Bian et al. 2013a), Matrigel (Sodunke et al. 2007), and derivatives of natural materials such as chitosan (Vllasaliu et al. 2012), alginate (Yamada et al. 2012) and silk fibers (Q. Zhang et al. 2012). They remain the most physiological hydrogels as they are components of the ECM *in vivo*. Two main drawbacks of natural hydrogels, however, make their final microstructures and properties difficult to control reproducibly between experiments. First, the fine details of their mechanical properties and their dependence on polymerization or gelation conditions are often poorly understood (Tibbitt and Anseth 2009). Second, due to their natural origin

(bovine fibrinogen (Thomson et al. 2013), rat tail collagen I (Geraldo et al. 2012)…) their composition may vary from one batch to another.

In contrast, synthetic hydrogels such as poly(ethylene glycol) diacrylate (PEGDA) (Guarnieri et al. 2010; Liu et al. 2012), poly(acryl amide) (Engler et al. 2006; Pathak and Kumar 2012), poly(vinyl alcohol) are more reproducible, although their final structure can also depend on polymerization conditions in a subtle way, so that a rigorous control of the preparation protocol, including temperature and environment control, may be necessary. Generally speaking, however, synthetic hydrogels offer more flexibility for tuning chemical composition and mechanical properties; users can, for example vary the concentration or molecular weight of the precursor, or alter the percentage of crosslinkers. They can also be selected or tuned to be hydrolysable or biodegradable over variable periods of time.

Cell adhesion ligands must be present in hydrogels to allow cells to adhere, spread, migrate and proliferate. There is a large variety of adhesion molecules, such as laminin (Christopherson, Song, and Mao 2009) and its derivatives (Sur et al. 2012), fibronectin (Douezan, Dumond, and Brochard-Wyart 2012), RGD peptide sequence carried by fibronectin (Cushing and Anseth 2007) and collagen (Al-Haque et al. 2012; L.-Y. Jiang and Luo 2013). It is therefore crucial to select the adhesion molecules for which the seeded cell type has the largest affinity to make adhesion effective. Natural hydrogels are bioactive and usually provide native adhesion sites. Conversely, synthetic hydrogels are inert, since their carbon skeleton presents no adhesion molecules or endogenous factors inducing proliferation and cell differentiation.

To enrich their potential as "bioactive" materials, synthetic hydrogels are generally supplemented with adhesion molecules (JA Burdick, Khademhosseini, and Langer 2004), either by covalent grafting (Tse and Engler 2010), adsorption (Tan et al. 2005) or electrostatic interaction (Kreke et al. 2005). Adhesion molecules can be grafted after hydrogel polymerization, or added to the pre-polymerized mixture and either physically trapped or chemically incorporated during polymerization. Finally, in the case of photoactivable materials such as PEGDA, adhesion molecules can be chemically modified to covalently attach to the hydrogel backbone. The grafting of PEG polymer has been thoroughly described in the review of Zhu et al (Zhu 2010).

The inertness of synthetic hydrogels may appear to be a disadvantage, since additional manipulation is needed to promote cell adhesion. However it allows a more flexible tuning of the different factors at play in cell fate. It can, for example, allow researchers to decouple mechanical and biochemical factors to assess independently the effect each factor has on cell behavior. This kind of uncoupling is hard to achieve in natural hydrogels. Increasing the mechanical load on cells by stiffening the hydrogel matrix is normally achieved by increasing the concentration of the gel. For a natural hydrogel, increasing the concentration of its components automatically increases the concentration of its endogenous adhesion molecules. In contrast, the concentration of adhesion molecules can be set independently of the

concentration of a synthetic hydrogel. Moreover, the chemistry of synthetic hydrogels enables a fine tuning of adhesion molecule density and distribution. This can be very useful, considering that, in vivo, the nature of ECM ligands, their density and spatial distribution are responsible for different cell functions.

The local concentration of adhesion molecules is critical, since a minimal concentration of adhesion molecules is required to induce cell adhesion on a substrate (JA Burdick, Khademhosseini, and Langer 2004). Sur et al have shown that adhesion molecule density also influences cell spreading and cell growth (Sur et al. 2012). They seeded Purkinje cells on a substrate composed of self-assembled peptides amphiphiles (PA) nanofibers and collagen I fibers. As the PA nanofibers comprise laminin epitopes, modifying the PA concentration changes the adhesion molecule concentration. On substrates with a low laminin epitope concentration, the dendrites only grew in 2D at the scaffold surface. For substrates having the same rigidity but a higher concentration of adhesion molecules, however, the dendrites also penetrated the scaffold. Moreover, a high concentration of laminin epitopes also increased the number of dendritic spines produced by the cells, resulting in a biomimetic network.

The distribution of ligands also affects cell morphology and migration by changing the orientation of the cytoskeleton. Fibroblasts growing on PEGDA hydrogels containing a gradient of RGD adhesion peptide elongate themselves towards the direction of increasing peptide density, while no specific orientation is observed on isotropic substrates (Guarnieri et al. 2010). Fluorescent labeling reveals that this morphology is correlated with an orientation of actin filaments parallel to the gradient (Figure 17). Fibroblasts also migrate in the direction of increasing RGD density and their velocity is directly correlated with the RGD gradient amplitude.

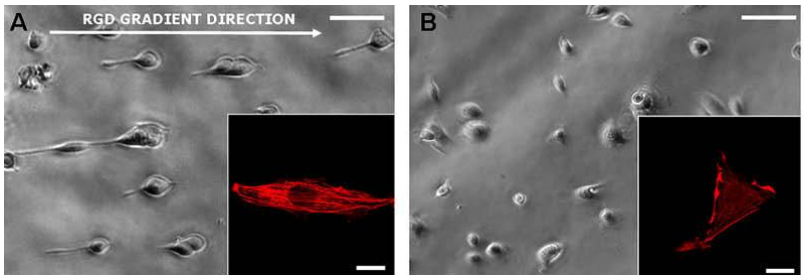

Figure 17: *Phase contrast microscope images of NIH3T3 fibroblast cells, seeded (A) on PEGDA hydrogel in the presence of a RGD gradient (slope = 1 mM.cm^{-1}; average RGD concentration = 1.5 mM) ; (B) on a control PEDGA hydrogel with a uniform distribution of RGD; after 4 h from cell seeding. Bar: 100 µm. CLSM images of phalloidin staining of cells after 24 h of culture. Bar: 20 µm.* (Guarnieri et al. 2010)

Finally, the global chemical composition of the scaffold is critical in tissue transplantation. It determines the inflammatory response of the host tissue to the implanted tissue. Furthermore, there is a correlation between the inflammatory response and the induction of vascularization of the implant. A severe inflammation prevents the formation of microvessels in the implants. Surprisingly, in the case

of an excellent biocompatibility of the implant, the low inflammatory response does not stimulate angiogenesis either. It seems that scaffolds inducing a slight inflammation are the best candidates for ensuring the appropriate vascularization of the implant (Laschke and Menger 2012).

II.1.2) Hydrogel physical properties

When used as a support for cell culture, hydrogels are most commonly synthesized as cylinders (Engler et al. 2006; Tse and Engler 2010) of variable thicknesses, and are either immersed in the medium or placed on a porous membrane above culture medium. Depending on the natural in vivo microenvironment of the cells to be cultivated, they can either be seeded on the surface of the hydrogel (e.g. epithelial and endothelial cells) or directly inside the hydrogel (e.g. mesenchymal cells).

Hydrogel porosity

The porosity of the hydrogels must therefore be sufficient to ensure a homogeneous supply of oxygen and nutrients throughout the hydrogel without damaging the gel structure and its mechanical properties. Various techniques have been investigated to precisely control the pore size (presented in more detail in Annabi's et al (Annabi et al. 2010) review).

- Solvent casting or particle leaching techniques rely on the use of porogens (salt, sucrose, sacrificial beads) suspended in a hydrogel solution (PEG, fibrin) and entrapped in the network formed by the hydrogel during polymerization. Their selective dissolution or diffusion by immersing the hydrogel in a solvent forms a porous hydrogel. The pore size of the hydrogel (40 to 400µm) is controlled by the size and concentration of the porogens (G. Y. Huang et al. 2011).

- Freeze drying is widely used in tissue engineering. It relies on fast freezing at very low temperatures causing thermodynamic instabilities and inducing local phase separation between the solvent and the polymer (collagen-chitosan, agarose ...). The solvent is then evaporated by vacuum sublimation during a lyophilization step. This method can be applied both to natural and synthetic hydrogels, but the control of pore size (10 to 120 µm (G. Y. Huang et al. 2011)) remains difficult, since it strongly depends on temperature kinetics. Furthermore, the structures formed are often unstable and can collapse.

- Gas foaming can also be used to generate hydrogels with pore sizes ranging from 100 to 600 µm (G. Y. Huang et al. 2011). Gas bubbles are formed in the hydrogel solution and the release of the gas during polymerization forms a network of interconnected pores. The gas-foaming agent commonly used is sodium bicarbonate, which generates carbon dioxide. This inexpensive technique does not involve organic solvent or reagents that could potentially impede cell or tissue viability.

A common limitation, of the above methods is that they generally yield an isotropic porous texture that is very different from the usual fibrillar microstructure of the ECM *in vivo*. This difference may have an influence on cell behavior, but this question has not been extensively addressed due to the lack of suitable experimental models. Another parameter closely related to the porosity of the hydrogel is the global stiffness of the scaffold. We have already mentioned that it can have a strong impact on cell differentiation. Also, in the case of transplantation, the global stiffness of the implant must not differ too much from that of the receiving organ, to ensure efficient transplantation.

Fibrillar structure

In vivo, native ECM is mainly composed of collagen, which has a fibrillar structure. Replicating and integrating such fibrillar structures *in vitro* is necessary to study their intrinsic influence on cell morphology, polarity and differentiation. Hydrogels allow users to generate fibrils with a wide range of diameters. Several techniques have been proposed for that purpose:

- Self-organization of peptides composed of an alternation of hydrophilic and hydrophobic groups. In water, these peptides organize into β-sheet structures. In a suitable electrolyte, however, they form an entanglement of nanofibers of controlled size (~10 nm). These peptides may also contain cellular adhesion peptide sequences (Schindler, Nur-E-Kamal, and Ahmed 2006). For more information about the use of self-assembling peptides in regenerative medicine, please refer to the review by Matson et al (Matson and Stupp 2012).

- Electrospinning can be used to form fibers by applying a current to a charged polymer at a capillary outlet. This technique allows users to tune of diameter of fibers from nano to micrometer scales, and to control their orientation and spacing. The fibers can be made of natural (collagen, elastin) or synthetic (polyacrylamide (Annabi et al. 2010; Schindler, Nur-E-Kamal, and Ahmed 2006)) hydrogels.

- Microfluidic co-flow of a polymer and a gelation solutions: the velocity of the two flows sets the diameter of the fibers (20 to 230μm) (Hwang et al. 2008).

- The spontaneous organization of polymerized collagen fibrils into fibers (0.5 to 1μm) can be achieved by raising the pH of the collagen solution to 7.4. Slowing polymerization leads to the formation of larger fibers (Geraldo et al. 2012; Raub et al. 2007), but fiber monodispersity remains difficult to control. Furthermore, it is difficult to orient the resulting fibers unless the researcher employs electrospinning or orientation in a microfluidic channel.

In general, an increase in fiber size decreases cell spreading, migration and proliferation (Christopherson, Song, and Mao 2009). It also modifies the morphology of cells and may induce different phenotypes. Indeed, if the fiber diameter is small as compared with cell dimensions, a single

cell adheres to several fibers and feels multi-directional traction forces, resulting in rounded cell shape. Conversely, on thick fibers, a cell adheres to one single fiber and the traction force is thus unidirectional. Cells exhibit an elongated morphology along the fiber axis thanks to the nucleus and cytoskeleton becoming reorganized parallel to the axis of fibers (Liao et al. 2008; H. B. Wang et al. 2010; Q. Zhang et al. 2012). For neural progenitor cells seeded on electrospun polyethersulfone fibers, distinct cell phenotypes are induced, depending on the fiber diameter. On thin, 200 nm diameter fibers these neural cells preferentially differentiate into glial cells presenting a round shape. On large fibers (700nm), they differentiate into neurons with elongated shapes (Christopherson, Song, and Mao 2009) (Figure 18).

a) 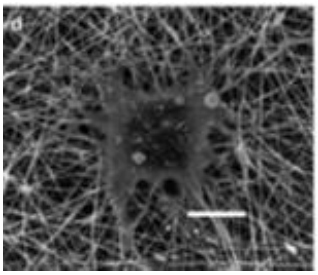 b) 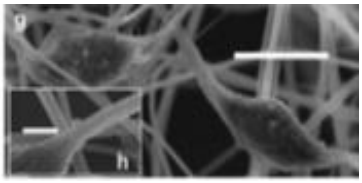

Figure 18: *SEM images of neural progenitor rat cells cultured on polyethersulfone fibers with various diameters various substrates for 5 days: a) Cells on 283-nm fiber mesh b) (g–h) Cells on 749-nm fibers. Imported from* (Christopherson, Song, and Mao 2009)

Hydrogel stiffness

Although fibrillar structures and the fibers diameter range are relatively similar throughout the human body, ECM stiffness is specific to each tissue. The mechanical "signature" of each tissue arises from tissue-specific differences in the amount of ECM present and its composition. For instance, connective tissues are characterized by a higher volume of ECM than other tissues. Lungs, blood vessels and skin are subjected to high levels of elastic deformation and contain a high ratio of elastic fibers. In contrast, cartilage, which is often compressed, is mainly composed of polysaccharides. Furthermore, the matrix surrounding neural cells is much softer (1 kPa) than the one surrounding muscle cells (10 kPa) (DuFort, Paszek, and Weaver 2011; Engler et al. 2006; Kaivosoja et al. 2012; Peyton et al. 2007). This stiffness difference is essential as it induces the migration of cells toward the region with the stiffness that promotes the best adherence. This phenomenon is called durotaxis or mechanotaxis (DuFort, Paszek, and Weaver 2011; Peyton et al. 2007; J. Y. Wong et al. 2003).

The type of substrate used to mimic the ECM *in vitro* dictates the range of rigidities that are accessible. These include: ~ 70 GPa for glass, ~ 0.2 to 1 MPa for PDMS (Al-Haque et al. 2012), ~ 0.5 to 40 kPa for PAA (Al-Haque et al. 2012; Pathak and Kumar 2012; Tse and Engler 2010), ~ 30Pa to 1.8kPa for collagen (Cross et al. 2010). For natural hydrogels such as collagen, increasing the collagen concentration increases the entanglement density, leading to more rigid hydrogels (Cushing and

Anseth 2007). Similarly, for synthetic hydrogels, increasing the concentration of cross-linkers results in stiffer matrices (Al-Haque et al. 2012; Bian et al. 2013b; Tse and Engler 2010).Using hydrogels to mimic ECM can thus be used to control the substrate stiffness and investigate its influence on cell fate.

Most cell types have the ability to sense and respond to the stiffness of the substrate through mechanotransduction pathways. A higher rigidity induces an increase in the number of focal adhesions, resulting in a global rise in cortical tension and tensile forces. Conversely, a matrix that is too soft does not support the tensile forces needed to ensure cell spreading and adhesion (Al-Haque et al. 2012; Pathak and Kumar 2012).

A theoretical description based on soft matter concepts provides an explanation of how matrix stiffness interferes with cell-matrix adhesion. In this model, tissues are considered as continuous media with an effective viscoelasticity and a surface tension that depends on cellular adhesion (Gonzalez-Rodriguez et al. 2012). The rheology of tissue spreading is modeled by a spread parameter S defined as $S = W_{sc} - W_{cc}$. W_{cc} represents the cell-cell adhesion energy per unit area, correlated with the density of molecules of intercellular junctions (cadherins). The term W_{sc} , which describes cell-matrix adhesion energy per unit area, takes into account both the molecular adhesion and matrix stiffness (Gonzalez-Rodriguez et al. 2012). The spread parameter S represents a balance between cell-matrix and cell-cell adhesion energy. If $S<0$, the energy of cell-cell adhesion is greater than the energy of cell-matrix adhesion. Cell aggregates do not spread and remain spherical. This situation is called partial wetting, by analogy with liquids. An increase in rigidity makes the cell-matrix adhesion more favorable and S becomes positive the aggregate spreads (complete wetting). For instance, murin sarcoma cell aggregates do not spread and remain in partial wetting on fibronectin-treated substrates with rigidities below 8kPa, whereas they do spread on substrates with rigidities above 12kPa (Douezan, Dumond, and Brochard-Wyart 2012). W_{sc} also depends on the densities of cell adhesion molecules and ligands of the substrate. By increasing the number of matrix adhesion molecules, the affinity of cells for the matrix increases, thus increasing cell-matrix adhesion energy and resulting in the spreading of the cell aggregate (figure 19).

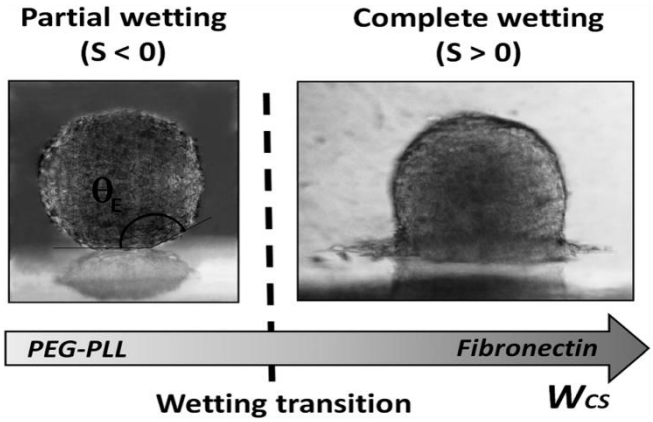

Figure 19: *Different wetting regimes observed for cellular aggregates spreading on a rigid surface. Depending on the molecules coating the surface, the aggregate can either remain spherical (partial wetting) if S < 0 (i.e. with a rich PEG-Poly L lysine (PLL)-coated surface) or spread with a precursor film of cells around the aggregate (complete wetting) if S > 0 (i.e. with a rich fibronectin-coated surface). Imported from* (Douezan, Dumond, and Brochard-Wyart 2012)

Matrix stiffness has a strong impact on cell differentiation, particularly on stem cell differentiation. Naïve mesenchymal stem cells seeded on substrates with different rigidities differentiate into neurons on soft substrate (0.1-1 kPa), into muscle cells on stiffer substrate (8-17kPa) and into osteoblasts on even stiffer substrate (25-40kPa) (Engler et al. 2006). Furthermore, studies performed on cell lines have shown that the differentiation is complete (i.e. specific function acquisition) only on substrates with tissue-like stiffness (Chatterjee et al. 2010; Engler et al. 2004). For instance, myocytes fused into myotubes regardless of substrate rigidity, but the striations required for muscle contractility only appeared for substrate stiffnesses of around 12kPa, consistent with in vivo muscle rigidity (Engler et al. 2004). Similarly, to activate the secretory function responsible for the mineralization of the extracellular matrix, osteoblasts needed to be cultured on substrates with a stiffness of 225kPa or higher (Chatterjee et al. 2010).

However, the ability of cells to sense substrate stiffness and respond to it also depends on how long those cells remain in contact with the specific substrate. Guvendiren et al have demonstrated this behavior using dynamic hydrogels (Guvendiren and Burdick 2012). Human mesenchymal stem cells were seeded on soft polymerized methacrylate hyaluronic acid that could be stiffened by UV exposure at different time points. The cells experiencing hydrogel of constant and low stiffness differentiated into adipocytes, whereas the cells grown on a substrate that was switched to a hard state after 1 to 3 days differentiated into osteocytes. When the substrate was stiffened on day 7, a mixture of adipocytes and osteocytes was observed. This heterogeneity was interpreted as being a consequence of heterogeneity in differentiation over time: a subset of the cell population had already differentiated and was unable to respond to changes in stiffness, while another part of the population remained undifferentiated and could still respond to these changes (Guvendiren and Burdick 2012). This

experiment exemplifies how dynamic hydrogels can be useful tools for studying the consequences of changes in the cell microenvironment on cell differentiation.

II.1.3) Importance of dynamic hydrogels

In vivo, extracellular matrices are dynamic structures constantly permeated by soluble molecules such as growth factors. Adhesion molecules are also constantly renewed, resulting in either modification or maintenance of their amount and distribution. Furthermore, the cell themselves are also able, in many instances, to modify and remodel their surrounding ECM structure and topography. This means that artificial ECMs will need to incorporate dynamic features if they are to accurately mimic *in vivo* physiology.

Mimicking ECM dynamics, however, is not straightforward. Although growth factors can be trapped inside a hydrogel, for example, they are usually released all at once by hydrogel swelling (Andreopoulos and Persaud 2006; Sano et al. 1998; van de Wetering et al. 2005). Growth factors can also be directly added to the culture medium, but this often generates a non-homogeneous distribution of growth factors between external and internal parts of the hydrogel, due to the diffusion of molecules from the medium into the gel.

For improved control, the chemistry of some hydrogels, especially PEGDA hydrogels, can be tailored to reproduce ECM dynamics. For example, chemically modified growth factors (growth factor-PEG methacrylate) and matrix metalloproteinases cleavable groups (A-PEG-cleavable structure-PEG-A) can be covalently photo-grafted to PEGDA networks (Phelps et al. 2010; Zhu 2010). Growth factors anchored to the substrate in this way are released only after the cleavage of the hydrogel by invading cells. The resulting diffusion of the growth factors is very slow (about 2 weeks) and is compatible with *in vivo* levels of VEGF (Phelps et al. 2010). It is particularly efficient in regenerative medicine, for implants scaffold, as the VEGF release enhances vascularization (Phelps et al. 2010). A similar strategy can be applied to control the concentration of nitrogen monoxide (NO), which can be complexed with acrylate-modified proteins and released over a period of months in the hydrogel to reduce the risk of thromboses (Bohl and West 2000). This ability to combine adhesion molecules, growth factors and different types of molecules modified with PEG methacrylate makes PEGDA a powerful “tailorable” support for tissue engineering.

Finally, artificial structures made from hydrogels are often considered to be a compromise between scaffolds that guide the formation of new tissue and a structure capable of being reshaped by the cells seeded in it. First, it is important that the cells secrete their own matrix to enhance their development and differentiation. The intrinsic structure of the artificial gel can stimulate the synthesis of ECM (B. M. Baker et al. 2012; Chatterjee et al. 2010; Miller et al. 2012). Peptide sequences can also be added to hydrogels to stimulate the production of the ECM by the cells seeded within the gel (Lee et al.

2006; Salinas and Anseth 2009). Cells that have secreted their own ECM can generally form functional tissues while maintaining the structure initially imposed by the artificial scaffold (Khademhosseini et al. 2007; Yamada et al. 2012), if that structure is sufficiently similar to the normal physiological one.

In numerous applications, and notably for implants, it may be necessary to get rid of the artificial hydrogel template once this functional state is achieved, so that the resulting tissue is surrounded only by its specific matrix. In that case, the gel merely plays the role of a sacrificial temporary template. Although most hydrogels can be hydrolysed over long periods of time, cleavable sequences or polyester segments that can be rapidly hydrolyzed can be inserted into the polymers to facilitate hydrogel remodeling (Zhu 2010). The cells themselves can also secrete enzymes to degrade the synthetic matrix that guided the development of their original form.

Given that biodegradability is a key desirable attribute of implants, dynamic hydrogels present a promising development for tissue engineering. The scaffold within such gels initially facilitates the handling of the implant and permits the physical interaction of transplanted tissue with the living organ. Subsequent hydrolysis of the scaffold enables the long term integration of the implant as an intimate part of the endogenous organ.

In most cases, artificial matrix induces cell differentiation and growth as a tissue. However the generated tissues often fail to self-organize in the three-dimensional shape they exhibit *in vivo* (e.g: intestinal cells grown on collagen substrate do not spontaneously shape into villi and crypt (Katano et al. 2015)). Therefore the topography relative to the engineered tissue should be imposed by the scaffold itself.

II.2 Microstructured 3D environments

Most cells reside in a 3D environment, meaning that cells growing on 2D substrates could acquire non-natural behaviors and morphologies (Santos et al. 2012). In 2D cultures, cells are in contact with a substrate on their undersides and medium on their upper sides. Intercellular interactions are limited to the edges of the cells. This configuration contrasts significantly with numerous *in vivo* environments where cells are in close contact with the extracellular matrix and neighboring cells over their entire surfaces (Santos et al. 2012). ECM topography influences cell adhesion, integrin distribution, morphogenesis and differentiation (Schindler, Nur-E-Kamal, and Ahmed 2006). Furthermore, different cell populations in most organs lie in definite relative spatial 3D positions, and experience interactions with other cells. Therefore, for many applications it is important to understand and reproduce three-dimensional morphologies, in order to achieve more realistic and physiological environments.

Therefore, a key goal in tissue engineering is to combine the spatial positioning power of microfabrication technologies with physiological environments as provided, for example, by artificial extracellular matrices. In this way, it may be possible to shape an artificial multicellular tissue into a three dimensional physiological structure corresponding to its related organ. In some case, this is a prerequisite for cells to reach their final state of differentiation and therefore perform their functions within the engineered tissue.

II.2.1) Spatially constrained 3D cultures

Although whole organs are macrostructures, they are built from cellular-scale microstructures. For instance, the diameter of a blood capillary or a kidney tubule is approximately between 8 and 10 µm, an intestinal villus is about 500 µm tall and a muscle fiber has a diameter of 10 to 100 µm. Microfluidics allows the user to structure or constrain the microstructure of hydrogels at the micrometer length scale (Shin et al. 2012). This spatial confinement favors the sorts of cell-cell interaction and paracrine communication experienced by cells *in vivo*, while maintaining cell-matrix interactions on physiologic dimensions. The use of hydrogels as artificial matrices ensure the cells a physiological environment as previously described.

Different microfluidic techniques have been developed to structure hydrogels at the micrometer scale. We briefly review these techniques below (Figure 20). For more details readers may refer to the reviews of Nikkhah et al.(Nikkhah et al. 2012), Annabi et al. (Annabi et al. 2010) and Huang et al. (G. Y. Huang et al. 2011).

Technique	Description	Resolution	Restriction
Soft lithography	Hydrogel molding with a master prepared by microfabrication techniques (e.g. photolithography, micromachining…)	~100nm	- many steps - Several specific equipments required
Generating fibers using fluid co-flow	Co axial flow of one or more crosslinkable polymer solution containing the cells with a solution containing the gelation agent	~10µm	Geometry limited to linear fibers
Stereolithography	Structuration of photopolymerizable hydrogel layer by layer with a laser	~1µm	- limited to photopolymerizable hydrogels - time consuming - expensive
Laser microstructuration	Structuration of hydrogel blocks by laser ablation	~1µm	- depth of structure limited by the penetration of light into the hydrogel - time consuming - expensive
Bioprinting	Precise deposition of various hydrogels using a printer	~10µm	- Limited to specific hydrogels - expensive

Figure 20: *Table of the main microfabrication techniques used to structure in three dimensions*

Based on these techniques, different authors have been able to produce hydrogel structures with dimensions comparable with those of the cellular-scale functional units of organs. For instance, Kunze and al (Kunze et al. 2011) studied dendritic growth in a hydrogel with a thickness equivalent to that of the cortical layers of the brain (0.12 to 0.4mm). The cellular response to molecular stimuli (NGF/B27) depended on the depth at which neurons were located in the layer. Such conclusions raise questions regarding the influence of cortical thickness heterogeneity *in vivo* on cellular response in neuroscience.

Controlling the size of the hydrogel can induce a higher level of differentiation in cells, resulting in the acquisition of specific functions. For example, myoblasts grown in collagen bands of 20µm width (compatible with the diameter of a muscle fiber) fused, formed myotubes and striations necessary for myocyte contraction. In contrast, when grown in porous macrogels, they failed to form striation (Engler et al. 2004).

Cellular confinement on dimensions that are similar to the scale of organ functional sub-units can also induce a self-organization of cells into micro-organs. Jiang et al (L.-Y. Jiang and Luo 2013), seeded endothelial cells on a collagen-coated hyaluronic acid structure with grooves of different widths (30 to 200µm) and a depth of 20µm. They observed that endothelial cells self-organize into blood vessels only for grooves with widths of between 30 and 50 µm. Using a similar array of grooves (25, 50 or 100µm wide), Chiu et al (Chiu et al. 2012) placed an arterial and a venous explants, each at one extremity of the groove network and found that capillaries grew between the two explants. In contrast to Jiang et al's findings, however, the diameters of these capillaries, which were characteristic of mouse myocardium capillaries (~10µm), were independent of the initial width of the grooves. Following the same protocol, the authors then grew oriented capillaries connecting human umbilical artery and vein explants. After 3 weeks, cardiomyocytes seeded onto the newly formed vascular bed showed enhanced function with lower excitation threshold and better organized sarcomeres, compared with the ones seeded on a control substrate without vascularization. Such experiments emphasize the importance of an integrated vascularization to engineer a tissue *in vitro*.

The ability to structure hydrogels on scales comparable to organ functional subunits also offers the possibility of organizing different cell types more precisely in space (C. P. Huang et al. 2009). This higher level of complexity is a major improvement over crude hydrogels where co-cultured cells are seeded randomly. The reproduction of the orderly spatial distribution of the different cell types, as seen *in vivo*, can induce differentiation and association of cells into tissues. For example, Yamada et al (Yamada et al. 2012) used a double-coaxial microfluidic device to grow a fiber, 80µm in diameter, that contained rat liver cells in its core and feeder cells in its shell. First, they used a co-flow of two alginate solutions, one containing liver cells and the other containing feeder cells, to surround the liver cell alginate solution with alginate containing feeder cells. Then, a cross-flow of a gelating solution

froze this organization by polymerizing the alginate. The migration of the cells into the hydrogel and their subsequent self-organization resulted in the formation of micro-organoids, whose structure was reminiscent of the hepatic cord of the liver lobule. Homotypic and heterotypic intercellular interactions induced the secretion of albumin and urea, characteristic of liver function.

These structured fibers are of major interest for regenerative medicine. Recently, the group of Shoji Takeuchi (Onoe et al. 2013) temporarily implanted a fiber whose core consisted of primary pancreatic islet cells embedded in type I collagen, in the renal parenchyma of a diabetic mouse (figure 10). The shell, which was made of alginate and agarose, discouraged any fibrotic reactions from the host, and the fiber morphology offered a large surface area facilitating contact between the implanted cells and the renal parenchyma. The pancreatic cells within the fiber almost immediately secreted insulin in response to a high concentration of glucose, while the same amount of dispersed primary islets exhibited no secretion (Figure 21). This supports the idea that the confinement of cells, coupled with the presence of ECM-protein-enriched hydrogel induces the development of specialized cell function. The resistant shell also facilitates the easy handling and removal of the fibers, two important considerations for implant therapeutic safety.

a)

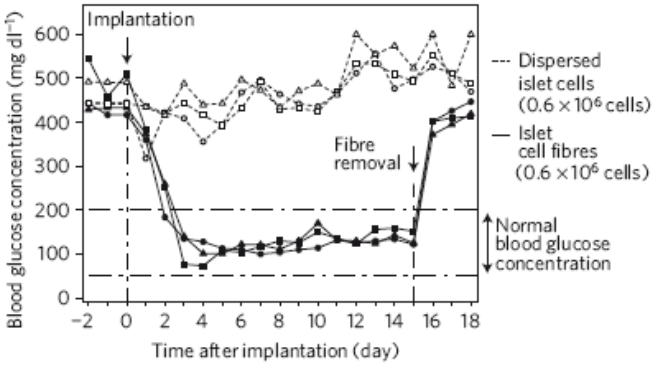

b)

Figure 21: *Images of the implantation of a 20-cm-long primary islet cell fiber into the subrenal capsular space of a recipient mouse after the implantation (a). Changes in the blood glucose concentration of three mice receiving 20-cm-long primary islet cell fibers (solid lines) and three mice receiving dispersed islet cells (dashed lines). Each symbol indicates an individual recipient. Fifteen days after implantation, the implanted fibers were removed from the subrenal capsular space.*(Onoe et al. 2013)

While the results are impressive for pancreatic implants, further structuring of the cellular environment is required for many other organs to reproduce the *in vivo* topography with greater verisimilitude. This accuracy is needed to induce cells to differentiate correctly and shape into the corresponding tissue.

II.2.2) 3D microstructured hydrogels: towards micro-organs

Here, we restrict our discussion to studies that have succeeded in reproducing physiological 3D structures and in directing cell growth and differentiation to form tissue-like structures. We will not review investigations performed on non-structured 3D aggregates, often called spheroids, nor discuss the use of micropillars as substrates.

Within current research into the development of *in vitro* micro-organs, one must distinguish between structures that reproduce the three-dimensional shape of an organ without achieving its functionality, and those with sufficient maturity to achieve a functionality that resembles to some extent that of the of the full organ.

Structures reproducing the three-dimensional shape of organs are usually obtained by first shaping the hydrogel, using, for example, bioprinting (Miller et al. 2012), stereolithographic projection (Gauvin et al. 2012) or molding with sacrificial layers (Esch et al. 2012; J. H. Sung et al. 2011). The microstructures have dimensions comparable to physiological ones and the use of porous hydrogels mimics the composition of the ECM. The biocompatibility of the material induces the growth and proliferation of cells (usually human cell lines).

The development of a confluent monolayer on these 3D hydrogels generates *in vitro* tissues with a structure very similar to the *in vivo* ones, such as blood capillaries (Gauvin et al. 2012) and villi (Figure 22) (J. H. Sung et al. 2011). The use of bio-printing has enabled researchers to precisely mimic the structure of blood capillaries and to surround such capillaries with a defined thickness of synthetic ECM containing fibroblasts (Miller et al. 2012; Norotte et al. 2009). Such co-culture increases the potential and realism of organs at the structural level.

Despite their high level of structure complexity, there is still a need to demonstrate the functionality of these cultures. For example, Sung et al (J. H. Sung et al. 2011) have analyzed an intestine villi model and shown that although the air-liquid interface characterizing the epithelium was lacking, the 3D structure induced a differentiation pattern closer to the *in vivo* one, with polarized cells at the top and less differentiated near the villous base, than in 2D culture. As a result, the permeability of the 3D micro organ and its trans epithelial electric resistance (TEER) were more analogous to the *in vivo* human values than a conventional 2D culture (Yu et al. 2012). Therefore, *in vitro* models that couple *in vivo*-like properties and the advantage of being seeded with human cells are now emerging as new tools for testing drug permeability in pharmacology (Yu et al. 2012).

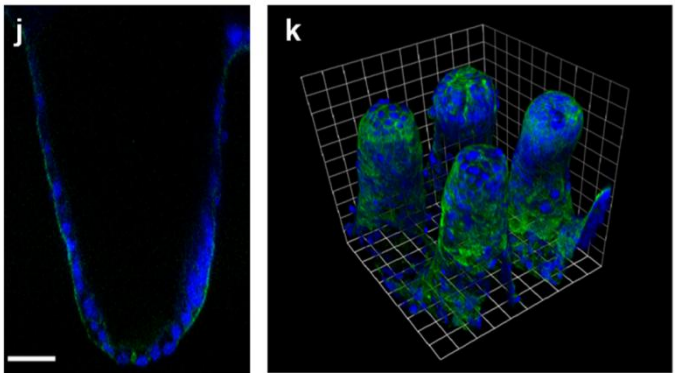

Figure 22: *Pictures of Caco-2 cells on 3D collagen villous structure: (j) X–Z section picture of single villous scale bar=43µm. (k) 3D villi with Caco-2 cells after 3D rendering (1 unit=37.6 µm) green actin blue nucleus. Imported from* (Esch et al. 2012)

Other artificial tissues still have some problems to iron out. For example, some micro-blood vessels are still filled with hydrogel, making blood flow inside the vessel impossible (Gauvin et al. 2012; Norotte et al. 2009). However, some *in vitro* capillary structures are also able to ensure a leak-free fluid flow in the lumen of the capillary (Miller et al. 2012; Yeon et al. 2012; Zheng et al. 2012). Injection of dextran into the lumen attests of the impermeability of the newly formed capillary (Miller et al. 2012; Yeon et al. 2012). Zheng et al (Zheng et al. 2012) probably achieved the most sophisticated structure so far, which permitted the flow of human blood flow in a microvascular network, based on hydrostatic pressure differences (Figure 23). The perfusion of human blood in this network revealed the interactions of the blood cells with the endothelial cells, reflecting both the physiological and the functional aspects of the structure formed.

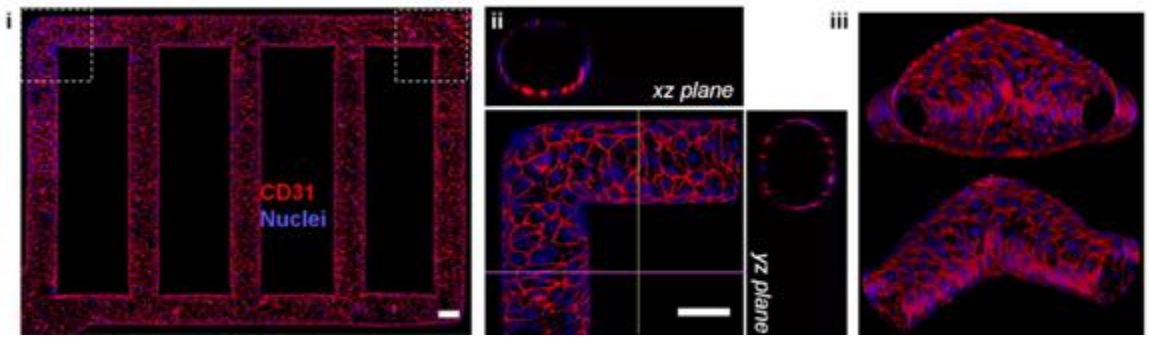

Figure 23: *Pictures of microvascular network in collagen scaffold: Z-stack projection of horizontal confocal sections of endothelialized microfluidic vessels (overall network, i) and views of corner (ii) and branching sections (iii). Red, CD31; blue, nuclei. (Scale bar: 100 µm.). Imported from* (Zheng et al. 2012)

The fact that such vascular structures can be integrated into human tissue implants is a hopeful step forwards in the development of engineered tissue. Unlike the micro-organs used for fundamental or drug testing studies, the scaffold structures designed for tissue transplantation must have a suitable size for achieving the desired function within the body. As such, they are often so large that

vascularization is necessary to provide enough 0_2 and nutrients for the long-term survival of the cells seeded at the center of the structure.

One approach is to stimulate angiogenesis after the scaffold has been transplanted (Laschke and Menger 2012). Angiogenic growth factors secreted locally due to the inflammatory response of the wound tissue at the transplant site can be sufficient to induce angiogenesis. Endothelial growth factors can also be added to the implant (see part 2.1.c). However, the growth of the host endothelial sprouts invading the implant is often too slow to prevent the death of cells at the center of big structures.

To overcome these limitations, a method called inosculation has been established (Laschke and Menger 2012). A preformed microvascular network is grown in the scaffold prior to its transplantation. Once implanted *in vivo*, sprouts of the host vasculature are expected to connect to the microvessel extremities of the implants, at a rate faster than "*de novo*" vascularization. For example, Baranski et al have used groove confinement to generate endothelial cord structures with collagen cores (see part 2.2.a), embedded them in fibrin gel and implanted them into mice (Baranski et al. 2013). This 'prevascularized' implant seemed to induce faster angiogenesis (within 3 days) than endothelial cells randomly seeded in the implants.

The newly formed vessels were composed of cells from both the implant and the host. Their cells were geometrically highly organized alongside the collagen cores of the endothelial cords. Randomly seeded cells, in the other hand, formed a disorganized morphology. Injection of FITC dextran through the mouse tail vein demonstrated that the cords of the whole implants had functionally anastomosed with the host vasculature. In contrast, substrates that had been randomly seeded showed perfusion that was limited to the periphery of the implants. Finally, the presence of ordered endothelial structure prior to implant transplantation seems to improve engineered tissue integration. For instance, hepatic cells enclosed in fibrin implants together with endothelial cords exhibited a greater albumin promoter activity, as compared to implants without cords (Baranski et al. 2013).

In addition to the growing interest in microvasculature as a tool to grow *in vitro* macroscale organs, microorgans themselves could offer great promise in the case of avascular transplantation in regenerative medicine, as they can also trigger vascularisation in vivo. A classic example of this is a medical case study by Revel et al (Revel et al. 2011). It concerns a woman who had one of her ovaries cryopreserved with the aim of restoring her fertility after invasive therapies. She requested fertility treatment years later, and two successive avascular slivers transplantations of her cryopreserved ovary were performed without a resulting pregnancy. The clinicians then adopted a new strategy where they implanted ovarian micro-fragments, which were called micro-organs in reference to the preservation of organ basic structure despite their microscopic thickness. The reduced thickness of the fragment allowed 0_2 and nutrients to penetrate the tissue, increasing the viability of the implants and resulting in their successful vascularization. This, in turn, enabled the delicate sensing of hormonal signaling

required for oocyte maturation. The fertility of the patient was restored, and resulted in the delivery of a healthy baby. This example highlights how synthetic microorgans could be deployed in the replacement macroscale tissues, in the context of avascular transplantation.

From this global introduction on the tools developed to provide physiological environment to cells *in vitro*, we can distinguish two prevailing approaches: one more focused reproducing the chemical and mechanical properties of the *in vivo* matrix uses bulk hydrogels without definite shape as cell substrates whereas microstructured devices concentrate more on the spatial organization of cells but rarely provide physiological microenvironment. The existing *in vitro* models of intestinal tissues follow the same trends: some groups combine physiological hydrogels with an optimal cocktail of signaling molecules to induce the spontaneous growth of intestinal tissue while some others impose the cells a spatial constrain either static (3D structure) or dynamic (peristaltic motion) perceived by intestinal cells *in vivo*.

III *In vitro* models of intestinal tissues, state of the art.

The intestinal tissue is particularly complex as it is constituted of various cell types: stem cells, transit amplifying cells, differentiated cells comprising: enterocytes, goblet cells, enteroendocrine cells, Paneth cells, Tuft cells and M cells. Therefore, growing intestinal tissue *in vitro* is more challenging than for other organs as the system should induce the differentiation and maintenance of these 8 different cell types whereas most organs are constituted of only one differentiated cell type. In addition *in vitro* intestinal tissue should have the ability to self-renew.

III.1. Growing intestinal organoids in artificial extracellular matrix

Organoids are *in vitro* multicellular structures shaped as cysts with budding parts (Figure 24).

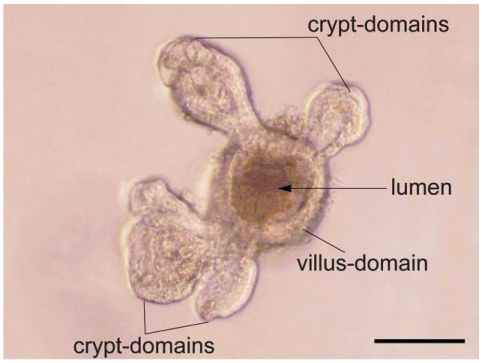

Figure 24: *Intestinal organoid. 4 days old organoid derived from single mice crypt stem cell. 4 'crypt like' structures bud out from the cystic central domain considered as villus-domain. Scale bar 100µm. Imported from (http://www.img.cas.cz/research/vladimir-korinek/research/)*

The intestinal organoids developed in the last 6 years by the group of Hans Clevers represent an important step forward in the *in vitro* culture of intestinal tissues as they recapitulate most of the

anatomical and functional characteristics of living intestinal epithelium. In their original study, Sato et al (Sato et al. 2009) isolated Lgr5 single stem cells from mice small intestine and embedded them in a natural hydrogel, Matrigel. Since it is derived from the basement membrane of mice sarcoma, Matrigel is enriched in laminin and therefore supports intestinal stem cell growth. Single stem cells first proliferated and formed hollow spherical structures called cysts. Then crypt like structures budded from the cyst (Figure 25 (i)). The number of budding structures increased with time via a phenomenon that resembled crypt fission. To stimulate cell survival and proliferation, the cell culture media had to be complemented with growth factors specific of the intestine: R-Spondin, a Wnt agonist was added together with Epithelial Growth Factors (EGF) to induce cell proliferation; and Noggin, a BMP inhibitor, was added to increase the number of crypts.

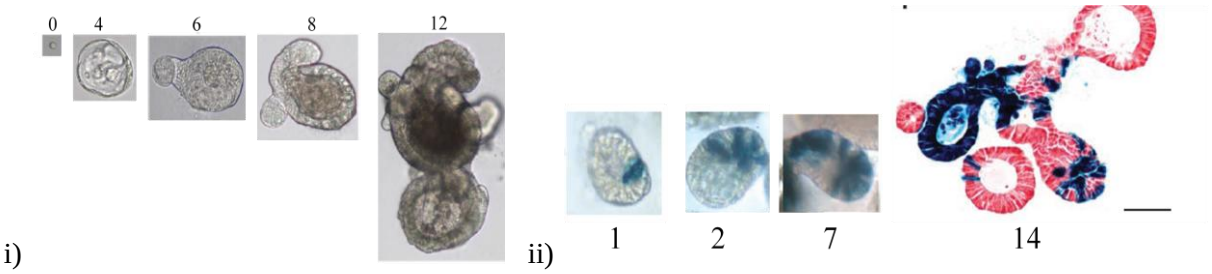

Figure 25: *Organoid formation. (i) Forming organoids starting from single Lgr5+ cell imaged at day 0,4 at magnification 40X at day 6 at magnification 20X, on day 8 at magnification 10X and on day 12 at magnification 4X. (ii) Lineage tracing of Lgr5+ stem cells. Lgr5 were identified on day 1 (tamoxifen and cre-recombinase construction); on day, 2 Lgr5 stem cells proliferated in the cystic structure; on day 7, crypts are entirely blue; and on day 14, Lgr5 progeny migrated out to the villi like structures. Magnifications and the values of scale bars were not specified). Adapted from* (Sato et al. 2009)

They observed that proliferative cells were mostly located in the lower part of the buds reinforcing the idea of buds being crypt like structures, and by inference the cystic parts between the buds were qualified as villi like structures. As they used the Cre recombinase genetic construction similar to the one they previously worked with to follow the lineage of Lgr5 expressing cells *in vivo*, they noticed that Lgr5 expressing cells were first located in the bottom of the 'crypts' and that their progeny progressively migrated along the bud (Figure 25 (ii)). This constant proliferation of stem cells is at the origin of the expansion of the organoids but is also counter balanced by the shedding of apoptotic cells that accumulate in the lumen of the organoids. Sato et al (Sato et al. 2009) also confirmed that Lgr5 cells alone were able to restore the differentiated cells types as they could identify enterocytes, Goblet cells, enteroendocrine cells and Paneth cells in the organoids.

In a second study (Sato et al. 2011), they refined their results and suggested that the initial combination a Paneth cell associated to a Lgr5 cell was essential to the formation of organoids. As a matter of fact they detected that Lgr5 alone were able to proliferate as organoids only if Wnt3a was added to the media whereas this additional factor was not needed in the presence of Paneth cells. Such observation confirmed the *in vivo* hypothesis that Paneth cells, intercalated between Lgr5 cells at the

bottom of the crypt, are secreting niche factors that are essential for survival and proliferation of Lgr5 stem cells.

Yan et al (Yan, Chia, and Li 2012) also succeeded in growing organoids but starting from +4 quiescent stem cells expressing Bmi1+ marker. Similarly, +4 stem cells spontaneously grew as organoids and differentiated cell types were found among their progeny (goblet, enterocyte and Paneth). Although they initially embedded +4 stem cells, they could localize Lgr5 cells in the lower part of the 'crypts'. This finding supports the concept of crypt plasticity as the quiescent +4 stem cells could adopt the Lrg5/CBC stem cell fate to regenerate the whole intestinal epithelium.

In the last four years, the technique of intestinal organoids was transposed to human stem cells (Finkbeiner et al. 2015; Spence et al. 2011). The adjustments added allow starting with human pluripotent stem cells instead of primary intestinal stem cells and therefore bypassing the delicate surgical procedure to extract primary cells. Human pluripotent stem cells first differentiate into endoderm, then differentiation of the endoderm into hintgut endoderm is induced. These two first steps are realized in 2D petri dish, while the maturation of hindgut endoderm into human intestinal organoids is achieved by seeding cells in 3D Matrigel. Similarly as mice primary cells, human cells formed organoids as they complete their differentiation (Spence et al. 2011). The major difference between human and mouse organoids is the presence of the mesenchymal cells associated with intestinal epithelium surrounding human organoids which is absent in mice organoids. As a matter of fact, human organoids derive from intestinal endoderm tissue that *in vivo* differentiate into both intestinal epithelium and mesenchyme. On the contrary, mice organoids result from the proliferation and differentiation of epithelial stem cells and as those cells are already committed to the epithelial lineage and therefore cannot differentiate into mesenchymal cells anymore. On the anatomical side, human intestinal organoids are more cystic and show only limited budding structures. However, when engrafted in mice kidney capsule they reorganized into the *in vivo* structure made of villi and crypts (Figure 26). Finkbeiner et al (Finkbeiner et al. 2015) compared the gene expressions of cultured and transplanted organoids. They noticed that the gene expression of cultured organoids was very similar to fetal intestine whereas transplanted organoids expressed advanced metabolic and host defense genes that characterize mature intestinal epithelium. However, when transplanted organoids were dissociated and seeded back in hydrogel they were incapable of reproducing the physiological architecture they exhibited when transplanted and reorganized as *in vitro* cultured organoids. These significant differences in morphology and gene expression between *in vitro* cultured organoids and engrafted organoids point out the essential role of humoral factors in intestinal tissue differentiation that are still challenging to reproduce *in vitro*.

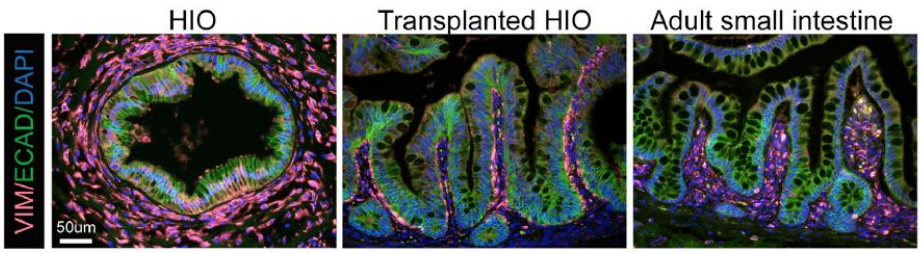

Figure 26: *Comparison between human intestinal organoids (HIO) in culture, human intestinal organoids transplanted in nude mice and human adult small intestine. The morphology of transplanted HIO is very similar to adult small intestine whereas cultured HIO are only poorly organized. Mesenchymal fibroblasts surrounding epithelial cells are labeled in pink (vimentin), epithelium is identified by E-cadherin labeling in green, all nuclei are labeled in blue. Imported from* (Finkbeiner et al. 2015).

Concerning applications, organoids provide many possibilities for drug screening, genomic sequencing and regenerative medicine (Barker 2014). Because of their *in vivo*-like shape and functionality, organoids represents *in vitro* models to study genetic diseases. Human organoids are particularly suited for drug screening as they abolish the problems related with species barrier that come along with drug testing on animals. In addition, organoids can be amplified *in vitro* and does not present any stress related gene expression over long periods of *in vitro* culture (up to 8 months) (Sato et al. 2009). They can be stored and therefore represent a biobank of intestinal tissue. In the case of intestinal mucosa inflammation like ulcers, the possibility to differentiate stem cells from the patient into viable tissue to replace the damaged mucosa should solve many problems related to isotype matching between donor and patient (Barker 2014; Sato and Clevers 2015).

However, although organoids already provide a very good model to study intestinal tissue *in vitro*, there is still room for improvement. As previously mentioned the architecture of the intestine is not fully restored as villi structures are missing in mice organoids. In addition, although differentiated cells were spotted in organoids, they were not restricted to the 'villi part' but were also located in the crypt like buds (Figure 27). In conclusion, the spatial segregation that goes along with the intestinal structure is not respected in organoids and might induce some false interpretation of the *in vivo* physiology of the intestine.

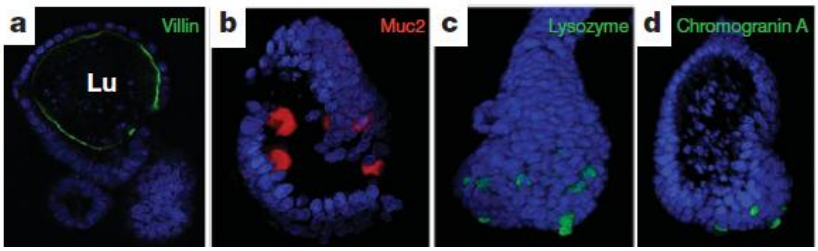

Figure 27: *Location of differentiated cells. 3 differentiated cells types are identified: (a) enterocytes by villin labeling, (b) Goblet cells by Muc2 labelling, (c) Paneth cells by lysozyme labeling and*

enteroendocrine cells by Chromogranin A labeling. Lu indicated the lumen of the organoids. Nuclei are labeled with Dapi. (Magnifications are not specified). Imported from (Sato et al. 2009)

Two groups tried to overcome this problem using microfluidics and microfabrication. They aim at reproducing the physical constrains sensed by cell *in vivo*, namely topography and peristaltic motion, to induce the formation of villi.

III.2 Gut- on-chip: growing intestinal tissue in microfabricated systems

A few years ago, the group of Donald Ingber developed a dynamic microdevice that does not include the replication of the 3D structure of the small intestine. They made the assumption that the peristaltic motion combined to the shear stress affecting the cells on both their apical (nutrients flowing in the lumen) and basal side (blood flow) would induce the spontaneous formation of crypts and villi (Kim et al. 2012). In their experiment they seeded Caco 2 cell line on a porous membrane (made in polydimethylsiloxane (PDMS)) placed in the center of a microfluidic channel. This membrane thus separated the apical lumen from the blood side (Kim and Ingber 2013). This chamber was flanked by two vacuum channels in PDMS and when vacuum was applied in these channels the central chamber was deformed at an amplitude and frequency mimicking the peristaltic motion (10% mean cell strain = cell deformation (Figure 28), 0,15Hz frequency).

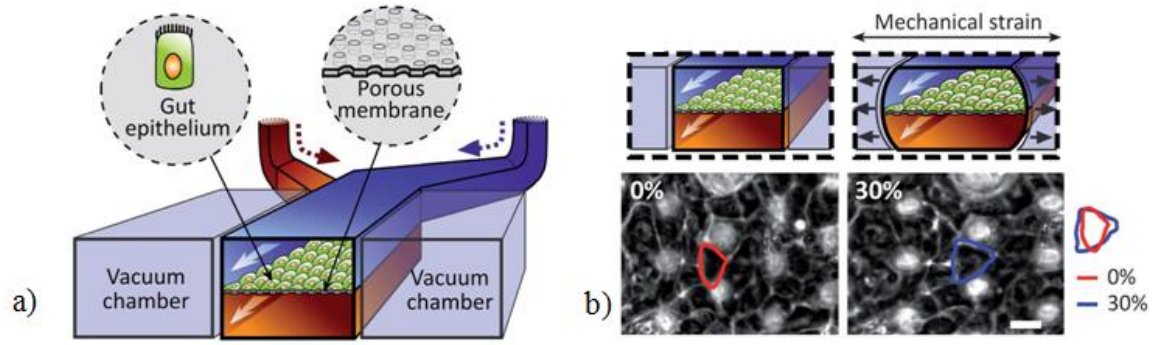

Figure 28: *Schematic presentation of the set up invented in Ingber lab. a) a central porous membrane with cells seeded at its apical pole divided the chamber into the luminal side and the blood side. Liquid was flown on both sides. Vacuum chambers are added on both sides of the cell culture chamber. b) The cyclic deformation gendered by cyclic motion induces cell deformation from 0 to 30% of the mean cell strain. Imported from* (Kim et al. 2012)

They observed that the shear stress caused by the flow of liquid in the central channel induced cell to polarize more than in a static transwell device. The addition of peristaltic motion polarized the cells even more. Hundred hours after the beginning of mechanical induction they noticed that confluent Caco2 monolayer spontaneously formed structure reminiscent to intestinal villi of approximately 70µm height (Figure 29).

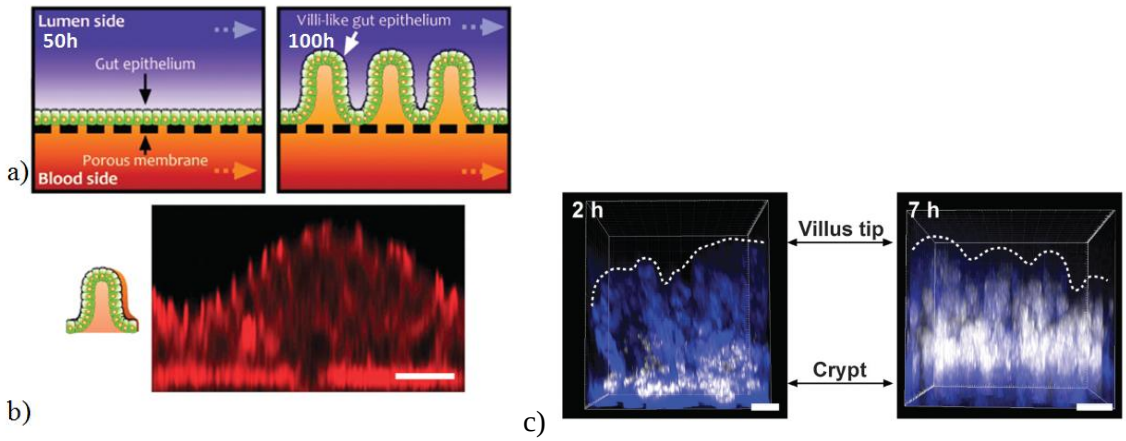

Figure 29: *Spontaneous formation of the villi and recapitulation of the proliferative and differentiated regions. a) Schematic representation of the flat epithelium after 50h of mechanical stimulation and the apparition of villi-like structures after 100h. b) picture of villi like structure (ZO-1 tight junction is labeled in red). c) localization of the dividing cells in the villi like structure 2hours and 7hours after Edu incubation. Scale bars: 20µm.*

They could localize the dividing cells in the crypt region of this structure via EdU labeling. The labeled cells seemed to migrate upwards to the tip of the so called villi (Figure 29). The 4 main differentiated cell types: enterocytes, Goblet cells, enteroendocrine cells and Paneth cells were all identified in the intestinal region where they belong *in vivo*. They concluded that their device efficiently induced the morphogenesis of Caco2 layer into a functional intestinal tissue (Kim and Ingber 2013).

The group of John C. March proposed a different approach to develop gut on chip as they seeded cells on a device that initially replicated the 3D structure of the villi. We already presented their previous study performed on collagen scaffold (J. H. Sung et al. 2011) in section (II.2.2)/ Figure 22). In their recent studies they realized a porous scaffold made of poly-lactic-glycolic acid (PLGA) polymer (Costello et al. 2014). To conceive the initial master, they first used laser ablation to dig holes of 500µm deep and 200µm diameter at the base in a thermoplastic polymer (Poly(methyl methacrylate) (PMMA)) mold. Laser ablation technique allowed them to create such high aspect ratio structures. They replicated the structure by curing PDMS on the PMMA mold. An agarose replica of the PDMS mold was used as template to make the final poly-lactic-glycolic acid (PLGA) structure (Figure 30). A sodium bicarbonate porogen solution was mixed to the PLGA solution prior to its polymerization to generate a porous scaffold. The PDMS intermediate as it is flexible facilitates unmolding of the agarose. Agarose was used as PLGA adhered less on this material.

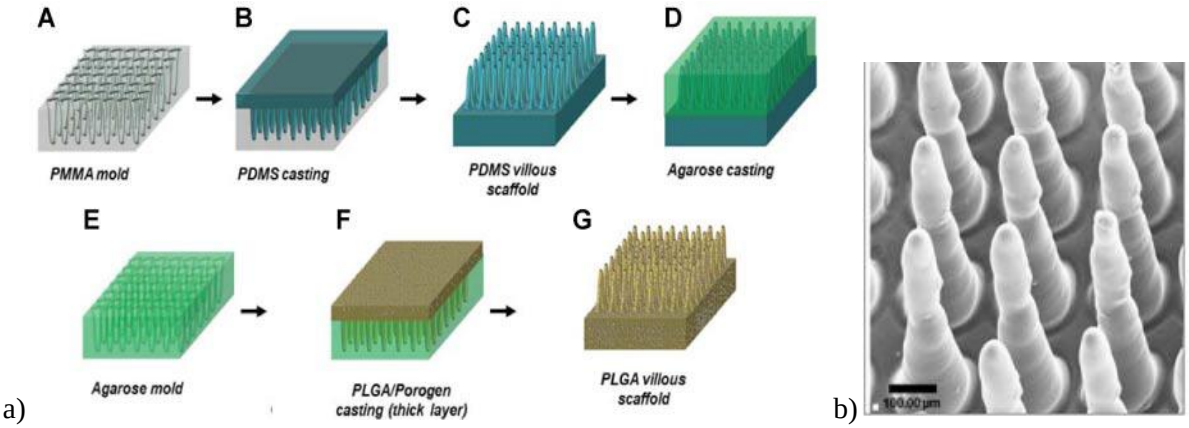

Figure 30: *Fabrication of the PLGA mold. a) Schematic representation of the different steps to process the PLGA mold. b) SEM picture of a non-porous PLGA mold obtained. Scale bar: 100µm.*

They coated their structure with Matrigel to make cell adhere. They first co-cultured Caco2 and HT29 cell lines on their device and they deduced that the 3D structured environment induced cell polarization (actin at the apical pole) and cell activity was promoted since the level of alkaline phosphatase (an enzyme active in the intestine) expressed was twice higher than in cells seeded on transwell devices. They also seeded primary crypts isolated from mice intestine. The primary cells successfully grew as a confluent monolayer on the structure. They observed the presence of differentiated cells by labeling Paneth cell at the base of the villus structure and Goblet cells on the villi (Figure 31).

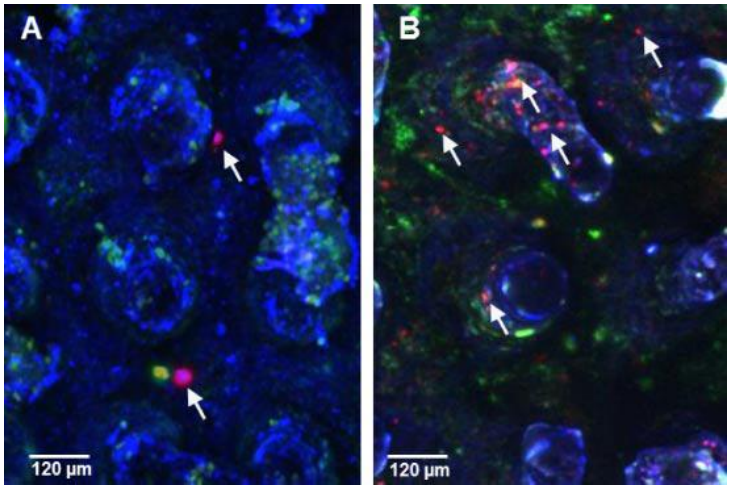

Figure 31: *Primary cells differentiation of the PLGA scaffold, 5 days after seeding. a) Paneth cells localized at the villi base (white arrows) stained for lysozyme (red). b) Goblet cells appear on the villi (white arrows) stained for Muc2 (red). Nuclei are labeled in blue and E-cadherin in green.*

Even if these two groups have demonstrated the possibility to grow cells in different biomimetic situation, none of them has provided cells with a physiological substrate or scaffold. In these papers, cells differentiation is only induced by mechanical strain applied on the seeded cells. In the first approach the mechanical strain is dynamic through peristaltic cyclic motion coupled to flow shear

stress whereas in the second device the mechanical strain is static and comes from the geometrical constrain of the structure.

The Ingber's paper reports that the height of the villi spontaneously formed under dynamic stimulation (approximately 75µm) is quite low compared to the in vivo topography of the villi (500 to 900µm in human). Since they seeded these structures only with cell line derived from colon carcinoma, it seems quite abusive to talk about cell differentiation. Furthermore, it is quite surprising to observe that Caco2 cells could differentiate into Paneth cells in intestinal crypt since Paneth cells are absent *in vivo* in colon. Following the same argument, the fact that physiological peristaltic motion, also experienced by colonic cells *in vivo*, would induce *in vitro* the spontaneous formation of villi that are normally absent in the colon is quite unexpected.

In the second approach the crypt region is missing in the design of the scaffold. However, primary cells seeded on this structure could still differentiate into Paneth cells which normally reside in the crypt. Another disputable point is that even though the authors proved that primary cells were able to differentiate into specific intestinal lineages; they did not provide evidence that intestinal stem cells were maintained during the course of their study.

Finally, in both approaches, the absence of matrix (Ingber) or its toxicity (March) do not allow fibroblast seeding in the substrate although they are proven to play a major role in the maintenance of cell homeostasis.

This last point is how my PhD project differs from the two previous models. The goal of this thesis is to reproduce both the chemical composition of the ECM of the intestine and its topography in order to induce the growth and differentiation of crypt stem cells into a functional tissue and to maintain its homeostasis through time. Every parameter of the system: chemical composition, stiffness and topography of the matrix, presence or absence of fibroblasts could be tuned and uncorrelated, so that, in turn, the influence of each parameter on intestinal homeostasis would be more easily read-out than *in vivo*. Finally, such *in vitro* device allows investigating other parameters, like 3D structure, that cannot be assessed *in vivo* since the loss of either crypts or villi would be lethal to mice.

CHAPTER 2: RESULTS

This section is divided in two parts. The first part describes the process we followed to synthesize a suitable matrix that recapitulate the intestinal environment, namely its chemical composition and its 3D structure. The second part is dedicated to the description of how we grew cell lines or mouse primary cells as an epithelium on this scaffold. The gut-on-chip device we generated is a simplified version of *in vivo* mice intestine but presented certain advantages inherent to *in vitro* systems. In particular, it allowed to uncouple different parameters and to change them individually without affecting others.

I How to engineer a scaffold that meets the specifications fixed by *in vivo* microenvironment?

In the previous section, we described the intestinal epithelium as a polarized cellular monolayer that adheres at its basal pole to the basement membrane. Underneath the basement membrane, the stroma is mostly constituted of a network of collagen I and fibroblasts. Actually, collagen I is the most abundant protein in mammals and the main constituent of all ECM in the body. It ensures the mechanical stability, strength and toughness of very different tissues ranging from cornea or skin to bone and dentine. This wide spectrum of mechanical properties is mainly related to changes in the organization of collagen fibers rather than chemical modifications except for bone and dentine in which the stiffness is increased by the inclusion of minerals (tiny calcium-phosphate mineral) into the collagen matrix (Fratzl 2008).

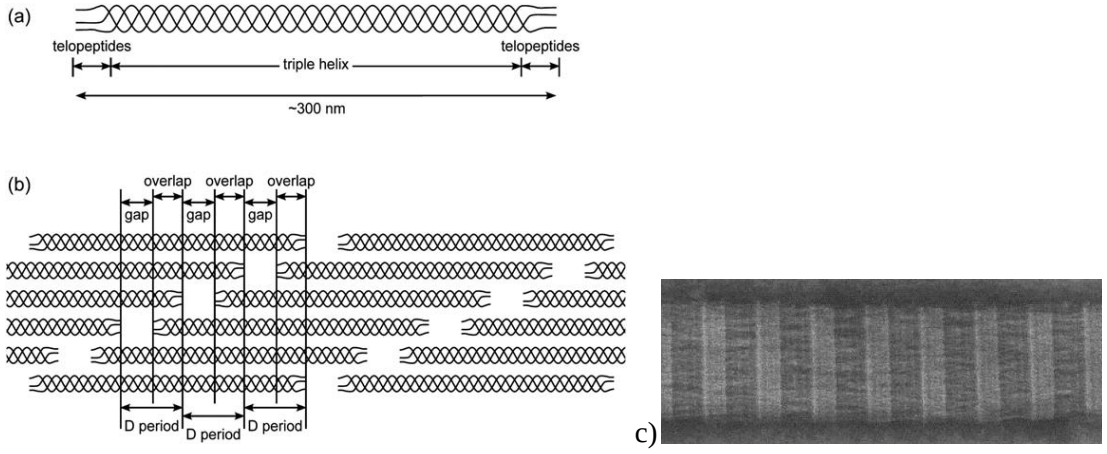

Figure 32: *Hierarchical structural assembly of collagen I. a) Schematic representation of three α chains assembled in a triple helical structure. b) Schematic representation of collagen molecules organized as a fibril with an axial D period. Imported from* (Streeter and de Leeuw 2011) *c) Electron*

micrograph of native fibril from rat tail tendon the visible periodic bands results from the D periodicity of the collagen fibers (×130,000). Imported from (Williams et al. 1978)

In vivo, collagen I molecules are constituted of three α chains that spontaneously organize into a triple helical structure of 300nm long and 1.5nm wide independently of the tissue considered (Fratzl 2008; Streeter and de Leeuw 2011) (Figure 32a). The formation of hydrogen bonds between adjacent amino acid small sequences (Gly-X-Y where X and Y can be any amino acids) result in a right handed triple helical structure with glycin residues in the core of the molecule and X,Y residues exposed to the surface (Fratzl 2008). The formation of triple helical structure is initiated at the C-telopeptide of collagen molecules. Collagen molecules then assemble into fibrils by longitudinal and parallel packing of collagen molecules. Concerning parallel packing, two adjacent collagen fibrils are offset from one another by a length of 64 to 67nm called D periodicity (see Figure 32b) (Fratzl 2008; Streeter and de Leeuw 2011). The D periodicity is typical of collagen fibrils and is responsible for their banded appearance due to changes in light reflection (Figure 32c). Fibrils formation is driven by electrostatic and hydrophobic interactions between hydrophobic amino residues exposed at the surface of collagen molecules that are buried into the core of the fibrils. It thus maximizes the contact between hydrophobic regions and minimizes the surface of hydrophobic residues in contact with solvent (Fratzl 2008; Kadler et al. 1996). The dimensions of the fibrils (length and diameter) vary depending on the tissue considered: fibrils from the tendons exhibit a micrometric diameter while they are only 40nm and 10nm wide in the cornea and in the cartilage respectively (Fratzl 2008). Proteoglycans of the matrix like lumican, fibromoduline or decorin interact with collagen fibrils and may regulate the growth of fibrils.

In vivo, the fibrillar network is further stabilized by intra and inter fibrillar cross-links. These cross-links are mostly performed by the lysyl oxidase (LOX), an enzyme secreted by fibroblasts. This enzyme converts lysine and hydroxylysine residues in N and C terminal telopeptides regions in the corresponding aldehydes which spontaneously condense to form covalent cross-links (Fratzl 2008). Overtime another type of crosslinking appears called glycation. Glycation occurs through spontaneous condensation between an amino group of a protein and a carbonyl group of a reducing sugar. This reaction is extremely slow because although glucose is the most abundant monosaccharide in mammals, it is quite absent in its aldehyde form (Tanaka et al. 1988).

As previously mentioned, our aim is to mimic physiological environment for intestinal epithelium. Because collagen I is the major constituent of the intestinal stroma, we chose collagen I hydrogels as materials to build our biomimetic device. From a tissue engineering perspective, despite the weak mechanical properties of collagen gels (Cross et al. 2010), collagen I spontaneously exhibits fibrillar structure and can be remodeled by cells. This last characteristic is a valuable asset for our model since collagen would at first provide the substrate for cells to grow in a given geometry and then it would allow them to secrete and organize their own matrix resulting in a mature autonomous tissue.

I. 1 Characterization of collagen I matrix

Collagen gel presents weak mechanical properties, thus the first challenge of my project was to find a good conditions to form fibrillar network with the characteristics of intestinal stroma found *in vivo* from a solution of collagen molecules. We scanned a range of collagen concentrations starting from low concentration commonly used in cell biology for 3D migration assays (~2mg/mL) (Geraldo et al. 2012; Sabeh, Shimizu-Hirota, and Weiss 2009) which happened to be to soft for our application, to highly concentrated collagen gels (10mg/mL). To generate the highly concentrated gels we extracted collagen from rat tail ourselves as commercial stock concentration was not high enough (from 9-11mg/mL). Both commercial and home-made collagen stock solution consisted of collagen molecules extracted from rat tails by dissolution in acetic acid. This extraction method was chosen over pepsinization, because pepsinized collagen present damaged telopeptides which are unable to initiate the formation of triple helical structure (Kadler et al. 1996).

Collagen molecules extracted by dissolution in acetic acid are mostly in the form of monomers but also includes cross-linked components (dimmers, trimers and some higher components) and are stored at 4°C to prevent polymerization.

The two main parameters that initiate fibrils formation are the pH neutralization of the acid stock solution of collagen and the rise in temperature from the initial 4°C. Depending on which step is first realized the resulting fibrils are shaped differently. If NaOH is added prior to the warming up of collagen, a step of nucleation forming 4D staggered dimmers occurs first, followed by a longitudinal elongation of these filaments. Finally, lateral fusion of those filaments gives rise to the banded fibrils (Figure 32 c). If the collagen is warmed up prior to neutralization, the nucleation step does not occur and instead both dimmers and early fibrils of collagen aggregate rapidly (Kadler et al. 1996). Since our aim is to synthetize collagen fibrils that are banded like *in vivo* ones, we first neutralized the collagen solution on ice and then allowed its polymerization by warming up the neutralized solution. The temperature of polymerization is also critical regarding collagen structure as a lower temperature slows down the polymerization kinetics and gives rise to larger fibrils. Following Geraldo et al study, we set the temperature of polymerization to room temperature as the fibrils generated are compatible with the size of *in vivo* ones (Geraldo et al. 2012). Williams et al (Williams et al. 1978) noticed that the presence of phosphate at an optimal concentration of 30mM improved the formation of banded fibrils. Since we had to be consistent with the osmolarity of cells we added phosphate saline buffer (PBS) at the physiological concentration of 15 mM in phosphate.

We first investigated the chemical and mechanical properties of commercial and home-made collagen to verify that there were no significant differences in the extracted collagen as they could induce different cell phenotypes. Thanks to the mass spectrometry platform in Institut Curie, we analyzed and compared the molecular composition of the collagen we extracted (i.e: home-made collagen) to the

commercial one (Figure 33). To perform such characterization, both collagen acid solutions were digested with trypsin prior to mass spectrometry analyses (see Material and Methods). Since enzymatic digestion could introduce some variability in the results, digestions and analyses were repeated three times by Vanessa Masson (Laboratoire spectrométrie de masse, Institut Curie).

HOME-MADE COLLAGEN Extracted from rat tail	COMMERCIAL COLLAGEN
Collagen α 1 chain	*Collagen α 1 chain*
Collagen α2 chain	*Collagen α2 chain*
Decorin	*Decorin*
Serum albumin	*Serum albumin*
Parvalbumin alpha	
Prolargin	
Serotransferrin	

Figure 33: *Comparison between the composition of home-made and commercial collagen solution*

According to this analysis, the collagen we extracted from rat tail had very similar protein composition compared to the purified commercial collagen. Quantitative analyses confirmed that the amount of both α chains were similar in the two types of collagen. In both samples, decorin was identified. Decorin is a proteoglycan composed of a core protein and a large glycosaminoglycan (GAG) moiety and belongs to the 'small leucine rich proteoglycan' (SLRP) family. The protein core binds collagen I fibrils and the hydrophilic anionic GAG chain attracts water in the interstitial space between fibrils and thus acts as a collagen fibrils spacer (Stamov et al. 2013). In decorin knockout mice collagen fibrils exhibit highly heterogeneous diameters and abnormal lateral fusion of thin and thick fibrils. In addition, the skin of those mice was more fragile than wild type one (Reed and Iozzo 2002). These observations suggest that decorin regulates the interactions between collagen molecules to generate fibrils homogeneous in diameter. Moreover, the presence of the GAG between fibrils favors the sliding of fibrils and therefore provides some elasticity to the collagen matrix (Stamov et al. 2013). The amount of decorin in home-made collagen was approximately 0.7 times the amount of decorin in the commercial collagen. Commercial collagen was thus richer in decorin and might be more elastic than home-made collagen. Serum albumin, a mammalian blood protein, is also detected in both collagen samples but is not involved in collagen fibrillogenesis. Three additional proteins were present in home-made collagen: serotransferrin, parvalbumin and prolargin. Serotransferrin is another blood protein that binds to iron, besides it may also stimulate cell proliferation. Parvalbumin alpha binds calcium ions and is more commonly found in the cytoplasma of muscular cells or in neurons where it regulates cytosolic calcium level. Prolargin like decorin belongs to the 'small leucine rich proteoglycan' family of proteins and it is mostly present in cartilage and skin. Prolargin also binds

fibrillar type I collagen and might be involved in collagen fibril formation although this has not yet been thoroughly examined in literature (Kalamajski and Oldberg 2010).

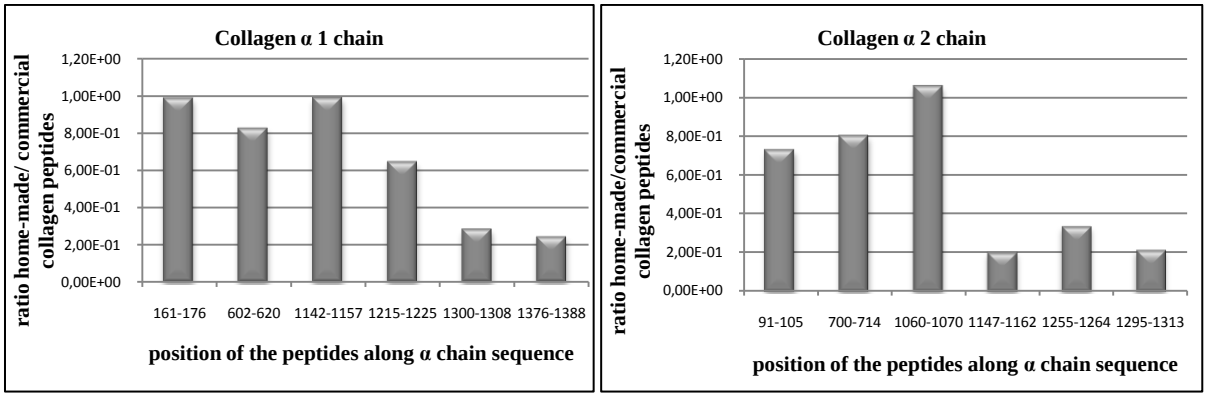

Figure 34: *Comparison of the quantity of peptides identified in home-made collagen vs commercial collagen depending on the position of the peptides along the protein sequence. Numbers on the x axis refer to the position of the amino acid in the protein sequence. The further the amino acids are the closer they are to the C telopeptide of the protein.*

During enzymatic digestion, trypsin recognizes lysine and arginine residues and cuts the protein sequence after these two specific peptides. Each protein sequence and the corresponding peptides obtained after trypsinization are recorded in a database. Therefore, the computational analysis of the peptides detected by mass spectrometry permits to get back to the protein they belong to. Furthermore, such analysis also enables to precisely locate the position of the peptide considered along the protein sequence. We could thus compare the quantity of peptide extracted for each collagen type depending on the peptide position along the collagen α chains sequences (Figure 34). We observed that peptides from the C-terminal part of both α1 and α2 chains were present in much lower quantity (5 times less) in home-made collagen. These results suggested that either C telopeptides were damaged during the extraction, which was quite unlikely since we performed acetic acid extraction, or that the amino acids of the telopeptides were chemically modified enabling their recognition by the enzyme performing the digestion. In the introduction of part II, we have reported that along rat aging, the collagen maturates and intra or inter fibrils cross-linking can occur resulting in amino acid modification. Since lysyl-oxydase cross linking converts lysine amino acids of N and C terminal telopeptides in their corresponding aldehyde and that the digestion enzyme we used cuts protein sequences after lysine or arginine, collagen cross-linking might explained the reduced number of C terminal peptides in home-made collagen. Therefore, home-made collagen might be more mature than commercial one. The results of the analyses also pointed out that the major drawback of collecting rat tails from different labs was that the age of the animals was not controlled, inducing some heterogeneity in the extracted collagen.

In conclusion, although there were slight differences, the composition of home-made collagen was very similar to the purified commercial collagen. Such analogous composition validated the use of the

home-made collagen as cell substrate. We thus expected cells to express the same cell phenotype on both collagens as they are very much alike. The possibility to use rat tail extracted collagen opened the possibility to use collagen in a broader range of concentrations than if we were restricted to commercially available concentrations.

Next, we investigated how collagen concentration affects collagen fibrillogenesis. This information is particularly valuable as most of the studies in literature are performed using collagen at low concentration (< 5mg/mL) (Brigham et al. 2009; Geraldo et al. 2012; Mason et al. 2013). Therefore, the description of collagen fibers shape at high collagen concentrations is limited. In addition, because slight differences in composition (presence of prolargin, various amount of decorin, absence of C-telopeptides) between commercial and home-made collagen could initiate some differences in collagen polymerization, we also compared the shape of the fibrils. Collagen solutions were mixed with fluorescently-labeled collagen (TAMRA-collagen) and observed under confocal microscope (Figure 35).

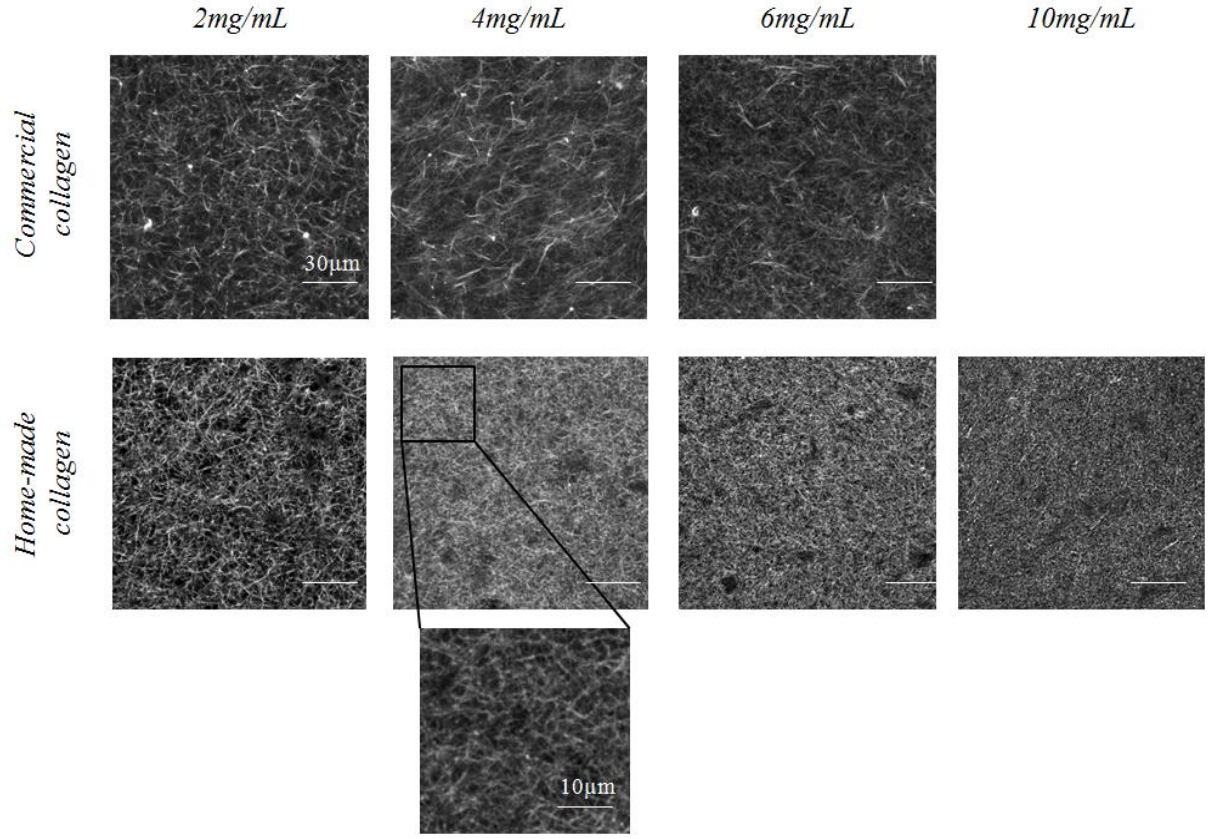

Figure 35: *Fibrillar collagen networks. Fluorescent images of commercial and home-made collagen gels at different concentrations. Scale bar of the first image is applicable to all images expect for the magnification of collagen 4mg/mL home-made.*

Depending on the type of collagen, the structure of the network appeared different. The fibrils were clearly visible on commercial collagen gels and on home-made collagen at 2mg/mL. In contrast, it seemed that home-made collagen at higher concentration failed to generate fibrillar structure.

However, the observation of those concentrated gels at higher magnification (Figure 35, for 4mg/mL) revealed that the fibrillar structure was still present in those gels but were so densely packed that they are hardly distinguishable. The fibrils of the commercial collagen also seemed larger compared to home-made collagen. We thus analyzed the fibrils diameter and approximate the mesh size of networks they formed depending on collagen type and concentration (Figure 36).

i)

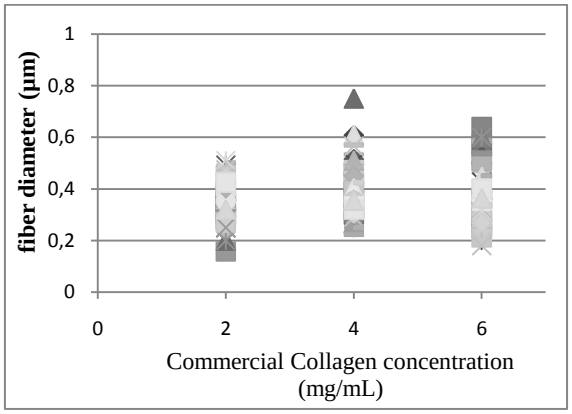

ii)

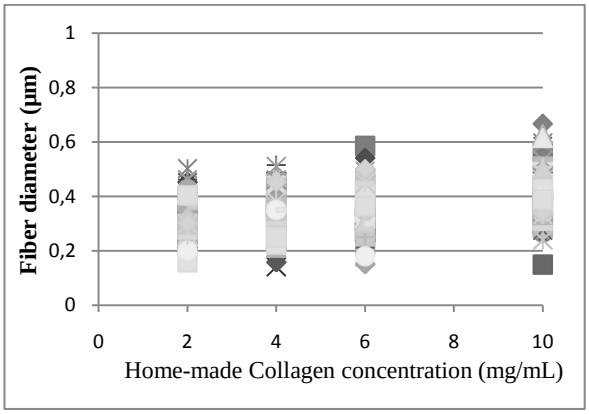

iii)

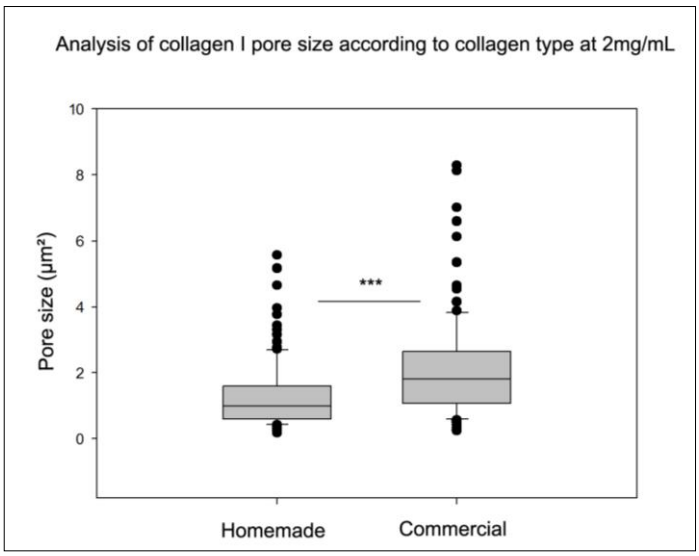

Figure 36: *Collagen gels characteristic dimensions. (i)&(ii) distribution of fibril diameters for commercial collagen and home-made collagen respectively. (iii) Plot box representative of the distribution of pores size for commercial and home-made collagen. ANOVA test was performed for statistical analysis*

The diameters were measured on 100 fibrils at each concentration and for each collagen type (Figure 36 (i) & (ii)). The mean fibril diameter was around 360nm regardless of collagen type or concentration. However, in every gel the fibrils were heterogeneous in size as their diameter range from 150nm to 600nm. Since fibrils mean diameter was constant regardless of collagen concentration, we deduced that an increase in collagen concentration directly correlated with an increase in the number of fibrils. This observation is in good agreement with the study of Cross et al (Cross et al. 2010) that found that an increase in collagen concentration resulted in a more reticulated gel but that

the mean diameter of the fibers remained constant even at 15mg/mL. The diameter we found ~340nm was a bit lower than the average fiber diameter ~500nm they reported but was in the same order of magnitude. In order to understand the differences in morphology between home-made collagen gels that seemed denser than commercial ones at a given concentration, we evaluated the pore size of those gels. This estimation could only be performed at 2mg/mL concentration since home-made collagen gels were too dense at higher concentrations (Figure 36(iii)). The mesh sizes were almost two times bigger in commercial compared to home-made collagen. If we refer to the mass spectroscopy analysis of the collagen composition, we noticed that C terminal peptides were missing or at least were present in smaller amount in home-made collagen compared to commercial ones. One explanation could be that the fibers constitutive of the peptidic α-chains of home-made collagen are shorter and thus generate smaller fibrils that arrange in a less porous hydrogel than the long fibrils of commercial collagen at the same concentration. Since these differences in hydrogel mesh size could induce important variations in the mechanical properties of home-made collagen compared to commercial hydrogel, we decided to study the rheology of those hydrogels.

As expected, the literature is unanimous on the fact that an increase in collagen concentration correlates with an increase in the hydrogel stiffness. Despite this consensus, the values found in literature for a given concentration vary depending on the rheological measurement performed: compression-stress measurement estimate the equilibrium modulus of 3mg/mL collagen to be around 30Pa (Cross et al. 2010). Using the same technique another study evaluated the equilibrium modulus of 1,5mg/mL collagen to be around 200Pa (Mason et al. 2013). Given these large variations, we evaluated ourselves the stiffness of our hydrogels depending on the concentration in order to correlate the differences between fibril shapes with rheological changes.

We had to find a method that could be performed on immersed hydrogels since collagen gels are highly sensitive to dehydration. As a matter of fact, when dehydration happens, the collagen surface in contact with air rapidly dries out resulting in a local over-concentration of the collagen fibrils compared to the rest of the gel. Rheological measurements performed on those gels would thus overestimate the real value of the gel stiffness. The texture of collagen gels is also challenging since they are very soft at low concentration and highly deformable. Classical rheological measurements are difficult to performed as deformation rate of collagen gels may fall below the limit of detection of most rheometers (Brigham et al. 2009). Furthermore, the measurements realized with rheometer always imply stress-strain measurements; the collagen is physically deformed and such deformation expulses the water out of the hydrogel. For soft hydrogels, such as collagen, the expulsion of water modifies the viscoelastic properties of the hydrogel and models describing poroelastic behavior have to be used to determine the viscoelastic properties of collagen (Cross et al. 2010). Finally the last limiting factors concerns the range of frequencies that can be investigated with conventional rheology which does not exceed 100Hz whereas the relaxation time of polymeric materials like collagen are

distributed over a large range of frequencies (Rubinstein and Colby 2003). Microrheology, on the contrary, permits to measure the rheological properties of a material over a wide range of frequencies from 1Hz to >1kHz (Shayegan and Forde 2013). This technique consists in deducing the mechanical properties of a material from the passive of diffusion of colloidal probes in the material or from an active diffusion of microbeads imposed by optical tweezers. Microrheology is thus by far less invasive than conventional rheology as it does not imply material deformation at the macroscale. The main drawbacks of this technique are the potential interaction of these micro-objects with the material and the spatial restriction of the obtained information to micrometer range due to the size of the objects used.

Considering the constraints imposed by collagen and the limitations of existing rheological techniques, we took advantage of the innovative technique developed by Laurence Talini ('Sciences et Ingénierie de la Matière Molle, UMR7615, ESPCI) to measure the rheological properties of materials. The method called surface fluctuation specular reflection (SFSR) deduces the rheological properties of a material from the thermal fluctuation of its free surface. It refers to the fluctuation dissipation relation that establishes the relation between the height fluctuations of a material free surface to its properties, namely surface tension, density and viscoelastic modulus (Pottier et al. 2011, 2013). This technique is particularly suited to study collagen rheology as it is fully non invasive. As a consequence, viscoelastic moduli are estimated in the linear regime where their values are independent of the strain and thus describe the intrinsic properties of collagen gels. In addition, the fact that the viscoelastic moduli are evaluated over a large frequency range (1-100kHz) permits to fully describe the mechanical properties of collagen gels.

On the practical side, a laser beam is focused at the free surface of the material; the fluctuation of this surface with temperature induces some spatial deviation of the reflected laser beam which is collected on a photodiode. The temporal noise recorded is converted into the frequency dependent fluctuation spectrum (S(f)) that can be expressed as follows: $S(f) = \int_0^\infty P_k(f)\phi(k)\, kdk$ where k represents the spatial mode of fluctuations and f the frequency. Function P represents the power spectral density of the surface modes. It depends on the spatial mode of fluctuation and on the frequency and describes both the mechanical properties of the material and its surface tension. Function ϕ is a weighting function of the spatial mode k and is directly related to the laser used. As a matter of fact, from all the modes k of fluctuation of the surface, the laser is mainly sensitive to the spatial mode k=1/R where R is the radius of the laser. If $1/k \gg R$ (Figure 37 (i)), the fluctuations are too low to be sensed by the laser, on the contrary if $1/k \ll R$ (Figure 37 (ii)), fluctuations are too narrow and fall below the sensibility of the laser. As a consequence, function ϕ corresponds to a band pass filter centered on k~1/R. Depending on the size of the laser that can be easily tuned, the surface fluctuation specular reflection (SFSR) method enables to perform measurement on length scales ranging from 1 to 100µm.

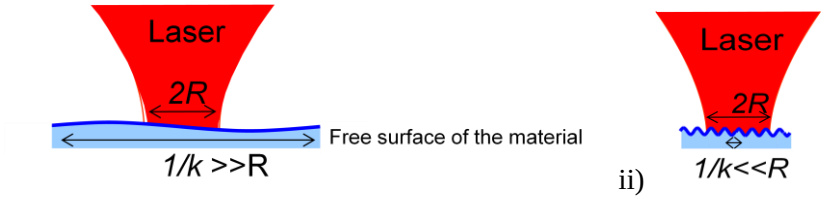

Figure 37: *Sensibility of the laser to the spatial mode of height fluctuations of a material surface. (i) Fluctuations are too large to be recorded by the laser. (ii) Fluctuations are too narrow to be sensed by the laser.*

All the measurements and analysis of this section were performed with Laurence Talini on flat and thick collagen hydrogels. Collagen gels were placed in the measurement cells immediately after unmolding and phosphate buffer solution (PBS) was added to prevent collagen dehydration. The volume of PBS added was set to reach the surface of collagen gels without covering it to avoid recording PBS fluctuations instead of collagen surface fluctuations. In order to verify that this configuration did not expose collagen gels to dehydration we compared rheological measured after unmolding to those performed after the same hydrogel had spent one entire day in the measurement cell. Since the two measurements overlapped, we confirmed that the amount of PBS added to the measurement cell was sufficient to prevent collagen from dehydration. The first measurement was performed with a laser beam of 3.5µm in radius. The frequency dependent fluctuation spectrum (S(f)) was evaluated on different regions of a home-made collagen at 4mg/mL (Figure 38(i)). The comparison of these spectrums revealed a spatial heterogeneity of the gel at this length scale. These results were consistent with the heterogeneity observed by Shayegan et al (Shayegan and Forde 2013) who performed microrheological measurements with 2.10 µm diameter beads trapped in optical tweezers. Such spatial heterogeneities can be explained by the fibrillar structure of collagen networks. We have previously demonstrated that the distribution of fibrils diameters was heterogeneous as they range between 150nm and 600nm. With regard to the size of the fibrils, it thus might be that at this high spatial resolution, both laser and beads could sense the heterogeneity between fibrils. In this respect, we decided to perform experiments with larger laser beams so that the heterogeneities related to fibrillar structure would be negligible.

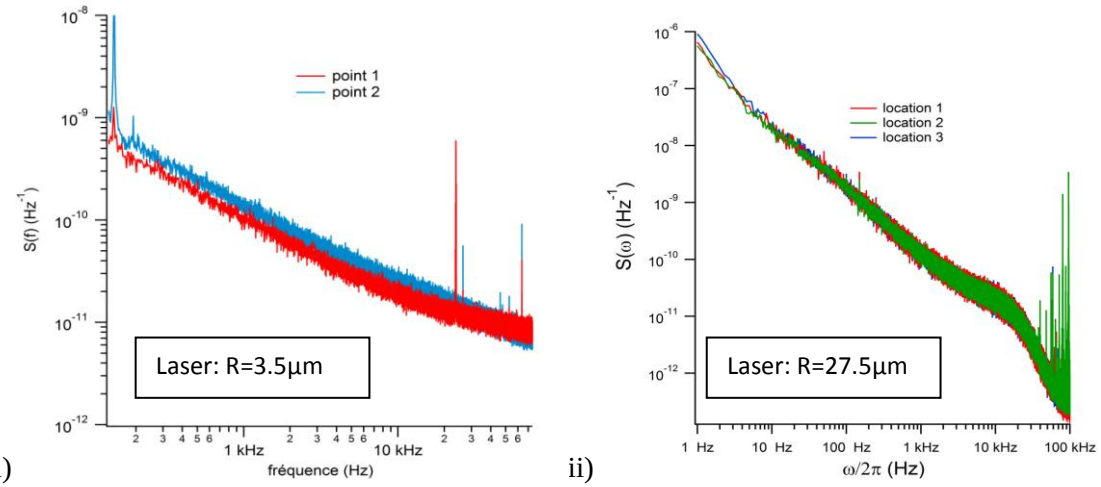

i) ii)

Figure 38: *Frequency dependent fluctuation spectrum of collagen gels at 2 different positions on the gel surface (4mg/mL home-made collagen). (i) Fluctuations recorded with a laser beam of 3.5µm in radius. (ii) Fluctuations recorded with a laser beam of 27.5µm in radius.*

On Figure 38 (ii), the measurements performed with a laser beam of 27.5µm in radius at three different locations on the same gel entirely overlap. It thus confirmed that the gel was not intrinsically inhomogeneous and that the heterogeneity recorded at higher spatial resolution might be related to the fibrillar structure of collagen networks.

Starting from the frequency dependent fluctuation spectrum (S(f)) computational analysis are then performed to extract the viscoelastic complex modulus variations with frequency G*(f) = G'(f) + i G''(f) where the real part G' represents the elastic modulus and the imaginary par G'' is the viscous modulus (Pottier et al. 2011, 2013). For hydrogels as collagen, the value of surface tension with air is needed to determine G*. Because hydrogels are in an intermediate state between liquids and solids, their surface fluctuations comprise terms relative to each state. One term corresponds to capillary waves characteristic of liquids and is dominated by surface tension effects. The second term corresponds to Rayleigh waves, dominated by elasticity, and is specific to solids. The surface tension had to be determined experimentally since the surface tension of soft polymeric gels may be different than the surface tension of their solvent and may vary with polymer concentration. As the surface tension is a constant that does not depend on frequency, comparing the measurements of the frequency dependent fluctuation spectrum with two different sizes of laser beam permitted to extract the value of the surface of tension of collagen. Additional measurements of 4mg/mL home-made collagen were thus performed with a laser beam of 41.3µm (Figure 39(i)). Since depending on the radius of the laser different spatial modes of fluctuations of the surface were recorded, the curves obtained with 41.3µm and with 27.5µm did not overlap anymore. The comparison of these two signals permitted to estimate the surface tension of home-made collagen for each concentration (Figure 39(ii)).

i)

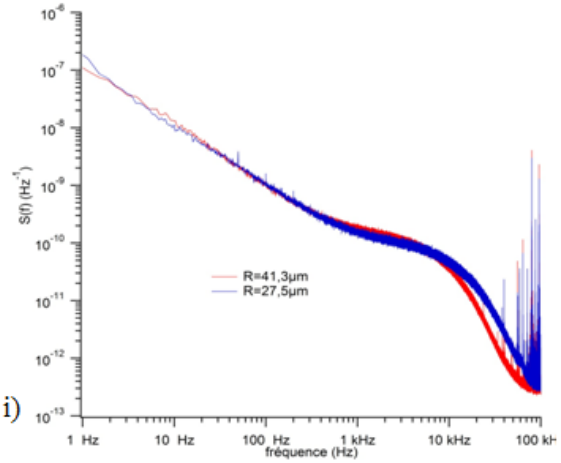

ii)

Home-made collagen concentration (mg/mL)	Surface tension (mN/m)
2	60
4	52
6	48
10	44

Figure 39: *Measurements of home-made collagen surface tension. (i) Fluctuation spectrum recorded with two laser beam sizes permits to extract surface tension value. (ii) Estimation of the surface tension values at each concentration of home-made collagen.*

Since collagen is a hydrogel, we expected its surface tension to be identical to the surface tension of PBS (~70mN/m). Our results demonstrate that the surface tension of collagen gels is always below the surface tension of PBS and that an increase in collagen concentration correlates with a decrease in the surface tensions values. Such tendency can be explained by the existence of hydrophobic domains in the collagen peptidic chain that preferentially adsorbed at the interface with air and thus decreased the surface tension of the hydrogel.

The surface tension values determined could thus be implemented in the frequency dependent fluctuation spectrum (S(f)) to extract the variations of the elastic modulus (G'(f)) and of the viscous modulus (G''(f)) with the frequency. Viscoelastic moduli were determined at different concentrations for both home-made and commercial collagen.

i)

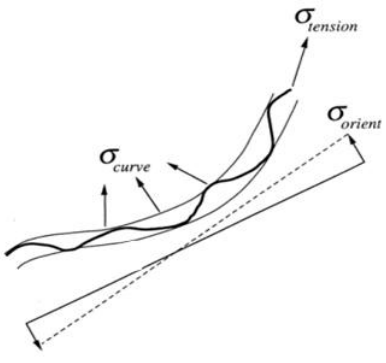

ii)

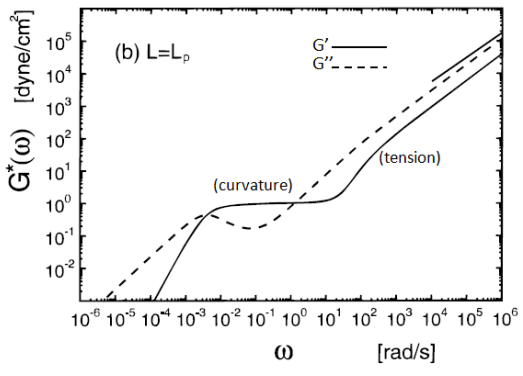

Figure 40: *Theoretical variation of viscoelastic moduli for semiflexible polymer solution. (i) Schematic representation of semiflexible polymer within a virtual tube showing the three types of stresses (curvature, tensional and orientational stress), applied to the polymer when the network is strained (ii) Calculated variations elastic modulus (solid line) and viscous modulus (dotted line) with frequencies.*

(curvature) and (tension) indicate frequency regimes in which G(w) is dominated by curvature or tension contribution. Adapted from* (Morse 1998).

In literature, biological polymer networks like actin and collagen are considered as semiflexible polymer networks. Morse (Morse 1998) extended the reptation in a tube model to describe the viscoelatic behavior of semi flexible polymers (Figure 40 (i)). According to his calculations, the variations of viscoelastic moduli as a function of frequency follow the model of Figure 40 (ii). The response of semiflexible polymer network to an oscillatory deformation is dominated by curvature stress at low frequency whereas tensional stress dictates the high frequency regime (Figure 40). The plateau in elastic moduli appearing in the curvature regime corresponds to the relaxation of the polymer chains. The value of G' at this plateau is called plateau modulus and can be exploited to understand the dynamic of the polymer chains considered. We expected our viscoelastic measurements performed on collagen gels to be in agreement with semi flexible polymer networks model.

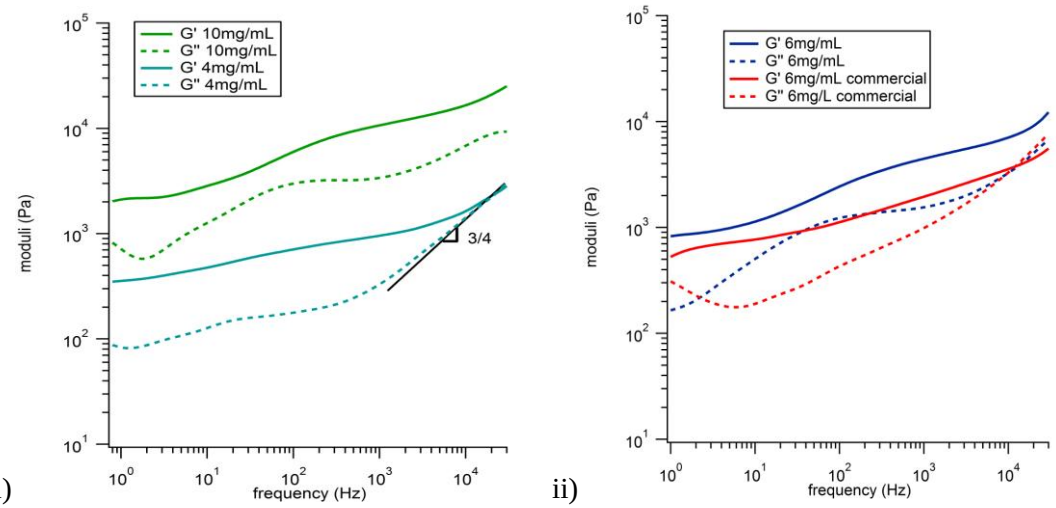

Figure 41: *Variation of viscoelastic moduli measured on collagen gels. (i) On home-made collagen at 10mg/mL and 4mg/mL. (ii) On home-made vs commercial collagen at 6mg/mL.*

At each concentration and independently of the type of collagen considered, both elastic and viscous moduli presented low variations corresponding to the plateau previously described in the curvature regime of semiflexible polymers. At high frequency, in the tension regime, we would expect variations elastic and viscous modulus with frequency to follow a power law ($G^*(f) \propto f^{\alpha}$ where $\alpha = 3/4$ for semiflexible biological polymer networks like actin). We could observed such variations for the viscous modulus of 4mg/mL collagen gels (Figure 41 (i)) but additional data at higher frequency were required to detect this regime for higher concentrations.

For every collagen sample, the elastic modulus values were larger than viscous modulus values indicating that collagen gels were elastic at all the frequencies investigated. By comparing elastic modulus variations at different concentrations for home-made collagen, we could also verify that, as expected, the higher the concentration of collagen was the stiffer collagen gels were (Figure 41).

We could only compare the viscoelastic moduli of home-made and commercial collagen at the concentration of 6mg/mL since commercial gels were too heterogeneous at lower concentration to extract the viscoelastic moduli. Although commercial and home-made collagen presented similar variations of their elastic moduli, the higher values of home-made collagen elastic modulus attested that home-made collagen was stiffer than commercial collagen (Figure 41(ii)).

In order to put our results in perspective with the studies found in literature, Young modulus values of collagen gels were extracted from the elastic modulus measurement. As a matter of fact, Young modulus is a physical quantity extensively used in tissue engineering to describe the stiffness of materials. We calculated Young modulus following the linear relation between Young modulus (E) and elastic modulus (G') established for incompressible medium: E=3 G'(commonly calculated with the value of G' at 1Hz). The values are reported in the following table (Figure 42).

Collagen concentration (mg/mL)	Young Modulus value for Home made collagen (kPa)	Young Modulus value for commercial collagen (kPa)
2	0.6	
4	1.05	
6	2.55	1.5
10	6	

Figure 42: *Young modulus values estimated depending on collagen concentration and collagen type*

According to the theoretical description of semi flexible network, the variation of plateau modulus values of elastic moduli at low frequency (Figure 40(ii)) with polymer concentration should follow a power law: $G' \propto C^{\beta}$ with $\beta=1,8 \pm 0,2$ (Gardel et al. 2003; Morse 1998).The value of β was determined for actin polymer networks (Gardel et al. 2003).We thus reported the values of elastic modulus we measured as a function of collagen concentration for two frequencies (1Hz and 10Hz) (Figure 43).

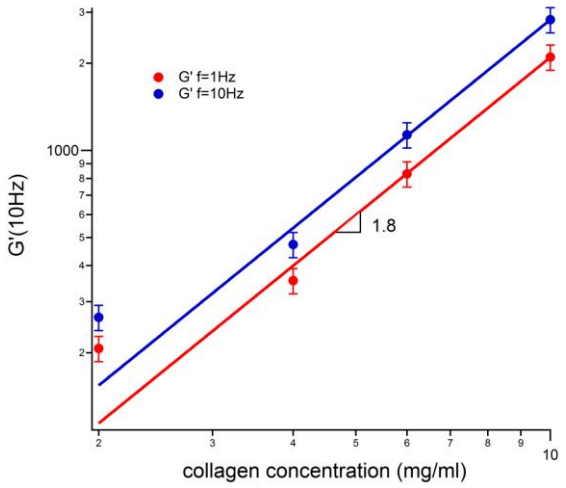

Figure 43: *Variations of plateau modulus values with home-made collagen concentration at different frequencies.*

Except for 2mg/mL concentration, the variations of elastic modulus with concentration respected the power law previously described at both frequencies. We thus confirmed that our measurements were in agreement with the common view shared in literature that considers collagen hydrogels as semi-flexible polymer networks.

Although we could not determine the viscoelastic moduli of the lower concentrations of commercial collagen as they were too heterogeneous to extract reliable values, the surface fluctuation specular reflection method informed us on the variations of viscoelastic moduli over a wide range of frequencies. In addition, since this method was non invasive, viscoelastic moduli were estimated in the linear regime and thus reflected the intrinsic viscoelastic properties of the hydrogel. We could extrapolate the values of Young Modulus which are considered as the reference values to describe the mechanical properties of hydrogels in the tissue engineering field. Another strong advantage of this technique is that the spatial resolution (in surface and volume) of the measurement was comparable to the size of cells (~10µm). Therefore there was a direct correlation between the mechanical properties evaluated and those sensed by the cells seeded in or on the hydrogel.

The characterization of collagen chemical and mechanical properties confirmed that we could use the collagen we extracted as its composition was very similar to the commercial one. With both collagens we managed to reproduce the fibrillar structure typical of the *in vivo* ECM. The close observation of these fibers revealed some differences in shape and distribution between the two collagens that result in significant deviation in stiffness at a given concentration. These variations in the mechanical properties are not negligible for the following parts of this study since it is very likely that the cells can sense them.

I 2 Structuring the collagen

Since our aim was to reproduce the topography of the small intestine, we needed to develop a method to structure the collagen in 3D that is compatible with the requirements imposed by collagen fibrillogenesis *in vitro* previously mentioned (§ II introduction).

Among the microfabrication techniques to structure hydrogels described in the introduction (§ I 2.2.a), most of them were not compatible with the kinetics of polymerization or with the properties of collagen gels. For instance, laser ablation could not be performed on a collagen as it imposes to have a surface in contact with air and the local heating due to laser illumination would cause a drying of the collagen. Bioprinting necessitates hydrogels that polymerize instantaneously when deposited on the substrate to keep the 3D structure imposed by the printing. The duration of collagen polymerization (~30 minutes) thus did not seem compatible with this technique. Finally, soft lithography and in particular replica molding techniques seemed to be the only option left. This technique consists in

creating a master in material that is rigid enough to act as a template to mold the hydrogel of interest and replicate a given 3D structure.

The first step of my project was thus to generate a template mold with the dimensions that mimic the intestine 3D structure in order to replicate this structure with collagen. The main difficulty in reproducing the global topography of mouse intestine lays in the high aspect ratio (height/ width) of both crypts and villi structures: about 2.5 for the villi and up to 5 in the crypt (Figure 44(i))

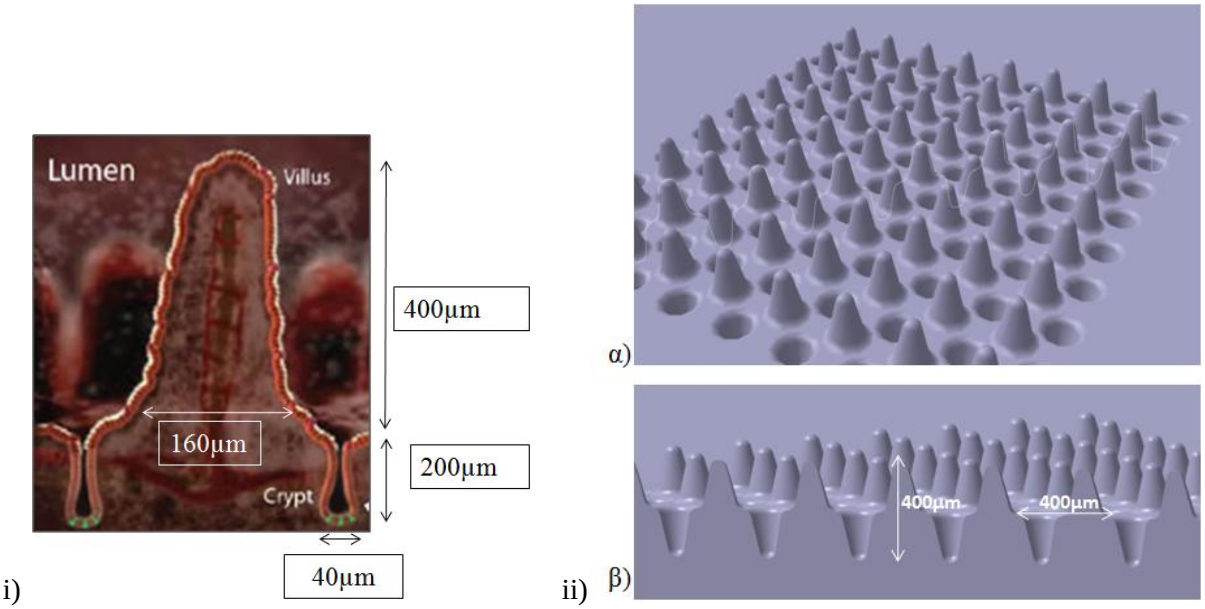

Figure 44: *Reproduction of the structure of the small intestine. (i)Transversal cut of mice of the small intestine annotated with dimensions of the crypt and villus entities. (ii) Graphical design of the mold to mimic the intestine on Katia software. (α) Global view of the structure of the succession of holes (~crypts) and conic spots (villus). (β) transversal cut of the structure (α) to visualize the 3D sinusoid of 400 µm in height with a 400 µm period.*

With regards to the height of the *in vivo* structures, conventional photolithography method to fabricate the mold was immediately rejected. Two microfabrication techniques commonly used in our lab were thus considered: micromilling and 3D printing. In an attempt to mimic the intestine topography while maintaining the microfabrication step at a reasonable complexity level, the first design generated was a three dimensional sinusoid of 400 µm in height with a 400 µm period (Figure 44(ii)). We focused on reproducing the convex curvature of the villi and the opposite concave curvature of the crypt found in the intestine even though the relative dimensions of crypt and villi were not respected. These opposite curvatures are missing in the device of Costello et al (Costello et al. 2014) which replicated only the villi part. Because those opposite curvatures may play an important role in the maintenance of the stem cell state in the crypt and/or facilitate the shedding of apoptotic cells at the villus tip, we insisted in replicating these geometrical features.

We first evaluated the potential of stereolithographic 3D printing. Stereolithography 3D printing involves layer by layer polymerization of a photosensitive resin using focused laser or LED light

source. Resolution is primarily defined by the size and the speed of the laser beam (here ~20 µm, 2200 mm/s), but also by the software which generates and control trajectory of the laser. We made several attempts, and encountered different difficulties regarding the mold fabrication as well as the PDMS demolding.. In addition, the 3D printing equipment failed to generate homogeneous and regular structures (Figure 45 (i)). Finally, the creation of an inverted curvature mimicking the crypts seemed too challenging, due to the accumulation of photocurable resin in those holes (Figure 45 (ii)). Further investigations are currently performed to optimize this process.

i) 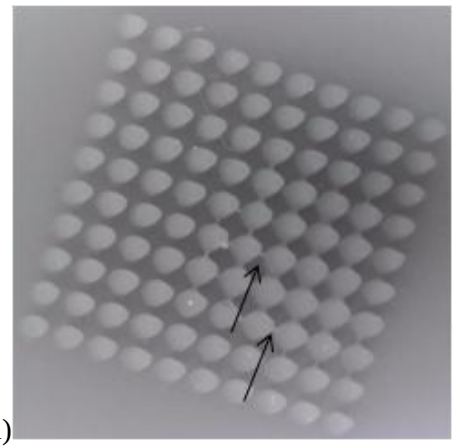 ii) 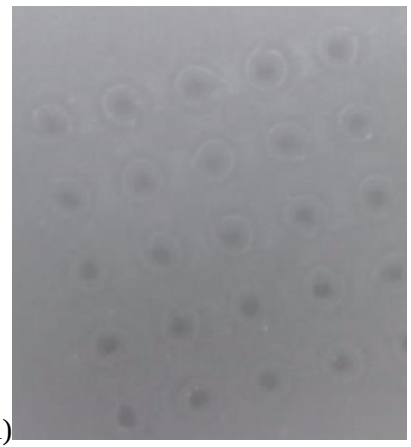

Figure 45: *3D printed structure. i) Irregular diameter of the printed pillars. Black arrows indicate connections between the pillars (x 10). ii) Traces obtained instead of holes with 3D printing (x10)*

A micromilling machine was thus used to fabricate the mold. Surfaces generated by micromilling technique are rougher than those obtained with photolithography because the structuring is realized by a miller instead of UV illumination. However, as it mechanically extrudes the material, micromilling generates higher structure than those obtained with photolithography. Since the structures we designed were high with a spatial resolution of about 5µm, micromilling was well suited for our application. The curvature of the bottom of the crypt was also limited by the existing tools since the smallest ball miller commercialized had a diameter of 100µm. Therefore it restricted the crypt curvature to this diameter. Furthermore, the width tool used also imposes the height of the structure that can be generated. The maximum depth of material that can be extruded with a given tool equals to twice its width: a 100µm driller can thus generate 200µm deep holes at maximum. Therefore, we were limited in the aspect ratio of the structure we generated. The 400µm 3D sinusoids seemed the best compromise to conserve confined curvature while maintaining a substantial height (Figure 46). The micromilling permits to generate an initial brass mold from which PDMS replica were obtained.

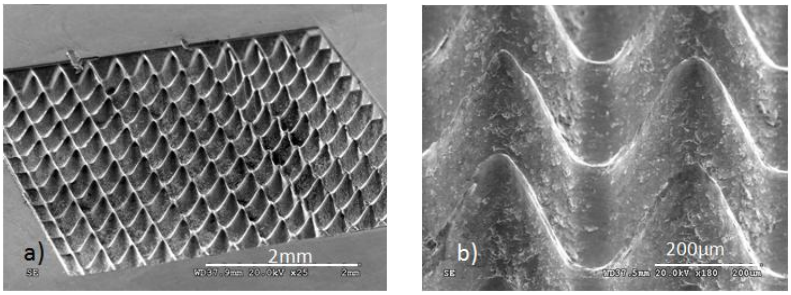

Figure 46: *Sinusoidal structure fabricated by micromilling on a brass mold. Scanning electron microscopy a) of the whole structure, b) focused on the sinusoidal shape.*

For sterility issues, collagen was not directly molded on the brass mold but through an intermediate PDMS replica (mold 1). The workflow of collagen molding process is illustrated in Figure 35. Since collagen was too soft to be directly handled, a PDMS mold with an inner cavity to hold the collagen gel was created to manipulate easily the collagen scaffold (mold 2). Neutralized collagen solution was prepared. Meanwhile mold 1 and 2 were assembled as an enclose chamber which facilitates the injection of the neutralized collagen solution. The inner cavity of mold 2 was treated so that collagen could adhere to its surface (see Material and methods). Collagen injection in an enclosed chamber also forces the collagen to enter all the microstructures of our mold and thus generated fewer bubbles at the bottom of the structure than if collagen solution was simply deposited. Once collagen had polymerized, collagen and its PDMS holder were unmolded. Starting from unmolding, the collagen was always kept immersed (Figure 47).

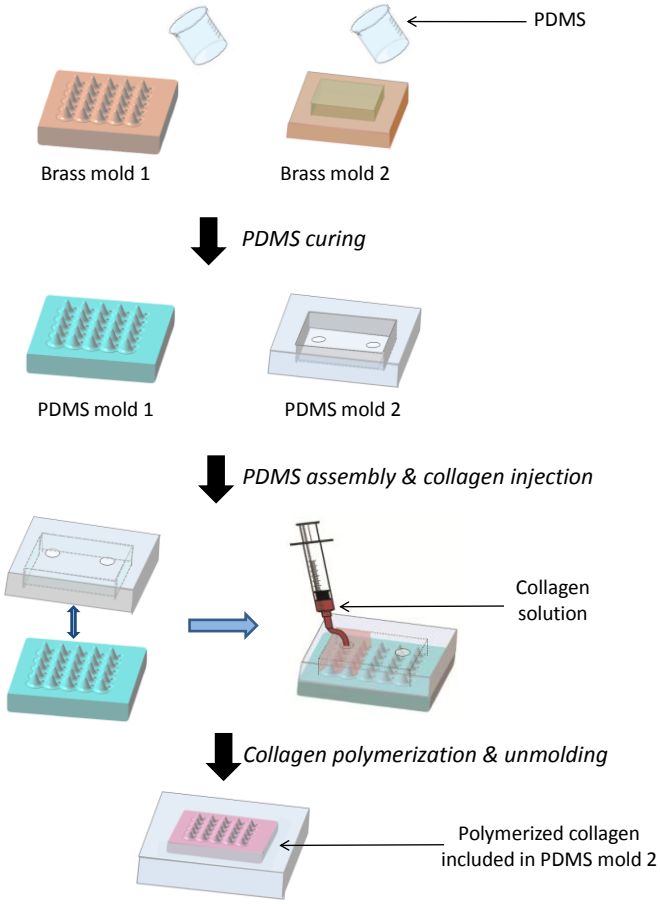

Figure 47: *Processing of the collagen scaffolds*

To evaluate our collagen molding strategy, we first verified that the structure imposed by the PDMS mold was identically replicated by collagen at each concentration. The height of the microstructures was measured using fluorescent collagen gels (TAMRA labelled collagen of concentration ranging from 2 to 6 mg/mL) after unmolding and compared to those of PDMS mold (Figure 48).

i)

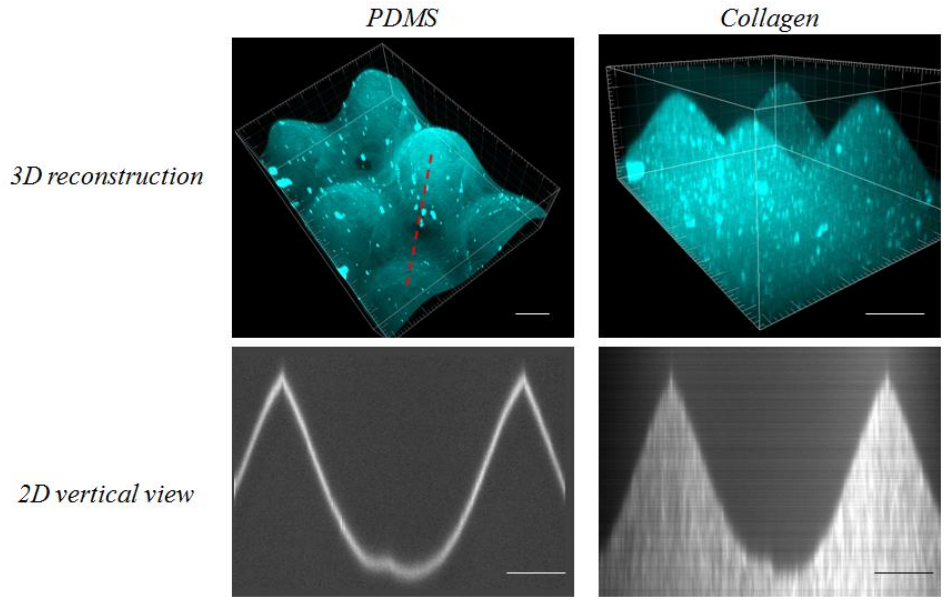

ii)

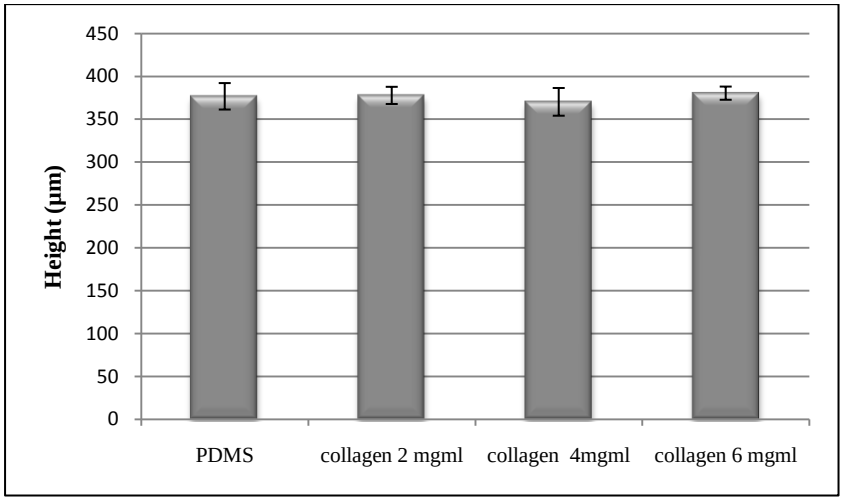

Figure 48: *Reproducibility of collagen molding. (i) 3D reconstruction of the PDMS mold coated with fluorescent BSA and its collagen replica and the corresponding 2D vertical views (along the dotted red line).Scale bars: 100µm (ii) Heights of the collagen microstructure after unmolding depending on the collagen concentration. Mean +/- SD, n=20.The heights are measured from 2D vertical views.*

As shown in Figure 48, the dimensions of the structure were successfully replicated during collagen molding in the range of collagen concentration investigated. It indicates that the polymerization did not cause any retraction in volume of initially injected liquid solution and that the gel did not swell once in contact with the solvent after unmolding. The error bars of collagen gels and PDMS were measured on different area for one replica and on different replica (Figure 48(ii)). The error bars on the PDMS mold directly translate the inhomogeneity of the height of the structure of the initial brass mold. Since the error bars of collagen gels were comparable to those of the PDMS we concluded that collagen faithfully reproduced PDMS structure and that working with collagen did not introduce additional variations to the scaffold structure.

Before seeding the cells on and within collagen gels, it was crucial to confirm that collagen structures were stable over time and did not collapse, especially at low concentrations. The same structures were thus measured at various time points for 20 days (Figure 49).

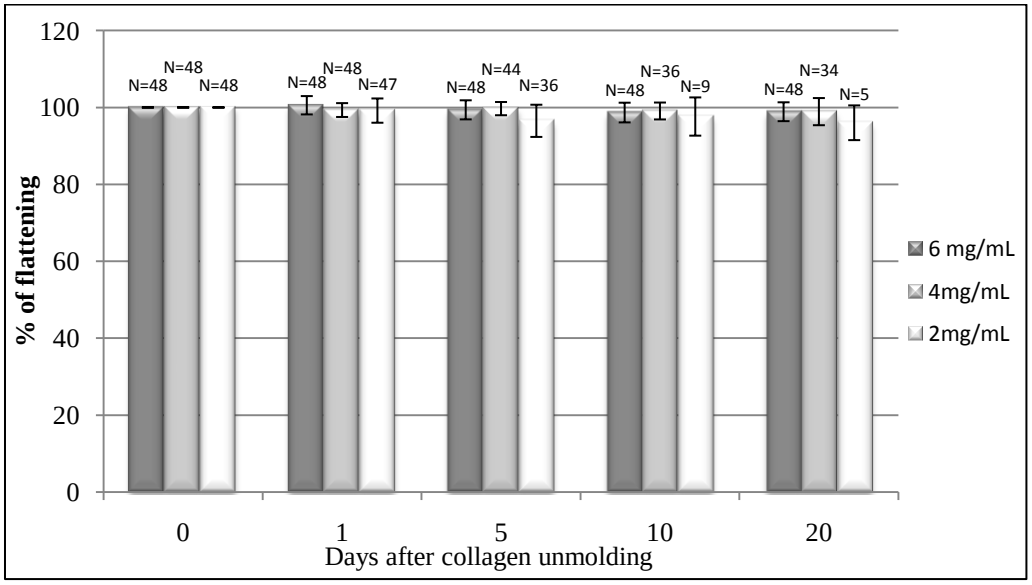

Figure 49: *Evaluation of the percentage of flattening of collagen microstructures through time.(N refers to the number of measurements)*

At each concentration, no significant decrease in height was observed over time and the standard deviation did not exceed 5% attesting of the reproducibility of the experiment and of the stability of the structures.

As we demonstrated that collagen gels successfully replicated the original brass mold and that these structures were stable over time, any variations in height after cell seeding will thus be attributable to cells deforming the structure.

I 3 Remodeling of the matrix by epithelial cells and fibroblasts

The biocompatibility of collagen scaffold does not need to be tested since it is a natural hydrogel extracted from rat tendons. The question was more whether epithelial cells would grow as a monolayer at the surface of the collagen or preferentially invade the collagen to grow in 3D.

Collagen scaffolds were first seeded with cell lines as they are more robust and easier to handle than primary cells. The epithelial human cell lines mostly derive from cancerous cells and are considered as representative cells of the tissue in which the carcinoma has developed. As an example, Caco2 and HT29 cells are derived from human colorectal adenocarcinoma and thus are considered as a model of human colonic epithelial cells. As cell lines derived from small intestine are not so widespread, we decided to work with one of these two cell lines. Finally, Caco2 colonic cell line was chosen over HT29 colonic cell line because the cells grew faster.

Caco2 epithelial cells were seeded on the top of the mold after unmolding. The structure was gently shacked to make the cells sink to the bottom of the structure (Figure 50(i)). The seeding concentration was set so that the cells did not reach confluence on the two days following the seeding since we wanted to confirm that our scaffold promotes not only cell spreading but also cell proliferation on the structure. As shown in Figure 50, Caco2 cells successfully adhered on the collagen scaffold attesting that collagen gels presented a sufficient amount of adhesion ligands on their surface. As they grew, cells spread as a monolayer covering the whole structures. We can thus conclude that the collagen 3D structures we synthesized were adapted to induce the spontaneous growing of dissociated epithelial cells into a confluent monolayer shaped in three dimensions at the micrometer scale.

i) 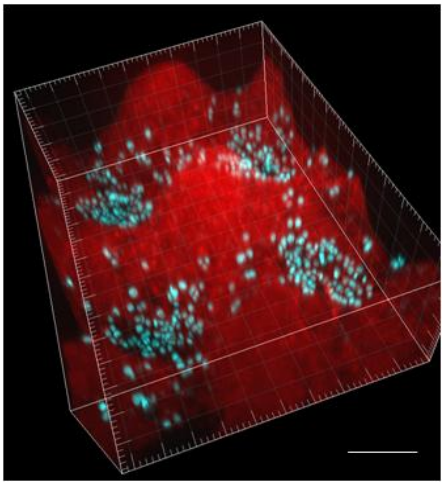 ii) 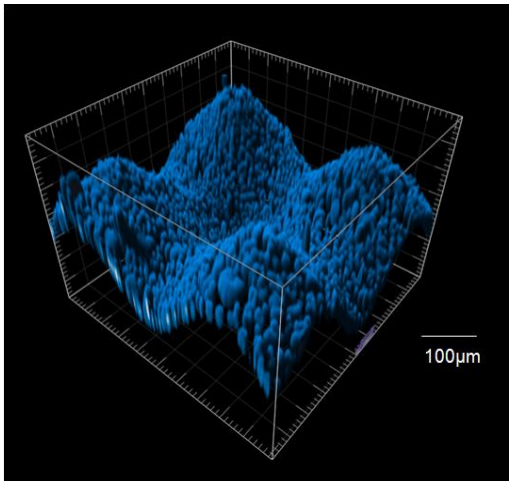

Figure 50: *From isolated single cells to confluent monolayer of Caco2 epithelial cells. (i) 3D reconstruction of Caco2 seeded at the bottom of the crypt on day 0. (Collagen at 10mg/mL labeled in red (TAMRA collagen),Caco2 nuclei in blue(Dapi), scale bar 100µm). (ii) 3D reconstruction of the confluent monolayer formed by Caco2 at the surface of the 10mg/mL collagen structure (Nuclei labeled in blue, Scale bar 100µm)*

However, the final dimensions of the structure covered with cells were lower than the initial dimensions of the collagen gels, as shown in Figure 51. The mechanical forces exerted by epithelial cells on the structure were strong enough to deform the structure. The results obtained showed a decrease in structure height ranging from 33% to 80% (after 5 days of culture), depending on the collagen concentration.

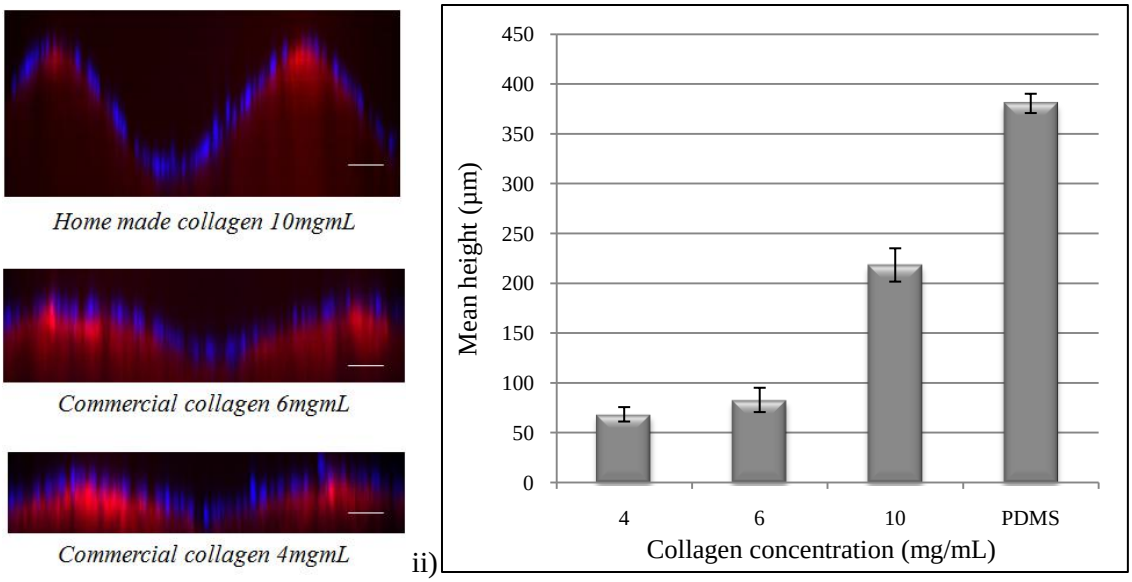

Figure 51: *Caco2 pulling on collagen structure. (i) Transversal cut of collagen structure at various concentrations covered with a monolayer of Caco2. Collagen is labeled in red (TAMRA collagen) and nuclei in blue (Dapi). Scale bars: 50µm (ii) Final height of the collagen structure seeded with Caco2 depending on the initial concentration of collagen. Mean +/- SD, n=20.*

As a control we verified that the PDMS structure was not modified by cell seeding. These results confirmed our previous rheological characterization of collagen hydrogels which indicated that an increasing collagen concentration correlated with a rise in stiffness of those gels (Young modulus being multiplied by a factor 6 between 4mg/mL and 10mg/mL collagen gels). However, even at high concentration these *in vitro* gels exhibit limited mechanical strength compared to *in vivo* matrix since they cannot resist the forces exerted by cells on their surface. Such poor mechanical properties can be explained by the absence of inter-fibrils cross-linking that normally occur *in vivo* and provide more elasticity and strength to the collagen matrices. Without cross-links collagen fibrils have the ability to slide along each other and thus the tension applied by cells might have caused a disentanglement of the fibrillar structure. Besides, arrangements of fibrils into super fibrillar structures which strengthen the matrix are dictated by mesenchymal cells like fibroblasts and thus cannot arise in our system.

In this perspective, fibroblasts cell lines were embedded in the collagen matrix. Concerning fibroblasts cell lines we chose fibroblasts that were extracted from mice embryos and immortalized called mouse embryonic fibroblasts (MEF). The main advantages of these cells compared to other fibroblasts are their ability to secrete matrix and to maintain the stemness of stem cells through their paracrine secretion. We thus expected fibroblasts to secrete their own matrix to provide the future primary epithelial cells a microenvironment more realistic than collagen matrix alone. We also assumed that once in contact with primary epithelial cells they will secrete molecules constitutive of the basement membrane which is present *in vivo* at the boundary between epithelial cells and stromal compartment. In addition, we expected mouse embryonic fibroblasts to maintain epithelial cells at the lower part of

the crypt in their stem cell state. Finally, on a more structural point of view we believed that fibroblasts would cross-link collagen fibrils and thus stiffen the whole scaffold.

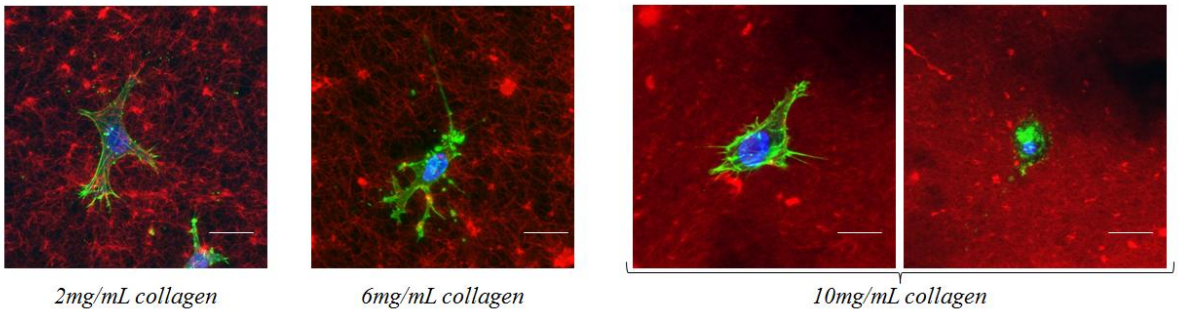

Figure 52: *Pictures of fibroblasts spreading in collagen at various concentrations (2, 6 and 10mg/mL) after 1 day of culture. Nuclei are labeled in blue, actin in green and collagen in red. Scales bar: 20µm*

Fibroblasts were added to neutralized collagen solutions prior to collagen injection in PDMS molds. We first verified that fibroblasts spread well in collagen scaffolds independently of collagen concentration (Figure 52). At low concentration (2mg/mL) fibroblasts spread more and developed larger processes than at higher concentration. The actin bundles seemed also more organized and larger as they were detectable at this resolution only for 2mg/mL concentration. The more collagen was concentrated the thinner fibroblasts protrusions were. At 10mg/mL collagen, fibroblasts barely spread (only 2 small protrusions on the right picture (Figure 52: 10mg/mL collagen) and almost 50% of the cells appeared round and unhealthy (Figure 52: 10mg/mL collagen picture on the left). With regards to the analysis of fibrils density depending on the concentrations, we concluded that the spreading of fibroblasts directly depended on the fibrils arrangement and the more fibrils were entangled, the more fibroblast experienced difficulties to spread.

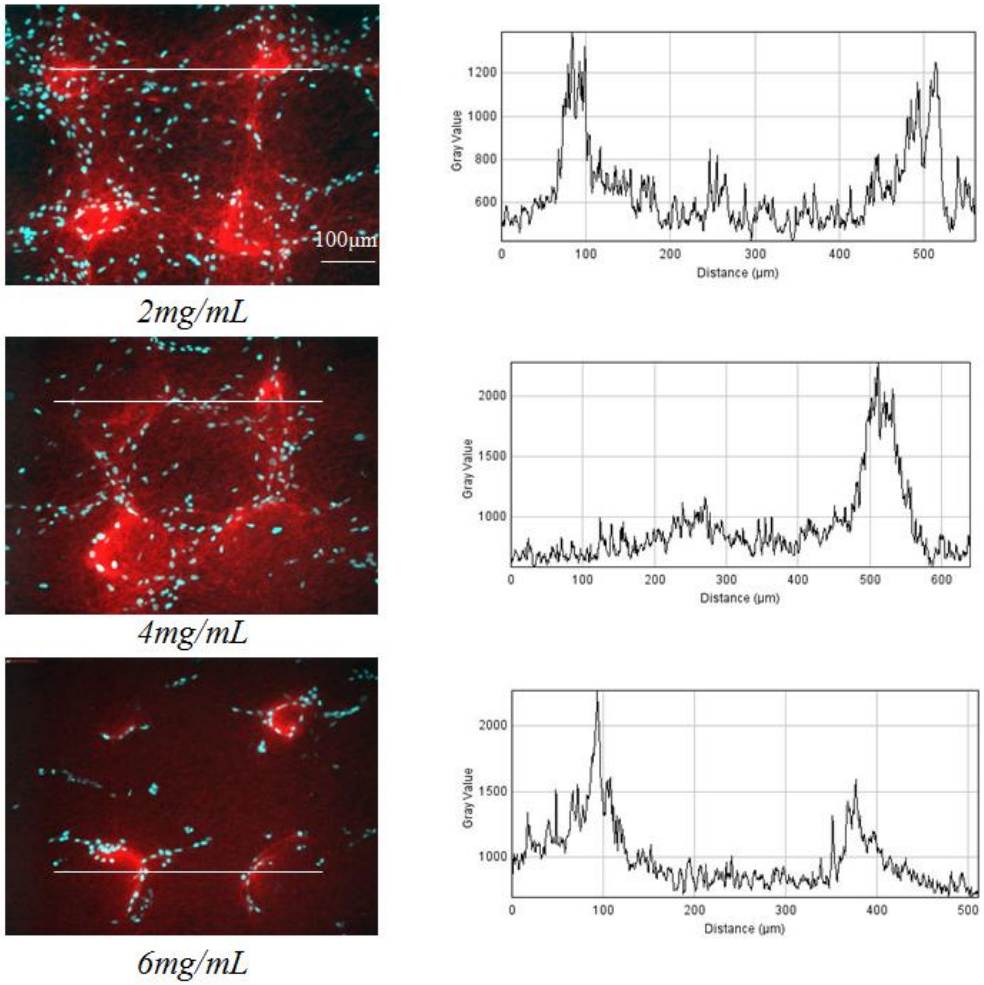

i)

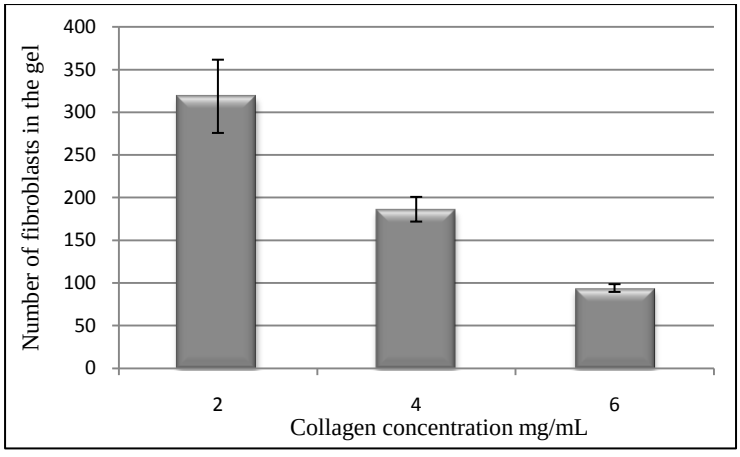

ii)

Figure 53*: Proliferation of fibroblasts in collagen gels after 5 days of culture. (i) 2D projection of the z stacks of collagen gels at different concentrations containing fibroblasts. Nuclei are labeled in cyan and collagen in red. Right: the fluorescent intensity of the collagen along the white lines on the pictures. (ii) Total number of fibroblasts in the collagen microstructures after 5 days depending on collagen concentration. Mean +/- SD, n=20.*

After 5 days of culture, we observed how fibroblasts had proliferated and expanded on the structure (Figure 53). Visually, the cells seemed to proliferate faster in less dense collagen gels (Figure 53 (i)). Indeed, the total number of cells was around 320 cells in 4 microstructures of 2mg/mL collagen gels

whereas we numbered only 100 cells in 6mg/mL collagen (Figure 53 (ii)). The exponential decrease of permeability with increasing concentration of collagen might explain the differences in fibroblasts morphology and proliferative rate (Cross et al. 2010; Ramanujan et al. 2002). Although we did not measure the permeability of our gels, Ramanujan et al calculated for different molecules the ratio of their diffusion coefficient obtained in collagen gels to those in free solutions (Ramanujan et al. 2002). They reported a value of 0.8 for 2mg/mL collagen independently of the size of the molecule considered. Thus, even in low concentration collagen, the diffusion is already lower than in solution. At 10 mg/ml of collagen this value dropped down to 0.6 for small molecules (hydrodynamic radius (Rh) <10nm) and below 0.3 for molecules with a hydrodynamic radius larger than 30nm. Therefore, depending on its concentration collagen may act as a significant barrier to diffusion and may impede fibroblasts survival. Another explanation refers to the differences in fibrillar structure relative to collagen concentration we observed previously. At 10 mg/mL the fibrils were so densely packed that pores were difficult to distinguish among fibrils. Fibroblasts could only spread once collagen was polymerized and the fibrils formed to support cell adhesion. Concerning concentrated collagen, it might be that the fibrils were so densely packed around the fibroblasts that they restrained their spreading. Finally, we also observed that at each concentration the shape and the amount of fibroblasts varied depending on their location within the gel. The deeper they were found in the collagen scaffold the less elongated and numerous they were. This observation suggests that diffusion is not homogeneous inside the collagen gels and that cells in the deeper parts of the hydrogels did not receive enough nutrients. To overcome this problem, collagen hydrogels were supplemented with foetal bovine serum and the other nutrients required for fibroblast proliferation before polymerization. These changes greatly improved fibroblasts survival at high concentration of collagen.

i) 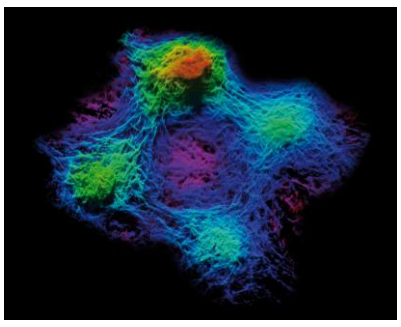

ii) 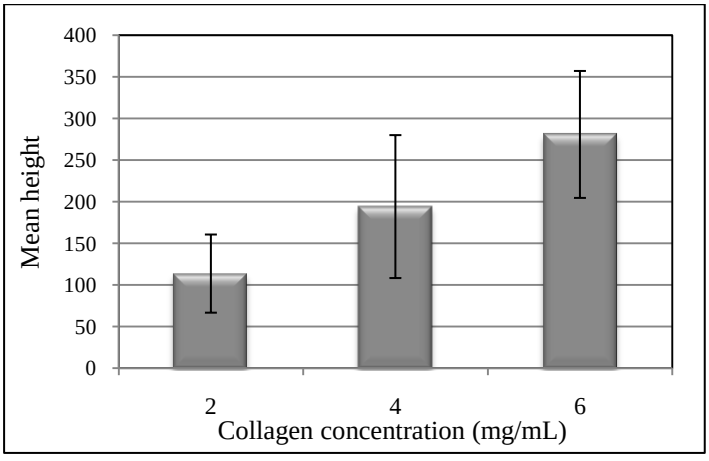

Figure 54: *Remodeling of the matrix by fibroblasts.(i) 3D reconstruction of the collagen matrix after the inhomogeneous pulling of fibroblasts. (ii) Final height of the collagen structure seeded with fibroblasts depending on the initial concentration of collagen Mean +/- SD, n=20.*

Besides their survival and spreading, we have also investigated the influence of fibroblasts on the collagen structure. We measured the residual height of the structures after 5 days of culture as for

Caco2 cells (Figure 54 (ii)). The same tendency was observed: the higher the concentration was the less the fibroblasts deformed the structure. Two hypotheses can explain this observation: either fibroblasts degraded the collagen matrix or they pulled on the structure. The Figure 41(i) is in favor of the second hypothesis. On this figure, the maximal collagen intensity found along the stack for each point is reported on the 2D projection. Therefore, if the collagen is homogeneous the signal should be constant on the 2D projection whereas if the collagen is locally more concentrated then this area should appear brighter than the rest of the structure. On 6 mg/mL collagen, the brightest areas clearly coincided with the presence of fibroblasts. Fibroblasts might thus locally concentrate collagen by pulling on the fibers and cause the flattening of the structure. On 4mg/mL collagen gels only some structures were flatten by the cells (i.e an increased in collagen fluorescent intensity was only noticed for some spots) whereas all the structures were damaged on 2mg/mL collagen (Figure 53(i)). Thus, as for Caco2 cells, the stiffer the gel was the less it was remodeled by cells. Although the comparison might not be relevant due to differences in shape and in proliferation with concentrations previously exposed. Cells that were more elongated and more numerous, at low collagen concentration, should have pulled more on the structures and therefore the gels, depending on their concentration, were not subject to the same amount of stress. Error bars were also significantly larger than the one of the Caco2 experiment. Although fibroblasts were homogeneously mixed in the collagen solution, their distribution in the scaffold varied from one microstructure to the other. Therefore, depending on the number of cells in the microstructure, the microstructure was deformed or not. This is evidenced on Figure 53(i) for 4mg/mL collagen: the top left microstructure which contains a low amount of cell was not flattened whereas the collagen of top right microstructure where cells are more numerous was locally concentrated. The 3D representation of the collagen matrix better represents this spatial heterogeneity. In addition, cell division through time increased locally the density of cells in the microstructure amplifying even more the heterogeneity between microstructures (Figure 54 (i)).

Together, these experiments demonstrated the ability to grow, both on and within the collagen structure we developed, cells that participate *in vivo* to the intestine homeostasis. Regarding, the mechanical stability of the structure, we observed that collagen at low concentration (<6mg/mL) is too soft to resist the forces exerted by the cells in and on the structure. Increasing collagen concentration considerably improves the mechanical properties of the gels but their low porosity significantly hinder fibroblasts survival and spreading inside the gels. Therefore the perfect substrate to constitute our scaffold would be a collagen hydrogel stiff enough to withstand cell forces but with an inner porosity that enables spreading and migration of fibroblasts in the matrix. In the following section, I explain my methodology to select the best approach that would comply with our requirements as well as the results obtained with different strategies.

I. 4 How to strengthen collagen 3D structures?

Based on literature, two major options available to enhance mechanical properties of collagen gel while preserving its porosity were either cross-linking the collagen fibrils to stabilize them and avoid their sliding or adding a stiffer hydrogel to the collagen to generate stiffer semi-interpenetrating polymer networks. We decided to perform our investigations with commercial collagen to avoid batch to batch variations as much as possible.

I. 4.1) Semi-interpenetrating polymer networks

The hydrogels resulting from the mixing of collagen with another cross-linked hydrogel without additional cross-linking between the two hydrogels are called semi-interpenetrating polymer networks which are a subclass of interpenetrating polymer networks.

Interpenetrating polymer network (IPN) are described by the International Union of Pure and Applied Chemistry (IUPA) as 'polymer comprising two or more networks that are at least partially interlaced on a molecular scale but not covalently bonded to each other and cannot be separated unless chemical bonds are broken' (Figure 55). The distinct polymers constituting the final IPN are thus independently cross-linked but not to each other. This absence of cross-linking between distinct polymer types differentiates IPN from grafted polymer and block copolymers (Lohani et al. 2014). In addition, IUPA specifies that 'a mixture of two or more preformed pre-formed polymer networks is not an IPN'. Polymers constitutive of the final IPN should then be mixed as reactants in solution before polymerization (Matricardi et al. 2013). Semi interpenetrating network (SIPN) refers to IPN in which only one constituent is a physical hydrogel meaning that its polymer chains are entangled but not covalently bond as in collagen (Matricardi et al. 2013). IPN and semi-IPN are intensively used in tissue engineering and drug delivery fields. Mixing two different hydrogels permits to couple their mechanical and chemical properties and lead to systems with improved features and therefore extent the scope of application of individual hydrogels (Banerjee, Ray, and Maiti 2010; Lohani et al. 2014; Matricardi et al. 2013).

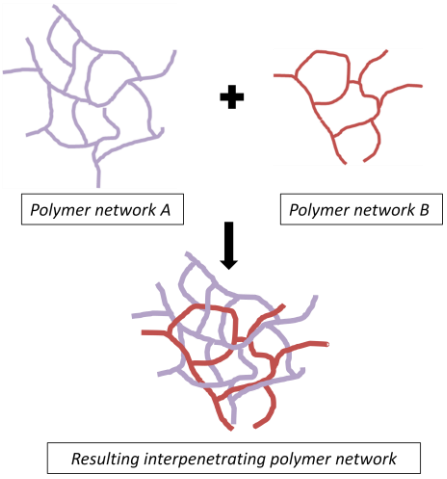

Figure 55: *Schematic presentation of interpenetrating polymer network*

Regarding collagen mechanical properties, we assume that mixing collagen with a stiffer cross-linked hydrogel could prevent fibrils sliding and thus improve the mechanical characteristics of collagen. To remain consistent with our initial goal of providing the cells an environment that resembles as closely as possible the *in vivo* one, we have selected polymers that are present *in vivo* in the ECM to supplement collagen hydrogels.

α) Hyaluronic acid/ collagen semi interpenetrating network

Hyaluronic acid (HA) is a large anionic polysaccharide chain composed by the repetition of a dimer of N-acetyl-D-glucosamine and D-glucuronic acid (J. A. Burdick and Prestwich 2011; Laurent, Laurent, and Fraser 1996). Its size can vary from 100 kDa to 8000 kDa. HA is ubiquitous in the human body and is the major constituent of synovial and soft connective tissue. HA molecules are organized in an entangled polymer network but they do not spontaneously form fibrillar reticulated network like collagen. The HA chains are hydrophilic and have the ability to retain water. This ability enables HA chains to act as lubricant in articulation joins. Another characteristic of HA is its high renewal rate estimated at 0.5 to 1 day which has a major impact on the osmotic pressure of the ECM (Laurent, Laurent, and Fraser 1996). Rapid changes in concentration of HA combined to the hydrophilic properties of its chains causes fluid flow in the matrix which contributes to morphologic changes of the ECM (§ 1.1 embryonic morphogenesis of the intestine).

In vitro, HA chains in solution exhibit low mechanical properties. Chemical modification of HA chains are thus necessary for them to covalently bond and form a hydrogel. This can be performed by addition/condensation chemistry or radical polymerization. By tuning the amount of cross-linker, Disher et al (Rehfeldt et al. 2012) succeeded to synthesize hyaluronan hydrogels with Young Modulus ranging from 0.1 to 100kPa. Rheological features of these hydrogels thus significantly differ from the native properties of HA (Collins and Birkinshaw 2012).

Depending on the chemical function grafted on the polysaccharide chains, HA hydrogels are either formed by chemical cross-linking or by photo-crosslinking. Chemical cross-linking is mostly performed on the alcohol function of N-acetyl-D-glucosamine and on the carboxylic function of D-glucuronic acid. In many cases they involved toxic cross-linker as 1-Ethyl-3-(3-dimethylaminopropyl) carbodiimide (EDC) or required the use a toxic solvent such as dimethylformamide (Collins and Birkinshaw 2012). Such toxicity would thus prohibit the seeding of fibroblasts in the solution prior to crosslinking. Chemical modifications of HA chains (like thiol modification) can induce spontaneous chemical crosslinking in aqueous solution but these reactions are slow since they are hindered by anionic repulsion of the HA chains (Shu et al. 2003). To overcome this kinetic limitation, additional cross-linker can be mixed to the HA solution: polyethylene glycol diacrylate (PEGDA) has been commonly used as cross-linker (J. A. Burdick and Prestwich 2011; Nimmo, Owen, and Shoichet 2011; Rehfeldt et al. 2012). The addition of a synthetic hydrogel to thiol-modified hyaluronic acid solution is necessary to successfully complete the formation of HA hydrogel.

As it will be discussed in the following section, there are arguments in favor of HA photo-crosslinking. In general manner photo-crosslinking allows a more effective control of HA crosslinking. It only occurs under UV exposure while chemical reaction can still happen after cell seeding if all reagents did not react and this may lead to modifications of the properties of the hydrogel during the course of the experiment. The degree of cross-linking can be tuned at various levels including the UV dose (time and power of exposure), the concentration of photo-initiator and the rate of functionalization of HA chains even though this last point is more difficult to control. Photo-crosslinking can be performed in aqueous solutions compatible with collagen solutions. It only requires the addition of photoinitiator which are small molecules that can be washed out after polymerization compared to the large PEGDA polymer chains that are included in the final chemically cross-linked hydrogel. A major drawback of photo-crosslinking is related to the fact that these photoinitiators are known to generate cytotoxic radicals. However, studies performed on photocrosslinked collagen-HA SIPN reported a great rate of survival of the cells embedded in those hydrogels (Brigham et al. 2009; Suri and Schmidt 2009, 2010; Suri et al. 2011).

Concerning mechanical properties, Suri and Schmidt (Suri and Schmidt 2009) showed that the photocrosslinking of HA improved the values of both the storage modulus G’ and the loss modulus G’’ by a factor of 10 to 100 compared to non cross-linked HA/ collagen hydrogels. They mentioned that increasing concentration of HA correlated with increasing values of storage modulus. Mechanical testing on collagen/HA SIPN reported mechanical features of hybrid hydrogels were mostly attributable to HA as the fracture stress of composite material was similar to metacrylated HA only (Brigham et al. 2009). However, addition of collagen to HA greatly improved cell survival, which was nearly inexistent in photocrosslinked HA alone. In a more general manner cells can only adhere to HA if they express one of the three following receptors: CD44, RHAMM or ICAM-1. This therefore

notably reduces the number of cell types that have the ability to survive on those hydrogels. A last point crucial to our device is the possibility to structure HA in three dimension at the microscale by UV exposure through a PDMS mold (Khademhosseini et al. 2006).

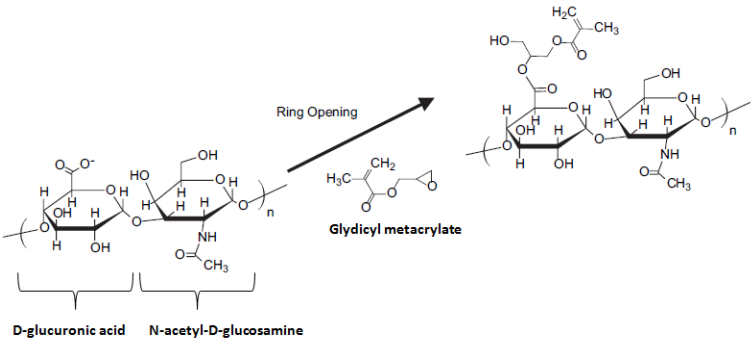

Figure 56: *Mechanism of the grafting of glycidyl methacrylate on hyaluronic acid chain. Imported from* (Bencherif et al. 2008) *with modifications*

Referring to literature we decided to graft glycidyl methacrylate groups as reactive functions to crosslink the HA moieties. Glycidyl methacrylate was selected instead of methacrylate groups since they appeared to be more reactive (Brigham et al. 2009; Suri and Schmidt 2009). Glycidyl metacrylate (GM) is expected to react with each glucuronic acid of the HA chains (Figure 56) (Bencherif et al. 2008). The first step consisted in grafting glycidyl methacrylate groups on HA and the percentage of methacrylation (the ratio of glycidyl methacrylated molecules grafted to total number glucuronic acid per chain) on the HA was further evaluated by nuclear magnetic resonance. Optimization of the grafting protocol and nuclear magnetic resonance analyses were performed with the precious help of Nadège Pantoustier ('Sciences et ingénierie de la matière molle-physico-chimie des polymers et des milieu dispersés' lab, UMR 7615, Ecole Supérieure de Physique et de Chimie Industrielles de la ville de Paris). The grafting optimization allowed achieving a grafting percentage of 50% (see Material and methods for protocol). According to literature, at this degree of methacrylation, hyaluronic acid should be added at a concentration of at least 50mg/mL to significantly improve the mechanical properties of HA-collagen SIPN (Brigham et al. 2009). Because we expected that the addition of HA to the matrix will reduce collagen matrix porosity and thus impede the survival of fibroblasts, the first set of experiments was performed at low collagen concentration (collagen at 4mg/mL) (§I. 3 Remodeling of the matrix by epithelial cells and fibroblasts). Irgacure was the photoinitiator chosen for its reduced cytotoxic properties (Panda et al. 2008). The GM-HA/collagen mixture was injected in the mold. The collagen was first allowed to polymerize, then the gel in the enclosed PDMS chamber was exposed to UV light (8mW/cm² for 5 minutes) to further crosslink the GM-HA and the resulting SIPN hydrogel was then unmolded and rinsed several times (see material and methods).

We first demonstrated that the scaffold biocompatibility was maintained with SIPN for epithelial cell lines. Caco2 epithelial cells successfully grew and spread as a monolayer on the hybrid GM-HA/collagen hydrogel. The final height of the microstructures was measured when the cells reach confluence (after 5 days as for collagen only) and was compared to the control 4mg/mL collagen gel seeded also with Caco2 cells (Figure 45).

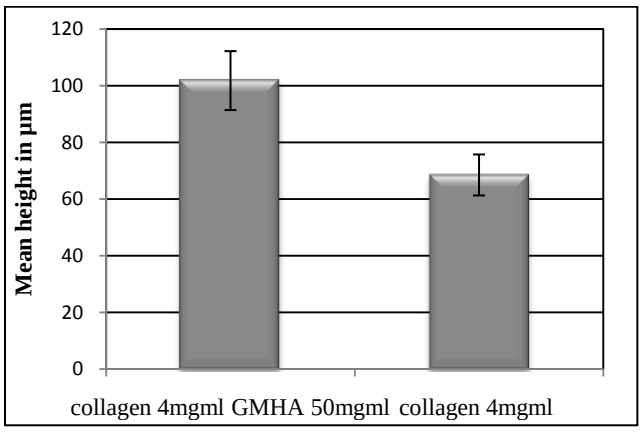

Figure 57: *Comparison of the final height of collagen-HA SIPN vs collagen scaffolds both seeded with Caco2. Mean +/- SD, n=20.*

As shown in Figure 57, the microstructures of HA/ collagen SIPN were less deformed by cells; the microstructures made GMA-HA/collagen were higher than the collagen ones. Thus, the interpenetrating hydrogel has slightly improved collagen mechanical properties. However, the final height was still far beyond the initial height of ~ 400 µm and also below the height obtained with highly concentrated collagen at 10 mg/mL (~ 230 µm). This result was surprising since we expected HA to notably improve the resistance of collagen gels to forces exerted by cells. Our hypothesis was initially supported by the modification of the fibrillar structure of the collagen gels by cross-linked HA observed by Brigham et al (Brigham et al. 2009). They examined the architecture of collagen and cross-linked HA independently and compared them to the network formed by the entangled collagen and cross-linked HA (Methacrylated HA: MeHA in their experiments) using scanning electron microscopy (SEM). They noticed that the HA/collagen SIPN structure was a mix of the fibrous structure of the collagen and of the flaky structure of cross-linked HA: collagen fibrils appeared interconnected with HA flakes (Figure 58). Since we neither performed SEM nor labeled fluorescently HA chains in our samples, we were not able to confirm their observations.

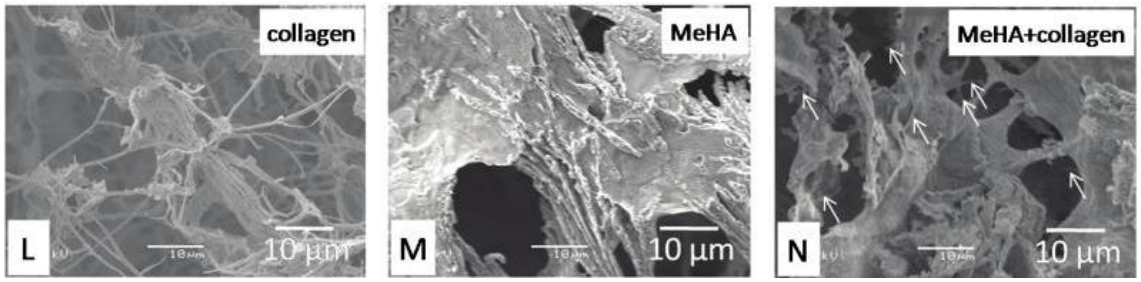

Figure 58: *Architecture of the Collagen/ HA SIPN experienced by cells. SEM micrographs (x 2000) of (L) the fibrous collagen, (M) the porous flaky cross-linked methacrylated HA and (N) the hybrid network of collagen fibrils (white arrows) interconnected with HA flakes in the collagen/HA SIPN. Imported from* (Brigham et al. 2009)

The preservation of a porous structure in the HA/collagen SIPN would have been in favor of fibroblasts survival in the scaffold. On the contrary, when we added mouse embryonic fibroblasts in the cross-linked HA/collagen matrix, they were all found dead on the first day of culture. Such lethal damage could either come from the free radicals generated in the matrix upon UV activation or directly from the UV radiation itself. The fibroblasts seeded in 4mg/mL collagen and UV irradiated at the same dose survived. Thus, even though previously it has been reported that NIH3T3 fibroblasts can survive in cross-linked scaffolds (Brigham et al. 2009), in our experiments, the radicals generated during UV radiation seemed to be lethal to the fibroblasts we used. We could have pursued this SNIP strategy, especially by tuning the toxicity of the polymerization step. One possibility would have been to decrease either the GMA-HA and/or photoinitiator concentration or the UV dose but since the improvement related to the addition of HA at this concentration was already really low compared to an increase in collagen concentration, we concluded that cross-linked HA was not adapted to our device and we thus did not investigate further this HA SIPN approach.

β) Fibrin/ collagen semi interpenetrating network

The second candidate we investigated to mix with collagen and to generate a stiffer SIPN was fibrin. Fibrin molecules are the products of the reaction occurring between fibrinogen and thrombin. Fibrinogen is a 45 nm long plasma protein highly synthesized together with thrombin in case of wound. Fibrinogen is constituted of a central region (E) bordered by two similar domains (D) (Figure 59 (i)). Thrombin first catalyzes the maturation of fibrinogen into fibrin molecules and then catalyzes the arrangement of fibrin molecules into a cross-linked fibrillar network (Figure 59 (ii)).

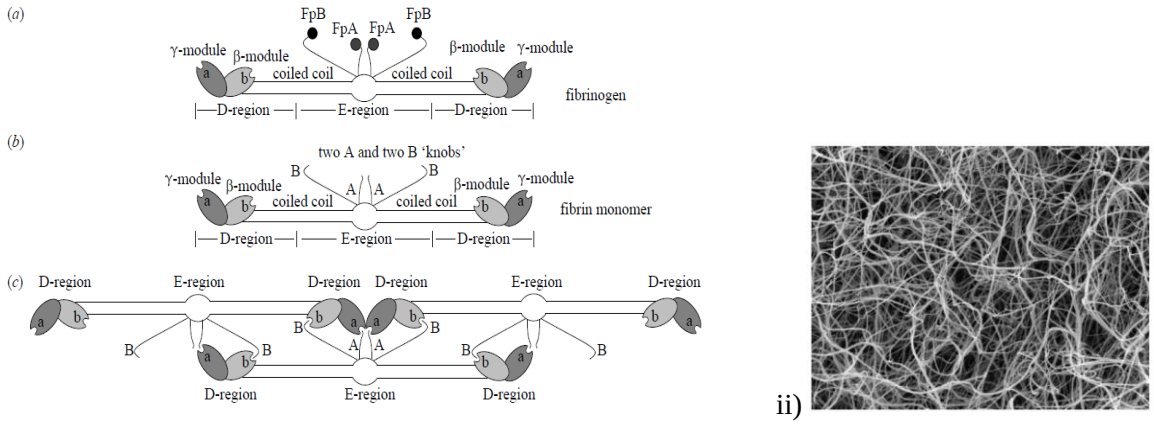

i) ii)

Figure 59: *Fibrin cross-linked fibrillar network. (i) a) fibrinogen monomer b) fibrin monomer resulting from molecular changes of A and B knobs catalyzed by thrombine c) assembly of fibrin monomers into protofibrilsalso catalyzed by thrombine. (ii) Scanning electron micrograph of 1mg/mL fibrin hydrogel. Full width of the figure is 62,5µm. Imported from* (Janmey, Winer, and Weisel 2009)

Fibrils are made of fibrin molecules laterally staggered so that D domains of one molecule are cross-linked to the E domain of the neighboring molecule. Fibrils are further arranged in supramolecular structures with lateral branching that result in a dense network (Mosesson, Siebenlist, and Meh 2001). *In vivo*, the first phase initiated after blood injury is hemostasis. During hemostasis, fibrin together with fibronectin clots in the wound and form a provisional matrix that closes the wound. Immune cells then deposit on this matrix during the inflammation stage to contain microorganism and to locally activate fibroblasts and epithelial cells. The provisional matrix chemoattracts the activated fibroblasts and stimulates them to secrete a new matrix. Provisional matrix also enhances vasculogenesis to irrigate the newly synthesized matrix. Throughout the wound healing process, the provisional matrix is gradually degraded by the surrounding macrophages (Strodtbeck 2001).

Fibrin network is also found in the contiguous matrix enclosing some tumors. In these particular cases, fibrin is assumed to be secreted by tumor cells themselves. Fibrin participates in stiffening the fibrotic stroma enveloping the tumor. It also promotes the vascularization of the tumor and acts as a filter against immune reaction from the body (Costantini and Zacharski 1992; Ghosh et al. 2008). Similarly circulating tumor cells are also protected from immune reaction that could occur in blood as they are surrounded with fibrin when they detach from the tumor (Lu et al. 2015).

The ability to use fibrin to easily generate biocompatible resistant and relatively stiff hydrogels (up to 5kPa (Duong, Wu, and Tawil 2009)), has found applications in tissue engineering and pharmaceutical communities. Thanks to its fast polymerization combined to its mechanical properties, fibrin is now commercialized as a surgical sealant (www.tisseel.com). Mechanical properties of fibrin hydrogel are mostly dictated by the initial fibrinogen concentration. Higher fibrinogen concentration generates denser, less porous and stiffer hydrogels. Thrombin only modifies slightly the rheology of those hydrogels (Duong, Wu, and Tawil 2009). The rigidity of highly concentrated hydrogels (34 mg/mL

fibrinogen) is sufficient to induce osteogenic differentiation while low concentration (5 mg/mL) fails to induce such differentiation (Catelas et al. 2006). Therefore, we considered that adding fibrin to our collagen hydrogels in SIPN configuration could improve their mechanical properties.

The slow degradation of fibrin *in vitro* and *in vivo* is also a considerable asset. *In vivo*, this moderate disintegration allows the large drug molecules encapsulated in the hydrogel to gradually diffuse in the area where the fibrin has been injected. Concerning *in vitro* application, fibrin is known to have ability to retain the molecules (growth factors or ECM molecules) secreted by embedded and surrounding cells (Janmey, Winer, and Weisel 2009). Fibrin would thus promote the maintenance of a niche-like environment in our device by first stimulating ECM secretion by fibroblasts (Pawelec et al. 2015; Ye et al. 2000) and then by holding the local molecules secreted by the surrounding cells. Furthermore, the degradation of fibrin over time can be limited by the addition of aprotinin in the medium (Ye et al. 2000). It would thus allow us to initially slow down the degradation of fibrin to constrain the cells in the given topography until they secreted their own matrix.

Finally the study of Koroleva et al (Koroleva et al. 2012) confirmed that fibrinogen could faithfully replicate the three dimensional microstructures from a PDMS mold by first pouring a fibrinogen solution on the PDMS mold and then adding the thrombin solution.

According to literature, fibroblasts encounter difficulties to survive and spread in fibrin hydrogel concentration exceeding 5mg/mL (Duong, Wu, and Tawil 2009). Thus, we decided to evaluate the influence of fibrin in a concentration below this value. From a more practical point of view, the fibrinogen concentration investigated in this study has been limited due to solubility issues. Fibrinogen had a low solubility in collagen neutralized solution. Fibrinogen/collagen mixture was not homogeneous when the collagen concentration exceeded 2mg/mL (Figure 60(i)). Starting from a neutralized collagen solution at 2mg/mL, the higher fibrinogen solution we could reach was 2mg/mL. This observation was supported by literature, since the total amount of protein (cumulative concentration of collagen and fibrin) in fibrin/ collagen SPIN was never reported to exceed 5mg/mL (Boudou et al. 2012; Cummings et al. 2004; Rao et al. 2012; Rowe and Stegemann 2006).

Fibrinogen/collagen solutions were injected in PDMS molds. Once collagen was polymerized, the hydrogels were unmolded and incubated with a solution of thrombin for 5 minutes to cross-link the fibrinogen into a fibrin network.

Contrary to the HA/collagen SNIP, the fibrin/collagen SIPN did not replicate perfectly the PDMS mold structure. A comparison of the final height of the structures revealed that the presence of cross-linked fibrin induced a global shrinking of almost 25% of the original size of the hydrogel (Figure 60 (ii)). To go further in the analysis, we compared collagen-fibrinogen hybrid hydrogel before and after the maturation into collagen-fibrin hybrid and we realized that the addition of thrombin was the cause

of the retraction of the hydrogel (Figure 60 (ii)). We thus considered the possibility to mix initially thrombin with the fibrinogen/collagen solution to induce first the cross-linking of fibrin and then the polymerization of collagen. However, we were not able to achieve this process as fibrin polymerized before the end of the injection of the solution in the mold.

i) 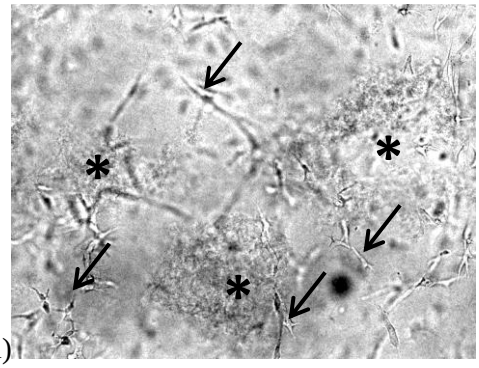

ii) 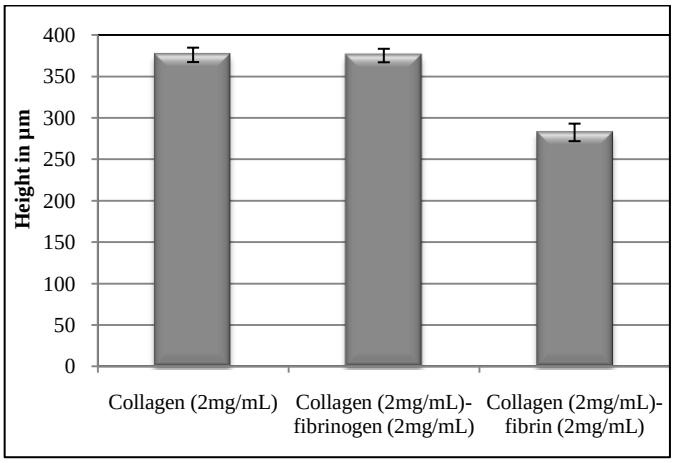

Figure 60: *Collagen/ Fibrin SIPN.i) Inhomogeneity of the SIPN obtained with 4mg/ml collagen and 2mg/mL fibrin. (*) present clots of fibrin in the collagen matrix and black arrows point fibroblasts seeded in the matrix. (ii) Histogram reporting the final height of the structures replicated either with collagen only, with collagen and fibrinogen or with collagen and fibrin which correspond to collagen-fibrinogen hydrogel subsequently cross-linked with thrombin. Mean +/- SD, n=20.*

Even though the cross-linking by thrombin generated some shrinking of the structure, fibrin could still be considered as an option. If fibrin-collagen SIPN was strong enough to resist cell tension, we could oversize the initial mold to compensate this shrinking. Unfortunately, fibrin-collagen SIPN was not stiff enough and the final height structures were not significantly higher (~ 75µm) than those obtained with 4mg/mL collagen (~68µm), both structures being seeded by Caco2. Furthermore, we noticed that Caco2 cells adhered less and took more time to reach confluence on fibrin-collagen SIPN compared to collagen alone as we had to wait for 10 days for cells to reach confluence compared to the usual 5 days. We assumed that if cell lines experienced difficulties to proliferate on such hydrogel it could be even worse for primary cells. Because of the low mechanical improvement combined with the limited cell proliferation, we did not investigate fibrin/ collagen alternative any further.

Even though the SIPN approach showed its ability to stiffen the collagen structure, this stiffening was limited and biocompatibility issues have been observed. We thus investigated another approach consisting in a direct cross-linking of collagen fibrils to stabilize the structure and prevent fibrils sliding.

I. 4.2 Chemical cross-linking of collagen fibrils

Among the various methods developed in literature to cross-link collagen, we excluded strategies involving chemical grafting on collagen fibers and enzymatic cross-linking. Indeed, we have previously shown that GM-HA photo-crosslinking generated (§ II.4.1.α) radicals that are lethal to

fibroblasts. In addition, the grafting of glycidyl methacrylate or methacrylic anhydre on collagen requires neutralizing the collagen stock solution. This reaction results in the precipitation of functionalized collagen and puts some question regarding a possible initiation of fibrillogenesis along this step (Tronci, Russell, and Wood 2013; Tronci et al. 2014). Therefore, functionalization of collagen by photocross-linking was not further considered. Polyhydroxyethylmethacrylate functionalization is also intensively used to engineer stiff dentin pulp starting from raw collagen but the chemical catalysts and solvent used to cross-link collagen are cytotoxic and thus would not be compatible with fibroblast seeding in the bulk of the microstructures (Jeyanthi and Rao 1990).

Concerning enzymatic cross-linking of collagen fibrils, it is often performed with lysyl oxydase enzyme (LOX) both *in vivo* and *in vitro* (see introduction of Chap2). One of the major disadvantages of working with enzymes is that they only catalyze a reaction between two products in a given conformation. In particular, LOX only cross-links collagen molecules in their native fibrillar form namely molecules that are 4D staggered (see § II). Since collagen molecules *in vitro* are not as well arranged as *in vivo*, collagen treated with LOX only presents 3 times more cross-links compared to control hydrogels and the elastic modulus of the gels is only improved by a factor 1.2 (a-M. Baker et al. 2012). We considered that this improvement was too low with regards to the longtime of incubation needed (at least 5 days).

In the earlier description of the *in vivo* collagen fibrillogenesis, we introduced two different modes of cross-linking that occur *in vivo*: condensation between lysines catalyzed by LOX and glycation (See introduction of Chap.2). Condensation of lysines was set aside for the reasons previously mentioned. We thus focused on reproducing glycation reaction since it would both strengthen collagen structures and be consistent with the chemical modification occurring *in vivo*.

α) Glycation

Collagen glycation spontaneously occurs *in vivo* and results from the condensation of reducing form of a glucose molecule and the amino group of collagen proteins. Reducing sugars represents a sugar opened chain with an aldehyde group. The kinetic of glycation reaction *in vivo* is limited by the low amount of glucose under the reducing form. Once the reducing sugar is formed there is a nucleophilic addition of the amino nitrogen on the carbon with the aldehyde function. This reaction is called Maillard reaction which produces a reactive intermediate called Shiff base and release a molecule of water. The Schiff base product then rearrange into Amadori product. Amadori products evolved in time into Advanced Glycated End products (AGE) through a combination of chemical reactions (dehydration, oxidation and cleavage) which is not clearly elucidated. Advanced glycated end products act as cross-linkers between collagen molecules (Figure 61).

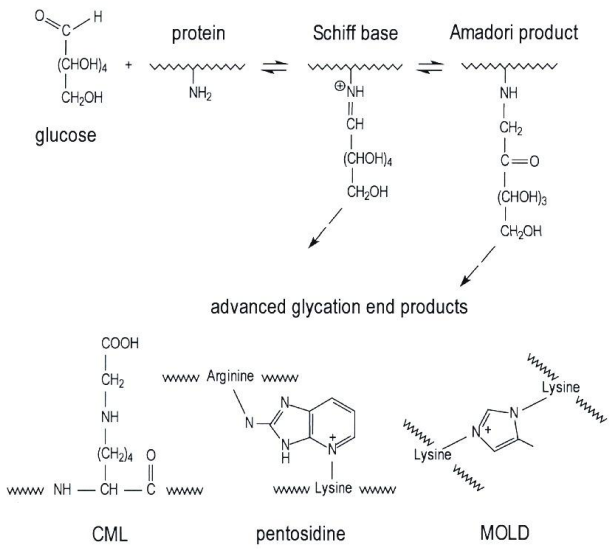

Figure 61: *Scheme of the chemical reaction that generates advanced glycation end products. 1) aldehyde form of glucose molecule reacts with protein, 2) Schiff base produced during nucleophilic addition of amine 3) molecular rearrangement into Amadori product and 4) evolution into advanced glycation end products like pentosidine, carboxymethyllysine (CML) and methyl glyoxal-lysine dimer (MOLD).*

In vitro the reaction can be accelerated by replacing glucose by ribose which is more reactive. Sugars can be added before or after collagen polymerization but an incubation of at least 3 days is needed to observe significant changes in collagen stiffness (Francis-Sedlak et al. 2009; Mason et al. 2013). Since the addition of concentrated sugar for such a long time in cell culture media could create a hypertonic environment causing the death of cells, we added ribose to collagen acid solution and leave it for 5 days at 4°C under constant shaking for ribose to graft on collagen molecules as reported in literature (Mason and Reinhart-King 2013; Mason et al. 2013). Addition of 200mM ribose to 1.5 mg/mL collagen increased the stiffness of the matrix by a factor 3 (Mason and Reinhart-King 2013; Mason et al. 2013). However, the authors noticed that fibrillogenesis and the resulting fibrils were altered by ribose for concentration exceeding 150mM: the nucleation phase was delayed and the collagen fibers were larger. Since the two studies are performed at low final collagen concentration (1.5mg/mL), we chose the same concentration to confirm their results. In addition, we chose an additional intermediate concentration of 4mg/mL as stock solution. More concentrated solutions would have been difficult to homogenize with ribose given their viscosity. The results of the deformation of the glycated structures by Caco2 cells are shown in Figure 61(i) for collagen at 4 mg/mL.

i)

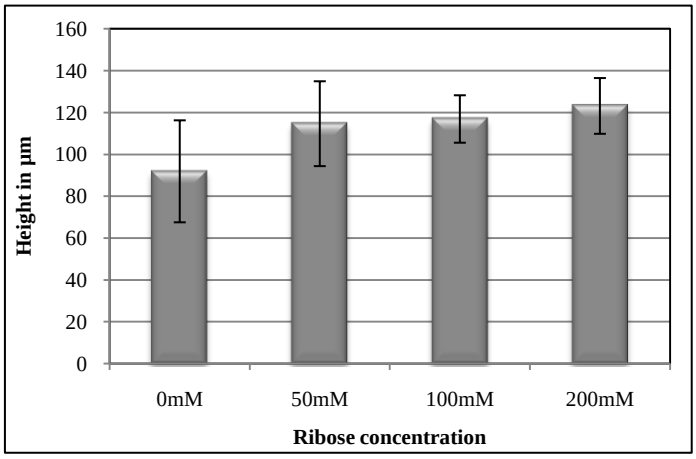

ii)

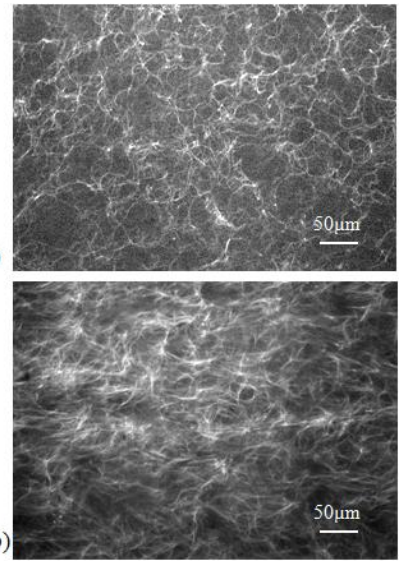

Figure 61: *Collagen cross-linked by glycation. (i) Table of the final height of 4mg/mL collagen gels seeded with Caco2 depending on the concentration of ribose they were incubated with. Mean +/- SD, n=20. (ii) Structure of 4mg/ml collagen fibrils (TAMRA collagen) (a)incubated for 7 days with 100mM ribose (b) control 4mg/mL collagen.*

The glycation of collagen by ribose does not alter the gels biocompatibility as Caco2 as cells were able to grow on the structure and the glycation improved to some extent the collagen gel stiffness (Figure 61 (i)). It seemed that 50mM ribose increased collagen stiffness but that a plateau was reached for higher concentration (Figure 61 (i)). As described in literature we also noticed some delay in the polymerization of collagen with ribose at 200 mM although we did not observe significant changes in collagen fibrils. Based on these encouraging preliminary results we incubated collagen (4mg/mL) with ribose (100 mM) for a longer time (7 days) expecting an increased stiffness of the material. We were surprised to observe that the fibril network appearance was modified by this longer reaction time. The collagen solutions took twice the normal time (about 1 hour) to polymerize after injection in PDMS molds and the resulting network almost completely lost its fibrillar structure and looked more like a cross-linked network (Figure 61 (ii)). These results confirmed the observation of Mason and Reinhart that a high the degree of glycation of collagen molecules severely impedes collagen fibrillogenesis. Finally, the hydrogel obtained in these conditions is so soft that it was not able to handle the structure after unmolding and the pores size was so large that the epithelial cells seeded on the top of the structure felt across the whole depth of the hydrogel. We thus concluded that the addition ribose effectively stiffen collagen hydrogels and seemed a good approach to mimic glycation reaction occurring *in vivo*. However, the improvement of the mechanical properties was not sufficient to resist the tension forces exerted by the cells, in particular because the use of ribose is limited by the range of concentration and reaction time applicable. In addition to impede fibrillogenesis, accumulation of AGE can also be damageable for the cells inside the matrix. Glycation reaction chemically modifies the proteins and therefore alters the signaling they convey to adhering cells. The presence of AGE activates specific receptors called receptors for advanced glycation end products (RAGE) that are

present in various cells types such as smooth muscles cells, macrophages, endothelial cells, microglia, and fibroblasts (Alikhani et al. 2005). RAGE activation in dermal fibroblasts has been reported to reduce matrix production (Owen et al. 1998) and to induce apoptosis through the activation of caspase 8 and 9 synthesis (Alikhani et al. 2005). In the highly glycated matrix of diabetic mice the speed of wound healing is slower due to a lower secretion of matrix and low proliferative rate of fibroblasts (Goova et al. 2001). Given the low mechanical improvement and the potential toxicity of highly glycated collagen matrix, we concluded that ribose was not the best candidate for our application.

Since this physiological alternative did not meet the requirements (especially regarding mechanical stability) to achieve a candidate structure for biomimetic intestine, we decided to investigate chemical cross-linkers that are known to effectively cross-link and stiffen collagen gels even if they could be cytotoxic.

β) Glutaraldehyde cross-linking

Glutaraldehyde is known to be toxic for cells as its aldehyde functions easily react with the amino group of the cell proteins. However, based on the same reaction process glutaraldehyde is also considered as a powerful collagen cross-linker.

Glutaraldehyde is mostly used in tissue engineering to cross-link collagen sponges rather than collagen hydrogels. Collagen sponges are made of collagen hydrogels that are freeze-dried and lyophilized. The resulting matrix is solid and porous and looks like a sponge. This porous structure can be reinforced by glutaraldehyde cross-linking (G. Chen, Ushida, and Tateishi 2001; Narotam et al. 1995). Collagen sponges are widely used as grafts in surgery. As an example, the DePuy Synthes Company commercialized bovine collagen grafts as dural graft implant (Duraform product). The use of collagen sponge bypasses the delicate step of stitching dural tissues after brain surgery. The cross-linking of these collagen sponges maintains the porous structure by reinforcing the whole architecture and also reduces immunogenicity of the grafts since it reacts with the amino functions of any proteins including those that could induce an immune reaction of the host. The porous structure of the sponge allows the migration of fibroblasts inside of the implants and the synthesis of a new matrix. Collagen sponges are particularly indicated in the case of dural implants since they can absorb cerebrospinal fluid without swelling (Narotam et al. 1995).

Glutaraldehyde cross-linking is also used to preserve the structure of porcine valves implanted into the heart of humans. Glutaraldehyde cross-linking reduces the degradation of the valve and as previously mentioned erase the last cells or proteins that could trigger immune reaction (Vesely 2005).

The use of glutaraldehyde cross-linked collagen as implants testify of the non toxicity of this matrix. Furthermore, osteoblasts proliferated two times faster in glutaraldehyde cross-linked collagen scaffold than on raw collagen scaffold certainly due to the increase in the matrix stiffness (D. C. Chen et al.

2007). In addition, osteoblasts were not able to contract the cross-linked matrix anymore as the surface of the scaffold remained constant after 7 days of culture compared to control samples that experienced a 50% decrease in size. This impressive improvement of mechanical properties of collagen hydrogels while maintaining their porous structure was particularly interesting for our device.

Bowes et al studied the reactivity of aldehyde to cross-link collagen depending on the number of carbons in their molecular backbone (from 2 to 6 carbons) (Bowes and Cater 1968). They observed that the maximal reactivity was obtained with the 5 carbon glutaraldehyde molecules. Glutaraldehyde in aqueous solution is present as a mixture of different forms from monomers (molecule I in Figure 62) to polymers that can all be declined in their opened or cyclic molecular forms (Figure 62).

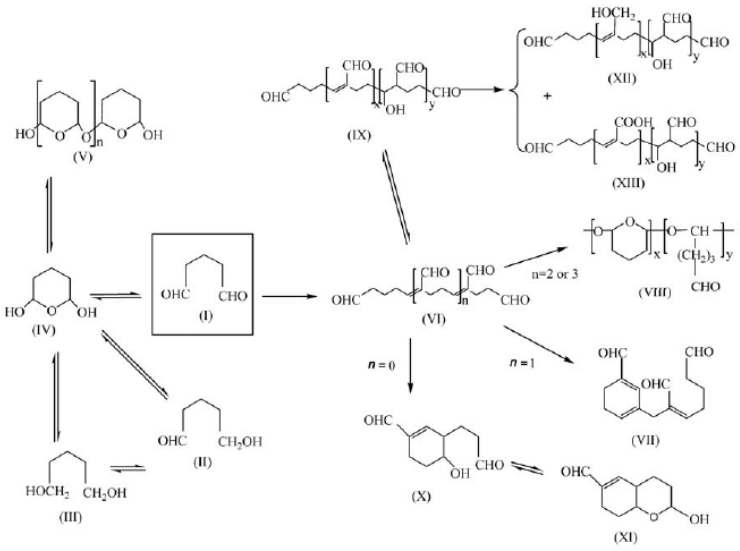

Figure 62: *Diagram of the various forms of glutaraldehyde in aqueous solution. Imported from* (Migneault et al. 2004)

Glutaraldehyde can interact with different functions of proteins like amine, thiol, phenol and imidazole. Among those functions, glutaraldehyde preferentially reacts with the ε amino groups of lysine. Given the various forms of glutaraldehyde in solution and the several possibilities of reactions of glutaraldehyde with the amino group of proteins (Figure 63), it is still unclear to determine which mechanism is responsible for collagen cross-linking with glutaraldehyde (Damink et al. 1995; Migneault et al. 2004). It is globally admitted that the first step of the reaction is the nucleophilic addition of the amino group of the protein on the aldehyde function of the glutaraldehyde to form a Schiff base (molecule III Figure 63).

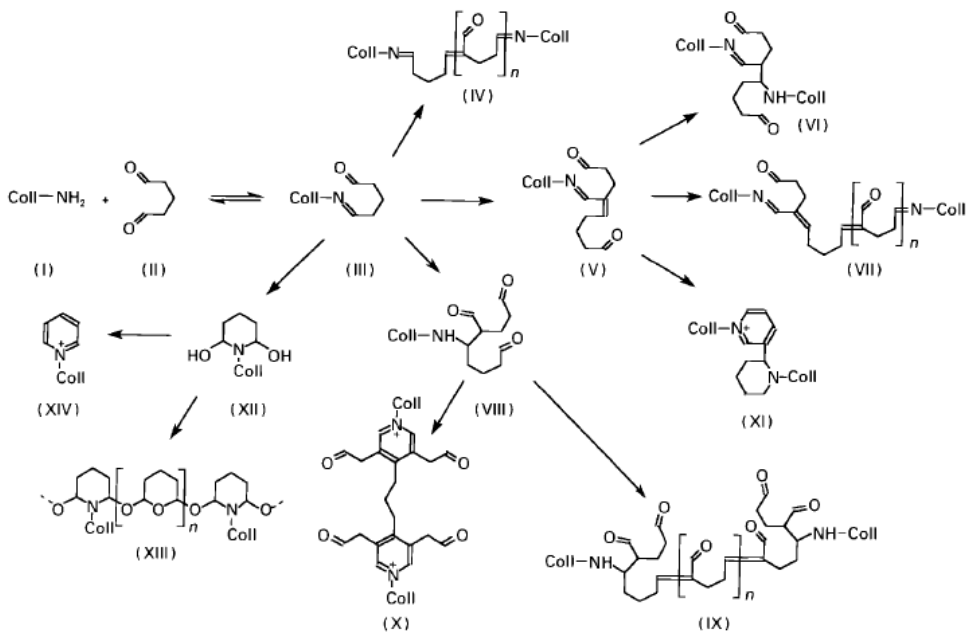

Figure 63: *Diagram of the various chemical reactions between glutaraldehyde (molecule II) and collagen (molecule I: Coll-NH2) in aqueous solution. Imported from* (Damink et al. 1995)

The Schiff base is an unstable form that tends to be hydrolyzed back into the two initial reagents under acidic condition. In neutral and basic condition the Schiff base is more stable and can spontaneously form a cyclic aminal (molecule XII Figure 63) in aqueous environment that can further react with glutaraldehyde molecules to crosslink two cyclic amino collagen molecules (molecule XIII Figure 63). The remaining aldehyde function of the Schiff base can also react again with an amino function of collagen molecules to cross-link two collagen molecules but the resulting molecule (IV) is hydrolytically unstable. It seems that the most frequent reaction in aqueous environments is the addition of another glutaraldehyde molecule on the Schiff base. This addition can happen through two different ways: an aldol-type condensation (resulting product component V) or a Mannich reaction (resulting product component VIII). Mannich reaction results from the nucleophilic addition of the amino group of the Schiff base on the aldehyde function of the glutaraldehyde while aldol-type condensation results from a nucleophilic addition of glutaraldehyde on Schiff base. Since component VIII is more stable than component V in water, collagen cross-linking derived from this component (X and IX) are the most frequently encountered. However, Mannich reaction is not the rule and collagen cross-links by glutaraldehyde are also composed of a mixture of the previously presented reactions (Damink et al. 1995; Migneault et al. 2004). Glutaraldehyde molecule in which only one over the two aldehyde functions has reacted to form a covalent bond can also be found in the hydrogels. As the molecules can later be toxic to the cells seeded on the hydrogel, collagen gels are usually first incubated in a solution that inactivated the last aldehyde functions. Glycine, the smallest amino acid is frequently used as its amino function reacted with aldehyde to form a Schiff base (Cheung and Brown 1982). Its small size eases its diffusion in collagen hydrogel and its composition is compatible with cells seeding.

We tested the efficiency of collagen crosslinking by glutaraldehyde on our device by immersing collagen scaffold in glutaraldehyde (0.5%(v/v)) solution after unmolding. After the 2 hours of incubation the collagen mold was transferred to the inactivating solution of glycine. After 2 days of washing Caco2 epithelial cells were seeded on the top of the collagen structures.

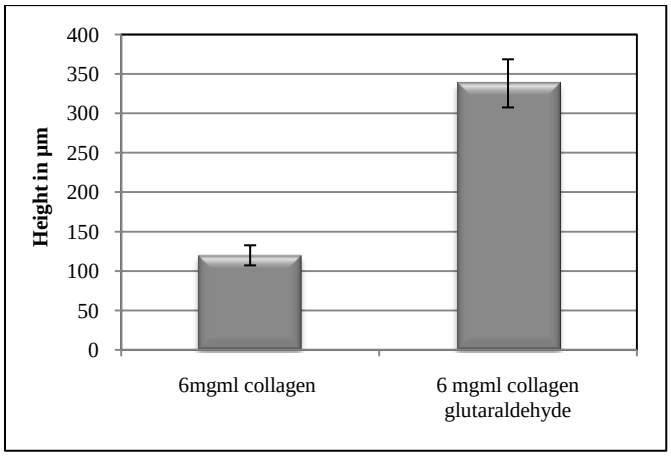

Figure 64: *Collagen and glutaraldehyde. Table comparing the final height of the structures once Caco2 have reached confluence. Mean +/- SD, n=20.*

Due to efficient inactivation and rinsing steps we have shown that adhesion and growth of Caco2 cells (it still took them 5 days to reach confluence) was not impeded by the preceding glutaraldehyde treatment. Once Caco2 were confluent, the measurement of the final structures reveled that glutaraldehyde significantly improved the mechanical properties of collagen. The mean value of the height of collagen cross-linked with glutaraldehyde was 338µm which is almost the initial height of the structure (~ 380µm) while the control was only 120µm for collagen at 6 mg/ml (Figure 64).

The main defect of glutaraldehyde is the toxicity of its aldehyde functions in solution that kept us from seeding the fibroblasts in collagen matrix prior to glutaraldehyde treatment. The only possibility left was to seed fibroblasts on the top of the structure and expect them to invade the cross-linked collagen matrix. Fibroblasts were thus seeded on the top of the structure and after 5 days their invasion in the collagen matrix was evaluated.

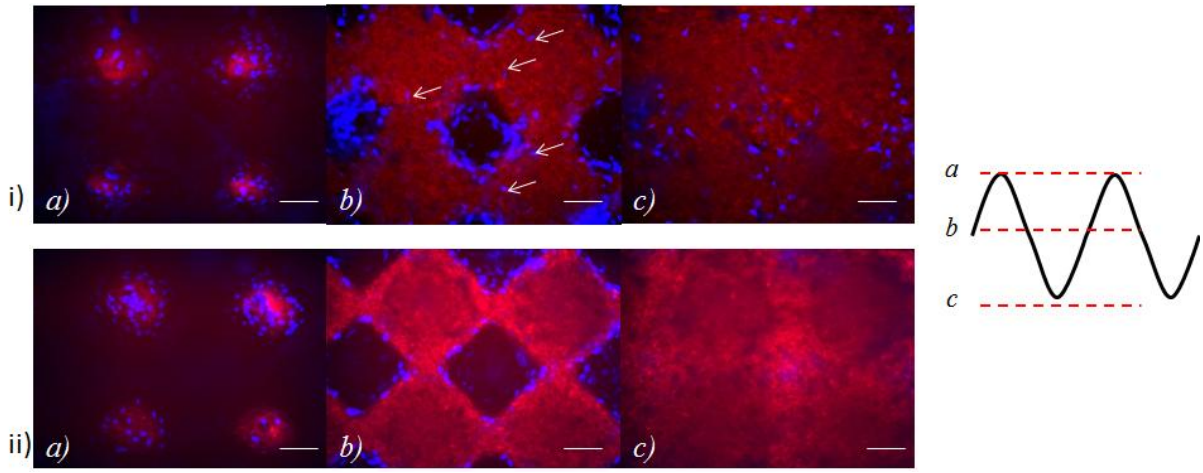

Figure 65: *Invasion of the fibroblasts inside the collagen matrix (i) control 6mg/mL collagen and (ii) 6mg/mL collagen treated with glutaraldehyde. Pictures are taken at various heights along the structure (a) top, (b) middle, (c) bottom of the structure reported on the scheme on the right. White arrows indicate invading fibroblasts. Red: TAMRA collagen/ blue: DNA (Dapi). Scale bar: 50µm.*

In control collagen scaffolds, some fibroblasts were observed inside the matrix of microstructures (White arrows Figure 65 (i, b)) and underneath the crypt parts (Figure 65 (i, c)). We concluded that the fibroblasts slightly invaded control collagen matrix after 5 days while they only colonized the surface of the structures on glutaraldehyde cross-linked scaffolds (Figure 65). In order to understand these differences in fibroblasts invasion, we verified if the glutaraldehyde treatment induced modification of the collagen fibrillar network. As the visualization of collagen fibrils and the estimation of pore size were facilitated at the lowest collagen concentrations we analyzed collagen gels at 2mg/mL and we assumed that the conclusions could be extended to higher collagen concentrations.

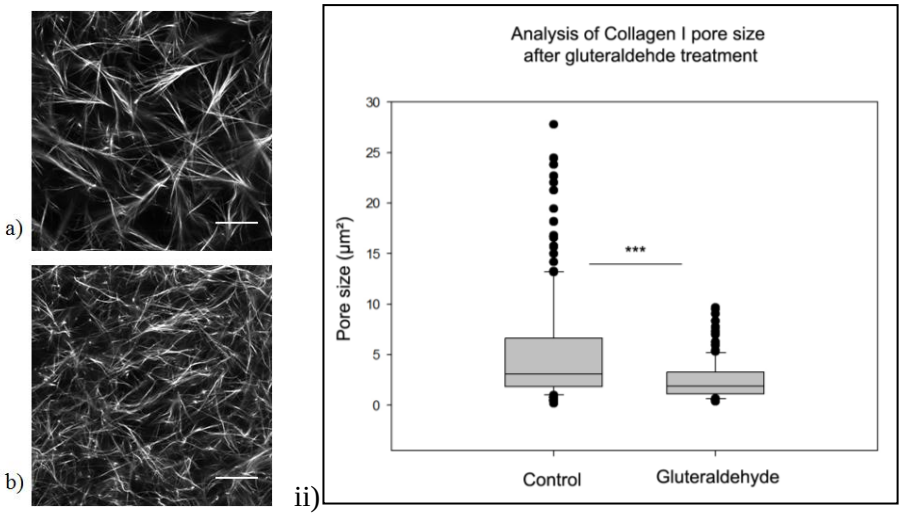

Figure 66: *Effect of glutaraldehyde treatment collagen fibrillar network. (i) Architecture of 2mg/mL collagen network (TAMRA labeled collagen). (a) Control collagen gel. (b) Collagen gel treated with 0.5% (v/v) glutaraldehyde for 2 hours. (ii) Plot box representative of the distribution of pores size for collagen alone and collagen treated with glutaraldehyde. ANOVA test was performed for statistical analysis. (n=200).Scale bars: 20µm*

Fibrillar structure of collagen gels was preserved after glutaraldehyde treatment even though the network appeared denser than for control collagen gels (Figure 66 (i)). Statistical analysis confirmed that the pore size was significantly lower on collagen gels treated with glutaraldehyde (mean pore size =2.50µm² ± 0.18) compared to control collagen gels (mean pore size =5.22µm² ± 0.37) (Figure 66 (ii)). The distribution of pore size was less expanded on glutarladehyde cross-linked collagen scaffolds than on collagen alone.

The fact that treating collagen scaffold with glutaraldehyde generated denser hydrogels could explain why fibroblasts experienced more difficulties to invade these matrices compared to collagen alone. As glutaraldehyde is known to cross-link collagen fibrils it should prevent the sliding of fibrils under fibroblasts tension and thus further obstruct the invasion of fibroblasts.

In addition to physically remodel matrices, fibroblasts are known to synthesize matrix metalloproteinases (MMPs) which are zinc dependent enzymes that lyse proteins of the ECM including collagen I (Ratnikov, Deryugina, and Strongin 2002; Wilhelm et al. 1986). *In vivo*, MMPs act as mediators of the ECM composition as they ensure the balance between ECM synthesis and degradation. As the notable increase in ECM synthesis related to fibrosis was coupled to an increase in synthesis of MMPs (Xie et al. 2014), we expected the stiffening of collagen matrix caused by glutaraldehyde treatment to promote MMPs synthesis. It might be that fibroblasts invasion related to MMPs activity is less effective and requires more time than invasion via physical remodeling of the matrix.

We could have wait longer than 5 days to see if induction of MMPs synthesis by fibroblasts required more time. We could also have tested lower glutaraldehyde concentrations or shorter incubation time to ease the migration of fibroblasts inside the collagen but we preferred to test the option of a less toxic molecule that would cross-link the collagen scaffold in a similar manner as glutaraldehyde but would allow the seeding of fibroblasts inside the matrix.

γ) Genipin cross-linking

Genipin has only been used for the last 20 years in tissue engineering compared to glutaraldehyde which has been extensively used since the 80's. It is considered to be 5000 to 10 000 times less toxic than glutaraldehyde but still being able to improve the mechanical properties of matrices in a comparable degree.

Genipin is extracted from fruits called Genipa Americana or Gardenia jasminoides Ellis under geniposide form. Geniposide is transformed into genipin by the enzymatic hydrolysis of the glucose on carbon 1 (Figure 67).

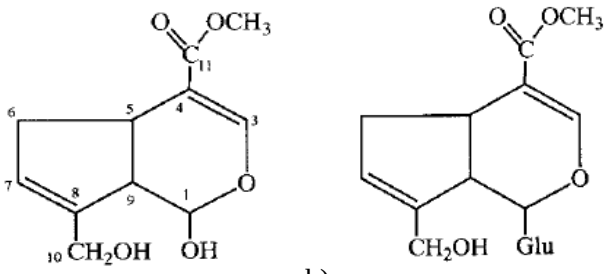

a) b)

Figure 67: *Chemical structure of the Genipin (a) and of the geniposide (b). Imported from* (Butler, Ng, and Pudney 2003)

Genoside represents 4 to 6% of the dried mass of the fruit. Gardenia jaminoides are used in Chinese medicine as diuretic, anti-inflammatory, choleretic, antiphlogistic. Genoside is lyzed into genipin in the digestive tract and no significant damage on the organism are reported. Genipin is also used as a food dye called gardenia blue as it forms blue pigments when it reacts with primary amine. This reduced toxicity of genipin compared to glutaraldehyde is favorable for implants that exhibit the same mechanical improvements but with reduced inflammatory reactions (Chang et al. 2002). Genipin also allows the seeding of cells in implants prior to cross-linking treatment. In this regard, collagen gels containing cells isolated from human dental pulp cross-linked with genipin could be stiffen enough to resist the mechanical tensions experienced at the center of dental implants (Kwon et al. 2015). In addition, human dental pulp cells were more advanced into ontogenic differentiation when seeded in genipin-collagen scaffold compared to collagen alone. Similarly, using genipin as cross-linker, Jeffords et al optimized the stiffness of their matrix (200 Pa) to induce an early differentiation of human mesenchymal stem cells into endothelial cells that was not achieved in control hydrogels (30 Pa) (Jeffords et al. 2015). Matrix degradation and swelling was also reduced when treated with genipin. The changes in cell behavior observed on collagen treated with genipin compared to collagen alone are mostly related to changes in stiffness since the size of collagen fibers, their number and cell adhesion are not modified (Sundararaghavan et al. 2009).

The low toxicity of genipin also offers the opportunity to treat damaged tissues *in situ*. In this perspective, genipin cross-linking of cartilage matrix is now considered to heal osteoarthritis (McGann et al. 2015). In osteoarthritis, cartilages are degraded due to an overexpression of degradative enzymes combined to an inflammation of the synovium. Genipin cross-linking would reduce the chemical degradation of the bone and improve its mechanical resilience as proven by *in vitro* experiments. Furthermore, the short duration of genipin treatment is compatible with surgery.

Genipin reacts with primary amines of proteins or polymers via two different reactions (Figure 68). The first one is a nucleophilic substitution of the ester group of the genipin by the amino group. Methanol is thus released following the addition of the primary amine. The second reaction results from the nucleophilic attack of the amine on the carbon C3 of the genipin molecule (Figure 67 for the

numbering) which causes the opening of the dihydropyran ring. The nucleophilic attack of the secondary amine formed in the first step of this reaction closes the opened ring via dehydration. The intermediate heterocyclic compound can rearrange and dimerize. The second reaction is prevalent in genipin cross-linking reactions as the nucleophilic substitution on the ester group is slow compared to nucleophilic attack on the carbon 3. This last reaction is at the origin of the blue color as the product of the reaction is a made of conjugated double bonds (Figure 69). Finally, this reaction can only happen in an oxygen environment since oxygen radicals activate the reaction.

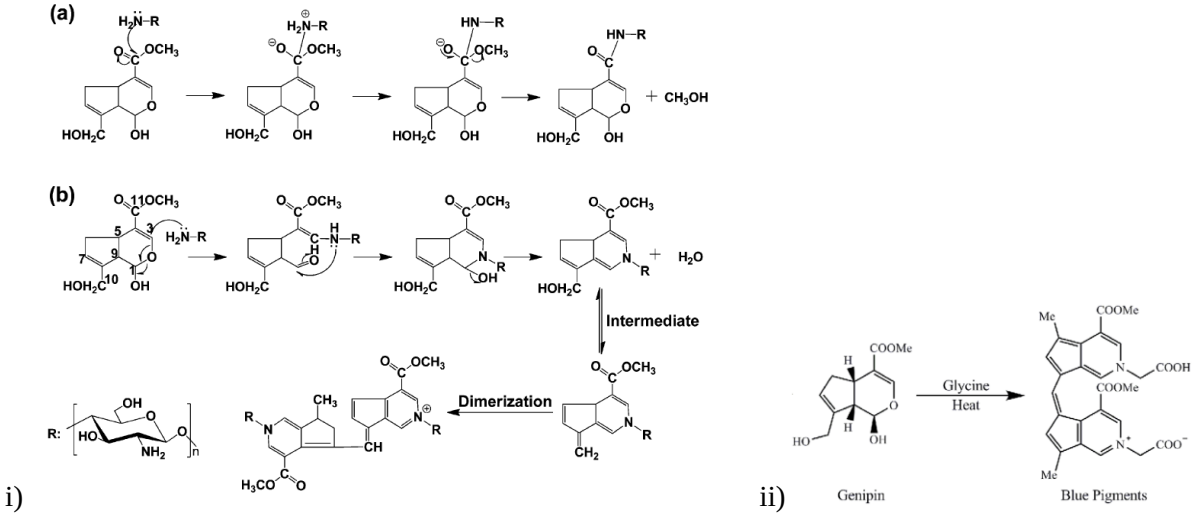

Figure 69: *Reaction of genipin with primary amines. i) Chemical process of the two reactions that can happen between genipin and primary amine: (a) Nucleophilic substitution & (b) nucleophilic attack on carbon C3. ii) Blue pigment is the product of reaction (b) when the primary amine is glycine. Imported from* (P. Wang et al. 2014; Q. S. Wang et al. 2012)

According to the previous studies that use genipin as a cross-linker, the stiffening of collagen gels depend both on the concentration of genipin used and on its incubation time (McGann et al. 2015; Sundararaghavan et al. 2008). The initial young modulus value of 2mg/mL collagen gels has increased by an order of magnitude (from 80 to 800 Pa) when incubated with 10mM genipin for 6 hours, whereas an incubation in 1mM for the same duration only improved the Young modulus to 100Pa (Sundararaghavan et al. 2008). However, when collagen gels were incubated in 1mM genipin for 12 hours their Young modulus reach a value of 500Pa.

According to the literature, genipin is starting to be cytotoxic at concentrations higher than 5mM independently of the duration of incubation tested (from 12 to 24 hours) (Fessel et al. 2014; Sundararaghavan et al. 2008). Since genipin at 1mM only significantly improved collagen mechanical properties for incubation time longer than 12 hours (Sundararaghavan et al. 2008), we decided to test the effect of three different concentrations of genipin: 0.5, 1 and 10mM for 12 hours incubation on 6mg/mL collagen .

i)

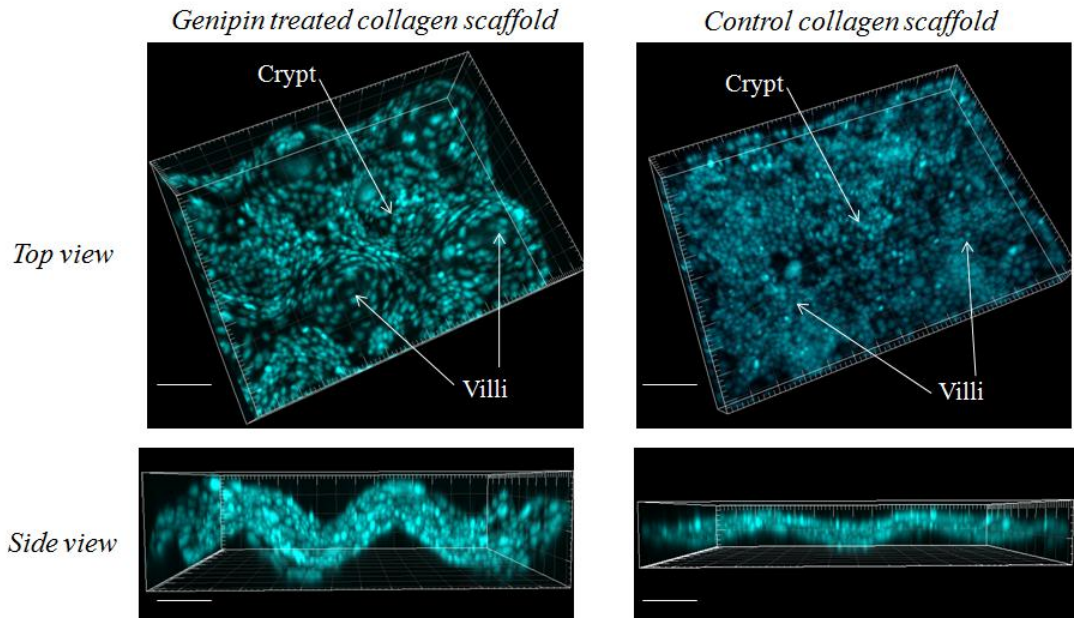

ii)

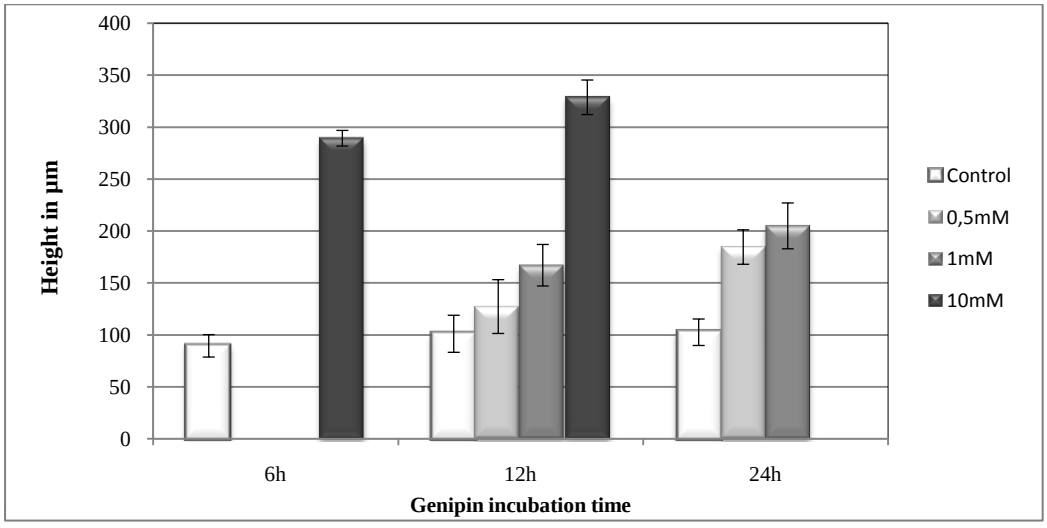

Figure 70: *The effect of genipin on collagen. (i) 3D reconstruction of 6mg/mL collagen scaffolds covered with Caco2 cells: Left: treated with 10mM genipin for 6 hours. Right: control collagen gels. (ii)Table comparing the final height of the structures once Caco2 have reached confluence depending on genipin concentration and incubation time using 6mg/mL commercial collagen. Mean +/- SD, n=20.*

Collagen gels were incubated in genipin solution after unmolding as for glutaraldehyde treatment. In order to avoid any toxicity of residual genipin, the gels were washed 3 times for 1 hour. Since no difference in cell adhesion or cell proliferation on the structure (confluence was reached in 5 days) were observed, we concluded that genipin treated collagen gels were not cytotoxic for Caco2 cells independently of the concentration of genipin used. When cells reached confluence, we measured height of collagen microstructures (Figure 70(ii)). As expected the higher the concentration of genipin was, the less the collagen was deformed. However, at low concentrations (0,5mM and 1mM) the improvements were still limited as the residual height was only increased by a factor ~1.5 at 1mM

genipin. On the contrary, the highest concentration successfully increased collagen stiffness as the residual height (~325µm) was almost equivalent to the height of the structure without cells (~380µm).

Meanwhile, we tested the cytotoxicity of each genipine concentration at 12 hours incubation for fibroblasts (mouse embryonic fibroblasts cell line, MEF) embedded in collagen matrix. As expected, 10mM genipine was by far the most cytotoxic, as only 10% of the cells survived the treatment compared to around 50% at lower concentrations.

Next, we investigated the influence of longer incubation time (24 hours) with the two less toxic concentrations. The increased gel stiffness induced by a longer incubation period suggested by literature was only verified at the lowest concentration (0.5mM). As the mechanical improvements were still low and the fibroblasts survival was diminished by longer incubation time, we decided to reduce the incubation time of the highest concentration: 10mM. The residual height was slightly lower for 10mM genipin incubated for 6 hours (~290µm) (Figure 70 (i)) compared to 12 hours incubation (~ 325µm). Concerning the survival of fibroblasts it was hard to conclude if 10mM genipin at 6 hours incubation was more harmful than the lower concentrations at 12 hours incubation.

Since our final goal was to use primary fibroblasts as they are more physiologically relevant cells, we investigated the effect of genipin on fibroblasts extracted from mice embryos (see Material and Methods for the extraction procedure). Primary fibroblasts were added to the neutralized collagen solution prior to injection. Once collagen gels were unmolded, the fibroblasts were left for one day in their normal medium to allow cells to spread and adhere before genipin treatment. Collagen matrices were then cross-linked with 10mM genipin for 6 hours. After treatment, collagen gels were rinsed thoroughly 3 times for one hour and fibroblasts were left in culture for 5 days. The residual height of collagen microstructures cross-linked with genipin and the shape of fibroblasts seeded inside the matrices were compared to control collagen gels.

i) 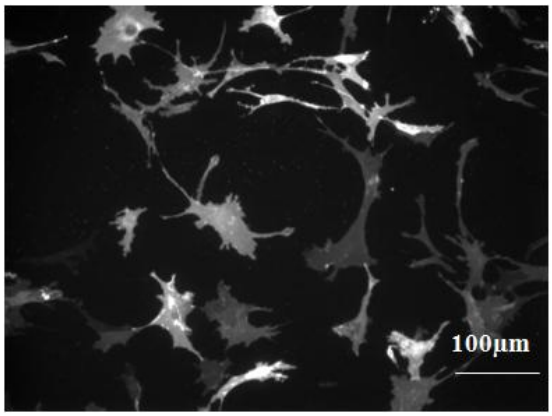

ii) 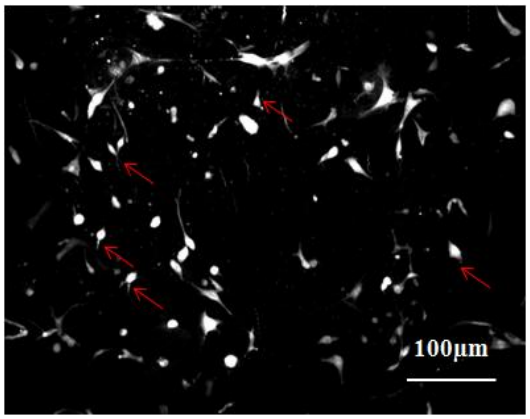

iii)

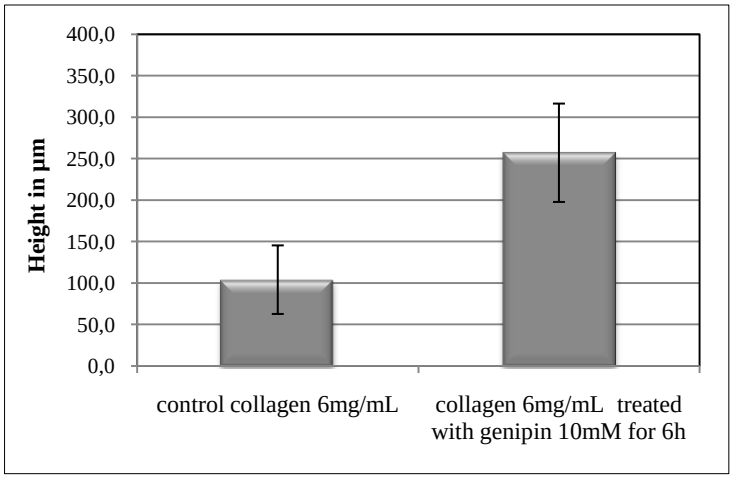

Figure 71: *Primary fibroblasts survival in genipin treated collagen (6mg/mL commercial collagen). (i) 2D projection of mouse embryonic fibroblasts present in control collagen microstructures after 5 days of culture. (ii) 2d projection of mouse embryonic fibroblasts present after 5 days of culture in collagen microstructures treated with 10mM genipin for 6 hours. Red arrows point at fibroblasts thin protrusion suggesting that cells are viabile although they may look roundish like dead cells at this magnification. (iii) Table comparing the residual heights of 6mg/mL collagen microstructures seeded with fibroblasts for 5 days whether they were treated with genipin or not. Mean +/- SD, n=20.*

According to the 2D projection of the fibroblasts seeded in collagen matrices (Figure 71 (i) &(ii)), the fibroblasts appeared more spread and stellate after 5 days of culture in control collagen compared to the spindle shape they exhibit in genipin treated matrix. Although many cells present some roundish shape characteristic of dead cells, they still manage to develop thin protrusions suggesting that they are viable (Red arrows Figure 71 (ii)). The survival rate of primary fibroblasts in collagen gels treated with 10mM for 6 hours was estimated to be around 20%. Primary fibroblasts seemed to be more resistant to genipin than immortalized fibroblasts cell line.

Since the spindle shape and the thin protrusions of fibroblasts in collagen gel treated with genipin evoked the shape of fibroblasts in highly concentrated collagen gels (see Figure 52), it was tempting to conclude that genipin cross-linking of collagen fibers resulted in denser collagen networks as for glutaraldehyde cross-linking. We verified this hypothesis by comparing the pore size of genipin treated to control collagen gels (Figure 72). As the visualization of pore size was facilitated at the lowest collagen concentrations we performed the measurements at 2mg/mL collagen and we assumed that the conclusions could be extended to higher collagen concentrations.

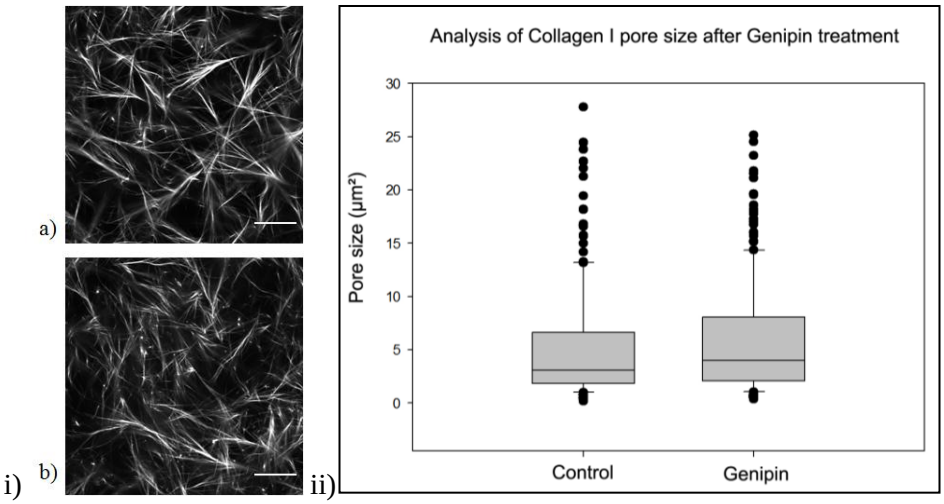

Figure 72: *Effect of genipin treatment collagen fibrillar network. (i) Architecture of 2mg/mL collagen network (TAMRA labeled collagen). (a) Control collagen gel. (b) Collagen gel treated with 10mM genipin for 6 hours. (ii) Plot box representative of the distribution of pores size for 2mg/mL collagen gels and 2mg/mL collagen gels treated with genipin ANOVA test was performed for statistical analysis (n=200). Scale bars: 20µm*

In contrast with glutaraldehyde treatments, genipin did not generate denser fibrillar networks. The fibrillar structure was still preserved and pore sizes of genipin treated collagen scaffolds (mean pore size =5.99µm² ± 0.39) were comparable to control collagen gels (mean pore size =5.22µm² ± 0.37). Since the mesh size was not modified, we assumed that the nature of reticulation point could explain the differences in fibroblasts shape observed. Collagen gels fibrils are entangled whereas after genipin treatment they are cross-linked. The presence of cross-links might restrict the sliding of fibrils necessary for cells to spread in collagen networks.

Regarding the final height of collagen microstructures, as for Caco2, genipin cross-linked collagen gels were much higher (~257µm) than non-treated collagen (~104µm). However, in the case of fibroblasts higher residual microstructure height might not directly correlate with improved mechanical resistance of collagen gels to cell forces. As a matter of fact, as fibroblasts spread more on control collagen gels, they should exert higher tension on those gels than on genipin treated collagen gels. Therefore, as treated and control gels might not be submitted to the same stress, the difference in the residual height observed probably overestimated the effective mechanical improvement related to genipin cross-linking.

The differences in height between control collagen and genipin treated collagen complicated the conclusions on how genipin may affect fibroblasts proliferation. According to the phenotypic changes induced by genipin, we would expect proliferation to be reduced in the presence of genipin. Surprisingly, fibroblasts seemed to be more numerous on the 2D projection of collagen microstructures treated with genipin after 5 days of culture (Figure 71 (i) &(ii)). However, since these microstructures were higher than control microstructures, the number of cells was thus integrated on a

larger volume of hydrogel. As a consequence, the number of cells per volume unit might be higher in control collagen gels. This quantification was still not satisfying as a reduction in height correlated with a local increase of collagen concentration: microstructures that were out of plane were condensed closer to the surface plane. As cells were initially homogeneously seeded in the hydrogels, local accumulation of collagen fibrils should lead to a local over-concentration of fibroblasts. The total number of cells from crypt to villus should thus remain constant despite the decrease in height. Considering all the arguments discussed, it seemed difficult to conclude on the influence of genipin on fibroblasts proliferation. Monitoring the proliferation of fibroblasts in real time would have helped us concluding on this effect.

With regards to our final goal which was to improve mechanical properties of collagen enough to resist cell tension, genipin together with glutaraldehyde seemed to be the best candidate so far, as the residual height once epithelial cells reached confluence was almost equivalent to the height without cells. One key advantage of genipin compared to glutaraldehyde was its reduced toxicity: fibroblasts could still be seeded in the matrix. However, genipin induced major changes in fibroblasts phenotype and was still cytotoxic to some extent. Since we observed that reduced incubation time improved fibroblasts survival, we might have tested shorter incubation time. The fact that reducing incubation time would also reduce the mechanical improvement related to the addition of genipin kept us from investigating lower concentrations. In fact, although 75% of the structure treated with 10mM genipin for 6 hours was still preserved when covered with epithelial cells, we considered that the addition of fibroblasts to the matrix would shrink even more the structure and thus we could not fall below this limit.

In conclusion, two main methods were investigated to improve the mechanical properties of collagen scaffolds: on the one hand, the addition of a stiffer hydrogel to the collagen to form a semi-interpenetrating network that would combine the fibrillar structure characteristic of *in vivo* ECM provided by collagen to the rigidity supplied by the second hydrogel; and the addition of a cross-linker to the collagen matrix to stabilize the collagen network. The spectrum of investigation of the first approach was mostly restricted by the limited solubility of the mixed hydrogels and the results obtained were always below the improvements that could be achieved only by increasing collagen concentration. Concerning collagen cross-linking, the most convincing results were obtained with cytotoxic cross-linkers. Genipin thus appeared as the best compromise between stiffening the collagen enough to preserve the initial 3D structure while limiting fibroblasts death induced by the addition of cytotoxic cross-linker.

In parallel to our investigation of the possibilities to stiffen the matrix, we studied more carefully how cells behaved on the 3D matrix and we included a basement membrane coating to our collagen matrix in order to grow organoids on our microstructured scaffold.

II How Caco2 cells behave on a microstructured scaffold

As described in the introduction, proliferative and differentiated cells are rigorously spatially partitioned in the intestine into dedicated morphological subunits - crypt and villi (exception are Paneth cells). The secreted factors actively contribute to the niche environment provided by crypts. However, our hypothesis is that the 3D structure of the crypt could also support the maintenance of stemness of intestinal stem cells.

II. 1. Influence of the 3D structure on the spatial location of proliferative cells

The influence of the 3D structure was first studied on Caco2 cell line, as we already optimized their culture conditions so that they colonized rapidly the 3D collagen structure.

We assumed that the confluence had to be reached for cells to integrate the differences in cortical tensions between crypts and villi at the tissue level. We considered that cells do not react to the 3D structure individually but that it is more a collective response. Cells could sense the topography of the environment individually and transduce the signal to the cytoskeleton via integrins, but they could also perceive the cortical tension of neighboring cells through cadherin junctions. The cells thus respond to the combination of both matrix and intercellular inputs. However, what is the tissue characteristic length at which differential cortical tensions could be integrated? If this length is negligible compared to the radius of crypt curvature, cell monolayer should not sense the curvature. On the contrary, if it is of comparable size, we hypothesized that local curvature will affect cell proliferation.

The proliferation of cells was evaluated 7 days after cells reached confluence. We considered that this period was sufficient for the monolayer to reach a steady state. The spatial location of proliferative cells on the structure was investigated at different stiffness: 4mg/mL (E~1.05kPa) and 10mg/mL collagen (E~6kPa) and PDMS (~2MPa). Because of the slight differences in collagen composition between commercial and home-made collagen and the mechanical heterogeneity of commercial collagen at 4mg/mL, we decided to perform this set of experiments only with home-made collagen. Similarly, to remain consistent on the chemical nature of adhesion molecules, PDMS molds were coated with collagen from the same batch.

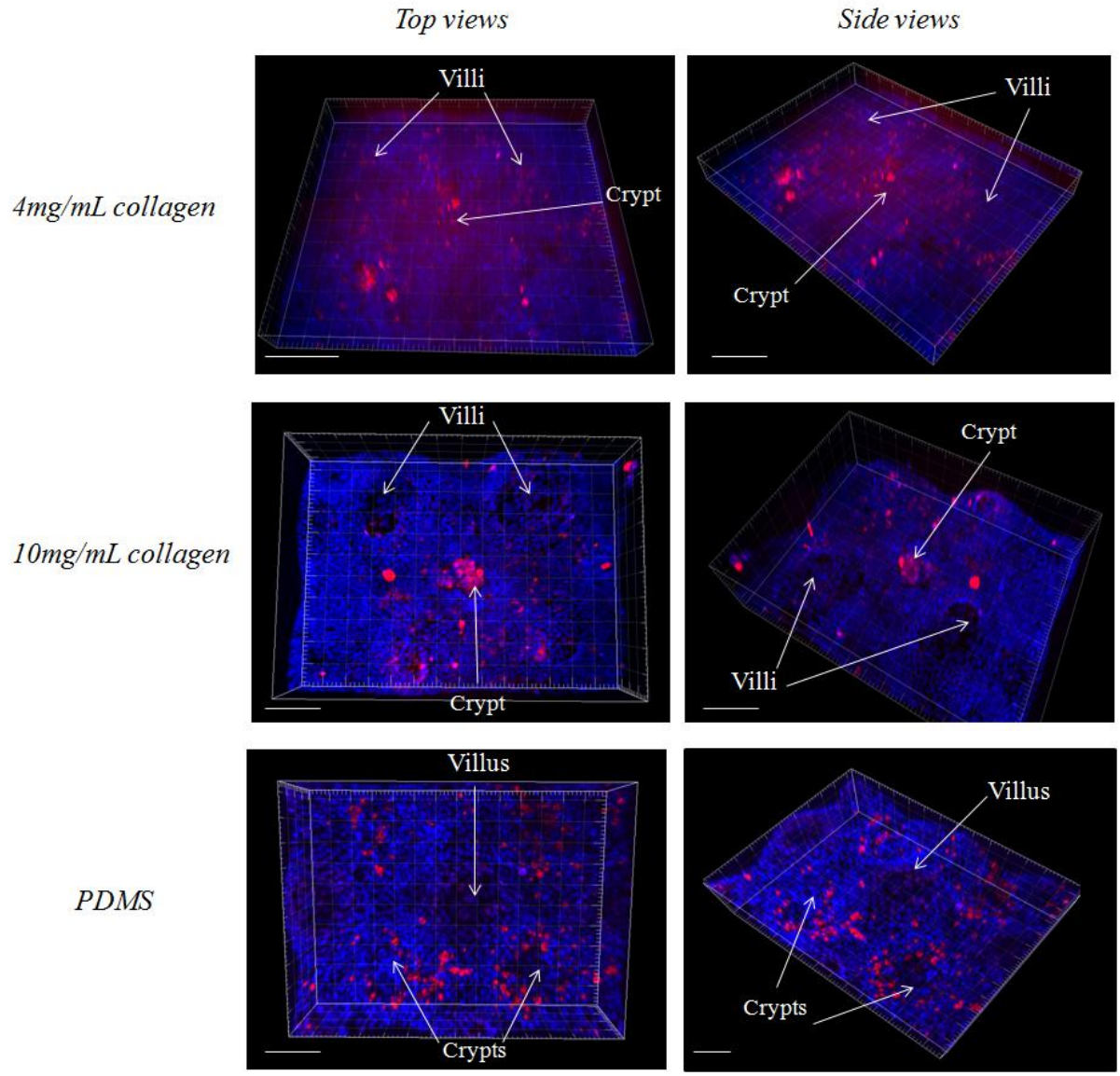

Figure 73: *Spatial location of proliferative cells depending on the stiffness of the scaffold. Top views and side views of the structures covered with Caco2 cells at different substrate stiffness (collagen 4 and 10mg/mL and PDMS)(blue, dapi labeled nuclei; Red: proliferative cells labeled with Ki67). (i) On collagen at 4mg/mL. Scale bars: 100µm.*

On highly concentrated collagen scaffold and on PDMS, we perceived a pattern of proliferative cells mostly located in the crypts. Thus, cells seemed to be able to sense and react to the topography of the environment. The notion that the matrix topography has the capacity to spatially control proliferation, was strengthen with the fact that these experiences were performed with cancer cell line that present abnormal proliferative mechanism. However, on 4mg/mL collagen, proliferative cells seemed randomly distributed. We have previously measured that on 4mg/mL the amplitude of the sinusoide was reduced to ~80µm in height when cells were confluent compared to the ~250µm on 10mg/mL collagen and 380µm on PDMS. It was thus difficult to conclude if the matrix was too soft for cells to sense topography or if the amplitude of the residual sinusoid was too low to be integrated by cells. To distinguish between those two possibilities, we intend to design a new mold with sinusoidal structures

of various amplitudes. Since the stiffness of the matrix will be equivalent on the whole mold the only variable will be the amplitude of the sinusoid.

Nevertheless, using the highest collagen concentration we showed that a given topography could induce patterns of proliferation. It implied that the tissue length upon which spatial heterogeneities were integrated was comparable to our 3D sinusoid of 400 µm in height with a 400 µm period. Next, we wanted to verify our hypothesis that proliferation pattern was only induced when cells reached confluence so that topographical constrained could be integrated at the scale of the whole tissue.

II. 2. Location of proliferative cells during the colonization of 3D structures

Two main processes could be expected during the progressive cell colonization of the scaffold: either cells proliferated randomly throughout the scaffold and after reaching the confluence cells away from the crypts stop proliferating; or, from day 0, only cells at the bottom of the crypts proliferated and the mitotic pressure they exerted induced the colonization of the scaffold by their neighboring cells.

To tackle this question, we monitored the location of proliferative cells at different time points (day 0, 1 and 3) on 10 mg/mL collagen. We focused on studying these potential effects on collagen rather than on PDMS as they were more representative of the composition and structure of *in vivo* extracellular matrices.

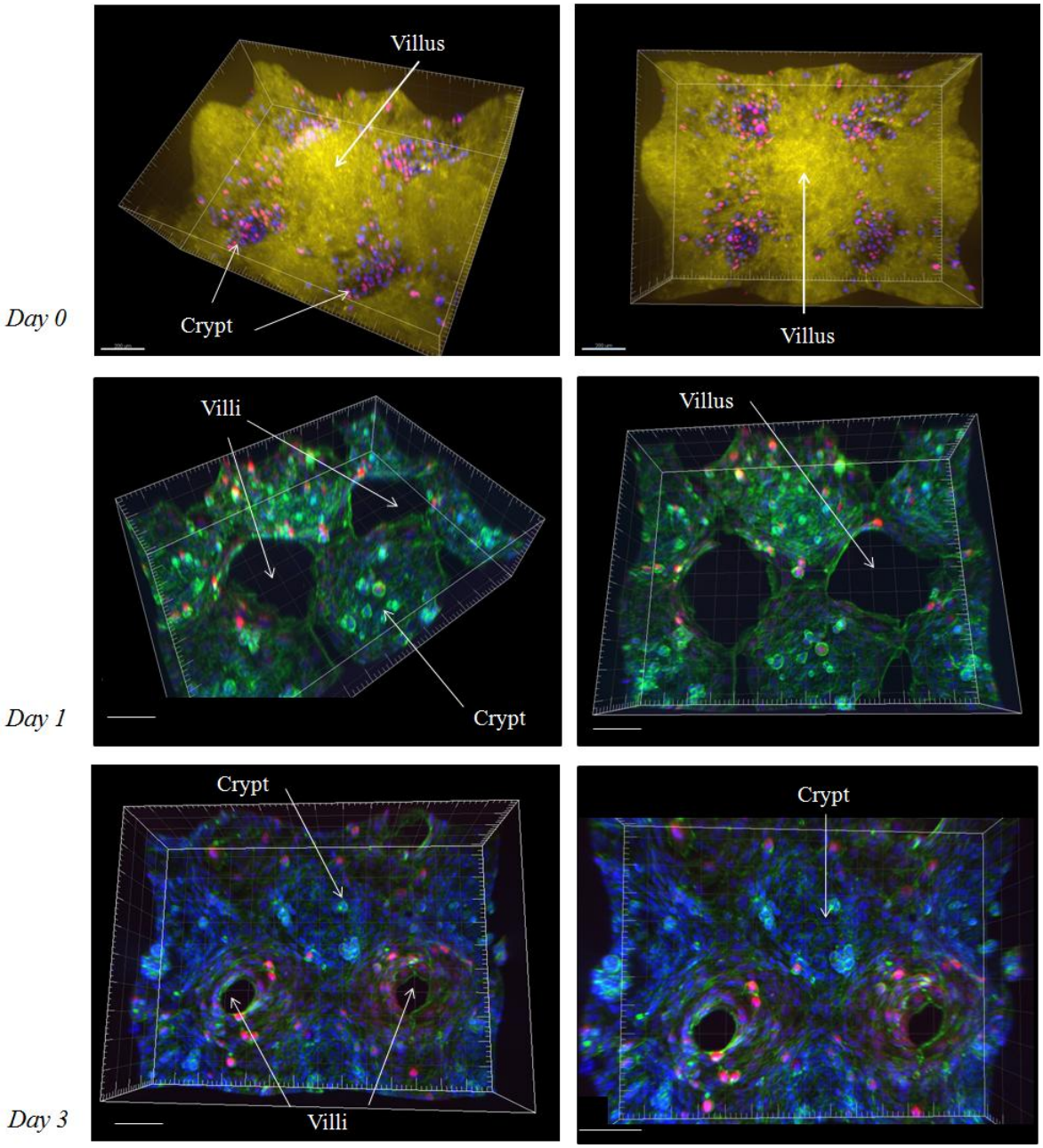

Figure 74: *Location of proliferative cells during the colonization of the 10mg/mL collagen scaffolds by Caco2 cells. 3D reconstruction of the z stacks. Scale bars, 100µm. Left panels: side view; Right panels: top views of the reconstruction. Day 0: Collagen is labeled in yellow, nuclei are labeled in blue (dapi) and proliferative nuclei in red (Ki67). Day 1 and Day 3: actin is labeled in green (Phalloidin), nuclei are labeled in blue (dapi) and proliferative cells in red (Ki67). Collagen was not represented on day 1 and 3 for clarity reasons. Scale bars: 100µm.*

On the first day of seeding (Figure 74, Day 0), the cells were located in the crypt and proliferative cells seemed homogeneously distributed. On day 1, the cells in the crypt already formed cohesive patches of cells that migrated out of the crypts. The patches of neighboring crypts seemed to have fused in a cohesive monolayer that colonized the villi. Proliferative cells were absent from the crypts and were mostly located on the first rows of cells at the migration front. The same pattern was observed on day 3.

With regard to the results observed at confluence, the proliferation patterns of proliferative cells clearly depended on the stage of expansion of cells on the structure. It seemed that as far as the whole structure was not covered with cells, proliferative cells were restricted to migration front. This phenomenon seemed logic as on 2D substrate, Caco2 cells preferentially proliferated where they have enough space to expand. When confluence was reached, the whole monolayer of epithelial cells seemed to rearrange so that proliferative cells were essentially observed only in the crypts. This suggested that spatial constriction provided by the matrix only induced a pattern of proliferation when cells were already confined by neighboring cells. In conclusion, our results strongly suggest that topography variations had to be integrated at the tissue scale rather than at the cell scale to induce any pattern of proliferation. In a prospective study, we will refine this analysis by comparing the pattern of proliferation immediately after cells have reached confluence and one week after confluence to determine the delay needed for cells to acquire their steady pattern of proliferation.

Another interesting feature observed in Figure 74 was the apparent synchrony of epithelial cells as they colonized the structure. Cells were organized as rings that surrounded villi and progressively constricted as they progressed toward the top of the villi (Figure 74: Days 1 and 3). We then investigated if this cooperative colonization was also observed on softer matrices.

II. 3. Matrix stiffness induced synchronized collective cell colonization of scaffolds

Because 4mg/mL and 10mg/mL induced different cell behavior regarding cell proliferation, we examined if these two collagen concentrations also induced different growing patterns. For the reasons previously exposed (II.2), we used home-made collagen in both conditions.

The motifs formed by cells as they colonized the different collagen matrices were imaged on the first day and third day after cell seeding.

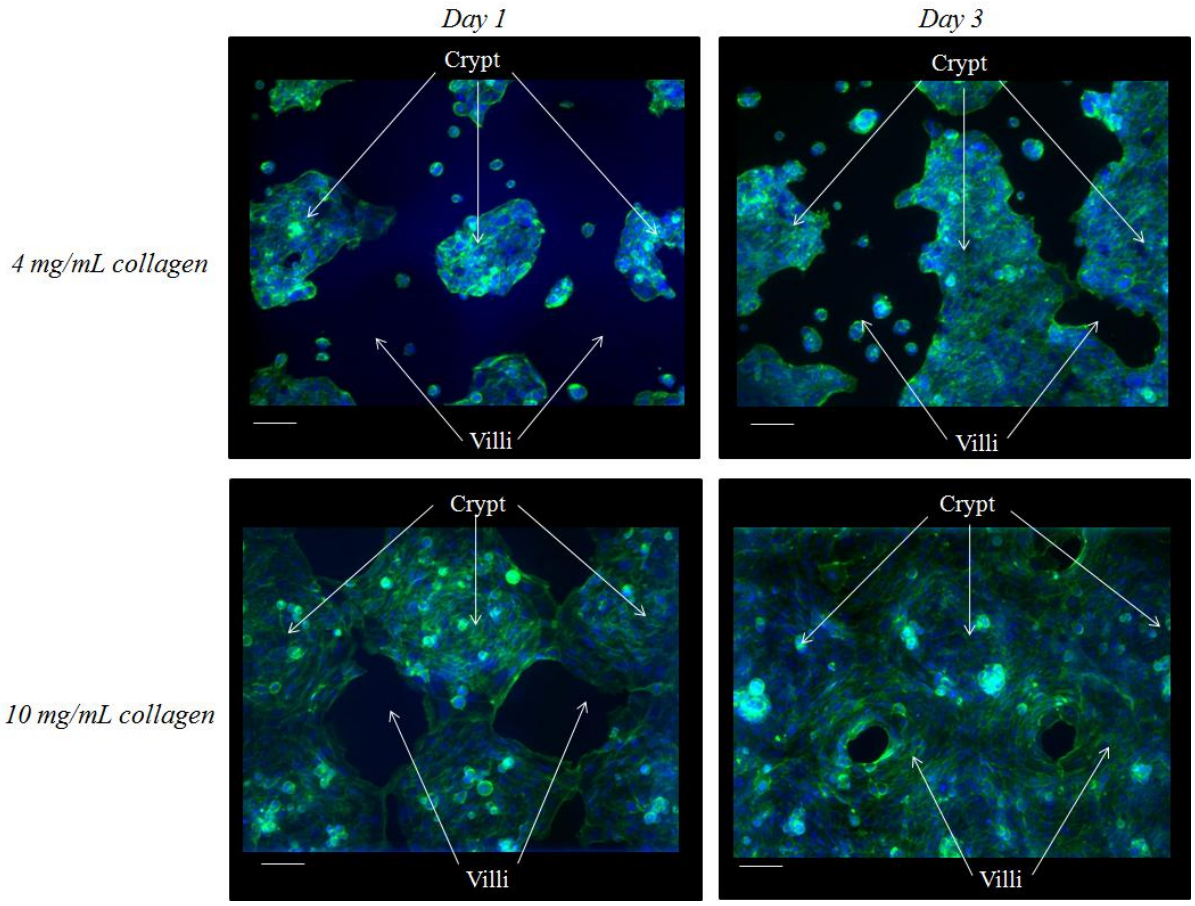

Figure 75: *Patterns of scaffold colonization by Caco2 cells depending on collagen concentration. 2D projections of the average fluorescence intensity of the z-stack. 2D projections were preferred over 3D reconstruction as it helped visualizing the growing patterns. Nuclei labeled in blue (DAPI), actin (phalloidin) in green. Scale bars: 100µm.*

According to the area covered by cells, Caco2 cells seemed to proliferate faster on 10mg/mL collagen compared to 4mg/mL. On day 1, the estimated number of cells adhering on collagen microstructures was, indeed, twice larger on collagen at 10mg/mL (~320) compared to 4mg/mL (~160). Similarly, on day 3, around 655 cells covered 10mg/mL collagen microstructures against 425 on 4mg/mL collagen. Furthermore, the constriction rings observed on 10mg/mL did not form on 4mg/mL collagen structure. Although cells were located in the crypts on day 1 on collagen 4mg/mL, they made random patterns on day 3. Cells did not appeared nicely synchronized around villi as they did on 10mg/mL collagen, but were rather arranged as randomly expanding patches of cells that at some point fused to form a confluent monolayer. This expansion mode of Caco2 cells was very similar to the one observed in 2D culture flasks.

As for proliferation, it was difficult to conclude if the different pattern observed were related to differences in stiffness of the matrix or in the amplitude of the sinusoid which decreased as the cells were growing on its surface at 4mg/mL concentration. As previously discussed, using a sinusoidal mold with different amplitudes will help us evaluating the relative influence of each factor. However,

the fact that cells covered a smaller area on 4mg/mL compared to 10mg/mL on day 3 even though the total surface at this concentration was reduced due to cell pulling suggested that matrix stiffness affected cell proliferation.

On 10mg/mL scaffolds, the expansion of Caco2 cells was very different than on 2D surfaces. The cells seemed to synchronize as they formed constriction rings that gradually climbed to cover the whole villi structure. We could thus conclude that microstructured surface induced specific modes of cell growing.

This part illustrated the importance of the 3D structure of organs since they induce specific patterns of proliferation and of growing. This further suggests that ECM do not only act as a passive structural support for cells since its relative variations in topography and geometry were integrated by cells and strongly influenced their behavior. Unfortunately, although the tendencies of growing and proliferation patterns were clearly visible on the pictures, it was not easy to perform statistical analysis because the density of nuclei was elevated once cells had reached confluence. In addition, as cells deformed substrate structures, the final size of crypts and villi relative to collagen concentration used should be implemented in the analysis. We are now developing a script that meet all the specification to accurately relate the proliferative cells to their position.

All the experiments above were conducted with epithelial cell line. Since these cells present abnormal proliferative dynamics, it was already surprising to observe that their anarchical proliferation could be spatially restrained by 3D structured environment. We thus expected primary cells to express similar patterns of proliferation. Such information would be even more meaningful and representative of *in vivo* situation, as they would be obtained with intestinal stem cells that *in vivo* possess all the potentiality to generate a whole intestinal epithelium. The ability of primary cells to differentiate would confirm our conclusions that, in addition to restrict proliferative stem cells to crypts, 3D microstructured environment would also induce the specific location of differentiated cells on the villi.

III From *in vivo* isolated intestinal crypts to an *in vitro* intestinal epithelium

The final goal of my PhD project was to grow a mice intestinal epithelium *in vitro* starting from mice stem cells. In this respect, we first developed a physiological scaffold that recapitulated both the composition and the morphology of the matrix. Adjustments were needed to have this matrix resist cell tension and required the use of genipin as the optimal cross-linker to stiffen collagen matrices.

In parallel to our studies on collagen strengthening, we started investigating the growth of primary cells on our collagen scaffolds in the early stages of the project. Although primary cells are the best candidate to generate a functional intestinal tissue *in vitro* that meet the specificities of *in vivo* intestine, they are sensitive and require more optimization to survive and grow on an *in vitro* device than epithelial cells lines. Their extraction from a living organism that provides multiple chemical

signals from various origins, was harmful to the cells. However, as described in the introduction, the elegant studies of Clevers group demonstrated that when primary cells were seeded in ECM hydrogel such as Matrigel and immersed in media supplemented with selected growth factors, stem cells associated to Paneth cells managed to survive and grow as organoids (Sato et al. 2011). This ability of stem cells to proliferate and differentiate *in vitro* encouraged us to use stem cells to repopulate our biomimetic structure. However, as collagen differs from Matrigel in molecular composition and organization as well as in the amount of bound growth factors, we anticipated that some improvements would be required to provide cell survival. We thus started working on these aspects in the initial phase of the project, in parallel with matrix improvement. Only recently, we have identified genipin as the best candidate to stiffen collagen matrix. This explains why only a few experiments were performed with organoids on a collagen matrix cross-linked with genipin.

This delicate part of the results was realized with the precious help of Anthony Simon, engineer in Danijela Vignjevic lab, who optimized organoid culture technique. The knowledge they acquired was crucial to perform the following experiments.

III.1. Growing primary intestinal epithelium on 3D microstructured collagen scaffold

As described in the introduction section, polarized epithelial cells adhere on the basement membrane with their basal side. The importance of this specialized network of ECM proteins in the maintenance of tissue homeostasis was clearly demonstrated as it supports cell migration and induces cell anoikis at the top of the villi (see § introduction). Reproducing this thin layer at the top of collagen matrix was thus primordial for us.

III.1.1) Coating strategies as basement membrane substitute

Matrigel was first considered as the best candidate to reproduce basement membrane as it is globally considered by biologists and bioengineerers as the hydrogel that resembles the most its complex composition. Furthermore, Matrigel has proven to support intestinal stem cell survival and proliferation *in vitro* (Sato et al. 2009). However, since it is extracted from mouse sarcoma tumors, it also presents constituents that are specific to cancers and thus could promote chaotic cell hyperproliferation. Moreover, its composition is not well established and may vary from batch to batch.

As basement membrane is mainly composed of laminin, this protein also figured as potential candidate to mimic basement membrane. Furthermore, it was shown to be a critical component of Matrigel that supports organoids development (Sato et al. 2009). Besides, an advantage of using laminin as coating agent is that it can be manipulated in precise concentrations in contrary to Matrigel.

Coating of collagen scaffolds was realized after unmolding. Since laminin and Matrigel are hydrogels that polymerize with increase in temperature, a cold diluted solution of either laminin or Matrigel was incubated at the surface of collagen structure at 37°C. The hydrogels molecules in contact with collagen surface entangled with collagen fibers as they polymerized and formed a thin layer of basement like hydrogel at the surface of the collagen structures. The concentrations of hydrogels used were first optimized and are reported in the Material and Methods section. Both hydrogels were mixed with cold fluorescent laminin prior to incubation to permit the observation of the final coating (Figure 58). The excesses of coating agent were washed before observation.

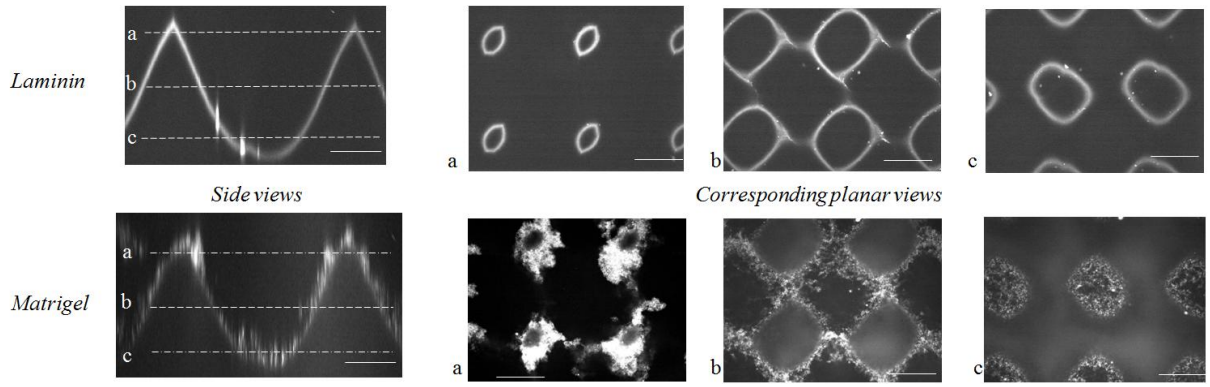

Figure 76: *Laminin and Matrigel coatings of the surface of collagen microstructures. On the left transversal cut of the coatings with the location of the different planes. (a, b, c) are the corresponding planar views :(a) top (b) middle and (c) bottom of the structure. Matrigel patches appearing after polymerization were particularly visible on the top view (a). Red-labeled laminin was added to both Matrigel and laminin. Scale bars are 100µm.*

As depicted in Figure 76, Matrigel coating seemed by far less homogeneous than laminin. Matrigel appeared to polymerize on the surface as patches that irregularly covered the collagen matrices. On the contrary, laminin seemed to homogeneously cover collagen surface as a thin layer. However, Matrigel could still be used as basement membrane substitute since it covered the whole scaffold without filling the crypts and the global morphology of the structure was still detectable (Side view Figure 76). The thickness of the coating was difficult to evaluate but was estimated to be around 0.5 to 1µm for laminin which was compatible with *in vivo* basement membrane (100-200nm).

III.1.2) Seeding isolated primary cells on collagen structure.

During mice dissection, epithelial cells were isolated from intestinal tissue as individual cells or as small clusters of not more than 4 cells. We first considered seeding the cell suspension immediately after their isolation as we expected differentiated cells to die and stem cells to recover from dissection and to colonize the whole structure. The collagen was molded at 10mg/mL as it was the stiffest hydrogel we had at that time, and then coated with Matrigel to mimic basement membrane.

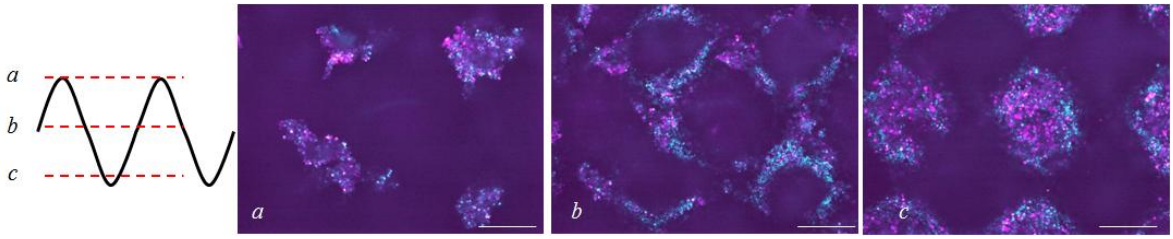

Figure 77: *Collagen structure covered with isolated primary cells. Planar views corresponding to the doted sections on the scheme: (a) top view, (b) middle and (c) bottom views. Nuclei are labeled in cyan (Dapi), actin in green (Phalloidin, not visible on the figure because cells were dead) and dead cells in red (caspase 3). Scale bars are 100µm.*

The seeding concentration of cells was chosen to be 10 times superior to the seeding concentration of Caco2 (0,5 million/ mL) as primary cells seeding population was constituted of a mix of differentiated and stem cells. The composition of the cell medium was similar to the medium used to grow organoids *in vitro* (cf Material and Methods). On the first day of culture the whole scaffold was covered with cells, attesting that isolated primary cells successfully adhered to Matrigel coating. Cell structure and labeling were similar 1 and 9 days after cell seeding (Figure 77). The entire height of the structure was preserved, meaning that the cells did not pull on the structure. In addition, we found that all cells were positive to caspase 3 indicating that cells did not survive. Unlike what we expected dead cells could still adhere to Matrigel.

In conclusion, it might be that isolated cells suffered from an important, even lethal stress when seeded directly on scaffold. We thus decided to first grow stem cells in 3D Matrigel to form organoids that will be in the second step seeded on the scaffold.

III.1.3) Seeding organoids on collagen scaffolds.

We hypothesized that organoids would be more likely to survive on collagen scaffolds than single cells because they already acquired the architectural organization characteristic of the intestine (stem cells associated to Paneth cells in contact with transit amplifying cells). In addition, differentiated cells that do not survive the isolation would die in Matrigel and consequently would not be transferred on the scaffold. However, cells in the organoids are already organized as an enclosed entity and the opening of this cohesive structure is required for cells to colonize the scaffold. The potential drawback of using organoids is that they would not open if the cystic conformation was more favorable than a monolayer.

Upon isolation, isolated intestinal cells were embedded in Matrigel and after 3 days cystic organoids (~100µm diameter) were extracted from Matrigel and seeded on collagen scaffolds coated either with laminin or Matrigel. The devices were gently shacked to make the organoids roll to the bottom of the crypts (Figure 78). The composition of the cell medium was similar to the medium used to grow

organoids *in vitro* (cf Material and Methods) to promote stem cell proliferation and growth on the structure.

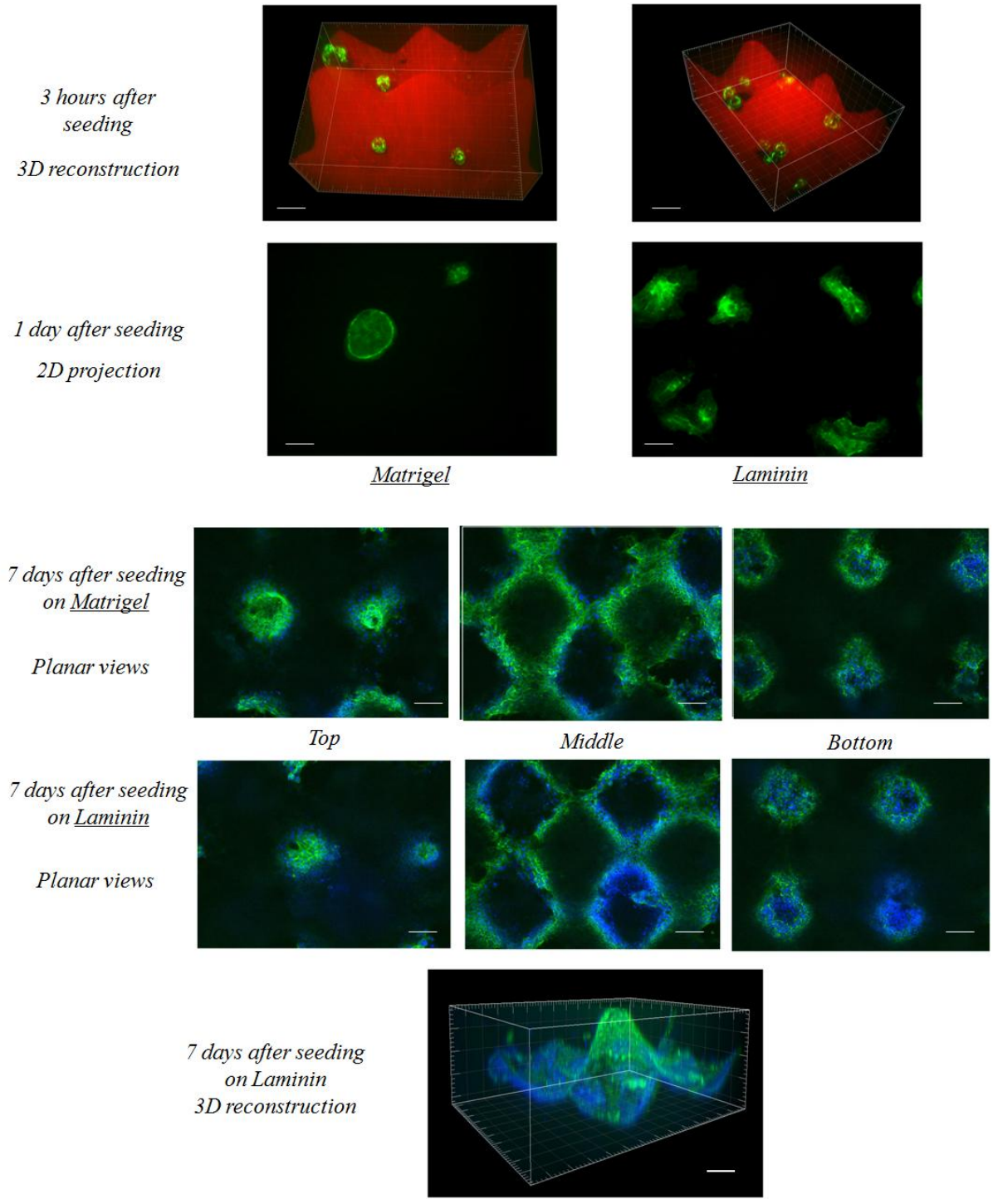

Figure 78: *Organoids growing as a monolayer on the collagen structure. 3 hours after seeding, cystic organoids adhered at the bottom of the scaffold. On day 1, they were still shaped as cysts on Matrigel (the hollow internal part does not appear on the 2D projection) or started to spread as monolayers on laminin. On day 7, the cells successfully covered the whole scaffold on both coatings. Collagen is labeled in red (TAMRA collagen), nuclei in blue (Dapi) and actin in green (Phalloidin). Scale bars are 100µm.*

After 1 day of culture, organoids successfully adhered to the scaffolds. However, organoids were differently shaped depending on the type of coating: on laminin, organoids opened up and started spreading on the structure, whereas they were still shaped as hollow balls on Matrigel coating (Figure 78). After 8 days of culture, organoids covered entirely some microstructures of both laminin and Matrigel-coated scaffolds. Their speed of growing was impressive as it was comparable to the proliferative rate of Caco2 which is abnormally elevated due to their cancer origin. In addition, no differences in cell shape were noticed between laminin and Matrigel coatings.

The opening of the cystic structure is a complex mechanism that requires breaking of the intercellular junctions. Thus, while on laminin coating, cellular-matrix junctions were favored over cell-cell junctions from the early time points, on Matrigel coating opening of the organoids occurred with some delay. Therefore, the nature or concentration of the molecules coated on the scaffold, might dictate the speed of the organoids opening. This point could not be clearly investigated since Matrigel constituents and their relative concentrations were not specified by the supplier.

Depending on the area of the device considered, some microstructures always remained unpopulated by cells. Although we shacked the organoid suspension in order to seed approximately one organoid per crypt, some of the crypts remained empty. As a consequence, villi surrounded by crypts that all contained one organoid were more rapidly covered with cells. In addition, the close vicinity of organoids on densely seeded areas might also stimulate cell proliferation through paracrine signaling among organoids.

Although both Matrigel and laminin coatings supported organoids spreading as a monolayer after 8 days of culture, we choose laminin over Matrigel for the following reasons: 1) Laminin coating was more homogeneous; 2) patches of Matrigel often detached from the scaffold after 10 days that might disturb epithelial monolayer; 3) the composition and the concentration of the laminin coating could be controlled.

The final height of 10mg/mL collagen scaffolds covered with the monolayer of primary cells was comparable to those obtained with Caco2 cells (~220µm), suggesting that the stress applied on collagen microstructure is comparable between primary cells and cell lines.

Finally, we investigated if epithelial cells could survive extended period of time after reaching confluence which is required to study epithelial homeostasis. Actin laminin indicated that the epithelial cell monolayer was still cohesive one week after confluence and indicated that primary epithelial cells were indeed still alive since this cohesion was lost with dead cells. As for Caco2 cells, we considered that 7 days was a reasonable period of time for the primary tissue to attain its steady state, and consecutively we could study proliferation and differentiation pattern.

Altogether our experiments demonstrated the importance of the microenvironment on morphogenesis as the substrate composition induced the disruption of the organized organoid 3D structure to allow their spreading. However, it also indicated that a minimal cell organization provided by organoids was necessary for cells to survive and colonize the scaffold as isolated individual cells did not survive on the structure.

III.2. Proliferation patterns of primary cells on collagen scaffolds.

Next we investigated if similarly to Caco2 cells, primary cells also presented a pattern of proliferation in response to constrains imposed by the 3D structure of the scaffold. Because the results obtained with Caco2 cells showed that there is a minimal amplitude in topography variations or stiffness that cells can sense and respond to, in addition to 10mg/mL collagen scaffolds, we also used PDMS mold that cannot be deformed.

PDMS mold were coated with laminin and Matrigel as collagen scaffolds were. However, we observed that organoids grew in a very different manner on PDMS molds compared to collagen scaffolds (Figure 79). After 7 days of culture, organoids covered less than a half of the scaffold. Although organoids seemed to open up since patches of cells organized as monolayer could be observed, some regions were still covered with unopened budding organoids.

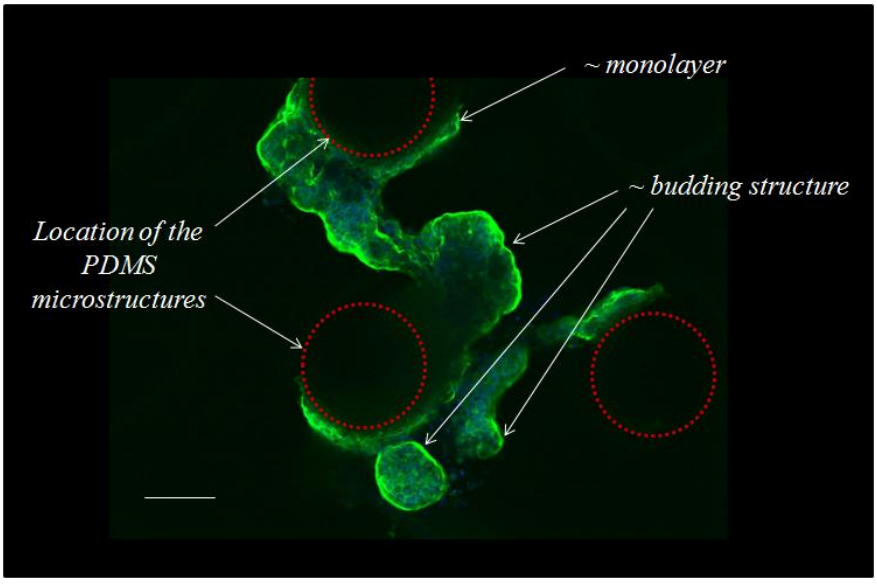

Figure 79: *Primary cells growing on PDMS microstructures coated with laminin. Top view of the organization of primary cells on PDMS. Nuclei are labeled in blue (Dapi), actin in green (Phalloidin) and the villi are represented in red. Scale bar is 100µm.*

Since PDMS was coated with Matrigel or laminin, similarly as collagen scaffolds, our hypothesis was that this different growing mode was induced by increased substrate stiffness. However, since the chemical composition and texture (fibrillar or not) differs between PDMS and collagen, it is difficult to postulate that stiffness is the only parameter that influence the growing of organoids. Currently, I

am performing additional experiments with genipin cross-linked collagen. Since fibrillar structure and chemical composition will be similar the conclusion on the importance of stiffness would be more certain.

In conclusion, natural hydrogels seemed to provide stiffness, texture and composition that induce *in vivo* like behavior to the tissue they support. In this respect, they presented a major asset for tissue engineering compared to synthetic substrates.

To investigate the location of proliferating cells, organoids were seeded on 10mg/mL collagen scaffolds. The location of proliferative cells was examined 7 days after the epithelial cells reached confluence.

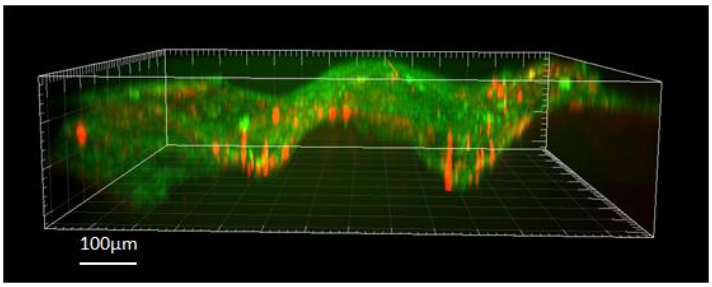

Figure 80: *Spatial location of proliferative primary cells on 10mg/mL collagen scaffold. Side view of 3D reconstruction. Actin is labeled in green (Phalloidin) and proliferative cells in red (Ki67). For clarity reasons nuclei were not represented.*

As for Caco2 cells, proliferative primary cells seemed mostly located in the crypts (Figure 80). We were tempted to conclude that the 3D confinement imposed by the microstructured matrix induced this spatial restriction of the proliferative cells to the crypt also observed *in vivo*. However, it was not clear if this specific location of proliferative cells was related to the initial positioning of the organoids in the crypt or effectively imposed by the matrix. As a matter of fact, the original position of the organoids could set the position of proliferative cells and their proliferation could locally generate a mitotic pressure that would induce the migration of their daughter cells along the villi. Therefore, monitoring the position of proliferative cells during the colonization of the structure, as we did for Caco2, would have helped us deciphering between these two hypotheses.

The restriction of proliferative cells to the crypts implied that differentiated cells should be found on the villi. In a preliminary set of experiment we attempted to label these cells with makers specific to each differentiated cell type of the intestinal epithelium. Ulex europacus agglutinin 1 (UEA) was used to identify both Goblet and Paneth cells as it bound to the carbohydrate secreted by these two types of cells. An antibody against villin, a protein associated to microvillar actin filaments, was chosen to identify enterocytes.

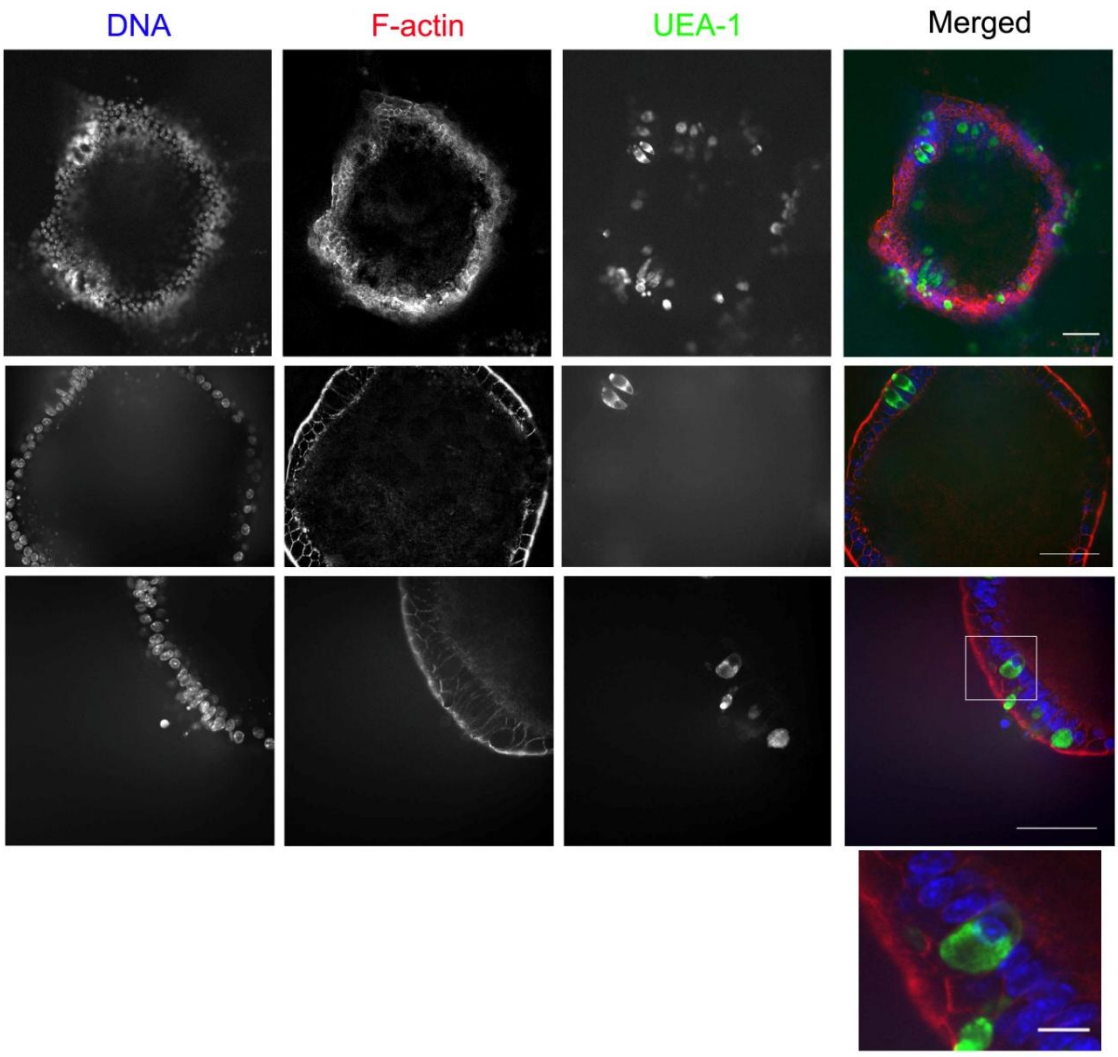

Figure 81: *Identification of differentiated cells in the primary epithelium at different locations. Goblet and Paneth cells were labeled with UEA (green cells) at the bottom (first row) , middle (second row) and top of the crypt (third row). On the enlargement of the last picture, secretory granules characteristic of Paneth cells are visible. Actin is labeled in red (Phalloidin), nuclei in blue and UEA in green. Scale bars: three rows: 50µm, enlargement: 10µm.*

Goblet and Paneth cells were successfully indentified on the structures both on the villi and in the crypts and confirmed the ability of cells to differentiate on our device. At a higher magnification the secretory granules characterics of Paneth cells were visible (Figure 81). Villin, however, was not visualized on our structure. Similarly, the staining of lysozyme a lytic enzyme exclusively synthesized by Paneth cells was not successful. Since these data were only preliminary, they need to be repeated with optimized staining protocols.

In conclusion, the pattern of proliferative cells observed with primary cells was consistent with the observations we made with Caco2 cells and more importantly was in agreement with the specific location of proliferative cells in the crypt *in vivo*. Such spontaneous spatial arrangement of cells confirmed the relevance of our device as an *in vitro* model to study intestinal homeostasis. The

presence of differentiated cells was partially demonstrated since Paneth and/or Goblet cells were localized on our scaffold.

III.3. Influence of fibroblasts on the primary epithelial cells growth

One of the main advantages of our *in vitro* platform was the ability to test how different parameters affect intestinal homeostasis. The fact that only one parameter varies at the time, also facilitated the read-out of the experiments compared to *in vivo* experiments in which the modification of one parameter could induce myriads of parallel effects. For example, using our device, we could test extreme situations like presence or absence of fibroblasts. That could not be experimented *in vivo* since it would be lethal for mice. Further, we could asses if fibroblasts present in the matrix are able to synthesize basement membrane together with epithelial cells. We also aim at investigating if fibroblasts promote epithelial cells migration by co-migrating with them, and finally if they participate in the maintenance of the stem cell state.

In order to mimic the *in vivo* configuration, primary fibroblasts were seeded in the collagen bulk. Since myofibroblasts are found in close contact with epithelial cells in the crypt, we also added some fibroblasts on the surface of collagen crypts directly under the laminin coating. Organoids were then seeded as previously described. Until now we only have preliminary data but as the observations were unexpected they were still reported in this manuscript.

In the firsts hours following organoids seeding, fibroblasts seemed to aggregate around organoids as if they were attracted by epithelial cells. On the following day, organoids were not cohesive anymore, they appeared as dissociated cells randomly distributed on the scaffold. We hypothesized that fibroblasts pulled the epithelial cells in the organoids and disrupted their intercellular junctions. One of the main defects of this experiment was that fibroblasts were not stained before seeding so they were hardly distinguishable from epithelial cells. However, by comparing the shape of cells we could still differentiated the elongated actin bundles characterizing fibroblasts from the more roundish shape of epithelial cells.

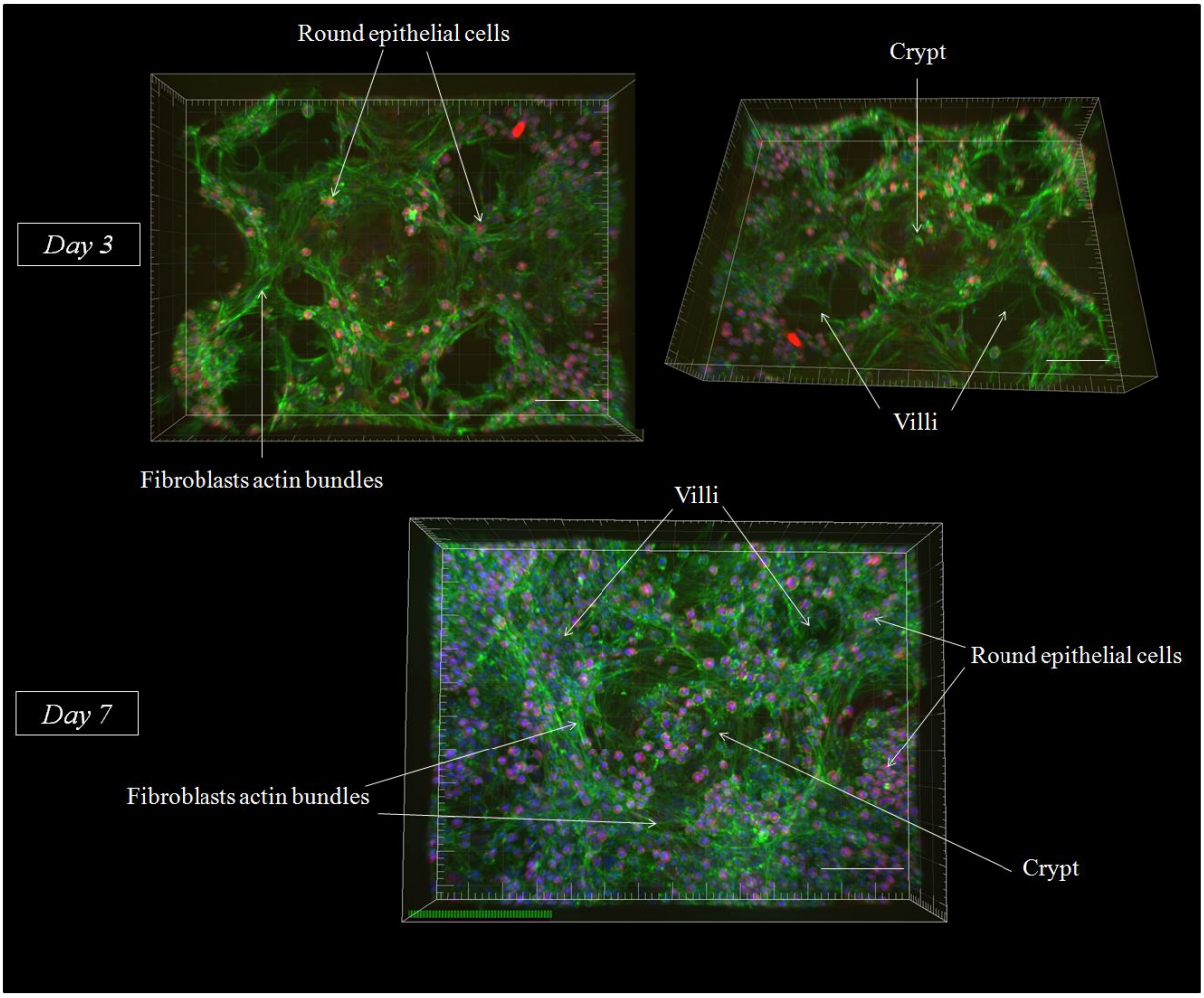

Figure 82: *Fibroblasts role in epithelial cells growing on collagen scaffolds. On day 3, fibroblasts actin bundles surrounded villi structure. Top view on the left and side view on the right. On day 7 the whole structure was populated with fibroblasts and epithelial cells. Nuclei are labeled in blue, proliferative nuclei in red (Ki67) and actin in green (Phaloidin). Collagen 10mg/mL, laminin coating.Scale bars are 100µm.*

After 3 days of culture, we noticed that fibroblasts, initially seeded in the crypts, proliferated and started colonizing the villi resulting in a dense network surrounding the structures. Epithelial cells appeared as individual cells but seemed all viable as they were all labeled as proliferative cells. After 7 days of culture, fibroblasts covered the whole structure. Epithelial cells were more numerous but still appeared as individual proliferating (Figure 82). This organization of cells induced by fibroblasts was dramatically different from the cohesive monolayer formed when organoids were seeded alone on the structure. Further experiments are needed to confirm and understand those results. However, this experiment suggested that fibroblasts can promote epithelial cell migration by pulling them apart. In addition, fibroblasts ability to maintain stem cell state was undeniable since all epithelial cells proliferated. However, we used mouse embryonic fibroblasts whose paracrine signaling and secreted matrix might induce different epithelial cell behavior, than the intestinal fibroblasts would. Mouse embryonic fibroblasts are normally used in conventional cell culture as a feeder layer to maintain the

stem cells in their stem state. The abnormal number of proliferative might be related to this aspect of mouse embryonic fibroblasts and could be different if intestinal fibroblasts were used. Since we did not succeed in culturing isolated mice intestinal fibroblasts *in vitro* until today, mouse embryonic fibroblasts were still the best alternative to our model.

In summary, in the presence of fibroblasts, epithelial cells did not longer form a monolayer, and the abnormally high number of them was in the proliferative state. These defects could be related to hyperproliferation of fibroblasts that rapidly became disproportionate in number compared to epithelial cells and increased notably both the tension applied on the organoids and the amount of factors they secreted. Decreasing the proliferation of fibroblasts would allow the epithelial monolayer to remain cohesive and would promote only locally the maintenance of cell proliferation. To test this hypothesis we are currently treating fibroblasts with mytomicin to stop fibroblasts proliferation; their migration and paracrine secretion should not be altered.

Even though most of these results are preliminary, we are still enthusiastic that the platform we have developed reasonably reproduced the main characteristics of the intestinal lamina propria. The transition from the cohesive cystic structure to a monolayer covering the microstructures induced by our matrix but not by PDMS molds suggests the importance of physiological matrix to promote *in vivo* like behavior. Furthermore, the reproduction of the spatial restriction proliferative cells to the crypts confirmed the level of realism of our matrix and gave some insights on the importance of the topography in tissue functions. Finally, our device also permitted to embed fibroblasts in the matrix while restricting epithelial cells to the matrix surface, which reproduce the anatomical organization of the intestinal tissue.

CHAPTER 3: DISCUSSION

I To which extent can one mimic *in vivo* environment?

Before 1980, ECM was considered as an inert space filling material that mechanically supports tissues. The bioactivity of the matrix is now more and more accepted since various alterations of the matrix have been identified as inducing severe diseases (Järveläinen 2009). As an example, coronary disease is caused by a modification of the ECM biochemical composition ECM that induces the agregation of lipoproteins and results in the formation of atherosclerotic plaques. Similarly, hypertension correlates with a stiffening of the blood vessels walls and pulmonary diseases like asthma with a loss of matrix elasticity or compliance.

Besides, these pathological aspects, it has also been demonstrated that biochemical and biomechanical properties of the ECM modulate cell adhesion, migration, proliferation, differentiation, phenotypic modulation and survival (Frantz, Stewart, and Weaver 2010). During morphogenesis, ECM can also act as a structural support that preserves the mechanical integrity of adult tissues and provides boundaries between adjacent tissues (Humphrey, Dufresne, and Schwartz 2014; Rozario and DeSimone 2010). All these functions depend on the tight regulation of ECM molecules synthesis and degradation in space and time. Since tissue engineering aims at reproducing the *in vivo* features of the ECM, the ideal artificial matrix should reproduce its biochemical and biophysical properties.

However, the composition and mechanical properties of *in vivo* ECM are not fixed but results from a dynamic equilibrium between ECM synthesis and degradation qualified as matrix homeostasis. Matrix homeostasis is maintained through a feedback mechanism between ECM constitution and fibroblasts activity as they are the main effectors of chemo-mechano transduction. Fibroblasts sense mechanical or chemical changes within ECM that in turn induce modifications in their phenotype and result in restoring ECM values back to normal (Frantz, Stewart, and Weaver 2010; Humphrey, Dufresne, and Schwartz 2014). To fully replicate *in vivo* ECM characteristics, *in vitro* matrix should allow its remodeling by residing cells to maintain matrix homeostasis during the course of the experiment (Frantz, Stewart, and Weaver 2010). It thus involves that the biophysical microstructure of the synthetic ECM allows matrix deposition and degradation by the cells on time and length scale similar to *in vivo* ECM (Tibbitt and Anseth 2009). In this respect, we chose collagen I matrix as it is the major component of ECM and its *in vitro* self-assembly is very similar to its *in vivo* fibrillar structure. Furthermore, collagen can be remodeled by cells whereas synthetic hydrogel like polyacrylamide or PEG cannot unless special matrixmetallo protease sequences are inserted in the hydrogel.

The other critical parameter was to reproduce the topography of the ECM of the intestine since 3D structure of other organs has been proven to play a major role in guiding tissue morphogenesis and differentiation *in vitro* (cf introduction). The spatial resolution of either complex organs like intestine or simple like blood vessels at micrometer scale has encouraged cross-disciplinary work among biologists, tissue engineers and microfabrication/ microfluidic technologists towards the development of organs-on-chip. However, there are still only limited examples that associate ECM like substrate with a biomimetic topography (cf introduction). So far, most of the microfluidic devices for cell culture present either a non-structured hydrogel included in a microfluidic system or an elastomeric microstructured substrate that fail to reproduce ECM specifications. The two groups that work on *in vitro* gut on chip both seed cells on elastomeric substrate structured (March group) or not (Ingber group). Even though those substrates are coated with ECM molecules, as they miss the micro-architecture specific of ECM (e.g. fibrillar structure and capacity to be remodeled by cells) as well as their mechanical properties; they might induce a different phenotype to the cells than if they were seeded in an ECM-like hydrogel.

Since our final goal is to elucidate the origin of biological phenomena happening *in vivo* (like cell proliferation or differentiation), it was mandatory that our system supports the *in vivo*-like phenotype of cells. In this perspective, we focused on reproducing the composition of *in vivo* intestinal ECM and its topography by adapting soft lithography techniques to the requirements imposed by collagen gels polymerization.

Thanks to the biocompatibility of collagen and to our microfabrication techniques, our device offered the possibility to reproduce the relative spatial organization of the different cell types constitutive of the intestine. Fibroblasts expanded in collagen gels whereas epithelial cells only spread on the surface of the matrix. Furthermore, we could also coat our substrate with a thin homogeneous layer of laminin that replicated intestinal basement membrane.

When we seeded cells either on the substrate or in the bulk, they deformed the initial structure due to the traction forces they exerted on the collagen hydrogel. This observation attested of the differences in mechanical properties between *in vivo* intestinal matrix that supports cell remodeling and migration and its *in vitro* analogous matrix made of collagen I. We thus focused on improving the mechanical properties of collagen scaffolds while remaining consistent with the physiological composition of the *in vivo* matrix. Increasing collagen concentration significantly improved the mechanical properties of the hydrogel but was directly correlated with a decrease in hydrogel porosity that impeded, to some extent, fibroblasts spreading and proliferation. Since we did not want to stress fibroblasts in a dense matrix as it could inhibit matrix secretion and induce lethal paracrine signaling to the adjacent epithelial cells, we looked for alternative option that could improve mechanical properties while providing sufficient porosity.

In our first attempts, we considered that the addition of a stiffer biomimetic hydrogel to the collagen To form semi interpenetrating polymer networks (SIPN) would stiffen the matrix while reducing collagen to a reasonable concentration. Most of the studies, we got inspired off to strengthen the collagen were performed on flat hydrogels at low concentration (around 2mg/mL). Therefore, without any topographical data on how cells retract the hydrogels, the only possibility to evaluate the relevance of a given candidate was to refer the rheological improvements measured performed by the authors. In many cases, the presence of an additional hydrogel limited the concentration of collagen (below or equal to 4mg/mL) we could work with because of reduced solubility of the two hydrogels. Furthermore, the mechanical improvements obtained were always below what we expected according to literature. As an example, in the study of Suri et al (Suri and Schmidt 2009), the rheological measurements estimated that the addition of 30mg/mL glycidyl metacrylated hyaluronic acid to 3mg/mL collagen increased by an order of magnitude the Young Modulus value of the hydrogel obtained compared to collagen. Based on these results, we expected roughly that adding 50mg/mL glycidyl methacrylated hyaluronic acid to 4mg/mL hydrogel, would result in an SIPN with an elastic modulus one order of magnitude higher than collagen hydrogel at 4mg/mL (1.05 kPa). The Young modulus of this resulting hybrid hydrogel should have been in the same range or even higher than the one of 10mg/mL collagen (6kPa). We thus expected the final height of the microstructures of hybrid hydrogel covered with epithelial cells to be higher than for 10mg/mL collagen. Surprisingly, the residual height of GM-HA- collagen hybrid was only 100µm height compared to the 220µm of 10mg/mL collagen. Similarly, based on the work reported by Rowe et al (Rowe and Stegemann 2006) on hybrid collagen/fibrin hydrogels, we obtained microstructures height much lower than expected. In both cases, we were not working higher collagen concentration than the authors, suggesting that the increase in stiffness related to the formation of an SIPN might be relative to the initial concentration of collagen: an added hydrogel that would increase by a factor 3 the Young modulus of a collagen at 2mg/mL, would not necessarily increase to the same extent the Young modulus of a collagen at an higher concentration since the starting matrix is stiffer.

Moreover, comparing Young Modulus values might not be sufficient to fully describe the system. Young modulus is an informative value that characterizes the elastic properties of bulk materials allowing the comparison between different materials. We used this physical parameter to compare collagen hydrogels in term of stiffness and it confirms our first assumption that the stiffer a material is the less the cell can deform it. However, this value does not illustrate the dynamic changes in viscoelastic properties of the material with strain. As cells exert some forces on the hydrogel, they might locally change its rheology and modify the Young Modulus value. As an example, Storm et al (Storm et al. 2005) noticed that although elastic moduli of biological hydrogels like collagen or fibrin remained initially constant with deformation, above a given percentage of deformation (around 10%) their storage moduli increased with deformation while the modulus of polyacrylamide remained

constant regardless of deformation. Therefore, the measurement of the variations in dynamic shear storage moduli with the strain amplitude would add some refinement on the mechanical characterization of hydrogels and could provide some more explanations on how a given hydrogel behave under cell tension. It would also help elucidating why distinct hydrogels with an apparent similar Young Modulus react differently under cell tension.

The other alternative to stiffen collagen gels was to crosslink collagen fibrils to prevent their relative sliding under stress applied by cells. Even if the different approaches applied increased collagen stiffness, chemical cross-linking with toxic molecule like glutaraldehyde or moderately toxic molecule like genipin was more effective than natural glycation reaction. The fact that collagen glycation, which occurs *in vivo*, was not sufficient *in vitro* to resist cell tension, attest of the importance of other mechanisms happening *in vivo*. As previously discussed, *in vivo*, collagen synthesis, molecular and supramolecular arrangements, cross-linking and degradation are performed by fibroblasts (Frantz, Stewart, and Weaver 2010). Fibroblasts themselves are integrated to the matrix they secrete and actively participate in the maintenance of the global tension of the ECM by physically and chemically organizing collagen from molecules to fibers (Humphrey, Dufresne, and Schwartz 2014). Since the accurate fibrillar arrangement realized by fibroblasts is quite impossible to reproduce *in vitro*, we intended to have fibroblasts secrete their own matrix in an enclosed chamber of PDMS which would constrain the matrix they produced in the desired final shape. Since the amount of matrix fibroblasts secrete *in vitro* is quite low (approximately 10µm thick in 5-9 days for NIH3T3 (Beacham, Amatangelo, and Cukierman 2006)), we mixed fibroblasts with collagen at low concentration (2mg/mL) so that they could secrete their matrix in the interstitial space of the collagen fibers to speed up the process. Unfortunately, we did not succeed in maintaining fibroblasts alive in the enclosed PDMS chamber even when we forced the circulation of medium. The apoptosis of fibroblasts might be related to a deficiency in CO_2 because of its limited diffusion through PDMS walls.

As a conclusion, our best attempt to mimic the intestinal ECM was to use self-assembled collagen I hydrogel that allows matrix remodeling and synthesis by the residing fibroblasts and to compensate its weak mechanical properties by using fairly toxic genipin cross-linker. Since we did not succeed in reproducing the highly ordered assembly of collagen fibers carried out by fibroblasts *in vivo*, we had to make a compromise between a physiological substrate made of collagen and the required addition of toxic cross-linker to preserve the topography once the matrix is submitted to cell tension.

Nevertheless, we could wonder if the ability of *in vivo* the intestinal mucosa to resist cell tension, migration and remodeling was an intrinsic feature or if the mechanical contribution of the underlying layers was required. As described in the introduction, the mucosa only contributes for 5-10% in the mechanical strength of the intestine compared to an input of 70-75% from the submucosa. As these two layers are in direct contact, it is likely that the properties of the mucosa are influenced by the

underlying submucosa and that the global biophysical environment experienced by the cells in the mucosa results from a combination of mechanical properties of both layers. In addition, blood capillaries that cross the submucosa may dynamically participate in the mechanical resistance of the mucosa matrix to cell tension because of the interstitial pressure applied by blood flow. Therefore, reproducing the exact biophysical properties of the environment perceived by cells is even more complex than expected as one layer of tissue does not recapitulate the integrity of the signals delivered to the cells.

Concerning the biochemical composition of the ECM, even though collagen I is the major constituent of ECM, our matrix does not completely reflect the refinement in composition of the intestinal ECM. To circumvent this deficiency, tissue engineers now isolate the matrix from the organ corresponding to the tissue they want to grow in order to preserve the biochemical composition of the original matrix (Jeffords et al. 2015). The isolated matrix are enzymatically digested, lyophilized and resuspended in solvent as for collagen solutions. However, they assemble less spontaneously than collagen gels and the use of an additional cross-linker like genipin is necessary (Jeffords et al. 2015). Concerning intestine, small intestine submucosa (SIS) hydrogel extracted from the submucosa layer has been considerably used recently as substrate for cell culture but not intestinal cell necessarily. Small intestine submucosa gels are composed of collagen I and III at 90%, type IV, V and VI collagen, glucosaminoglycan, fibronectine and heparin (T. Jiang et al. 2009). Although such matrices reproduce more faithfully the composition of *in vivo* matrix compared to collagen I scaffold, they introduce some complexity in the interpretation of the results as they are less biochemically and biophysically controlled than traditional hydrogels. Furthermore, we were interested in replicating the intestinal mucosa rather than its submucosa.

In vivo epithelial cells rely on the basement membrane at their basal pole. In order to reproduce this layer of specialized ECM, we coated our collagen scaffold with laminin which is the major constituent of basement membrane *in vivo*. Although the global composition and the thickness of the layer were consistent with *in vivo*, our coating was homogenously distributed on the collagen surface and thus lacked the specific spatial distribution of basement membrane constituents along the crypt-villus axis found in the small intestine. Since this definite patterns of constituent might support epithelial migration and differentiation (see § introduction), our replicated basement membrane might be less effective than *in vivo* one.

In conclusion, the expanding tissue engineering field provided us some tools to reproduce accurately the composition of the matrix and alternative options to approach the stiffness sensed by cell *in vivo*. In parallel the techniques developed by microfabrication engineered and microfluidics permit to increase the level of sophistication of these matrix by structuring in 3D these matrices to reproduce the

topography sensed by cells at the microscale. However, there is still room for improvement to reach the level of complexity of *in vivo* matrix.

II How the mechanical and physical cues of the matrix affect epithelium behavior.

The rheological measurements performed with the fluctuation specular reflection method revealed important increase of collagen gels Young Moduli (from 0.6 kPa to 6kPa) with collagen concentration (from 2 to 10mg/mL). According to literature, substrate stiffness affects the intercellular and cell-matrix adhesions state as well as the cytoskeletal tension of cells. These three parameters are somehow related since integrins and cadherins, that respectively mediate cell-matrix and cell-cell adhesions, interact with the cytoskeleton. Wang et al (Y.-K. Wang et al. 2003) noticed that integrin α2β1 of cells seeded on soft collagen gels acted as a mechanosensor and induced a decrease in focal adhesions numbers compared to the cells grown on stiff glass substrate coated with collagen. Similarly, Ladoux et al (Ladoux et al. 2010) observed that an increase in hydrogel stiffness correlated with a more spread phenotype, a more organized cytoskeleton and an increase in the forces transmitted through cadherin junctions. Furthermore, they noticed that disrupting cytoskeleton assembly directly reduced the forces exerted through cadherin junctions. They concluded that the strength of cadherin junctions depends both on substrate stiffness and on the intrinsic tension of cytoskeleton.

As a consequence, we expected in our experiments the global tension of the monolayer to be larger on stiffer collagen matrix.

II.1 Evaluation of epithelial tissue forces on the structure.

Currently, the two main methods to measure the traction forces exerted by cells on a substrate are the micro-force sensor arrays and the traction force microscopy (Martiel et al. 2015; du Roure et al. 2005; Tambe et al. 2011). Micro-forces sensor arrays are constituted of a collection of PDMS micropillars on which cells are seeded. The forces exerted by the cells are deduced from the measurements of micropillar deflection at the cell periphery (du Roure et al. 2005). Regarding traction force microscopy, cell are seeded on the surface or embedded in a hydrogel substrate that contains fluorescent microbeads. The stress field applied by cells on the hydrogel is deduced from the computational analysis of beads displacements (Tambe et al. 2011). In both techniques, information on the Young Modulus of the hydrogel or PDMS is necessary to evaluate cell traction forces.

We first considered our scaffold as a third alternative to estimate the traction forces exerted by an entire tissue. Since the initial geometry of the hydrogel and its Young modulus were established, the surface tension applied by the tissue on the hydrogel could be deduced from the comparison of the hydrogel final geometry when cells had reached confluence with its geometry without cells. In addition, the fact that collagen could be considered as an elastic hydrogel was confirmed by our rheological analysis which indicated that the visoelastic properties of collagen gels were dominated by

their elastic component. However, according to literature, biological gels are particular since they present a nonlinear elasticity and stiffen as they are strained (Figure 83 (i)) (Storm et al. 2005). This particularity is related to their filamentous architecture. Biological fibrillar networks are considered by polymer physicists as semi flexible polymer networks compared to PDMS, polyacrylamide or polyethylene glycol made of flexible chains that present a linear elasticity (cf polyacrylamide on Figure 83). Our rheological measurements confirmed that collagen gels could be assimilated as semi-flexible polymer networks since the variations of plateau modulus values as a function of collagen concentration was in good agreement with the scaling law model describing semi-flexible polymer networks (Figure 83 (ii)).

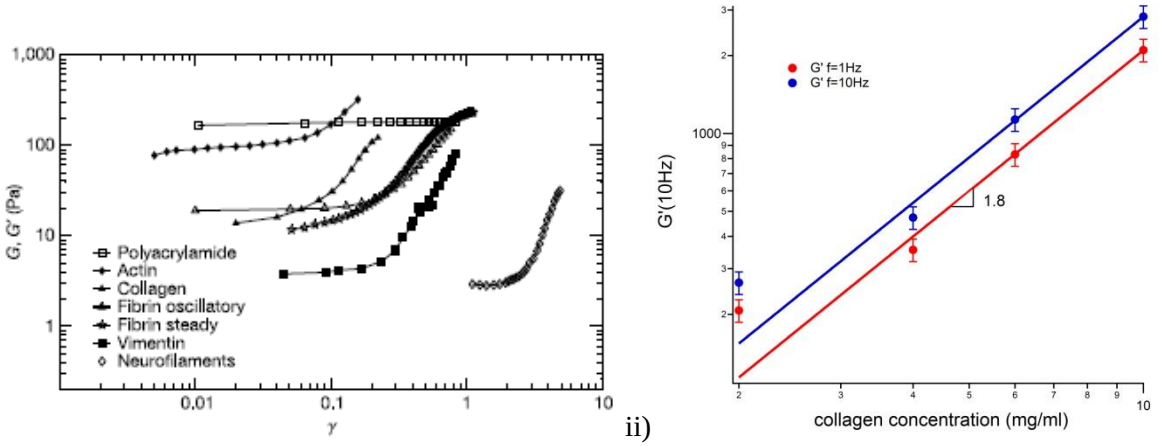

i) ii)

Figure 83: *Collagen gels as semi flexible polymers. (i) Dynamic storage moduli G'as a function of the dimensionless strain γ applied. Imported from* (Storm et al. 2005).*(ii) Reproduction of Figure 43, that confirmed elastic moduli as a function of collagen concentration follows the power low* $G' = c^{\alpha}$ *with* $\alpha = 1,8$ *characteristic of biological semi-flexible polymers.*

The low strain regime of semi flexible polymers is dominated by chains entropy (i.e the switch of filaments from bended state to a stretched state and their alignment in the direction of the strain reduces the number of conformations available for the system) (Storm et al. 2005; Winer, Oake, and Janmey 2009). At higher strain, semi-flexible filaments are in their stretched conformation and further stretching of these filaments adds an enthalpic contribution to the force-extension relation responsible for the increase of the elastic modulus. The values of strain that corresponds to the transition from linear to non-linear elasticity depend on the persistence length of the polymers considered. For flexible polymers (PDMS, polyacrylamide, polyethylene glycol), the persistence length lp is very small compared to the contour length Lc (i.e maximum end-to-end distance of a linear polymer chain) and this transition occurs at very high strain (higher than 100%). On the contrary, for semi-flexible polymer the persistence length and the contour length are of comparable order of magnitude and this transition appears at lower strain (10%).

i) 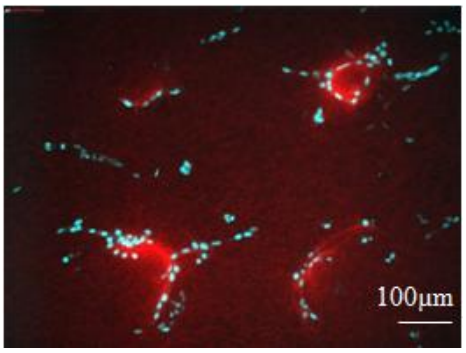

ii) 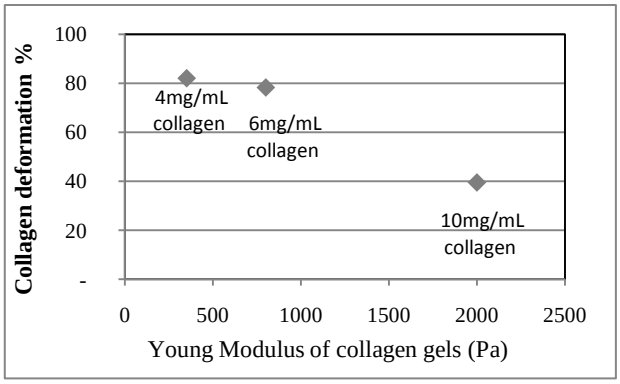

Figure 84: *Cells remodel fibrillar collagen network. (i) Reproduction of Figure 53(i) 2d projection of the z stacks of collagen gel at 6mg/mL containing fibroblasts. Nuclei are labeled in cyan (dapi) and collagen in red (TAMRA collagen). (ii) Collagen deformation by Caco2 cells in % as a function of the initial value of the Young Modulus of collagen gels.*

The rearrangement of collagen fibrils with strain and their local concentration under cell tension was particularly visible on the experiments we performed with fibroblasts where the local aggregation of fibers coincided with cells location (Figure 84 (i)). Since deformations we measured were all above 10% for Caco2 at the collagen concentrations we used (Figure 84(ii)), we considered that our experiments might already stand in the non-linear regime of elasticity of the collagen and that the Young modulus we measured might not be valid anymore. However, the estimation of storage modulus increase with concentration made by Storm et al (Storm et al. 2005) were obtained by shear-measurements while it is likely that forces applied by cells in our system were compressive or stretching forces. The strain value at which the transition from linear to non-linear elasticity occurs for collagen in our device might thus be different. As we were not certain to have the accurate values of collagen Young modulus, we could not deduce the tension applied by the epithelial monolayer on collagen structures. Additional dynamic rheological measurements of the variations of collagen Young Modulus under compression or traction would give us this missing information.

Although further rheological measurements need to be performed to fully characterize the system, our device presents interesting feature regarding the possibility to measure the tension applied by a whole cellular monolayer. Furthermore, the fact the estimation of the tissue forces could be performed on a microstructured environment that recapitulate the complexity of the *in vivo* matrix (fibrillar collagen and topography), makes the measurements even more representative of the tensions developed by tissues *in vivo* and provide additional information to the already existing traction-forces measurement methods.

In conclusion, we could not precisely estimate if distinctive cortical tensions were induced depending on the stiffness of the substrate cells were seeded on. However, the differential patterns of growth displayed by cells as they colonized the structure whether they were seeded on collagen 4mg/mL or

10mg/mL and the reduced proliferative rate of cells on 4mg/mL collagen strongly suggested that matrix features can influence cell collective behavior.

II.2 Emergence of collective coordinated colonization induced by the combination of matrix stiffness and topography.

In literature, collective cell behavior describes cell movements that are organized over characteristic length scales that are larger than the individual elements constituting the system (R. K. Vedula et al. 2013). In this respect, on both 4mg/mL and 10mg/mL concentration, Caco2 epithelial cells colonize the scaffold collectively, since they were organized as cohesive patches of cells with discernible migration fronts rather than as individual cells that migrate randomly.

On 10mg/mL, collective cell colonization seemed, however, more coordinated and synchronized than on 4mg/mL. The distinct patches of cells formed in each crypt fused as they migrated out of the crypt and synchronized as a unique monolayer that colonized the villi. Conversely, on 4mg/mL the cell patches formed randomly and grew regardless of the topography initially imposed by the matrix. As previously discussed, it was difficult to determine if the stiffness of the matrix was the only parameter responsible for such difference or if the amplitude of the topography was also at play.

Studies realized on 2D substrates of different stiffness provided some information on the different mode of collective migration developed by epithelial cells depending on the stiffness of the substrate (Ng et al. 2012). Rosa et al (Ng et al. 2012) measured the correlation of velocities and direction of cell migration and observed that on soft substrates only the first rows of cells contributed to cell migration while on stiffer substrate cells at 500µm from the leading edge still positively contribute to directional cell migration. In addition, actin fibers at 400µm from the leading edge were clearly aligned in the direction of migration whereas no clear organization was perceived on softer hydrogels. To precisely evaluate the role of cytoskeleton tension in this large scale coordination of cell migration, the authors inhibited myosin II. They observed a decrease in migration speed and in persistence length and thus deduced that the internal tension of cell was involved. Since analogous effect was induced by the inhibition of cadherin junctions, the authors concluded that an internal minimal tension of cells imposed by the substrate was required to ensure a long range intercellular transmission of the direction of migration. Similarly, we could hypothesize that on our device, a minimal internal tension was required for cells to sense the topography. On 4mg/mL, only the first rows of cells would be coordinated and the integration of the local variation of topography on this reduced length scale would be too small compared to the amplitude of the sinusoid (400µm). On the contrary, on stiffer hydrogels the variation of topography would be integrated in length scale comparable to the characteristic length of the sinusoid.

On the highest collagen concentration, the rings formed during structure colonization were very similar to circular wound closure shapes observed on 2D substrate (Cochet-Escartin et al. 2014). In both configurations, an actin ring formed at the edge of the monolayer (Figure 85). Labeling of myosin II light chain on our structure would show if an analogous actomyosin contractile cable also assembled at the migration front.

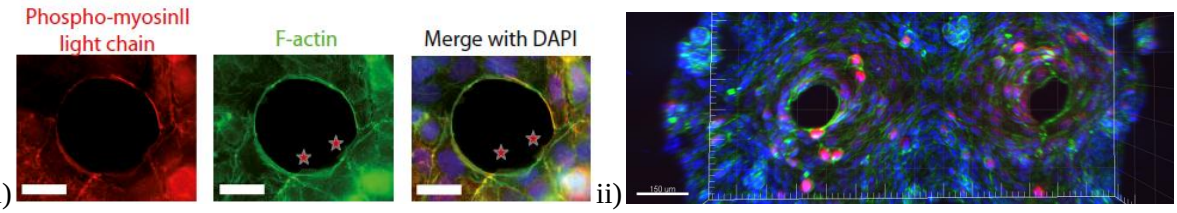

Figure 85: *Constriction rings forming in 2D and 3D conformations. (i) Wound healing rings formed with Madin-Darby canine kidney epithelial cells on 2D substrate (Myosin II labeled in red, F actin in green and nuclei in blue. Scale bar 25µm).Imported from* (Cochet-Escartin et al. 2014)*(ii) rings forming at the migration front of Caco2 on day 3(Reproduction of Figure 74: proliferative cells labeled in red, actin in green and nuclei in blue scale bar 150µm).*

Collective migration and wound healing have been extensively studied on 2D substrate (Cochet-Escartin et al. 2014; Reffay et al. 2014; Tambe et al. 2011). Working with stencil or micropatterning allows to reproduce in 2D the complex geometry experienced by cells *in vivo*. Working in plane permits to abrogate any side effect related to the third dimension and thus facilitates the read out of the experiments. Wound healing and migration studies on 2D substrates exposed two main types of migration occurring *in vitro*. The first model demonstrates the existence of leader cells at the migration front that actively migrate and provide local guidance cues to the cells that passively follow them. The second model suggests that all cells actively contribute to the monolayer migration. They collectively orient and migrate in the direction of the maximal principal stress which also corresponds to the direction that minimizes the intercellular shear stress. To establish if one of this two mechanisms directed cell colonization on our model we could perform traction microscopy analysis on our model. However, implementing this technique to our model might be very complex due to the 3D geometry that would require important calculation given the height of the microstructure.

Micropatterning techniques also permit to study the influence of constrained geometry on collective migration. Planar studies of spatially constrained cellular migration revealed that cells developed different modes of migration depending on the level of constrain imposed by the matrix. On large stripes (400 mm), Madin-Darby canine kidney (MDCK) epithelial cells migrate slowly with a linear progression, and show some vortex in their velocity orientation profile. Conversely, on narrow stripes (20 mm), cells migrate faster, with some fluctuations due to cyclic contraction-elongation. Additionally, the velocity field direction aligns with the stripe axis, suggesting that cell confinement induces a more organized and directed tissue migration (S. R. K. Vedula et al. 2012). Using our model, we could verify if such variations were observed on 3D structured substrates with different

curvature and if the migration mode depends more on the confinement imposed by the structure than on the stiffness of the matrix. Since the interaction with the matrix also regulated the spatial positioning of intercellular junction, the different migration modes might generate distinct colonization patterns on the structure (Tseng et al. 2012).

Although additional experiments are needed to investigate which parameter between stiffness and spatial constriction influence the most cells spreading and growing on the structure, our model clearly demonstrated the influence of mechanotransduction in morphogenesis. Concerning intestinal tissue, epithelium morphogenesis coincides with the spatial restriction of proliferative cells to the crypt. This spatial segregation between proliferative and differentiated cells (expect for Paneth cells) is later maintained in the adult tissue. Similar pattern of proliferation was observed on our microstructured matrix where proliferative cells were mostly located in the crypts.

II.3 Local rigidity and geometry sensing integrated at the tissue scale regulates spatial positioning of proliferative cells.

The influence of cytoskeleton tension on cell proliferation has already been established thanks to micropatterning techniques. As an example, assymetrical patterns of adhesion molecules induce cell shape anisotropy and this spatial heterogeneous distribution of cytoskeleton governs the orientation of the mitotic spindle (Théry et al. 2005). Similarly, the decrease in intracellular tension induced by a lower adhesion molecules density prevents the progression of cell cycle. A minimal intracellular tension is thus required for cells to enter in S phase (DNA synthesis phase) (S. Huang, Chen, and Ingber 1998). Interestingly, the fact that molecular actors of the cell tension are also involved in cellular checkpoints that govern the transition to S phase further supports the important role of mechanical tension in the regulation of cell proliferation. For instance, the level of RhoGTPase in its active form, a small enzyme that controls actin polymerization and cytoskeletal tension trough its downstream effectors, regulates the transition to S phase (Nelson et al. 2005). These observations support our vision that the proliferative pattern on our device might derive from pattern of differential cellular tension.

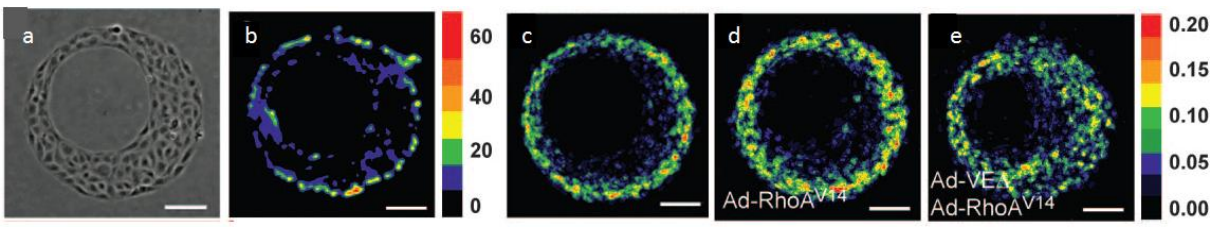

Figure 86: *Proliferative cells location coincides with the regions where the higher traction forces are exerted on substrate. (a) Confluent monolayer of MDCK epithelial cells grown on a 2D pattern. (b) Colorimetric map of the traction forces applied on the substrate. Colorimetric scale is in nN. (c-d) Colorimetric map of proliferative cells. (c) control situation. (d) RhoA is over expressed increasing cytoskeletal tension. (e) RhoA is overexpressed and cadherin junction formation is inhibited.*

Colorimetric scale: a pixel value of 0.20 indicates that 20% of cells at that location proliferated. Scale bars are 100µm. Adapted from (Nelson et al. 2005).

The influence of tension on cell proliferation has also been studied at the tissue scale on micropatterns of different shapes (Figure 86 (a)). Nelson et al (Nelson et al. 2005) observed that once cells reached confluence, the location of proliferative cells coincides with the regions were the cells developed the highest traction forces on the substrate (Figure 86 (b)&(c)). They noticed that increasing cellular tension increased and enhanced the pattern observed (Figure 86 (d)). They deduced that cytoskeletal tension was directly involved in the establishment of such proliferative pattern. However, when this increase in cellular tension was coupled with blockage of cadherin junction formation, the pattern of proliferation was absent and proliferative cells were uniformly distributed in the monolayer (Figure 86 (e)). These experiments suggest that cytoskeletal tension is required for cells to locally sense the geometry of the matrix but that long range transmission through intercellular junction of these local heterogeneities in tension is necessary to induce pattern of proliferation. The authors translated their 2D observation to a 3D pyramidal array and similarly noticed that proliferative cells were mostly located in the valleys, which were computationally defined as the regions that induced higher cells traction stress (Figure 87). This last observation is in agreement with the preferential location of proliferative cells in the crypts that somehow correspond to their valleys. Crypts would thus correspond to the area where the internal tension of cell is the highest. An analogous computational model of the tension experienced by cells depending on their position on our structure would confirm this statement.

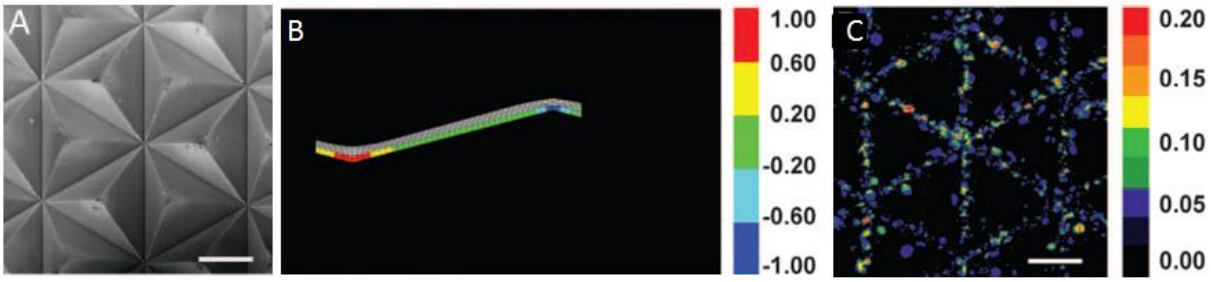

Figure 87: *Pattern of proliferation on 3D substrate. A) Scanning electron microscopy picture of the substrate. B) Computational calculation of the relative maximum principal tractional stress exerted by cells on the surface. C) Colorimetric map of proliferative cells on the substrate. Scale bars are 100µm. Adapted from* (Nelson et al. 2005).

Deducing the mechanism occurring on 3D structure from situations observed on 2D substrates seemed, however, controversial. On 2D squared or round patterns, cells appeared to be only under tension whereas compressive forces might also occur on 3D structures. Intuitively, we assumed that cells in the crypt were more under compression considering the concave geometry of crypts combined to the mitotic pressure developed by proliferative cells in this area. Conversely, on the convex

curvature of the villi, we expected cells to be under tension. Therefore, on 3D substrate, the type of strain sensed by the cells should also be considered to describe the system more accurately.

On our device, proliferative cells were located in the crypt only when the tissue reached its steady state. In the colonization phase, proliferative cells were present at the migration front. In this early stage, the argument of proliferative cells being preferentially located at the highest tractional stress would suggest that the cells at the migration front were initially the most tensed. The tensile force developed by cells at the migration front would thus be higher than the tension imposed by the substrate in the crypt. This model would be in favor of the leader cell model were most of the traction forces are concentrated in the first rows of cells at the migration front. This hypothesis suggests that when confluence was reached the tensile stress at the front disappeared and the mechanical stress applied to the monolayer was only dictated by substrate confinement inducing the translocation of proliferative cells to the crypt. Another possibility is that before confluence, the proliferative cells were preferentially located in the less densely populated area independently of the substrate topography. When confluence was reached, all cells were equally confined and the proliferative patterned appeared, suggesting that spatial constriction provided by the matrix only induced a pattern of proliferation when cells were already confined by neighboring cells.

We observed that on 4mg/mL collagen proliferative cells were not restricted to the crypts but were rather randomly distributed on the surface of the structure. Since cells pulled on the structure as they colonized it, it was hard to distinguish if the absence of pattern was related to the lower stiffness of this matrix or to the reduced height of the structure. If Nelson et al (Nelson et al. 2005) reported the dimensions of their pyramidal array, we could draw conclusions on the relative importance of each parameter. If their computational scheme was printed to scale, the structure they designed should have a period of 200µm and a height around 30µm. Our 4mg/mL collagen structure presented a residual height of 60µm for a 400µm period. Since the dimensions are comparable and their substrate seemed to be rigid, it would imply that the stiffness of the matrix seemed to be the critical parameter for cells to sense the matrix. It would thus suggest that a sufficient cellular tension imposed by the matrix would be required for cells to sense matrix topography. This conclusion remains just a hypothesis since all information required was not provided in the article.

The fact that proliferative pattern was adopted by two types of cells with distinct origin (primary or cell line) emphasizes the importance of mechanical features (cell tension, distorsion) in tissue homeostasis. In addition, the fact that our matrix induced primary cells to replicate the spatial segregation between differentiated and proliferative cells found in intestinal tissue attested of the physiological relevance of our device.

II.4. How is our model useful compared to organoids?

Intestinal organoids that were developed by Sato et al (Sato et al. 2009) are more and more exploited as *in vitro* tools to study intestinal homeostasis (Farin, Van Es, and Clevers 2012; Katano et al. 2015; Yan, Chia, and Li 2012). They present a good alternative to *in vivo* studies as they are easier to manipulate since *in vitro* techniques like siRNA can be directly applied on them. The possibility to amplify them and passage them as cells from cell line is also a major advantage as it considerably reduces the number of mice required to conduct an experiment. However, they do not completely recapitulate the morphology of the intestine as the architecture of the villi is missing. The buds are constantly growing and their number is permanently increasing whereas the number of crypts remains constant in number and in shape in adult intestine (Figure 88).

i)  ii) 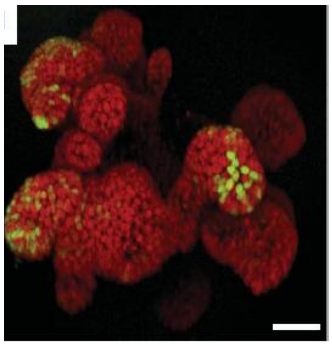

Figure 88: *Organoids expansion in time. (i) 13 days old organoid. Transmission picture x4 magnification. (ii) After 3 week in culture. 3D reconstruction, scale bar 50µm, Lgr5 cells are labeled in green and nuclei in red. Imported from* (Sato et al. 2009)

Concerning these two aspects our device was more representative of the *in vivo* situation since we set the architecture of the matrix. We determined the dimensions and the spatial positioning of villi and crypt so that the global morphology was fixed and steady as in the small intestine. The finite boundaries imposed by our matrix plays a similar role than the external muscular layers that restrain the expansion of the intestinal epithelium *in vivo*. The absence of spatial constraint in the organoids culture may induce different cell behavior compared to *in vivo* situation. The permanent expansion of the organoids also attests that the tissue never reaches its steady state since the number of mitotic cells is not balanced by the number of apoptotic cells. Consequently, organoids do not appear as the best model to study intestinal tissue homeostasis *in vitro*.

In culture, the environment of organoids embedded in Matrigel is very simple since only the composition of the basement membrane is imitated. Our device reproduced both, the mucosa made of collagen and fibroblasts, and the basement membrane. Furthermore, their relative proportions are preserved since only a thin layer of laminin coats the collagen scaffold. These several layers also permits to spatially separate the different types of cells in agreement with the compartmentalization observed *in vivo*: fibroblasts are present in the matrix and separated from the epithelial cells by the basement membrane.

On a more practical point of view, our device provides the ability to control and investigate distinct parameters that cannot be monitored in organoid traditional culture. In this respect, we could vary the stiffness, composition and geometry of the substrate or include other cell types to the system. As an example, replacing collagen substrate by PDMS, pointed out the influence of the matrix stiffness on the opening of the organoids. Organoids spreading on our device required the disruption of intercellular junctions. If we applied the model developed by Gonzalez et al (Gonzalez-Rodriguez et al. 2012) on the spreading of aggregates on a surface, organoids would only spread on a matrix if the cell-matrix adhesion are more energetically favorable to the system than cell-cell adhesion. These authors have established a model in which the spread parameter S was defined as $S = W_{sc} - W_{cc}$, where W_{cc} and W_{sc} represent the cell-cell adhesion energy per unit area and the cell-matrix adhesion energy per unit area, respectively (Gonzalez-Rodriguez et al. 2012). The density of adhesion molecules and the matrix stiffness are implemented in the cell adhesion energy while the number of cadherin is defined as the main actor of cell-cell adhesion energy. Since the same coating was realized on both collagen and PDMS and similar organoids were deposited on the structure, we assumed that the density of adhesion molecules and cadherin was equivalent in the two situations. Matrix stiffness would then be responsible for the differences in spreading. However, Douezan et al (Douezan, Dumond, and Brochard-Wyart 2012) suggest that the stiffer the matrix is the more the tissue spread. The fact that we observed the exact inverse phenomenon on our structure might be explained by the origin of the cells considered. Most of the studies are performed with cell lines. Those cells are cultured on very stiff substrates and implicitly a selection is made since only the cells that adhere on these substrates survive. When transferred onto our device, these cells like Caco2 experienced more difficulty to proliferate on soft substrates than on stiffer ones. On the opposite, primary cells that were extracted from a soft intestinal tissue spread more on soft collagen substrate than on stiff PDMS substrate. It would indicate that cells proliferate and spread more on substrates that have rigidity comparable to their original substrate (i.e plastic flasks or *in vivo* ECM).

The fact that organoids did not spread on PDMS stiff substrate did not imply that primary cells were not able to colonize stiff structure since Costello et al (Costello et al. 2014) succeeded to grow primary intestinal cells on their PLGA scaffolds whose rigidity is estimated to be around 1-10MPa (Mattioli-Belmonte et al. 2008). Unlike us, they managed to grow a monolayer of primary cells directly from the crypt they isolated. However, the physiological substrate that permit the seeding of fibroblasts and the crypt like structure were absent from their model. In addition, the specific location of proliferative cells was not reported in their study. Nevertheless, they could identify differentiated Goblet and Paneth cells. We could identify the same differentiated cells types on our device as UEA labeled both cells types but an additional labeling could help us discriminate Goblet cells from Paneth cells. Although those are only preliminary data, the addition of fibroblasts seemed to stimulate cell proliferation. This over-proliferation might be related to the type of fibroblasts and their density which

directly translated into increased amount of factors they secretes that can induce the maintenance of proliferative state. Factors promoting epithelial stem cells maintenance and stimulating epithelial growth are also contained in the cell culture media: R-Spondin which is a Wnt agonist was added together with Epithelial Growth Factors (EGF) to induce cell proliferation and Noggin, a BMP inhibitor, was added to increase the number of crypts. These factors were initially required for primary cells to recover from intestinal isolation and to form organoids but they might inhibit cell differentiation at later stages on our scaffolds. They might be too concentrated and consequently they could "hide" the differentiation signals coming from the matrix. In the future we could investigate if a reduction of growth factors concentration promotes differentiation of epithelial cells.

The other *in vitro* gut-on-chip system developed in Ingber lab (Kim and Ingber 2013), proposes an alternative approach as the final geometry of the intestine was not initially imposed to cells but imposed by cyclic strains applied on a membrane that mimicked peristaltic motion. In this device, the physiological aspect of the substrate that could enable the seeding of fibroblasts is again missing. However, their study performed on Caco2 cells suggests that peristaltic motion could initiate villi formation and cell differentiation. The addition of a peristaltic motion to our device might further stimulate the differentiation process.

CHAPTER 4: CONCLUSION

In the last ten years, several techniques developed in the microfabrication field have been adapted to cell biology to better apprehend cell physiology from individual cells to tissue. As an example, micropatterning provided some explicit insights on how ECM adhesion molecule can affect cell polarity, cortical tension, the positioning of division axis and even cell differentiation (Burute and Thery 2012; Kilian et al. 2010; Théry 2010; Théry et al. 2005). Observing tissues on controlled 2D substrates also permitted to elucidate the driving forces of collective cell migration at the monolayer scale (Reffay et al. 2014; du Roure et al. 2005; S. R. K. Vedula et al. 2012). The next challenge for cell biology is to extend the information collected on planar substrate to the third dimension.

3D hydrogel matrices are now considered as tools to better mimic the *in vivo* environment of cells and new questions are emerging with them. Several studies demonstrated that the stiffness of the matrix, its fibrillar structure and even the alignment of matrix fibrils could induce differential cell behavior (Christopherson, Song, and Mao 2009; Engler et al. 2006; Xu et al. 2014). In this project, we could experience the notable influence of matrix stiffness on tissue morphogenesis. Such differences point out the need to standardize the protocols to generate artificial matrices and the techniques to characterize them in order to draw reliable comparisons between the experiments performed in different labs. Despite these existing variations between matrices, 3D cell culture really improved the level of realism of cell culture compared to 2D culture as cell phenotype, gene expression and polarity are similar to the *in vivo* (Villasante and Vunjak-Novakovic 2015). In this respect, cell culture in hydrogels are now estimated as a valuable asset for clinical studies as the quantity of drug needed to visualize an effect are lower than on 2D system and are more compatible with *in vivo* quantities (Aref et al. 2013).

Organs on chip are also considered as an emerging technology that could benefit drug screening as they present additional advantages to those related to 3D cell culture. Depending on their design, micofabricated chips permit to reproduce the spatial organization of different cell type, to precisely control the microenvironment of cells and to recreate physiological topography or dynamic stress experienced by cells (Kim et al. 2012; van der Meer et al. 2010; Zheng et al. 2012). The ability to control the relative spatial positioning of various cell types is now exploited to develop human body-on-chip in which human cells constitutive of different organs are seeded in distinct chambers interconnected as the organs are in the body (Bhatia and Ingber 2014; J. H. Sung, Kam, and Shuler 2010). Such device would permit to study the side effects induced by a drug that initially targets one specific organ (Bricks et al. 2015; Prot et al. 2014).

To date, only few systems combined the physiological environment provided by artificial matrices with the advantages displayed by organ on chip. In my PhD project, we adapted and optimized the microfabrication techniques to structure substrates at the micrometer scales developed in organ on chips to mold hydrogel matrices that respect the anatomical dimensions of mice intestine. Thus, we coupled the influence of physiological substrate provided by collagen I gels to a 3D structure replicating the physical constraints perceived by intestinal epithelium *in vivo*. This unique combination induced the spatial restriction of proliferative cells to the crypts. Furthermore, the presence of fully differentiated cells such as Goblet and Paneth cells attested of the functionality of the 3D intestinal tissue engineered. The joined influence of the composition and morphology of the matrix to induce the differentiation of cells into a functional tissue is also well illustrated in regenerative medicine. In recent attempts to transplant a liver, it appeared that the conservation of the organ's 3D structure and its extracellular matrix after decellularization was sufficient to recreate a whole functional tissue starting from isolated primary hepatocytes (Uygun et al. 2010).

Altogether, our device provides the first *in vitro* model of functional intestinal tissue with physiologically relevant geometries and microenvironment. This platform presents the advantages of *in vitro* devices as all the parameters (i.e stiffness, curvature, composition of the matrix, type of cells) are controlled and can be investigated independently paving the way to new both biological and biophysical investigations. Since we focused on the physiological aspect of the matrix we generated, we expect the conclusions we will draw about the mechanisms driving intestinal homeostasis to be representative of the *in vivo* situation.

With regards to the research topics studied in the two labs in which I realized my PhD project, biological questions concerning how bacteria interact with intestinal epithelium or how the expansion of cancerous primary organoids differs from normal organoids can already be addressed with the actual device. Additional features like an internal microvasculature or peristaltic motion can be implemented by adapting technologies existing in organ on chips models to our system. The inclusion of these dynamic aspects to our system will further increase the level of realism of our *in vitro* platform. Finally, this model can also be oversized and seeded with human primary cells to study inflammatory intestinal diseases like Crohn disease or intestinal ulcers.

The fast expanding organ on chip community constantly provides innovative techniques to mimic *in vivo* environment and holds the promise of an integrated *in vitro* model that would recapitulate the complexity of living bodies. Concerted efforts from different fields (i.e microfabrication, fluidic, biology, soft matter…) are necessary to reach this goal and these cross-talks participate to the richness of this interdisciplinary community.

CHAPTER 5: MATERIAL AND METHODS

Cell lines

Human colon cancer cells Caco2, mouse embryonic fibroblasts (MEF C57BL/6) were obtained from America Type Culture Collection (ATCC). Caco2 and NIH3T3 cells were cultured in DMEM (Gibco) supplemented with 10% (v/v) foetal bovine serum (Invitrogen) in 5% CO_2 humidified air culture incubator. MEF cells were cultured in DMEM supplemented with 5% (v/v) foetal bovine serum, 1mM sodium pyruvate (Gibco) and 1X MEM non essential amino acids (Gibco) in 5% CO_2 humidified air culture incubator.

Crypt isolation and organoid culture

All experiments were carried out in accordance with European Community Council Directives.

Mices were sacrificed by isoflurane sedation (1errane, Baxter) followed by cervical dislocation and all efforts were made to minimize suffering. The small intestine was isolated and cleared from its inner materials with cleaning solution (2% (v/v) antibiotic-antimycotic (Gibco), 1% (v/v) gentamicin (Gibco) in cold sterile PBS). The intestine was opened longitudinally, cut into pieces of 3cm long and incubated in the cleaning solution with constant shaking at 4°C twice for 15 minutes. The tissue was then cut in smaller pieces (5mm long) and transferred to a 2mM EDTA solution for 30 minutes at 4°C. The supernatant was discarded and replaced by cleaning solution. The tissue was gently dissociated by pipetting 10 times the tissue solution using a 10mL pipette. The supernatant was kept on ice (=fraction 1), replaced by fresh cleaning solution and the tissue solution was pipetted again. New fractions were collected until fraction 4 which was centrifuged at 1000rpm for 3 minutes at 4°C. The pellet was resuspended in cleaning solution, filtered through a 70µm filter and centrifuged at 400g for 6 minutes. The pellet was resuspended in Matrigel (Corning) half diluted in cold PBS and plated in 48 well plates. The Matrigel was allowed to polymerise for 30 minutes in 5% CO_2 humidified air culture incubator. After polymerisation, organoid culture medium (DMEM F12 Invitrogen) supplemented with growth factors (EGF 20ng/mL (Peprotech), FGF 10ng/mL (Peprotech), Noggin 100ng/mL(Peprotech), Glutamax 2,5% (v/v) (Gibco), R-Spondin 500ng/mL (R&D System), B27 1X (Gibco), N2 1X (Gibco))was added.

Mouse embryonic fibroblasts (MEF) isolation:

Mouse embryos were dissected at 16 days post coitum. Limbs, internal organs and heads were removed from embryos. The carcasses were placed in a 50mL sterile conical tube containing PBS and rinsed three tumes with sterile DMEM without serum. The carcasses were minced into very small pieces with surgical blade. Minced embryos were transferred to tube containing 10mL of 2mM EDTA

solution and 5grams of sterile glass beads (5 mm in diameter, Sigma-Aldrich). The suspension was incubated for 30 minutes at 37°C. After incubation, 10mL of 2mM EDTA solution were added to tissue suspension. A magnetic stirrer was added to the suspension which was incubated for another 30 minutes at 37°C with stirring. 10mL of 2mM EDTA solution were added another time to tissue suspension and incubation step with stirring was repeated. Cell suspension was then decanted into two 50mL tubes each containing 3mL of foetal bovine serum. The cell suspension was centrifuged at 1000 rpm for 5 minutes and the pellets were resuspended in 50mL DMEM supplemented with 10% foetal bovine serum. The number of viable nucleated cells were counted using Trypan Blue. 5. 106 cells were then plated in 175 cm^2 culture flasks containing DMEM supplemented with 10% foetal bovine serum. The medium was changed the next day and grew at confluence before being passage at 1:6.

Specific labelling were performed on the cell culture obtained to verify that only MEF where isolated and not other cell types survived. As the cells were all positive for vimentin (an intermediate filament particularly expressed in fibroblasts) and negative for E-cadherin, we confirmed that the cells we isolated were fibroblasts.

i) 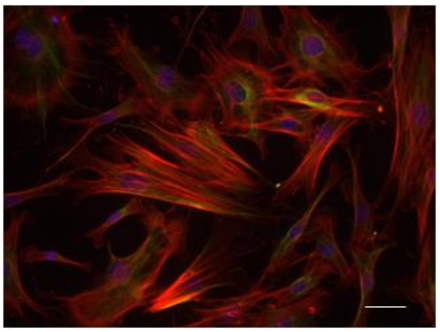 ii) 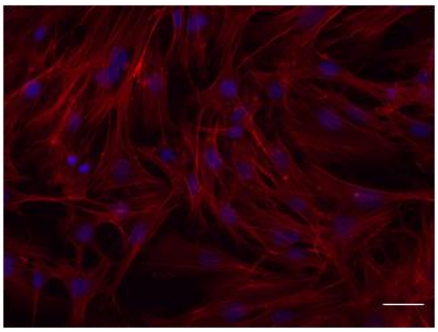

Figure 83: *Primary mouse embryonic fibroblasts isolated. (i) MEF were vimentin positive (Vimentin in green, actin in red, nuclei in blue) and (ii) cadherin negative (cadherin in green, actin in red and nuclei in blue).*

Collagen I labeling

Rat tail collagen I (non-pepsinized; Corning) dissolved in acetic acid 0.2% (v/v) was dialyzed over night against labeling buffer (0.25M NaHCO3, 0.4M NaCl, pH 9.5) at 4°C. Tetramethylrhodamine (TAMRA, Invitrogen) was resuspended in DMSO according to manufacturer's instructions to reach a final concentration of 1mg/mL. TAMRA solution was then mixed with collagen in (1:1) ratio and stirred overnight at 4°C. Free dye was removed by dialyzing the labelled collagen against labelling buffer overnight at 4°C. To restore the TAMRA-labelled collagen to its initial solvent a dialysis was performed over night against acetic acid 0.2% (v/v) at 4°C. The final volume of TAMRA-labelled collagen was measured and its final concentration was calculated considering the initial volume and concentration of the collagen stock solution used. TAMRA-labelled collagen was stored at 4°C.

Collagen I extraction

Rat tails were left in 70% ethanol for 15 minutes. The skin was removed from the tail. The vertebrae were broken and the segments were pulled from the rest of the tail. Each tendon was pulled out with

forceps and placed in 70% ethanol. The tendons were then placed in sterile distilled water where the bundles were separated into thinner strands. The strands were transferred to sterile acetic acid 0.2% (v/v) for 5 days. The extract was first centrifuged at 3000g for 30 minutes. Then the supernatant was collected and centrifuged at 8800g for 90 minutes. The supernatant was lyophilized and the collagen was stored at -20°C.

Fabrication of PDMS molds

Two molds were fabricated: one with an inner cavity to hold the collagen (mold 2) and the other with the structure to mold the collagen (mold 1). Both designs were drawn on Katia software and micro milled in aluminum. PDMS (Sylgard 184, Dow Corning) components were mixed in weight ratio of 1/11 curing agent to 10/11 base. Air bubbles were removed by applying vacuum. Liquid PDMS was then poured on both molds and cured at 60°C for 4 hours. The PDMS molds were then autoclaved to prevent contamination.

Surface treatment of the PDMS mold

The surface of mold 1 was plasma activated (plasma cleaner Harrick). The inner cavity of the mold was filled with a 2% (v/v) (3-aminopropyl)triethoxysilane (APTES) solution for 30 minutes. Silane solution was aspirated and the inner cavity of the PDMS mold was filled with deionised water for 5 minutes to wash the residual silane. The water was then replaced by a 0,5% (v/v) glutaraldehyde solution for 30 minutes. As described above, the mold is then washed twice for 10 minutes with deionised water and left in deionised water at 4°C overnight.

Preparation of collagen gels solutions

The volume of collagen required was calculated regarding the concentration of the stock collagen solution and the final collagen concentration needed. The desired volume of collagen of the stock solution was transferred to a 2mL tube using a pipette dedicated to viscous liquids (Transferpettor, 500µL, BrandTech). To prepare fluorescent collagen solution, TAMRA labelled collagen was mixed to non labelled collagen in weight ratio of 1/10 of labelled collagen to 9/10 of non labelled collagen. The neutralizing solution, to reach a final pH of 7.4, was prepared in another tube. The neutralizing reagents consisted of PBS (10X), culture medium (Gibco DMEM glutamax), Fetal Bovine serum (Gibco), sodium pyruvate (100mM Gibco), MEM non-essential amino acids (MEM NEAA 100X, Gibco) and NaOH 1M. The proportion of each constituent was calculated as follows:

V_{PBS}= 0,1* V_{final}

V_{NaOH}= 0,022* $V_{Collagen}$ for commercial collagen and 0,04* $V_{Collagen}$ for home made collagen and TAMRA labelled collagen

$V_{Fetal\ Bovine\ Serum}$=0,1* V_{final}

$V_{MEM\ NEAA}$=0,01* V_{Final}

$V_{Sodium\ Pyruvate}$= 0,01* V_{Final}

$V_{DMEM} = V_{Final} - V_{PBS} - V_{Collagen} - V_{NaOH} - V_{Fetal\ Bovine\ Serum} - V_{MEM\ NEAA} - V_{Sodium\ Pyruvate}$

The solution of neutralizing reagent was mixed on ice and pipetted on the top of collagen. For high final collagen concentration (<8 mg/mL) the gel was gently mixed on ice with a sterile spatula to avoid any bubbles. For lower concentration the gel was mixed with a pipette. If bubbles formed, the mixture was centrifuged at 1000g at 4°C for 1 minute. The pH of the solution was controlled to be at 7,4 before adding the cells.

For scaffold containing fibroblasts, the mixed neutralized gel was prepared by deducing the volume of the cell suspension from the volume of DMEM. The final concentration of fibroblast was 2.10^5cells/mL in the gel.

Injection-molding of the collagen in microstructured PDMS chamber (see Figure 47)

Two holes (4mm diameter, Huot Instruments) were punched in the cavity of mold 1. Tape was placed around the microstructures on mold 2 to plasma activate only the area with the microstructures (plasma cleaner Harrick). This surface oxidation induced the wetting of the collagen on the PDMS microstructures such that the entrapment of bubbles was minimized. The two molds were assembled and hermetically sealed with two clips. A small silicon tygon tube (0,032", Cole Parmer Instrument Company) was inserted in the injection hole of mold 1.

The collagen solution was drawn into a 1mL syringe. A 1mL cone was cut and placed at the tip of the syringe. The solution was injected through the tube in the PDMS enclosed chamber. The collagen was left to polymerize in the PDMS under the hood at room temperature for 30 minutes. Once the collagen was polymerized the clips were removed and the PDMS chamber was immersed in culture medium. The two parts of the mold were gently pulled apart using tweezers and mold 2 was removed. Since the PDMS was immersed, the medium directly wetted the collagen after unmolding. The collagen attached to PDMS mold 1 was kept immersed to avoid collagen drying.

Cell seeding on the collagen scaffold

Caco2 epithelial cells were seeded directly on the collagen scaffold. The liquid at the surface of the collagen scaffold was replaced by 300µL of the cell suspension (5. 10^5 cells/mL). The cells were left to adhere on the collagen structure for one hour in the incubator. The PDMS scaffolds were then turned upside down on two sticky PDMS pads in a petri dish (22,1cm²). The medium was added (5mL) and immediately filled the space between the collagen and the bottom of the petri dish by capillarity. The 'upside down' position of the scaffold minimized the accumulation of dead cells at the bottom of the crypt, due to gravity. The sticky PDMS pads prevented the collagen/PDMS scaffold from floating.

Concerning organoids, laminin coating (§ Laminin coating) was realized prior to organoids seeding. In the same way as for the Caco2 cells, 300µL of the organoids solution were deposited on the collagen

surface (approximately 40 organoids per device) and gently shacked to make organoids fall into crypts. Device were left for 3 hours in the incubator for cells to adhere. The PDMS scaffolds were then immersed in cell culture medium.

Laminin coating

Laminin stock solution (1mg/mL in Tris HCL buffer, Invitrogen) was diluted to 0,02mg/mL in cell culture medium and kept on ice. The liquid at the surface of the immersed collagen scaffold was replaced by 300µL of the laminin solution. Laminin coating solution was left on the collagen for 30 minutes in the incubator. The laminin solution was then removed and the collagen was washed with media for 5 minutes. In the case of fluorescent coating fluorescent laminin (§ Laminin labelling) was mixed to non labelled laminin in weight ratio of 1/10 fluorescent laminin to 9/10 unlabelled laminin.
For PDMS surface coating, the microstructured area was plasma activated. 300µL of the laminin solution were deposited on the top activated surface and again left for 30 minutes in the incubator. The laminin solution was removed and washed with media for 5 minutes.

Matrigel coating

Matrigel (Corning) was diluted to 10%(v/v) in culture medium and kept on ice. The liquid at the surface of the immersed collagen scaffold was replaced by 300µL of the Matrigel solution. The Matrigel coating solution was left on the collagen for 30 minutes in the incubator. The Matrigel solution was then removed and the collagen was washed with media for 5 minutes. In the case of fluorescent coating, 2,5%(v/v) of fluorescent laminin is added to the coating solution. For PDMS surface coating, the microstructured area was plasma activated. 300µL of the Matrigel solution were deposited on the top activated surface and again left for 30 minutes in the incubator. The Matrigel solution was removed and washed with media for 5 minutes.

Laminin labelling

Laminin was dialyzed for 2 days against PBS at 4°C. The PBS was changed twice a day. On the third day the PBS was replaced by labelling buffer (4mM Na_2CO_3, 46mM $NaHCO_3$). The laminin was dialyzed overnight at 4°C in the labelling buffer. The conjugation was performed following the procedure from the manufacturer (GE Healthcare Life Sciences, Cy3 mono-reactive dye pack). To remove free dyes, the fluorescent laminin solution was dialyzed over night against labelling buffer. Then the labelling buffer was exchanged with PBS for an overnight dialysis. The concentration of labelled laminin was determined by fluorescence spectroscopy.

Collagen and Glycidyl Metacrylated Hyaluronic Acid (GMHA) (in collaboration with Nadège Pantoustier, ESPCI)

Hyaluronic acid (Lifecore, 29kDa) was dissolved in 50: 50 water: acetone by stirring overnight at room temperature. On the following day, glycidyl methacrylate and triethylamine were added to the hyaluronic acid (HA) solution in 20 fold molar excess and stirred overnight. The solution was then

dialysed against water for 2 days. The water was changed every 2 hours on the first day and twice a day on the second day. The solution was lyophilised, desiccated and stored at -20°C in the dark. The ratio of glycidyl methacrylate grafted by HA molecule was determined by magnetic nuclear resonance (MNR).

The GMHA stock solution was prepared at 100mg/mL in water. The final concentrations tested were 50mg/mL for the GMHA and 1% (wt) for the photoinitiator (Irgacure 2959, Ciba). The volumes of both reagents were deduced from the volume of medium in collagen solutions and were added once the collagen was neutralized. The GMHA-collagen solution was injected in the PDMS molds and allowed to polymerise at room temperature. The GMHA-collagen gel was exposed to the UV light (LCL5 Hamamatsu, 8mW/cm²) through the PDMS mold for 30s. The gels were immediately unmolded and rinsed three times for 5 minutes and every 15 minutes for one hour.

Collagen and Fibrin

Firbinogen from bovine plasma (Sigma) was diluted in PBS to 20mg/mL. The volume of fibrinogen was deduced from the volume of medium and was added to the neutralised collagen solution to reach a final concentration of 2mg/mL. The fibrinogen-collagen solution was injected in the PDMS mold and left to polymerise for 30 minutes at room temperature. Once unmolded the liquid at the surface of the immersed fibrinogen-collagen scaffold was replace by a thrombin solution (from bovine plasma, Sigma) diluted to 1,25U/mL in PBS. The thrombin solution was left for 5 minutes on the collagen and then rinsed twice for 15 minutes.

Collagen and ribose

D-Ribose (Sigma) was diluted in 0,1%(v/v) acetic acid to prepare a stock solution at 0,5M. The solution was filtered through 0,22µm filter.

Collagen stock solution (Corning) (3mg/mL or 6mg/mL) were mixed with ribose stock solution to reach final concentrations of 0, 50, 100 or 200mM ribose. The collagen solutions were left to glycate at 4°C for 4 days. Glycated collagen was then used as normal collagen (see § Preparation of collagen solutions).

Collagen and silica particles

The commercial silica solution (LUDOX HS-40, Sigma) was diluted to a stock solution of 20mg/mL in 0,2 (v/v)% acetic acid. The silica particles were mixed to the collagen acidic solution. Final concentrations of silica particles tested were 0.5, 1, 1.5 and 2mg/mL. To neutralize the solution of silica particles mixed to the collagen, the volume of sodium hydroxide was determined according to the following equation:

V_{NaOH}= 0,4 * $V_{Silica\ particles}$ + 0,22* $V_{Collagen}$ for commercial collagen or 0,4* $V_{Collagen}$ for home-made collagen and TAMRA labelled collagen

The solution of neutralising reagents was gradually added to the solution to avoid aggregation of silica particles. The neutralized solution was then injected in the PDMS mold as for normal collagen.

Collagen and glutaraldehyde

The collagen gels were prepared as described in § Preparation of collagen solutions and § Injection-molding of collagen.

Once polymerised the collagen gels were unmolded and incubated in a solution of 0,5% (v/v) glutaraldehyde (Euromedex) in PBS at room temperature for 2 hours. The glutaraldehyde solution was replaced by a 2% (w/v) glycin solution (Lifetechnologies) to neutralise the residual glutaraldehyde. The glycine solution was refreshed after 15 minutes. The collagen gels were left overnight in glycine and the solution was renewed again twice on the following day. The glycine solution was replaced by medium and the collagen gels were left overnight in the medium. The medium was replaced on the following day.

Collagen and Genipin

Genipin (Abcam) was diluted in DMSO to a 2000mM stock solution. Stock solution was kept at -20°C and unfrozen at room temperature 1 hour before use. Fresh diluted genipin solutions were prepared on the day of treatment to minimise the reaction of genipin with the media. The solution tested were 0,5mM, 1mM and 10mM.

The collagen gels were prepared as described in § Preparation of collagen solutions and § Injection-molding of collagen. Once polymerised the collagen gels were unmolded and incubated in genipin solutions for 6h, 12h or 24h. Collagen gels were rinsed twice with media. The medium solution was then refreshed every hour for 3 hours to remove the residual genipin.

Collagen sample preparation for rheology experiments

Great attention was paid on the flatness of the PDMS since it dictated the flatness of the final collagen gels. PDMS rings of 1cm inner diameter and 0,5cm height were cut out. Two holes (Ø 0,75mm, Harris Uni Core) were punched in the wall of the ring and a small PTFE tube (O.D 1,07mm, Cole Parmer) was inserted in one of them. Since the hole of the tube was too thin to directly inject the collagen with the syringe, a larger tygon tube (I.D 0,031", O.D. 0,093", Cole Parmer Instrument Company) was adapted at the end of the thin tube to avoid any leakage during collagen injection. Two pieces of PDMS (1cm*1cm) were adjusted on the top and bottom of the ring to form an enclosed chamber, hermetically sealed with two clips.

Collagen solution was prepared as described in § Preparation of collagen solution and drawn into a 1mL syringe. A 1mL cone was cut and placed at the tip of the syringe. The solution was injected through the tubing in the PDMS enclosed chamber. The collagen was allowed to polymerise at room temperature. Before collagen unmolding, the chamber dedicated to rheology measurements was filled up with PBS. The Clips and PDMS pieces enclosing the PDMS ring were rapidly removed.

Immediately after the PDMS ring containing the collagen was transferred into the PBS bath. The collagen was gently detached from the PDMS ring wall using tweezers. The PBS level was adjusted to reach the limit of the upper surface of the collagen gel to prevent the collagen from drying. The collagen was not completely immersed to avoid the recording of the fluctuations of the PBS solution instead of those of the collagen gel surface.

Rheology measurements (methods developed by Laurence Talini, ESPCI)

Measurements of the viscoelastic modulus of the collagen at various frequencies were performed using the technique of surface fluctuation specular reflection (SFSR) spectroscopy developed in the Sciences et Ingénierie de la Matière Molle / Physico-chimie des Polymères et Milieux Dispersés (SIMM/PPMD) lab of the ESPCI.

Collagen samples were prepared as described in § Collagen sample preparation for rheology experiments.

The laser beam (diameter of laser beam: 41.3µm, 27.5µm or 3.5µm) was reflected by a prism and focused on the surface of the collagen gels. The surface deviated the laser beam which was reflected a second time by the prism. The reflected laser beam was collected on the center of the detector composed of a two-quadrant photodiode. The difference in voltages between the two quadrants directly quantifies the fluctuations in height of the surface of the sample. The duration of the acquisition varied from 1 to 5 minutes to investigate a larger range of frequencies. The signals recorded were analyzed by Laurence Talini (detailed calculations are available in the following papers:(Pottier et al. 2011, 2013)). Subsequently the diagram of viscoelastic modulus vs frequency was plotted.

Immunofluorescence

The cells were fixed with 4% (v/v) paraformaldehyde (Electron Microscopy Sciences) in PBS for 30 minutes. When matrigel was used, 0,25% (v/v) glutaraldehyde (Euromedex) was added to the paraformaldehyde solution to prevent its degradation. The collagen was rinsed 3 times with PBS for 5 minutes. The cells were permeabilised in a 1% (v/v) triton (Triton 100X, Euromedex) solution. The permeabilizing solution was rinsed in PBS for 5 minutes. The cells were incubated in the solution containing the primary antibody overnight at 4°C. The samples were washed three times in PBS supplemented with 0,05%(v/v) Tween 20(VWR) to remove the primary antibodies bounded to the collagen fibbers. The solution containing secondary antibodies, Dapi and Phalloidin was incubated for 2 hours at room temperature. After incubation, the scaffolds containing the cells was rinsed 3 times for 30 minutes in PBS containing 0,05%(v/v) Tween 20. The samples were stored in PBS at 4°C until imaging.

Identification of collagen by nanoLC-Mass Spectrometry/Mass Spectrometry (MS) analysis (Protocol developed by Vanessa Masson and Loew Damarys)

Collagen samples (50 µg) were dissolved in 110 µL of 25 mM NH_4HCO_3 and denaturated at 60°C for 3h. Samples were then centrifuged at 12000g for 20 min at 20°C. 5µg of each were digested by using 0.2 µg Trypsine/LysC (Promega) in 10 µL of 25 mM NH_4HCO_3 for 4 hours at 37 °C (protocol adapted from (G. Zhang et al. 2006)). 1µl of digested samples was reconstituted in 5 µl solution A (2% (v/v) acetonitrile/water, 0.1% (v/v) formic acid), and transferred to a HPLC vial for nanoLC-MS/MS analysis. Peptides were analyzed (6 µL) using an RSLCnano system (UltiMate 3000, Thermo Scientific) connected to an AB Sciex TripleTOF® 6600 mass spectrometer. Sample separation was achieved on an analytical C18 column (75 µm id x 500 mm long, packed with 3 µm particles with 100 Å pore size, C18 PepMap™, Dionex S.A.) using a linear gradient of 77 min (from 1 to 25% (v/v)) of solvent B (100% (v/v) acetonitrile, 0.085% (v/v) formic acid) at 300 nL/min and an oven temperature of 40 °C. Data acquisition was performed using Analyst TF (1.7), set for the positive-ion mode with an electrospray (ESI) voltage of 2.5 kV, a curtain gas of 30 psi, an ion source gas 1 of 15 psi and an interface heater at 75°C.

Data were searched against the SwissProt rattus database containing 7930 sequences using Mascot™ 2.4 Software. Enzyme specificity was set to trypsin and a maximum of three miss cleavages was allowed. Oxidized methionine, N-terminal acetylation and carbamidomethyle cysteine were set as variable modifications. The mass tolerances in MS and MS/MS were set to 10 ppm and 0.1 Da, respectively. The resulting Mascot files were further processed using myProMS (Poullet, Carpentier, and Barillot 2007) where we fixed the false discovery rate (FDR) for all peptide and protein identification to less than 5%.

Microscopy and imaging

Collagen gels and 3D cell cultured were imaged using an upright confocal spinning disk (Roper/Zeiss) equipped with 10x/0,3 NA (working distance 5,2mm) objective, 405nm, 491nm, 561nm and 634nm lasers and controlled by Metamorph imaging software (Universal Imaging). To image the experiments on 3D microstructured substrates, Z stacks acquisitions were set to start 20µm above the 3D structure and to end 20µm bellow the 3D structure. Flat bulks were imaged starting 20µm above the surface until 400µm below the surface. Z stacks were acquired every 2 to 5µm depending on the level of resolution needed. Images were processed on Image J software to get 2D profiles of the microstructures and to measure them. Imaris software was used to project the Z stacks in 3D.

BIBLIOGRAPHY

Al-Haque, Shahed et al. 2012. "Hydrogel Substrate Stiffness and Topography Interact to Induce Contact Guidance in Cardiac Fibroblasts." *Macromolecular bioscience* 12(10): 1342–53.

Alikhani, Zoubin et al. 2005. "Advanced Glycation End Products Enhance Expression of pro-Apoptotic Genes and Stimulate Fibroblast Apoptosis through Cytoplasmic and Mitochondrial Pathways." *Journal of Biological Chemistry* 280(13): 12087–95.

Andreopoulos, Fotios M, and Indushekhar Persaud. 2006. "Delivery of Basic Fibroblast Growth Factor (bFGF) from Photoresponsive Hydrogel Scaffolds." *Biomaterials* 27(11): 2468–76.

Annabi, Nasim et al. 2010. "Controlling the Porosity and Microarchitecture of Hydrogels for Tissue Engineering." *Tissue engineering. Part B, Reviews* 16(4): 371–83.

Aref, Amir R et al. 2013. "Screening Therapeutic EMT Blocking Agents in a Three-Dimensional Microenvironment." *Integrative biology : quantitative biosciences from nano to macro* 5(2): 381–89.

Baker, a-M et al. 2012. "Lysyl Oxidase Enzymatic Function Increases Stiffness to Drive Colorectal Cancer Progression through FAK." *Oncogene* (March): 1–6.

Baker, Brendon M et al. 2012. "Sacrificial Nanofibrous Composites Provide Instruction without Impediment and Enable Functional Tissue Formation." *PNAS* 109(35): 14176–81.

Banerjee, Subham, Somasree Ray, and Sabyasachi Maiti. 2010. "Interpenetrating Polymer Network (IPN): A Novel Biomaterial." *International Journal of Applied Pharmaceurics* 2(1):28-34.

Baranski, Jan D et al. 2013. "Geometric Control of Vascular Networks to Enhance Engineered Tissue Integration and Function."*PNAS* 110(19): 7586–91.

Barker, Nick et al. 2007. "Identification of Stem Cells in Small Intestine and Colon by Marker Gene Lgr5." *Nature* 449(7165): 1003–7.

Barker, Nick. 2014. "Adult Intestinal Stem Cells: Critical Drivers of Epithelial Homeostasis and Regeneration." *Nature reviews. Molecular cell biology* 15(1): 19–33..

Basora, N et al. 1999. "Expression of Functionally Distinct Variants of the beta(4)A Integrin Subunit in Relation to the Differentiation State in Human Intestinal Cells." *The Journal of biological chemistry* 274(42): 29819–25.

Batlle, Eduard et al. 2002. "B-Catenin and TCF Mediate Cell Positioning in the Intestinal Epithelium by Controlling the Expression of EphB/EphrinB." *Cell* 111(2): 251–63.

Beacham, Da, Md Amatangelo, and E Cukierman. 2006. "Preparation of Extracellular Matrices." *Current Protocols in Cell Biology*: 1–21.

Beaulieu, J F. 1992. "Differential Expression of the VLA Family of Integrins along the Crypt-Villus Axis in the Human Small Intestine." *Journal of cell science* 102 (3): 427–36.

Bencherif, Sidi a. et al. 2008. “Influence of the Degree of Methacrylation on Hyaluronic Acid Hydrogels Properties.” *Biomaterials* 29(12): 1739–49.

Benoit, Yannick D., Jean-François Groulx, David Gagné, and Jean-François Beaulieu. 2012. “RGD-Dependent Epithelial Cell-Matrix Interactions in the Human Intestinal Crypt.” *Journal of Signal Transduction* 2012(Section 2): 1–10.

Bhatia, Sangeeta N, and Donald E Ingber. 2014. “Microfluidic Organs-on-Chips.” *Nature biotechnology* 32(8): 760–72.

Bian, Liming et al. 2013a. “The Influence of Hyaluronic Acid Hydrogel Crosslinking Density and Macromolecular Diffusivity on Human MSC Chondrogenesis and Hypertrophy.” *Biomaterials* 34(2): 413–21.

Bian, Liming et al. 2013b. “The Influence of Hyaluronic Acid Hydrogel Crosslinking Density and Macromolecular Diffusivity on Human MSC Chondrogenesis and Hypertrophy.” *Biomaterials* 34(2): 413–21.

Bohl, K S, and J L West. 2000. “Nitric Oxide-Generating Polymers Reduce Platelet Adhesion and Smooth Muscle Cell Proliferation.” *Biomaterials* 21(22): 2273–78.

Boudou, Thomas et al. 2012. “A Microfabricated Platform to Measure and Manipulate the Mechanics of Engineered Cardiac Microtissues.” *Tissue Engineering Part A* 18(9-10): 910–19.

Bowes, J H, and C W Cater. 1968. “The Interaction of Aldehydes with Collagen.” *Biochimica et biophysica acta* 168(2): 341–52.

Bricks, Thibault et al. 2015. “Investigation of Omeprazole and Phenacetin First-Pass Metabolism in Humans Using a Microscale Bioreactor and Pharmacokinetic Models.” *Biopharmaceutics & Drug Disposition* 36(5): 275–93.

Brigham, Mark D et al. 2009. “Mechanically Robust and Bioadhesive Collagen and Photocrosslinkable Hyaluronic Acid Semi-Interpenetrating Networks.” *Tissue engineering. Part A* 15(7): 1645–53.

Burdick, JA, A Khademhosseini, and R Langer. 2004. “Fabrication of Gradient Hydrogels Using a Microfluidics/photopolymerization Process.” *Langmuir* 20(13): 8–11.

Burdick, Jason A, and Glenn D Prestwich. 2011. “Hyaluronic Acid Hydrogels for Biomedical Applications.” *Advanced materials* 23(12): 41–56.

Burdick, Jason a., and William L. Murphy. 2012. “Moving from Static to Dynamic Complexity in Hydrogel Design.” *Nature Communications* 3: 1269.

Burute, Mithila, and Manuel Thery. 2012. “Spatial Segregation between Cell-Cell and Cell-Matrix Adhesions.” *Current opinion in cell biology* 24(5): 628–36.

Butler, Michael F., Yiu Fai Ng, and Paul D a Pudney. 2003. “Mechanism and Kinetics of the Crosslinking Reaction between Biopolymers Containing Primary Amine Groups and Genipin.” *Journal of Polymer Science, Part A: Polymer Chemistry* 41(24): 3941–53.

Catelas, Isabelle et al. 2006. “Human Mesenchymal Stem Cell Proliferation and Osteogenic Differentiation in Fibrin Gels in Vitro.” *Tissue engineering* 12(8): 2385–96.

Chang, Yen, Chen Chi Tsai, Huang Chien Liang, and Hsing Wen Sung. 2002. "In Vivo Evaluation of Cellular and Acellular Bovine Pericardia Fixed with a Naturally Occurring Crosslinking Agent (genipin)." *Biomaterials* 23(12): 2447–57.

Chatterjee, Kaushik et al. 2010. "The Effect of 3D Hydrogel Scaffold Modulus on Osteoblast Differentiation and Mineralization Revealed by Combinatorial Screening." *Biomaterials* 31(19): 5051–62.

Chen, Dai Chian et al. 2007. "Osteoblastic Response to Collagen Scaffolds Varied in Freezing Temperature and Glutaraldehyde Crosslinking." *Journal of Biomedical Materials Research - Part A* 80(2): 399–409.

Chen, Guoping, Takashi Ushida, and Tetsuya Tateishi. 2001. "Development of Biodegradable Porous Scaffolds for Tissue Engineering." *Materials Science and Engineering C* 17(1-2): 63–69.

Cheng, H, and C P Leblond. 1974. "Origin, Differentiation and Renewal of the Four Main Epithelial Cell Types in the Mouse Small Intestine. V. Unitarian Theory of the Origin of the Four Epithelial Cell Types." *The American journal of anatomy* 141(4): 537–61.

Cheung, H Y, and M R Brown. 1982. "Evaluation of Glycine as an Inactivator of Glutaraldehyde." *The Journal of pharmacy and pharmacology* 34(4): 211–14.

Chiu, Loraine L Y et al. 2012. "Perfusable Branching Microvessel Bed for Vascularization of Engineered Tissues." *PNAS*109(50): E3414–23.

Christopherson, Gregory T, Hongjun Song, and Hai-Quan Mao. 2009. "The Influence of Fiber Diameter of Electrospun Substrates on Neural Stem Cell Differentiation and Proliferation." *Biomaterials* 30(4): 556–64.

Clarke, R M. 1972. "The Effect of Growth and of Fasting on the Number of Villi and Crypts in the Small Intestine of the Albino Rat." *Journal of anatomy* 112(Pt 1): 27–33.

Clevers, Hans. 2013. "The Intestinal Crypt, a Prototype Stem Cell Compartment." *Cell* 154(2): 274–84. http://dx.doi.org/10.1016/j.cell.2013.07.004.

Cochet-Escartin, Olivier, Jonas Ranft, Pascal Silberzan, and Philippe Marcq. 2014. "Border Forces and Friction Control Epithelial Closure Dynamics." *Biophysical Journal* 106(1): 65–73.

Collins, Maurice N., and Colin Birkinshaw. 2012. "Hyaluronic Acid Based Scaffolds for Tissue Engineering–A Review." *Carbohydrate Polymers*.

Costantini, Vincenzo, and Leo R. Zacharski. 1992. "The Role of Fibrin in Tumor Metastasis." *Cancer and Metastasis Reviews* 11(3-4): 283–90.

Costello, Cait M. et al. 2014. "Synthetic Small Intestinal Scaffolds for Improved Studies of Intestinal Differentiation." *Biotechnology and Bioengineering* 111(6): 1222–32.

Crosnier, Cécile, Despina Stamataki, and Julian Lewis. 2006. "Organizing Cell Renewal in the Intestine: Stem Cells, Signals and Combinatorial Control." *Nature reviews. Genetics* 7(5): 349–59.

Cross, Valerie L et al. 2010. “Dense Type I Collagen Matrices That Support Cellular Remodeling and Microfabrication for Studies of Tumor Angiogenesis and Vasculogenesis in Vitro.” *Biomaterials* 31(33): 8596–8607.

Cummings, Christopher L., Debby Gawlitta, Robert M. Nerem, and Jan P. Stegemann. 2004. “Properties of Engineered Vascular Constructs Made from Collagen, Fibrin, and Collagen-Fibrin Mixtures.” *Biomaterials* 25(17): 3699–3706.

Cushing, Melinda C, and Kristi S Anseth. 2007. “Materials Science. Hydrogel Cell Cultures.” *Science (New York, N.Y.)* 316(5828): 1133–34.

Damink, L. H H O et al. 1995. “Glutaraldehyde as a Crosslinking Agent for Collagen-Based Biomaterials.” *Journal of Materials Science: Materials in Medicine* 6(8): 460–72.

Desaki, J, T Fujiwara, and T Komuro. 1984. “A Cellular Reticulum of Fibroblast-like Cells in the Rat Intestine: Scanning and Transmission Electron Microscopy.” *Archivum histologicum Japonicum. Nippon soshikigaku kiroku* 47(2): 179–86.

Douezan, Stéphane, Julien Dumond, and Françoise Brochard-Wyart. 2012. “Wetting Transitions of Cellular Aggregates Induced by Substrate Rigidity.” *Soft Matter* 8(17): 4578.

DuFort, Christopher C, Matthew J Paszek, and Valerie M Weaver. 2011. “Balancing Forces: Architectural Control of Mechanotransduction.” *Nature reviews. Molecular cell biology* 12(5): 308–19.

Duong, Haison, Benjamin Wu, and Bill Tawil. 2009. “Modulation of 3D Fibrin Matrix Stiffness by Intrinsic Fibrinogen-Thrombin Compositions and by Extrinsic Cellular Activity.” *Tissue engineering. Part A* 15(7): 1865–76.

Egorov, V. I., V. Schastlivtsev, R. a. Turusov, and a. O. Baranov. 2002. “Participation of the Intestinal Layers in Supplying of the Mechanical Strength of the Intact and Sutured Gut.” *European Surgical Research* 34(6): 425–31.

Egorov, Viacheslav I. et al. 2002. “Mechanical Properties of the Human Gastrointestinal Tract.” *Journal of Biomechanics* 35(10): 1417–25.

Engler, Adam J et al. 2004. “Myotubes Differentiate Optimally on Substrates with Tissue-like Stiffness: Pathological Implications for Soft or Stiff Microenvironments.” *The Journal of cell biology* 166(6): 877–87.

Engler, Adam J, Shamik Sen, H Lee Sweeney, and Dennis E Discher. 2006. “Matrix Elasticity Directs Stem Cell Lineage Specification.” *Cell* 126(4): 677–89.

Esch, Mandy Brigitte et al. 2012. “On Chip Porous Polymer Membranes for Integration of Gastrointestinal Tract Epithelium with Microfluidic ‘Body-on-a-Chip’ Devices.” *Biomedical microdevices* 14(5): 895–906.

Farin, Henner F., Johan H. Van Es, and Hans Clevers. 2012. “Redundant Sources of Wnt Regulate Intestinal Stem Cells and Promote Formation of Paneth Cells.” *Gastroenterology* 143(6): 1518–29.e7.

Fessel, Gion et al. 2014. “Dose- and Time-Dependent Effects of Genipin Crosslinking on Cell Viability and Tissue Mechanics - toward Clinical Application for Tendon Repair.” *Acta biomaterialia* 10(5): 1897–1906.

Finkbeiner, Stacy R. et al. 2015. “Transcriptome-Wide Analysis Reveals Hallmarks of Human Intestine Development and Maturation In Vitro and In Vivo.” *Stem Cell Reports* 4(6): 1140–55.

Fisher, Matthew B, and Robert L Mauck. 2013. “Tissue Engineering and Regenerative Medicine: Recent Innovations and the Transition to Translation.” *Tissue engineering. Part B, Reviews* 19(1): 1–13.

Van der Flier, Laurens G, and Hans Clevers. 2009. “Stem Cells, Self-Renewal, and Differentiation in the Intestinal Epithelium.” *Annual review of physiology* 71: 241–60.

Fouquet, Stéphane et al. 2004. “Early Loss of E-Cadherin from Cell-Cell Contacts Is Involved in the Onset of Anoikis in Enterocytes.” *Journal of Biological Chemistry* 279(41): 43061–69.

Francis-Sedlak, Megan E. et al. 2009. “Characterization of Type I Collagen Gels Modified by Glycation.” *Biomaterials* 30(9): 1851–56.

Frantz, Christian, Kathleen M Stewart, and Valerie M Weaver. 2010. “The Extracellular Matrix at a Glance.” *Journal of cell science* 123(Pt 24): 4195–4200.

Fratzl, Peter. 2008. Collagen: Structure and Mechanics *Collagen: Structure and Mechanics*.

Frey, Mark R, Anastasia Golovin, and D Brent Polk. 2004. “Epidermal Growth Factor-Stimulated Intestinal Epithelial Cell Migration Requires Src Family Kinase-Dependent p38 MAPK Signaling.” *The Journal of biological chemistry* 279(43): 44513–21.

Furuya, Sonoko, and Kishio Furuya. 2007. “Subepithelial Fibroblasts in Intestinal Villi: Roles in Intercellular Communication.” *International Review of Cytology* 264(07): 165–223.

Furuya, Sonoko, and Kishio Furuya.. 2013. 304 International Review of Cell and Molecular Biology *Roles of Substance P and ATP in the Subepithelial Fibroblasts of Rat Intestinal Villi*. 1st ed. Elsevier Inc.

Gardel, M L et al. 2003. “Microrheology of Entangled F-Actin Solutions.” *Physical review letters* 91(15): 158302.

Gauvin, Robert et al. 2012. “Microfabrication of Complex Porous Tissue Engineering Scaffolds Using 3D Projection Stereolithography.” *Biomaterials* 33(15): 3824–34.

Geraldo, Sara et al. 2012. “Do Cancer Cells Have Distinct Adhesions in 3D Collagen Matrices and in Vivo?” *European journal of cell biology* 91(11-12): 930–37.

Gerbe, François, Catherine Legraverend, and Philippe Jay. 2012. “The Intestinal Epithelium Tuft Cells: Specification and Function.” *Cellular and Molecular Life Sciences* 69(17): 2907–17.

Ghosh, Kaustabh et al. 2008. “Tumor-Derived Endothelial Cells Exhibit Aberrant Rho-Mediated Mechanosensing and Abnormal Angiogenesis in Vitro.” *PNAS* 105(32): 11305–10.

Glentis, Alexandros, Vasily Gurchenkov, and Danijela Matic Vignjevic. 2014. "Assembly, Heterogeneity, and Breaching of the Basement Membranes." *Cell adhesion & migration* 8(3): 1–10.

Gonzalez-Rodriguez, D., K. Guevorkian, S. Douezan, and F. Brochard-Wyart. 2012. "Soft Matter Models of Developing Tissues and Tumors." *Science* 338(6109): 910–17.

Goova, M T et al. 2001. "Blockade of Receptor for Advanced Glycation End-Products Restores Effective Wound Healing in Diabetic Mice." *The American journal of pathology* 159(2): 513–25.

Gracz, a D, and S T Magness. 2014. "Defining Hierarchies of Stemness in the Intestine: Evidence from Biomarkers and Regulatory Pathways." *American journal of physiology. Gastrointestinal and liver physiology* 307(3): G260–73.

Guarnieri, D et al. 2010. "Covalently Immobilized RGD Gradient on PEG Hydrogel Scaffold Influences Cell Migration Parameters." *Acta biomaterialia* 6(7): 2532–39.

Guvendiren, Murat, and Jason a Burdick. 2012. "Stiffening Hydrogels to Probe Short- and Long-Term Cellular Responses to Dynamic Mechanics." *Nature communications* 3: 792.

Helary, Christophe et al. 2005. "Fibroblast Populated Dense Collagen Matrices: Cell Migration, Cell Density and Metalloproteinases Expression." *Biomaterials* 26(13): 1533–43.

Hinz, Boris. 2006. "Masters and Servants of the Force: The Role of Matrix Adhesions in Myofibroblast Force Perception and Transmission." *European Journal of Cell Biology* 85(3-4): 175–81.

Holzapfel, Boris Michael et al. 2015. "'Humanized Models of Tumour Immunology in the 21 St Century: Convergence of Cancer Research and Tissue Engineering.'" *STEM CELLS*:

Hosoyamada, Yasue, and Tatsuo Sakai. 2005. "Structural and Mechanical Architecture of the Intestinal Villi and Crypts in the Rat Intestine: Integrative Reevaluation from Ultrastructural Analysis." *Anatomy and Embryology* 210(1): 1–12.

Huang, Carlos P et al. 2009. "Engineering Microscale Cellular Niches for Three-Dimensional Multicellular Co-Cultures." *Lab on a chip* 9(12): 1740–48.

Huang, Guo You et al. 2011. "Microfluidic Hydrogels for Tissue Engineering." *Biofabrication* 3(1): 012001.

Huang, S, C S Chen, and D E Ingber. 1998. "Control of Cyclin D1, p27(Kip1), and Cell Cycle Progression in Human Capillary Endothelial Cells by Cell Shape and Cytoskeletal Tension." *Molecular biology of the cell* 9(11): 3179–93.

Humphrey, Jay D, Eric R Dufresne, and Martin a Schwartz. 2014. "Mechanotransduction and Extracellular Matrix Homeostasis I E R." *Nature Publishing Group*: 1–11.

Hwang, Chang Mo et al. 2008. "Microfluidic Chip-Based Fabrication of PLGA Microfiber Scaffolds for Tissue Engineering." *Langmuir : the ACS journal of surfaces and colloids* 24(13): 6845–51.

Janmey, Paul a, Jessamine P Winer, and John W Weisel. 2009. "Fibrin Gels and Their Clinical and Bioengineering Applications." *Journal of the Royal Society, Interface / the Royal Society* 6(30): 1–10.

Järveläinen, H. 2009. “Extracellular Matrix Molecules: Potential Targets in Pharmacotherapy.” *Pharmacol Rev*. 61(2): 198–223.

Jeffords, Megan E. et al. 2015. “Tailoring Material Properties of Cardiac Matrix Hydrogels To Induce Endothelial Differentiation of Human Mesenchymal Stem Cells.” *ACS Applied Materials & Interfaces* 7(20): 11053–61.

Jeyanthi, R, and K P Rao. 1990. “In Vivo Biocompatibility of Collagen-Poly(hydroxyethyl Methacrylate) Hydrogels.” *Biomaterials* 11(4): 238–43.

Jiang, Li-Yang, and Ying Luo. 2013. “Guided Assembly of Endothelial Cells on Hydrogel Matrices Patterned with Microgrooves: A Basic Model for Microvessel Engineering.” *Soft Matter* 9(4): 1113.

Jiang, Tao et al. 2009. “Preparation and Biocompatibility of Polyvinyl Alcohol-Small Intestinal Submucosa Hydrogel Membranes.” *Journal of Medical and Biological Engineering* 29(2): 102–7.

Kadler, K E, D F Holmes, J a Trotter, and J a Chapman. 1996. “Collagen Fibril Formation.” *The Biochemical journal* 316 (Pt 1: 1–11.

Kaivosoja, Emilia et al. 2012. “Chemical and Physical Properties of Regenerative Medicine Materials Controlling Stem Cell Fate.” *Annals of medicine* 44(7): 635–50.

Kalamajski, Sebastian, and Ake Oldberg. 2010. “The Role of Small Leucine-Rich Proteoglycans in Collagen Fibrillogenesis.” *Matrix Biology* 29(4): 248–53.

Katano, Takahito et al. 2015. “Gastric Mesenchymal Myofibroblasts Maintain Stem Cell Activity and Proliferation of Murine Gastric Epithelium in Vitro.” *The American Journal of Pathology* 185(3): 798–807.

Katari, Ravi, Andrea Peloso, and Giuseppe Orlando. 2015. “Tissue Engineering and Regenerative Medicine: Semantic Considerations for an Evolving Paradigm.” *Frontiers in Bioengineering and Biotechnology* 2(January): 1–6.

Kaur, P, and C S Potten. 1986a. “Cell Migration Velocities in the Crypts of the Small Intestine after Cytotoxic Insult Are Not Dependent on Mitotic Activity.” *Cell and tissue kinetics* 19(6): 601–10.

Kaur, P, and C S Potten.. 1986b. “Effects of Puromycin, Cycloheximide and Noradrenaline on Cell Migration within the Crypts and on the Villi of the Small Intestine. A Model to Explain Cell Movement in Both Regions.” *Cell and tissue kinetics* 19(6): 611–25.

Khademhosseini, Ali et al. 2006. “Micromolding of Photocrosslinkable Hyaluronic Acid for Cell Encapsulation and Entrapment.” *Journal of Biomedical Materials Research - Part A* 79(3): 522–32.

Khademhosseini, Ali et al. 2007. “Microfluidic Patterning for Fabrication of Contractile Cardiac Organoids.” *Biomedical microdevices* 9(2): 149–57..

Kilian, Kristopher a, Branimir Bugarija, Bruce T Lahn, and Milan Mrksich. 2010. “Geometric Cues for Directing the Differentiation of Mesenchymal Stem Cells.” *PNAS*107(11): 4872–77.

Kim, Hyun Jung, Dongeun Huh, Geraldine Hamilton, and Donald E Ingber. 2012. “Human Gut-on-a-Chip Inhabited by Microbial Flora That Experiences Intestinal Peristalsis-like Motions and Flow.” *Lab on a chip* 12(12): 2165–74.

Kim, Hyun Jung, and Donald E Ingber. 2013. “Gut-on-a-Chip Microenvironment Induces Human Intestinal Cells to Undergo Villus Differentiation.” *Integrative biology : quantitative biosciences from nano to macro* 5(9): 1130–40.

Komuro, T, and Y Hashimoto. 1990. “Three-Dimensional Structure of the Rat Intestinal Wall (mucosa and Submucosa).” *Archives of histology and cytology* 53(1): 1–21.

Komuro, Terumasa. 1988. “The Lattice Arrangement of the Collagen Fibres in the Submucosa of the Rat Small Intestine: Scanning Electron Microscopy.” *Cell and Tissue Research* 251(1): 117–21.

Koroleva, Anastasia et al. 2012. “Fabrication of Fibrin Scaffolds with Controlled Microscale Architecture by a Two-Photon Polymerization–micromolding Technique.” *Biofabrication* 4(1): 015001.

Kreke, Michelle R et al. 2005. “Modulation of Protein Adsorption and Cell Adhesion by Poly(allylamine Hydrochloride) Heparin Films.” *Biomaterials* 26(16): 2975–81.

Kucharzik, T et al. 2000. “Role of M Cells in Intestinal Barrier Function.” *Annals of the New York Academy of Sciences* 915: 171–83.

Kunze, Anja, Michele Giugliano, Ana Valero, and Philippe Renaud. 2011. “Micropatterning Neural Cell Cultures in 3D with a Multi-Layered Scaffold.” *Biomaterials* 32(8): 2088–98.

Kwon, Young-Sun et al. 2015. “Genipin, a Cross-Linking Agent, Promotes Odontogenic Differentiation of Human Dental Pulp Cells.” *Journal of Endodontics* 41(4): 501–7.

Ladoux, Benoit et al. 2010. “Strength Dependence of Cadherin-Mediated Adhesions.” *Biophysical Journal* 98(4): 534–42.

Langer, R. 2000. “Tissue Engineering.” *Molecular therapy : the journal of the American Society of Gene Therapy* 1(1): 12–15.

Laschke, M W, and M D Menger. 2012. “Vascularization in Tissue Engineering: Angiogenesis versus Inosculation.” *European surgical research. Europäische chirurgische Forschung. Recherches chirurgicales européennes* 48(2): 85–92.

Laurent, T C, U B Laurent, and J R Fraser. 1996. “The Structure and Function of Hyaluronan: An Overview.” *Immunology and cell biology* 74(2): A1–7.

Lee, H Janice et al. 2006. “Collagen Mimetic Peptide-Conjugated Photopolymerizable PEG Hydrogel.” *Biomaterials* 27(30): 5268–76.

Li, Peng et al. 2007. “Homeostatic Control of the Crypt-Villus Axis by the Bacterial Enterotoxin Receptor Guanylyl Cyclase C Restricts the Proliferating Compartment in Intestine.” *The American journal of pathology* 171(6): 1847–58.

Liao, I-Chien, Jason B Liu, Nenad Bursac, and Kam W Leong. 2008. “Effect of Electromechanical Stimulation on the Maturation of Myotubes on Aligned Electrospun Fibers.” *Cellular and molecular bioengineering* 1(2-3): 133–45..

Liu, Zongbin et al. 2012. “Covalently Immobilized Biomolecule Gradient on Hydrogel Surface Using a Gradient Generating Microfluidic Device for a Quantitative Mesenchymal Stem Cell Study.” *Biomicrofluidics* 6(2): 24111–112.

Lohani, Alka, Garima Singh, Shiv Sankar Bhattacharya, and Anurag Verma. 2014. “Interpenetrating Polymer Networks as Innovative Drug Delivery Systems.” *Journal of drug delivery* 2014(Figure 1): 583612.

Lopez-Garcia, Carlos, Allon M Klein, Benjamin D Simons, and Douglas J Winton. 2010. “Intestinal Stem Cell Replacement Follows a Pattern of Neutral Drift.” *Science (New York, N.Y.)* 330(6005): 822–25.

Louvard, D, M Kedinger, and H.P. Hauri. 1992. “Intestinal epithelial cell : Establishment and Maintenance of Functions Cellular Structures.” *Annu. Rev. Cell Biol.* 8: 157–95.

Lu, Da-yong et al. 2015. “Tumor Fibrin / Fibrinogen Matrix as a Unique Therapeutic Target for Pulmonary Cancer Growth and Metastases.” 3(1): 1–4.

Madison, Blair B et al. 2005. “Epithelial Hedgehog Signals Pattern the Intestinal Crypt-Villus Axis.” *Development (Cambridge, England)* 132(2): 279–89.

Marsh, M N, and J S Trier. 1974a. “Morphology and Cell Proliferation of Subepithelial Fibroblasts in Adult Mouse Jejunum. I. Structural Features.” *Gastroenterology* 67(4): 622–35.

Marsh, M N, and J S Trier. 1974b. “Morphology and Cell Proliferation of Subepithelial Fibroblasts in Adult Mouse Jejunum. II. Radioautographic Studies.” *Gastroenterology* 67(4): 636–45.

Martiel, Jean-Louis et al. 2015. “Measurement of Cell Traction Forces with ImageJ.” In , 269–87.

Mason, Brooke N, and Cynthia a Reinhart-King. 2013. “Controlling the Mechanical Properties of Three-Dimensional Matrices via Non-Enzymatic Collagen Glycation.” *Organogenesis* 9(2): 70–75.

Mason, Brooke N. et al. 2013. “Tuning Three-Dimensional Collagen Matrix Stiffness Independently of Collagen Concentration Modulates Endothelial Cell Behavior.” *Acta Biomaterialia* 9(1): 4635–44.

Matricardi, Pietro et al. 2013. “Interpenetrating Polymer Networks Polysaccharide Hydrogels for Drug Delivery and Tissue Engineering.” *Advanced Drug Delivery Reviews* 65(9): 1172–87..

Matson, John B, and Samuel I Stupp. 2012. “Self-Assembling Peptide Scaffolds for Regenerative Medicine.” *Chemical communications (Cambridge, England)* 48(1): 26–33.

Mattioli-Belmonte, M. et al. 2008. “Rapid-Prototyped and Salt-Leached PLGA Scaffolds Condition Cell Morpho-Functional Behavior.” *Journal of Biomedical Materials Research - Part A* 85(2): 466–76.

McGann, Megan E. et al. 2015. “Genipin Crosslinking of Cartilage Enhances Resistance to Biochemical Degradation and Mechanical Wear.” *Journal of Orthopaedic Research*: n/a – n/a..

Van der Meer, Andries D et al. 2010. “A Microfluidic Wound-Healing Assay for Quantifying Endothelial Cell Migration.” *American journal of physiology. Heart and circulatory physiology* 298(2): H719–25.

Meineke, F. a., C. S. Potten, and M. Loeffler. 2001. “Cell Migration and Organization in the Intestinal Crypt Using a Lattice-Free Model.” *Cell Proliferation* 34(4): 253–66.

Mifflin, R C, I V Pinchuk, J I Saada, and D W Powell. 2011. “Intestinal Myofibroblasts: Targets for Stem Cell Therapy.” *American journal of physiology. Gastrointestinal and liver physiology* 300(5): G684–96.

Migneault, Isabelle, Catherine Dartiguenave, Michel J. Bertrand, and Karen C. Waldron. 2004. “Glutaraldehyde: Behavior in Aqueous Solution, Reaction with Proteins, and Application to Enzyme Crosslinking.” *BioTechniques* 37(5): 790–802.

Miller, Jordan S et al. 2012. “Rapid Casting of Patterned Vascular Networks for Perfusable Engineered Three-Dimensional Tissues.” *Nature materials* 11(9): 768–74.

Morse, David C. 1998. “Viscoelasticity.” *Macromolecules* 31(98): 7044–67.

Mosesson, M W, K R Siebenlist, and D a Meh. 2001. “The Structure and Biological Features of Fibrinogen and Fibrin.” *Annals of the New York Academy of Sciences* 936: 11–30.

Narotam, P K et al. 1995. “A Clinicopathological Study of Collagen Sponge as a Dural Graft in Neurosurgery.” *Journal of neurosurgery* 82: 406–12.

Neal, J V, and C S Potten. 1981. “Description and Basic Cell Kinetics of the Murine Pericryptal Fibroblast Sheath.” *Gut* 22(1): 19–24.

Nelson, Celeste M et al. 2005. “Emergent Patterns of Growth Controlled by Multicellular Form and Mechanics.” *PNAS* 102(33): 11594–99.

Ng, Mei Rosa, Achim Besser, Gaudenz Danuser, and Joan S. Brugge. 2012. “Substrate Stiffness Regulates Cadherin-Dependent Collective Migration through Myosin-II Contractility.” *Journal of Cell Biology* 199(3): 545–63.

Nikkhah, Mehdi, Faramarz Edalat, Sam Manoucheri, and Ali Khademhosseini. 2012. “Engineering Microscale Topographies to Control the Cell-Substrate Interface.” *Biomaterials* 33(21): 5230–46.

Nimmo, Chelsea M., Shawn C. Owen, and Molly S. Shoichet. 2011. “Diels-Alder Click Cross-Linked Hyaluronic Acid Hydrogels for Tissue Engineering.” *Biomacromolecules* 12(3): 824–30.

Norotte, Cyrille, Francois S Marga, Laura E Niklason, and Gabor Forgacs. 2009. “Scaffold-Free Vascular Tissue Engineering Using Bioprinting.” *Biomaterials* 30(30): 5910–17.

Onoe, Hiroaki et al. 2013. “Metre-Long Cell-Laden Microfibres Exhibit Tissue Morphologies and Functions.” *Nature Materials*..

Owen, W F et al. 1998. “Beta 2-Microglobulin Modified with Advanced Glycation End Products Modulates Collagen Synthesis by Human Fibroblasts.” *Kidney international* 53(5): 1365–73.

Panda, Priyadarshi et al. 2008. “Stop-Flow Lithography to Generate Cell-Laden Microgel Particles.” *Lab on a Chip* 8(7): 1056.

Parker, F G, E N Barnes, and G I Kaye. 1974. “The Pericryptal Fibroblast Sheath. IV. Replication, Migration, and Differentiation of the Subepithelial Fibroblasts of the Crypt and Villus of the Rabbit Jejunum.” *Gastroenterology* 67(4): 607–21.

Pathak, Amit, and Sanjay Kumar. 2012. “Independent Regulation of Tumor Cell Migration by Matrix Stiffness and Confinement.” *Proceedings of the National Academy of Sciences of the United States of America* 109(26): 10334–39.

Pawelec, K. M., R. J. Wardale, S. M. Best, and R. E. Cameron. 2015. “The Effects of Scaffold Architecture and Fibrin Gel Addition on Tendon Cell Phenotype.” *Journal of Materials Science: Materials in Medicine* 26(1).

Peifer, Mark. 2002. “Developmental Biology: Colon Construction.” *Nature* 420(6913): 274–75, 277.

Peyton, Shelly R., Cyrus M. Ghajar, Chirag B. Khatiwala, and Andrew J. Putnam. 2007. “The Emergence of ECM Mechanics and Cytoskeletal Tension as Important Regulators of Cell Function.” *Cell Biochemistry and Biophysics* 47(2): 300–320.

Phelps, Edward a et al. 2010. “Bioartificial Matrices for Therapeutic Vascularization.” *PNASa* 107(8): 3323–28.

Pinto, Daniel, Alex Gregorieff, Harry Begthel, and Hans Clevers. 2003. “Canonical Wnt Signals Are Essential for Homeostasis of the Intestinal Epithelium.” Gebes & development 17(14) : 1709–13.

Potten, C S. 1977. “Extreme Sensitivity of Some Intestinal Crypt Cells to X and Gamma Irradiation.” *Nature* 269(5628): 518–21.

Potten, C S, L Kovacs, and E Hamilton. 1974. “Continuous Labelling Studies on Mouse Skin and Intestine.” *Cell and tissue kinetics* 7(3): 271–83.

Potten, Christopher S, Gary Owen, and Dawn Booth. 2002. “Intestinal Stem Cells Protect Their Genome by Selective Segregation of Template DNA Strands.” *Journal of cell science* 115(Pt 11): 2381–88.

Pottier, Basile et al. 2011. “High Bandwidth Linear Viscoelastic Properties of Complex Fluids from the Measurement of Their Free Surface Fluctuations.” *Soft Matter* 7(17): 7843.

Pottier, Basile et al. 2013. “High Frequency Linear Rheology of Complex Fluids Measured from Their Surface Thermal Fluctuations.” *Journal of Rheology* 57(2): 441–55.

Poullet, Patrick, Sabrina Carpentier, and Emmanuel Barillot. 2007. “myProMS, a Web Server for Management and Validation of Mass Spectrometry-Based Proteomic Data.” *Proteomics* 7(15): 2553–56.

Prot, Jean Matthieu et al. 2014. “First Pass Intestinal and Liver Metabolism of Paracetamol in a Microfluidic Platform Coupled with a Mathematical Modeling as a Means of Evaluating ADME Processes in Humans.” *Biotechnology and bioengineering* 111(10): 2027-2040.

Quyn, Aaron J. et al. 2010. “Spindle Orientation Bias in Gut Epithelial Stem Cell Compartments Is Lost in Precancerous Tissue.” *Cell Stem Cell* 6(2): 175–81.

Ramanan, Vyas et al. 2014. “New Methods in Tissue Engineering : Improved Models for Viral Infection.” *Annual Review of virology* 1: 475–99.

Ramanujan, Saroja et al. 2002. “Diffusion and Convection in Collagen Gels: Implications for Transport in the Tumor Interstitium.” *Biophysical journal* 83(3): 1650–60.

Rao, Rameshwar R. et al. 2012. “Matrix Composition Regulates Three-Dimensional Network Formation by Endothelial Cells and Mesenchymal Stem Cells in Collagen/fibrin Materials.” *Angiogenesis* 15(2): 253–64.

Ratnikov, Boris I, Elena I Deryugina, and Alex Y Strongin. 2002. “Gelatin Zymography and Substrate Cleavage Assays of Matrix Metalloproteinase-2 in Breast Carcinoma Cells Overexpressing Membrane Type-1 Matrix Metalloproteinase.” *Laboratory investigation; a journal of technical methods and pathology* 82(11): 1583–90.

Raub, Christopher B et al. 2007. “Noninvasive Assessment of Collagen Gel Microstructure and Mechanics Using Multiphoton Microscopy.” *Biophysical journal* 92(6): 2212–22.

Reed, Charles C., and Renato V. Iozzo. 2002. “The Role of Decorin in Collagen Fibrillogenesis and Skin Homeostasis.” *Glycoconjugate Journal* 19(4-5): 249–55.

Reffay, M et al. 2014. “Interplay of RhoA and Mechanical Forces in Collective Cell Migration Driven by Leader Cells.” *Nature Cell Biology* 16(3): 217–23.

Rehfeldt, Florian et al. 2012. “Hyaluronic Acid Matrices Show Matrix Stiffness in 2D and 3D Dictates Cytoskeletal Order and Myosin-II Phosphorylation within Stem Cells.” *Integrative Biology* 4(4): 422.

Revel, Ariel et al. 2011. “Micro-Organ Ovarian Transplantation Enables Pregnancy: A Case Report.” *Human reproduction (Oxford, England)* 26(5): 1097–1103.

Du Roure, Olivia et al. 2005. “Force Mapping in Epithelial Cell Migration.” *Proceedings of the National Academy of Sciences of the United States of America* 102(7): 2390–95.

Rowe, Shaneen L., and Jan P. Stegemann. 2006. “Interpenetrating Collagen-Fibrin Composite Matrices with Varying Protein Contents and Ratios.” *Biomacromolecules* 7(11): 2942–48.

Rozario, Tania, and Douglas W. DeSimone. 2010. “The Extracellular Matrix in Development and Morphogenesis: A Dynamic View.” *Developmental Biology* 341(1): 126–40.

Rubinstein, Michael, and Ralph H. Colby. 2003. “Polymer Physics.” : 456.

Sabeh, Farideh, Ryoko Shimizu-Hirota, and Stephen J Weiss. 2009. “Protease-Dependent versus -Independent Cancer Cell Invasion Programs: Three-Dimensional Amoeboid Movement Revisited.” *The Journal of cell biology* 185(1): 11–19.

Salinas, Chelsea N, and Kristi S Anseth. 2009. “Decorin Moieties Tethered into PEG Networks Induce Chondrogenesis of Human Mesenchymal Stem Cells.” *Journal of biomedical materials research. Part A* 90(2): 456–64.

San Roman, Adrianna K., Chenura D. Jayewickreme, L. Charles Murtaugh, and Ramesh a. Shivdasani. 2014. “Wnt Secretion from Epithelial Cells and Subepithelial Myofibroblasts Is Not Required in the Mouse Intestinal Stem Cell Niche in Vivo.” *Stem Cell Reports* 2(2): 127–34.

Sangiorgi, Eugenio, and Mario R Capecchi. 2008. “Bmi1 Is Expressed in Vivo in Intestinal Stem Cells.” *Nature genetics* 40(7): 915–20.

Sano, a, T Hojo, M Maeda, and K Fujioka. 1998. “Protein Release from Collagen Matrices.” *Advanced drug delivery reviews* 31(3): 247–66.

Sansom, Owen J. et al. 2004. “Loss of Apc in Vivo Immediately Perturbs Wnt Signaling, Differentiation, and Migration.” *Genes and Development* 18(12): 1385–90.

Santos, Edorta, Rosa M Hernández, José Luis Pedraz, and Gorka Orive. 2012. “Novel Advances in the Design of Three-Dimensional Bio-Scaffolds to Control Cell Fate: Translation from 2D to 3D.” *Trends in biotechnology* 30(6): 331–41.

Sato, Toshiro et al. 2009. “Single Lgr5 Stem Cells Build Crypt-Villus Structures in Vitro without a Mesenchymal Niche.” *Nature* 459(7244): 262–65.

Sato, Toshiro et al.. 2011. “Paneth Cells Constitute the Niche for Lgr5 Stem Cells in Intestinal Crypts.” *Nature* 469(7330): 415–18..

Sato, Toshiro, and Hans Clevers. 2015. “SnapShot: Growing Organoids from Stem Cells.” *Cell* 161(7): 1700–1700.

Schindler, Melvin, A Nur-E-Kamal, and Ijaz Ahmed. 2006. “Living in Three Dimensions.” *Cell biochemistry and biophysics* 45(14): 215–27.

Schmidt, G H, D J Winton, and B a Ponder. 1988. “Development of the Pattern of Cell Renewal in the Crypt-Villus Unit of Chimaeric Mouse Small Intestine.” *Development (Cambridge, England)* 103(4): 785–90.

Shayegan, Marjan, and Nancy R. Forde. 2013. “Microrheological Characterization of Collagen Systems: From Molecular Solutions to Fibrillar Gels.” *PLoS ONE* 8(8): 23–28.

Shin, Yoojin et al. 2012. “Microfluidic Assay for Simultaneous Culture of Multiple Cell Types on Surfaces or within Hydrogels.” *Nature protocols* 7(7): 1247–59.

Shu, Xiao Zheng, Yanchun Liu, Fabio Palumbo, and Glenn D. Prestwich. 2003. “Disulfide-Crosslinked Hyaluronan-Gelatin Hydrogel Films: A Covalent Mimic of the Extracellular Matrix for in Vitro Cell Growth.” *Biomaterials* 24(21): 3825–34.

Shyer, a. E. et al. 2013. “Villification: How the Gut Gets Its Villi.” *Science* 342(6155): 212–18.

Simon-Assmann, P et al. 1988. “Epithelial-Mesenchymal Interactions in the Production of Basement Membrane Components in the Gut.” *Development (Cambridge, England)* 102(2): 339–47.

Simon-Assmann, P. et al. 1995. “Extracellular Matrix Components in Intestinal Development.” *Experientia* 51(9-10): 883–900.

Simon-Assmann, Patricia et al. 1990. “Synthesis of Basement Membrane Proteins in the Small Intestine.” *Digestion* 46(2): 12–21.

Snippert, Hugo J. et al. 2010. “Intestinal Crypt Homeostasis Results from Neutral Competition between Symmetrically Dividing Lgr5 Stem Cells.” *Cell* 143(1): 134–44.

Sodunke, Temitope R et al. 2007. “Micropatterns of Matrigel for Three-Dimensional Epithelial Cultures.” *Biomaterials* 28(27): 4006–16.).

Spence, Jason R et al. 2011. “Directed Differentiation of Human Pluripotent Stem Cells into Intestinal Tissue in Vitro.” *Nature* 470(7332): 105–9.

St Clair, W H, and J W Osborne. 1985. “Crypt Fission and Crypt Number in the Small and Large Bowel of Postnatal Rats.” *Cell and tissue kinetics* 18(3): 255–62.

Stamov, Dimitar R. et al. 2013. “Quantitative Analysis of Type I Collagen Fibril Regulation by Lumican and Decorin Using AFM.” *Journal of Structural Biology* 183(3): 394–403.

Storm, Cornelis et al. 2005. “Nonlinear Elasticity in Biological Gels.” *Nature* 435(7039): 191–94.

Streeter, I, and Nh de Leeuw. 2011. “A Molecular Dynamics Study of the Interprotein Interactions in Collagen Fibrils.” *Soft Matter* (7): 3373–82.

Strodtbeck, Frances. 2001. “Physiology of Wound Healing.” *Newborn and Infant Nursing Reviews* 1(1): 43–52.

Sundararaghavan, Harini G. et al. 2008. “Genipin-Induced Changes in Collagen Gels: Correlation of Mechanical Properties to Fluorescence.” *Journal of Biomedical Materials Research - Part A* 87(2): 308–20.

Sundararaghavan, Harini G., Gary a. Monteiro, Bonnie L. Firestein, and David I. Shreiber. 2009. “Neurite Growth in 3D Collagen Gels with Gradients of Mechanical Properties.” *Biotechnology and Bioengineering* 102(2): 632–43.

Sung, Jong Hwan et al. 2011. “Microscale 3-D Hydrogel Scaffold for Biomimetic Gastrointestinal (GI) Tract Model.” *Lab on a chip* 11(3): 389–92.

Sung, Jong Hwan, Carrie Kam, and Michael L Shuler. 2010. “A Microfluidic Device for a Pharmacokinetic-Pharmacodynamic (PK-PD) Model on a Chip.” *Lab on a chip* 10(4): 446–55.

Sung, Kyung Eun et al. 2009. “Control of 3-Dimensional Collagen Matrix Polymerization for Reproducible Human Mammary Fibroblast Cell Culture in Microfluidic Devices.” *Biomaterials* 30(27): 4833–41.

Sur, Shantanu et al. 2012. “A Hybrid Nanofiber Matrix to Control the Survival and Maturation of Brain Neurons.” *Biomaterials* 33(2): 545–55..

Suri, Shalu et al. 2011. “Solid Freeform Fabrication of Designer Scaffolds of Hyaluronic Acid for Nerve Tissue Engineering.” *Biomedical microdevices* 13(6): 983–93.

Suri, Shalu, and Christine E Schmidt. 2009. “Photopatterned Collagen-Hyaluronic Acid Interpenetrating Polymer Network Hydrogels.” *Acta biomaterialia* 5(7): 2385–97.

Suri, Shalu, and Christine E Schmidt. 2010. “Cell-Laden Hydrogel Constructs of Hyaluronic Acid, Collagen, and Laminin for Neural Tissue Engineering.” *Tissue engineering. Part A* 16(5): 1703–16.

Tambe, Dhananjay T et al. 2011. “Collective Cell Guidance by Cooperative Intercellular Forces.” *Nature materials* 10(6): 469–75.

Tan, Jian, Richard a Gemeinhart, Mandy Ma, and W Mark Saltzman. 2005. “Improved Cell Adhesion and Proliferation on Synthetic Phosphonic Acid-Containing Hydrogels.” *Biomaterials* 26(17): 3663–71.

Tanaka, S, G Avigad, B Brodsky, and E F Eikenberry. 1988. “Glycation Induces Expansion of the Molecular Packing of Collagen.” *Journal of molecular biology* 203(2): 495–505.

Teller, Inga C. et al. 2007. “Laminins in the Developing and Adult Human Small Intestine: Relation with the Functional Absorptive Unit.” *Developmental Dynamics* 236(7): 1980–90.

Théry, Manuel et al. 2005. “The Extracellular Matrix Guides the Orientation of the Cell Division Axis.” *Nature cell biology* 7(10): 947–53.

Théry,Manuel. 2010. “Micropatterning as a Tool to Decipher Cell Morphogenesis and Functions.” *Journal of cell science* 123(24): 4201–13.

Thomson, Kassandra S et al. 2013. “Prevascularized Microtemplated Fibrin Scaffolds for Cardiac Tissue Engineering Applications.” *Tissue engineering. Part A* 19: 1–11.

Tibbitt, Mark W, and Kristi S Anseth. 2009. “Hydrogels as Extracellular Matrix Mimics for 3D Cell Culture.” *Biotechnology and bioengineering* 103(4): 655–63.

Tomasek, James J et al. 2002. “Myofibroblasts and Mechano-Regulation of Connective Tissue Remodelling.” *Nature reviews. Molecular cell biology* 3(5): 349–63.

Trier, J. S., C. H. Allan, D. R. Abrahamson, and S. J. Hagen. 1990. “Epithelial Basement Membrane of Mouse Jejunum. Evidence for Laminin Turnover along the Entire Crypt-Villus Axis.” *Journal of Clinical Investigation* 86(1): 87–95.

Tronci, Giuseppe et al. 2014. “Multi-Scale Mechanical Characterization of Highly Swollen Photo-Activated Collagen Hydrogels.” *Journal of The Royal Society Interface* 12(102): 20141079–

Tronci, Giuseppe, Stephen J. Russell, and David J. Wood. 2013. “Photo-Active Collagen Systems with Controlled Triple Helix Architecture.” *Journal of Materials Chemistry B* 1(30): 3705.

Tse, Justin R, and Adam J Engler. 2010. “Preparation of Hydrogel Substrates with Tunable Mechanical Properties.” *Current protocols in cell biology / editorial board, Juan S. Bonifacino ... [et al.]* Chapter 10(June): Unit 10.16.

Tseng, Qingzong et al. 2012. “Spatial Organization of the Extracellular Matrix Regulates Cell-Cell Junction Positioning.”*PNAS* 109(5): 1506–11.

Uygun, Basak E et al. 2010. “Organ Reengineering through Development of a Transplantable Recellularized Liver Graft Using Decellularized Liver Matrix.” *Nature medicine* 16(7): 814–20.

Vedula, R K, a Ravasio, C T Lim, and B Ladoux. 2013. “Collective Cell Migration: A Mechanistic Perspective.” *Physiology* 28(6): 370–79.

Vedula, Sri Ram Krishna et al. 2012. “Emerging Modes of Collective Cell Migration Induced by Geometrical Constraints.” *PNAS* 109(32): 12974–79.

Verhulsel, Marine et al. 2014. “A Review of Microfabrication and Hydrogel Engineering for Micro-Organs on Chips.” *Biomaterials* 35(6): 1816–32.

Vesely, Ivan. 2005. “Heart Valve Tissue Engineering.” *Circulation Research* 97(8): 743–55.

Villasante, Aranzazu, and Gordana Vunjak-Novakovic. 2015. “Tissue-Engineered Models of Human Tumors for Cancer Research.” *Expert Opinion on Drug Discovery* 10(3): 257–68..

Vllasaliu, Driton et al. 2012. “Absorption-Promoting Effects of Chitosan in Airway and Intestinal Cell Lines: A Comparative Study.” *International journal of pharmaceutics* 430(1-2): 151–60.

Vogel, Viola, and Michael Sheetz. 2006. “Local Force and Geometry Sensing Regulate Cell Functions.” *Nature reviews. Molecular cell biology* 7(4): 265–75.

Wang, Han Bing et al. 2010. “Varying the Diameter of Aligned Electrospun Fibers Alters Neurite Outgrowth and Schwann Cell Migration.” *Acta biomaterialia* 6(8): 2970–78.

Wang, Peng et al. 2014. “Molecularly Imprinted Layer-Coated Hollow Polysaccharide Microcapsules toward Gate-Controlled Release of Water-Soluble Drugs.” *RSC Advances* 4(50): 26063..

Wang, Qiang Song et al. 2012. “Dietary Blue Pigments Derived from Genipin, Attenuate Inflammation by Inhibiting LPS-Induced iNOS and COX-2 Expression via the NF-??B Inactivation.” *PLoS ONE* 7(3): 1–11.

Wang, Y.-K. et al. 2003. “Rigidity of Collagen Fibrils Controls Collagen Gel-Induced Down-Regulation of Focal Adhesion Complex Proteins Mediated by 2 1 Integrin.” *Journal of Biological Chemistry* 278(24): 21886–92.

Van de Wetering, Petra, Andrew T Metters, Ronald G Schoenmakers, and Jeffrey a Hubbell. 2005. “Poly(ethylene Glycol) Hydrogels Formed by Conjugate Addition with Controllable Swelling, Degradation, and Release of Pharmaceutically Active Proteins.” *Journal of controlled release : official journal of the Controlled Release Society* 102(3): 619–27.

Wilhelm, S M et al. 1986. “Human Fibroblast Collagenase: Glycosylation and Tissue-Specific Levels of Enzyme Synthesis.” *PNAS* 83(11): 3756–60.

Williams, B. R., R. A. Gelman, D. C. Poppke, and K. Piez. 1978. “Collagen Fibril Formation. Optimal in Vitro Conditions and Preliminary Kinetic Results.” *Journal of Biological Chemistry* 253(18): 6578–85.

Winer, Jessamine P., Shaina Oake, and Paul a. Janmey. 2009. “Non-Linear Elasticity of Extracellular Matrices Enables Contractile Cells to Communicate Local Position and Orientation.” *PLoS ONE* 4(7).

Wong, Joyce Y, Alan Velasco, Padmavathy Rajagopalan, and Quynh Pham. 2003. “Directed Movement of Vascular Smooth Muscle Cells on Gradient-Compliant Hydrogels †.” *Langmuir* 19(5): 1908–13.

Wong, Melissa Hirose. 2004. “Regulation of Intestinal Stem Cells.” *The journal of investigative dermatology. Symposium proceedings / the Society for Investigative Dermatology, Inc. [and] European Society for Dermatological Research* 9(3): 224–28.

Xie, Jing et al. 2014. “Substrate Stiffness-Regulated Matrix Metalloproteinase Output in Myocardial Cells and Cardiac Fibroblasts: Implications for Myocardial Fibrosis.” *Acta Biomaterialia* 10(6): 2463–72.

Xu, Yanyi et al. 2014. “Cardiac Differentiation of Cardiosphere-Derived Cells in Scaffolds Mimicking Morphology of the Cardiac Extracellular Matrix.” *Acta Biomaterialia* 10(8): 3449–62.

Yamada, Masumi et al. 2012. “Controlled Formation of Heterotypic Hepatic Micro-Organoids in Anisotropic Hydrogel Microfibers for Long-Term Preservation of Liver-Specific Functions.” *Biomaterials* 33(33): 8304–15.

Yan, Ks, La Chia, and Xingnan Li. 2012. “The Intestinal Stem Cell Markers Bmi1 and Lgr5 Identify Two Functionally Distinct Populations.” *Pnas* 109(2): 466–71.

Ye, Qing et al. 2000. “Fibrin Gel as a Three Dimensional Matrix in Cardiovascular Tissue Engineering.” *European Journal of Cardio-thoracic Surgery* 17(5): 587–91.

Yen, Tzung-Hai, and Nicholas a Wright. 2006. “The Gastrointestinal Tract Stem Cell Niche.” *Stem cell reviews* 2(3): 203–12.

Yeon, Ju Hun et al. 2012. “In Vitro Formation and Characterization of a Perfusable Three-Dimensional Tubular Capillary Network in Microfluidic Devices.” *Lab chip* 12(16): 2815–22.

Yu, Jiajie, Songming Peng, Dan Luo, and John C March. 2012. “In Vitro 3D Human Small Intestinal Villous Model for Drug Permeability Determination.” *Biotechnology and bioengineering* 109(9): 2173–78.

Zhang, Guifeng et al. 2006. “Mass Spectrometric Analysis of Enzymatic Digestion of Denatured Collagen for Identification of Collagen Type.” *Journal of Chromatography A* 1114(2): 274–77.

Zhang, Qiang et al. 2012. “Preparation of Uniaxial Multichannel Silk Fibroin Scaffolds for Guiding Primary Neurons.” *Acta biomaterialia* 8(7): 2628–38.

Zheng, Ying et al. 2012. “In Vitro Microvessels for the Study of Angiogenesis and Thrombosis.” *Proceedings of the National Academy of Sciences of the United States of America* 109(24): 9342–47.

Zhu, Junmin. 2010. “Bioactive Modification of Poly(ethylene Glycol) Hydrogels for Tissue Engineering.” *Biomaterials* 31(17): 4639–56.